

**UNIVERSITY OF SÃO PAULO**  
**CHEMISTRY INSTITUTE**  
Graduate Program in Biological Sciences (Biochemistry)

JOÃO VICTOR CABRAL COSTA

**Mitochondrial Ca<sup>2+</sup> Handling in the  
Central Nervous System:**  
*the role of the mitochondrial Na<sup>+</sup>/Ca<sup>2+</sup> exchanger (NCLX)  
in astrocyte metabolism and function*

Ca<sup>2+</sup> Mitochondrial no Sistema Nervoso Central:  
*o papel do trocador de Na<sup>+</sup>/Ca<sup>2+</sup> mitocondrial (NCLX)  
no metabolismo e função de astrócitos*

Corrected version.

São Paulo

Data do depósito na SPG

03/10/2022



JOÃO VICTOR CABRAL COSTA

**Mitochondrial Ca<sup>2+</sup> Handling in the  
Central Nervous System:  
*the role of the mitochondrial Na<sup>+</sup>/Ca<sup>2+</sup> exchanger (NCLX)  
in astrocyte metabolism and function***

Ca<sup>2+</sup> Mitochondrial no Sistema Nervoso Central:  
*o papel do trocador de Na<sup>+</sup>/Ca<sup>2+</sup> mitocondrial (NCLX)  
no metabolismo e função de astrócitos*

*PhD Thesis presented to the Chemistry Institute,  
University of São Paulo, Brazil, to obtain the  
degree of Doctor of Science in Biological Sciences  
(Biochemistry).*

*Supervisor: Prof. Dr. Alicia Juliana Kowaltowski*

São Paulo

2022

Autorizo a reprodução e divulgação total ou parcial deste trabalho, por qualquer meio convencional ou eletrônico, para fins de estudo e pesquisa, desde que citada a fonte.

Ficha Catalográfica elaborada eletronicamente pelo autor, utilizando o programa desenvolvido pela Seção Técnica de Informática do ICMC/USP e adaptado para a Divisão de Biblioteca e Documentação do Conjunto das Químicas da USP

Bibliotecária responsável pela orientação de catalogação da publicação:  
Marlene Aparecida Vieira - CRB - 8/5562

C117m Cabral-Costa, João Victor  
Mitochondrial Ca<sup>2+</sup> Handling in the Central Nervous System: the role of the mitochondrial Na<sup>+</sup>/Ca<sup>2+</sup> exchanger (NCLX) in astrocyte metabolism and function / João Victor Cabral-Costa. - São Paulo, 2022.  
119 p.

Tese (doutorado) - Instituto de Química da Universidade de São Paulo. Departamento de Bioquímica.

Orientador: Kowaltowski, Alicia

1. astrócitos. 2. mitocôndrias. 3. cálcio. 4. lactato. 5. metabolismo. I. T. II. Kowaltowski, Alicia, orientador.





Universidade de São Paulo  
Instituto de Química

"Ca<sup>2+</sup> Mitocondrial no Sistema Nervoso Central: o papel do trocador de Na<sup>+</sup>/Ca<sup>2+</sup> mitocondrial (NCLX) no metabolismo e função de astrócitos"

**JOÃO VICTOR CABRAL COSTA**

Tese de Doutorado submetida ao Instituto de Química da Universidade de São Paulo como parte dos requisitos necessários à obtenção do grau de Doutor em Ciências obtido no Programa Ciências Biológicas (Bioquímica) - Área de Concentração: Bioquímica.

---

Profa. Dra. Alícia Juliana Kowaltowski  
(Orientadora e Presidente)

**APROVADO(A) POR:**

---

Prof. Dr. Danilo Bilches Medinas  
IQ - USP

---

Prof. Dr. Julio Cesar Batista Ferreira  
ICB - USP

---

Prof. Dr. Eduardo Rigon Zimmer (por videoconferência)  
UFRGS

SÃO PAULO  
26 de outubro de 2022



To my wonderful wife, Juçara,  
for her unconditional support through the roughest of patches,  
for her kindness, brilliance, and strength,  
for making us go beyond complementarity,  
synergistically creating the best of us.



## ACKNOWLEDGEMENTS

I have sailed through the sea of mountains of Minas Gerais, navigating down to São Paulo to become a scientist, and across the ocean to Spain, to further develop my PhD project. I got to know many people, animals, and places that, each in their own way, directly or indirectly, were the reason I was able to keep moving and travel thus far. I was met with nothing less than friendship, kindness, and support; more than I ever imagined and could deserve. To them, I hold my deepest gratitude and respect.

I have an immeasurable appreciation by the guidance and example **Alicia Kowaltowski** has offered me. She was my very first supervisor when I started doing science as a 2<sup>nd</sup> year undergraduate student. Her brilliant mind, strong leadership, and kindness were one of the main reasons I decided to come back to her lab 7 years later to pursue my PhD. Rigorous, when necessary, and gentle, when needed. I owe you, Alicia, a great debt of gratitude for this opportunity to grow and discover myself.

To all my *mito-peers* I have crossed paths through these MitoLab years: I also owe you a mole of thanks. To **Camille Caldeira** (amazing lab manager/equipment tamer/life advisor), for all the patience, support, and serenity. To **Pamela Kakimoto** (*tovarishch farmacêutica* and wonder twin), for the fellowship and solidarity – both scientifically and personally. To **Bruno Chaussê** (the brainiest jester I know), for the ever-present encouragement and hopefulness. To **Oswaldo Pereira** (master of science, witty comments, and *pirouettes*), for granting me the opportunity to learn, err, and improve while discovering the complexity of mentoring. To **Vitor Ramos** (honorary *mineiro*, loyal fellow with his ever-calm countenance), for listening, cheering, and supporting me. To **Eloísa Vilas-Boas** (lab karaoke accomplice), for all the pleasant days by the Oroboros and fluorimeters, kindly sharing experiences and advices, and for the inspiration to move on. To **Ariel Cardoso** (fanatic *palmeirense*, pro snooker player), for mentoring my first steps in a lab and stimulating my critical thinking and writing skills. To all colleagues and friends that helped me to overcome obstacles with constructive criticism, including **Fernanda Cunha, Sergio Menezes, Julian Serna, Julia Martini, Luis Luévano, Felipe Macedo, Débora Rocha, Fernanda Cerqueira, Ignacio Amigo, Bruno Queliconi, Erich Tahara**, for easing the burden of tough processes and brightening the day with chit-chats, stories, puns, jokes, parodies, and countless liters of coffee.

I am also grateful to **Marcus Oliveira, Alexandre Bruni, Roberta Andrejew, Isaias Glezer, Carolina Munhoz, Cristoforo Scavone, Paula Kinoshita, Diana Andreotti, Larissa**

**de Sá, Bruno da Costa Rodrigues**, whose scientific and technical inputs were crucial to the progress of this thesis. A special thanks to the kind-hearted **Nilton Barreto** (*in memoriam*). This project would also have not gotten off the ground without the contributions of **John W. Elrod, Antonio Martínez-Ruiz**, and **Pablo Hernansanz-Agustín**, which I deeply appreciate.

I would like to thank **Edson Alves Gomes** and **Sirlei Oliveira**, for the amazing technical support; as well as all the *Biotério de Produção e Experimentação FCF-IQ/USP* staff, in the name of **Silvânia Neves, Renata Spalutto**, and **Flávia Ong**, for the untiring support and guidance in animal care. Indeed, I would like to acknowledge the immeasurable importance of all laboratory animals that were involved, directly or indirectly, in this study.

My warmest thanks to my journal club colleagues **José Carlos de Lima Júnior, Pamela Kakimoto, Bruno Chaussê, Marcel Vieira-Lara**, and **Nathalia Dragano**, for all insightful comments, uplifting discussions, and the supportive environment. More than just meeting fellow metabolic enthusiasts, our weekly *Foro de Mitocôndria* was one of the reasons I was able to make it to the end.

I also must also acknowledge my gratitude to the *Jornada Científica dos Acadêmicos de Farmácia e Bioquímica* (JCAFB-FCF/USP), in the name of **Primavera Borelli, Alice Serpentino, Sabrina Epiphany, Jeanine Giarolla**, and **Juliana Ract**, from where a good chunk of my motivation came. Each step toward a common goal – the possibility of more social justice for all – hit me like a shot of hope. In addition, I am deeply thankful to the many inspiring interactions with **Laura Marise, Raimundo da Silva, Ana Bonassa**, and the whole *Nunca Vi I Cientista* crew – brilliant science communicators that I hold in high regard.

My sincere gratefulness also goes to **Caio Zeidler** and **Anderson Baraldo**, brothers that life has kindly gifted me and whose presence, patience, merriment, integrity, and friendship helped me to endure numerous hardships, acquainting me with antifragility.

I thankfully acknowledge the inspiration I was lucky to receive from many great educators, including **Marisa Medeiros, Fernando “Titio”, Giovanni Marques, Primavera Borelli, Iolanda Cuccovia, Tania Marcourakis**, and **Fernando Abdulkader**. A debt of gratitude is owed to **Luciane Capelo**, for greatly kindly catalyzing a major milestone in my scientific and personal life. I would like to express my deepest appreciation to **Caio Mazucanti**, whose enthusiasm for Science (with a capital S) really shaped my path into science, for he was the responsible to introduce me to the world of neurometabolism.

\*\*\*

Fue precisamente un trabajo de **Juan Pedro Bolaños** que me involucró en el área de Neurometabolismo, a quien debo expresar mi más sincero agradecimiento. No sólo por haber inspirado a seguir por este camino, pero, más importantemente, por haber abierto las puertas de su laboratorio y recibirme, orientarme y ayudarme como uno de los suyos. Su apoyo, ejemplo y liderazgo fueron cruciales para dar forma a mi futuro como científico.

Y todo eso no existiría si no fuera por la amabilidad y la amistad de tantas personas que me acogieron y compartieron sus vidas e historias, haciendo que este año traiga memorias equivalentes a una década entera. Muchas gracias a **Brenda Morant** y **Paula Alonso**, por amablemente catalizar mi mudanza y aclimatación, como si esto hubiera sido siempre mi sitio. A **Daniel Jiménez**, por las charlas de ánimo y por la incansable alegría. A los hermanitos **Israel Manjarréz** y **Jesús Hermosín**, por recordarme de concentrar siempre en el lado positivo, incluso de las pequeñas cosas. A **Rubén Quintana**, **Marina García**, **Cristina Rodríguez** e **Irene Sánchez**, por todos los consejos, las ayudas y el aliento. A **Sandra Martínez**, **Silvia Gomila**, **Regina Mengual**, **Sara Yunta**, **Sonia González** y **Verónica Bobo**, por la compañía, conversaciones y risas. A **Angeles Almeida**, **María Delgado** e **Emilio Fernández**, por las orientaciones, críticas y el apoyo. A **Mónica Resch**, **Estefanía Prieto**, **Lucía Martín** e **Mónica Carabias**, por la paciencia y el soporte técnico impecable. Y a **Vanessa Carvalho** (*querida conterrânea*), por no dejarme olvidar de mis esencias y orígenes.

No puedo dejar de expresar mi profunda gratitud a **Carlos Vicente-Gutiérrez**, por acoger mis proyectos, dudas, ansiedades y sueños; y a **Natalia Medina**, por el cariño y acogimiento. A **Jesús “Chustín” Agulla**, por no escatimar esfuerzos para garantizar que todo caminara bien. A **Rebeca Lapresa**, por toda la preocupación en hacerme sentir bien e integrado; incluso por el cariño de **Moka** (¡qué regalo me diste!). Ustedes, amigos, han sido mi fuente de esperanza e inspiración.

Debo agradecer de manera especial a **Amparo Vega** y **Juan Bermejo**, que me adoptaron como miembro de la familia en un momento tan crítico. Mis queridos padres españoles, estaré eternamente agradecido por vuestra amabilidad, cariño y atención; con vosotros, y en la compañía de **Platón**, no hubo confinamiento, distancia ni angustia que me afectara sin que yo fuera antes acogido y consolado.

\*\*\*

Sobre família, antes de tudo, tenho de agradecer à minha amada mãe, **Maria do Carmo** (*in memoriam*), cujo caráter, bondade, alegria e amor seguem me iluminando. Aquele seu sorriso ainda reverbera na minha memória e influencia cada passo que eu dou. Agradeço ao meu querido pai, **Jésus**, pelos questionamentos, conselhos e incondicional incentivo. Foi seu o meu primeiro abraço como aspirante a farmacêutico, o “empurrão” decisivo que, em meio a um universo de escolhas, me trouxe até aqui. Também sou muito grato à minha *mãedrasta*, **Edilene**, pela amizade, palavra e respeito, por ter me adotado com tanto carinho. Agradeço aos meus sogros, **Carlos e Lamara**, que sempre me acolheram carinhosamente. Seus olhares, abraços e incentivos foram o combustível que me moveu por todo esse caminho.

À **Débora**, que plantou em mim, aos 6 anos, a semente da curiosidade e admiração pelas ciências naturais, quando me integrou ao seu “Clubinho da Ciência”. Seu apoio incondicional, amor e “jeitinho” iluminaram o meu caminho e moldaram a pessoa que sou e a que desejo ser. Ao **Nicholas**, querido compatriota, pelo intenso apoio, pelos saraus e churrascos, além, claro, pelo invejável repertório de piadas, trocadilhos e paródias. À **Patrícia**, meu exemplo de bravura e resiliência, por me ensinar a importância de se motivar pelo *amanhã* sem perder a essência do *hoje*. À **Cristiane**, que desbravou e me guiou em meus primeiros caminhos acadêmicos, por meio de seus conselhos, ensinamentos e pelo seu impecável exemplo. Meus medos, ansiedades e preocupações se tornavam pequenos perto da sua fortaleza, perseverança e acolhimento.

Aos meus queridos sobrinhos e afilhados, **Anna Beatriz, Miguel, João Henrique, Isabela, Victor, Manuela, Eric e Lis**, por me lembrarem da importância da espontaneidade, da leveza e da curiosidade; por me ensinarem que a admiração pela *complexidade do simples* nos ensina muito mais que a busca pela *simplicidade do complexo*.

À **Zara**, nosso anjinho de quatro patas, parceira de aventuras que encheu nossa casa de carinho, nos confortou em tantos momentos de angústia e partilhou da alegria de conquistas.

Por fim, à **Juçara**, minha companheira de vida, meu alicerce, *sostanza dei giorni miei*. Você é a razão pela qual eu hoje estou aqui, e poder compartilhar os dias com você é uma dádiva, um presente que a vida me deu e pelo qual sou eternamente grato.

\*\*\*

Finally, I appreciate the financial support from *Fundação de Amparo à Pesquisa do Estado de São Paulo* (FAPESP, grants #2013/07937-8; 2017/14713-0; 2019/22178-2; 2020/06970-5), *Coordenação de Aperfeiçoamento de Pessoal de Nível Superior* (CAPES), and *Conselho Nacional de Desenvolvimento Científico e Tecnológico* (CNPq), which were crucial to the execution of this work. All illustrations were created with Biorender.com.



*“Há um menino, há um moleque  
Morando sempre no meu coração  
Toda vez que o adulto balança ele vem pra me dar a mão*

*Há um passado no meu presente  
O sol bem quente lá no meu quintal  
Toda vez que a bruxa me assombra o menino me dá a mão*

*E me fala de coisas bonitas que eu acredito  
Que não deixarão de existir  
Amizade, palavra, respeito, caráter, bondade, alegria e amor*

*Pois não posso, não devo  
Não quero viver como toda essa gente insiste em viver  
E não posso aceitar sossegado qualquer sacanagem  
Ser coisa normal*

*Bola de meia  
Bola de gude  
Um solidário não quer solidão  
Toda vez que a tristeza me alcança um menino me dá a mão*

*Há um menino, há um moleque morando sempre no meu  
coração  
Toda vez que o adulto fraqueja ele vem pra me dar a mão”*

(Nascimento; Brant, 1988)



## ABSTRACT

Cabral-Costa JV. **Mitochondrial Ca<sup>2+</sup> Handling in the Central Nervous System: the role of the mitochondrial Na<sup>+</sup>/Ca<sup>2+</sup> exchanger (NCLX) in astrocyte metabolism and function.** 2022. 119 p. PhD Thesis – Graduate Program in Biological Sciences (Biochemistry). Instituto de Química, Universidade de São Paulo, São Paulo.

Mitochondria are specialized organelles involved in many cellular processes, including redox balance, macromolecule biosynthesis, and energy metabolism. In the central nervous system, mitochondrial dysfunctions are associated with many pathophysiological mechanisms central toward neurological disorders such as stroke, Amyotrophic Lateral Sclerosis, and Alzheimer's, Parkinson's, and Huntington's diseases. One of the common hallmarks of these diseases lies in the mitochondrial Ca<sup>2+</sup> handling system. Mitochondria have the ability to uptake and release Ca<sup>2+</sup> through the mitochondrial calcium uniporter complex (MCUc) and Na<sup>+</sup>/Ca<sup>2+</sup> exchanger (NCLX), respectively. This Ca<sup>2+</sup> cycling, apart from shaping cytosolic Ca<sup>2+</sup> levels, can modulate distinct mitochondrial metabolic pathways. In astrocytes, the most abundant macroglial cell type in the brain, Ca<sup>2+</sup> signaling plays a central role controlling cellular homeostasis and function, influencing several brain processes such as synaptic plasticity, circuit integration, behavior, and neurodegeneration. However, apart from influencing cell proliferation and survival, little was known to date regarding the role of NCLX on astrocyte physiology. Searches in public RNA-seq databases led us to observe that astrocytes have over-enriched *Nclx* transcription when in comparison to neurons or total brain areas, reinforcing our hypothesis that NCLX may present further critical physiological functions in this cell type. To study these functions, we inhibited NCLX activity – pharmacologically and genetically – in mouse primary culture astrocytes. *In vitro* NCLX inhibition increased cytosolic Ca<sup>2+</sup> clearance and induced a metabolic shift, increasing glycolytic flux and lactate secretion. *In vivo* deletion of NCLX specifically in hippocampal astrocytes improved mouse performance in behavioral tasks, while cognitive impairment was induced by neuronal-specific NCLX deletion. These data reveal a novel role of NCLX as a modulator of glucose metabolism in astrocytes, with functional cognitive impacts.

**Keywords:** astrocyte, mitochondria, calcium, NCLX, lactate, metabolism.

## RESUMO

Cabral-Costa JV. **Ca<sup>2+</sup> Mitocondrial no Sistema Nervoso Central: o papel do trocador de Na<sup>+</sup>/Ca<sup>2+</sup> mitocondrial (NCLX) no metabolismo e função de astrócitos.** 2022. 119 p. Tese (Doutorado) – Programa de Pós-Graduação em Ciências Biológicas (Bioquímica). Instituto de Química, Universidade de São Paulo, São Paulo.

Mitocôndrias são organelas altamente especializadas, envolvidas em diversos processos celulares, incluindo o balanço redox, biossíntese de macromoléculas e metabolismo energético. No sistema nervoso central, disfunções mitocondriais são associadas com vários mecanismos patofisiológicos centrais de doenças neurológicas, como acidente vascular encefálico, Esclerose Lateral Amiotrófica, e as doenças de Alzheimer, Parkinson e Huntington. Neste contexto, um importante fator em comum é o manejo de Ca<sup>2+</sup> mitocondrial. Mitocôndrias possuem a habilidade de captar e liberar Ca<sup>2+</sup> por meio do complexo do uniporter de cálcio mitocondrial (MCUc) e do trocador Na<sup>+</sup>/Ca<sup>2+</sup> (NCLX), respectivamente. Este transporte de Ca<sup>2+</sup>, além de moldar os sinais de Ca<sup>2+</sup> citosólicos, pode contribuir com a modulação de diferentes pontos de vias metabólicas mitocondriais. Em astrócitos, a célula macroglial mais abundante e uma das mais importantes do cérebro, a sinalização de Ca<sup>2+</sup> apresenta um papel central no controle da homeostase e função celular, influenciando diversos processos cerebrais, como plasticidade sináptica, integração de circuitos cerebrais, comportamentos e neurodegeneração. Contudo, além de influenciar a proliferação e sobrevivência, pouco se conhece sobre o papel do NCLX na fisiologia de astrócitos. Pesquisas em bases de dados públicas de RNA-seq nos levaram a identificar que o transcrito do *Nclx* se encontra enriquecido em astrócitos em comparação com neurônios ou o material total de áreas do cérebro, reforçando nossa hipótese de que o NCLX deve apresentar outras funções fisiológicas críticas neste tipo celular. Para abordar esta questão, a atividade do NCLX foi modulada – farmacológica e geneticamente – em cultura primária de astrócitos. A inibição do NCLX *in vitro* intensificou a depuração de Ca<sup>2+</sup> citosólico e induziu um remodelamento metabólico, aumentando o fluxo glicolítico e a secreção de lactato. A deleção genética do NCLX *in vivo*, em astrócitos no hipocampo, aprimorou o desempenho de camundongos em testes comportamentais, em contraste a um prejuízo comportamental induzido pela deleção neuronal de NCLX. Estes resultados revelam um novo papel do NCLX como modulador do metabolismo de glicose em astrócitos, capaz de gerar impactos cognitivos.

**Palavras-chave:** astrócitos, mitocôndrias, cálcio, NCLX, lactato, metabolismo.

## SUMMARY

<b>GENERAL INTRODUCTION .....</b>	<b>19</b>
References.....	24
<b>CHAPTER 1 – Neurological disorders and mitochondria .....</b>	<b>27</b>
Summary .....	28
Cabral-Costa and Kowaltowski, 2020 .....	1 (29)
Abstract .....	1 (29)
1 Introduction .....	1 (29)
2 Ischemic stroke.....	2 (30)
3 Alzheimer’s disease.....	3 (31)
4 Amyotrophic Lateral Sclerosis (ALS).....	3 (31)
5 Huntington’s disease .....	4 (32)
6 Parkinson’s disease.....	4 (32)
7 Conclusions .....	5 (33)
Funding.....	5 (33)
Abbreviations .....	5 (33)
References .....	5 (33)
<b>CHAPTER 2 – Mitochondrial Ca<sup>2+</sup> handling as a cell signaling hub: lessons from astrocyte function .....</b>	<b>37</b>
Summary.....	38
Cabral-Costa and Kowaltowski, 2022 .....	1 (39)
Abstract .....	1 (39)
Introduction .....	2 (40)
Mitochondrial Ca <sup>2+</sup> homeostasis .....	3 (41)
<i>Mitochondrial Ca<sup>2+</sup> influx</i> .....	4 (42)
<i>Mitochondrial Ca<sup>2+</sup> efflux</i> .....	4 (42)
<i>Mitochondrial permeability transition pore (mtPTP)</i> .....	6 (44)
Astrocytic Ca <sup>2+</sup> signaling .....	6 (44)
<i>Astrocytic mitochondrial Ca<sup>2+</sup> handling</i> .....	7 (45)
Open questions .....	10 (48)
Summary .....	10 (48)
Abbreviations .....	10 (48)
Acknowledgements .....	11 (49)
References .....	11 (49)

**CHAPTER 3 – *In vivo* and *in vitro* manipulation of the mitochondrial Na<sup>+</sup>/Ca<sup>2+</sup> (NCLX) exchanger: general methodological approaches..... 55**

3.1 Summary .....	56
3.2 <i>In vivo</i> NCLX deletion and behavioral assessment.....	57
3.3 Mouse astrocyte primary cultures .....	62
3.4 <i>In vitro</i> metabolic assessment .....	68
3.5 Influence of stressful stimuli on NCLX expression.....	71
3.6 Concluding remarks .....	76
3.7 References .....	77

**CHAPTER 4 – Mitochondrial sodium/calcium exchanger NCLX regulates glycolysis in astrocytes, impacting on cognitive performance ..... 81**

Summary .....	82
Cabral-Costa et al., 2022 .....	1 (83)
Title page .....	1 (83)
Abstract.....	2 (84)
Introduction.....	3 (85)
Results.....	5 (87)
Discussion.....	12 (94)
Materials and methods .....	15 (97)
RNAseq public databases .....	15 (97)
Animal care .....	15 (97)
Cell cultures.....	16 (98)
Seahorse assays .....	17 (99)
<i>ATPrate test</i> .....	17 (99)
<i>MitoStress test</i> .....	17 (99)
Glycolytic flux.....	18 (100)
Lactate secretion and glucose consumption .....	18 (100)
Viral transduction .....	18 (100)
Stereotaxic surgery .....	19 (101)
Behavioral assays .....	19 (101)
<i>Open Field test</i> .....	20 (102)
<i>Novel Object Recognition test</i> .....	20 (102)
<i>Y-maze test</i> .....	20 (102)
Calcium imaging .....	21 (103)

Statistical analyses .....	21 (103)
Data availability .....	22 (104)
Acknowledgements .....	22 (104)
Funding.....	22 (104)
Conflict of interest.....	22 (104)
Author contributions.....	22 (104)
References .....	23 (105)
Figure supplements.....	28 (110)
<b>CONCLUDING REMARKS .....</b>	<b>115</b>
References.....	117
<b>ANNEX LIST.....</b>	<b>119</b>





## GENERAL INTRODUCTION

Metabolism lies within the core definition of what we know as life, which entails the collaboration between this process and the ability to reproduce (Dupré; O'Malley, 2009). In this context, Erwin Schrödinger (1992, p. 47) poetically defined its importance:

‘What then is that precious something contained in our food which keeps us from death? That is easily answered. Every process, event, happening – call it what you will; in a word, everything that is going on in Nature means an increase of the entropy of the part of the world where it is going on. Thus a living organism continually increases its entropy – or, as you may say, produces positive entropy – and thus tends to approach the dangerous state of maximum entropy, which is of death. It can only keep aloof from it, *i.e.* alive, by continually drawing from its environment negative entropy – which is something very positive as we shall immediately see. What an organism feeds upon is negative entropy. Or, to put it less paradoxically, the essential thing in metabolism is that the organism succeeds in freeing itself from all the entropy it cannot help producing while alive.’

Metabolic pathways thus may be defined as a series of enzymatic reactions in which molecules are used to synthesize biomolecules (anabolism), or, conversely, more complex biomolecules are broken down to generate energy and/or obtain simpler molecules (catabolism, Fig. 1) (Voet; Voet, 2011, p. 561).

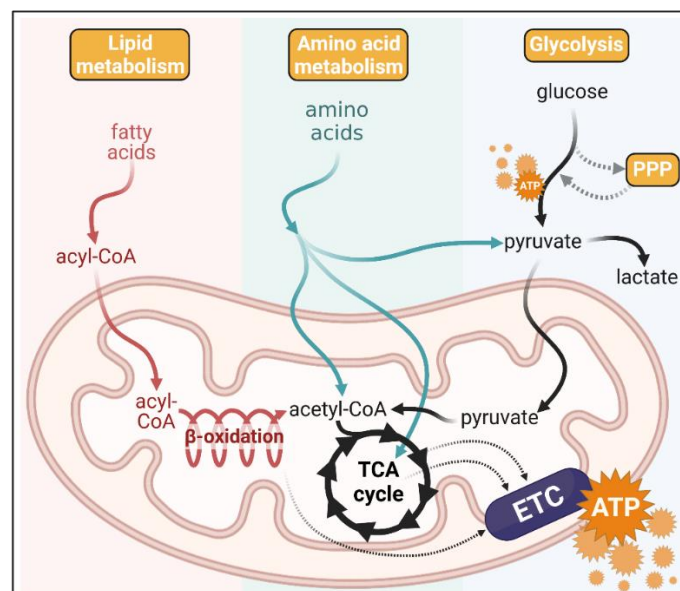


**Figure 1. Schematic overview of major catabolic pathways.** General overview of lipid, amino acid, and carbohydrate metabolism, integrating with mitochondrial-dependent oxidative phosphorylation and energy production (adapted from Loussouarn et al., 2021). (TCA: tricarballic acid; ETC: electron transport chain; PPP: pentose-phosphate pathway).

As an illustration of this process, the glycolytic pathway (Fig. 2) positively contributes toward energy production (Voet; Voet, 2011, p. 596) by promoting glucose catabolism, culminating in lactate (which can then be secreted by cells) or pyruvate (which can be transported for further oxidation by mitochondria) production, and generating adenosine triphosphate (ATP) and reduced equivalents of nicotinamide adenine nucleotide (NADH). NADH can then be shuttled into the mitochondrial matrix and oxidized by the electron transport chain.

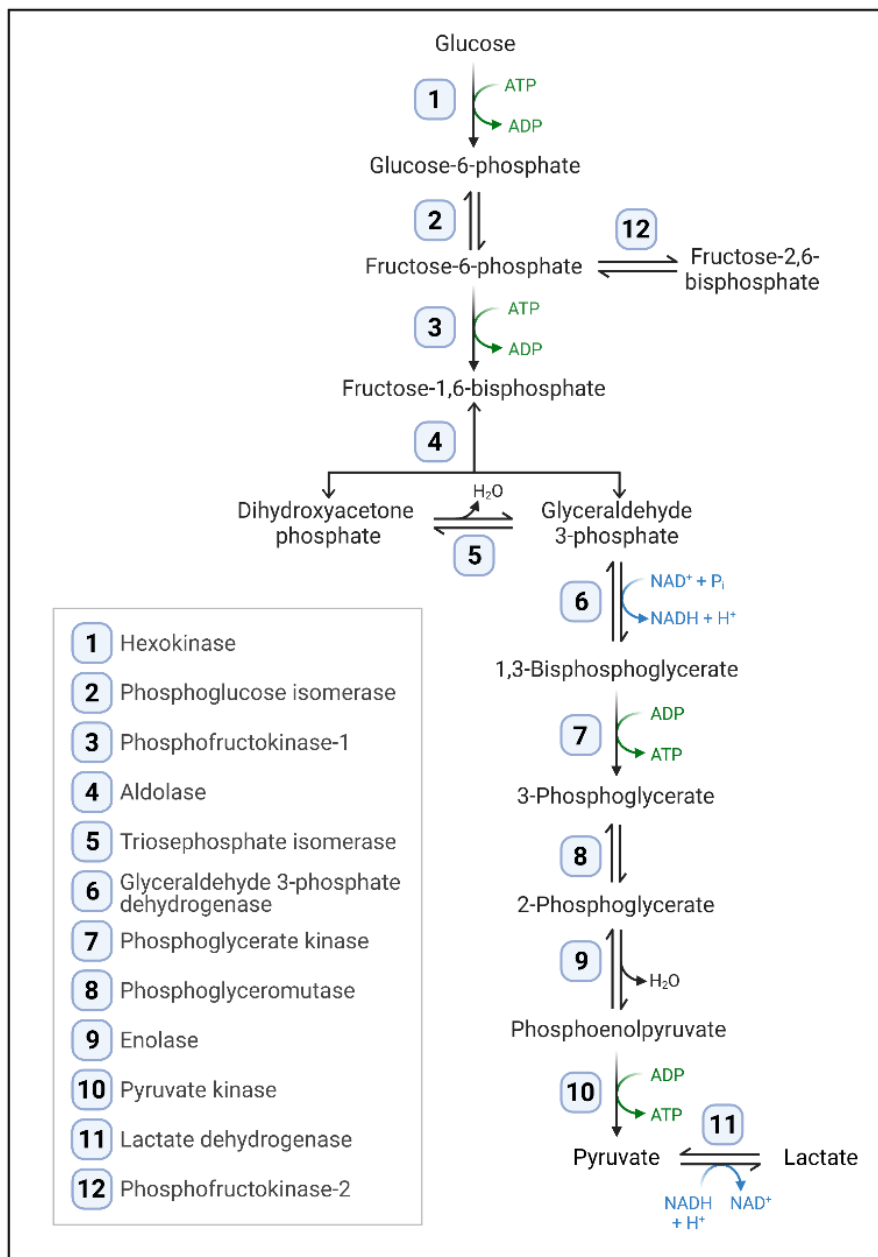


**Figure 2. Glycolytic pathway.** Major reactions of glycolysis and respective enzymes, highlighting adenine di (ADP) and triphosphate (ATP) output, as well as the reduction/oxidation of nicotinamide adenine dinucleotide (NAD<sup>+</sup>/NADH).

Most of these metabolic pathways are intrinsically integrated with mitochondrial physiology. Mitochondria are specialized organelles comprised of two membranes (outer and inner mitochondrial membranes, OMM and IMM, respectively), the latter of which engulfs the mitochondrial matrix (Nunnari; Suomalainen, 2012). These organelles are found as a heterogeneous population with diverse morphologies and sizes. They display the ability to fuse and divide, and undergo routine turnover (Ferree; Shirihai, 2012).

Apart from their well-known participation in energy metabolism, contributing toward ATP production (Fig. 2), mitochondrial functions span widely, including maintaining redox balance (oxidant production and quenching), ammonia assimilation, and acting as macromolecule biosynthesis hub, including the anabolism of nucleotides, heme, glucose, fatty acids, cholesterol, and amino acids (Spinelli; Haigis, 2018). In this sense, mitochondrial dysfunctions lead to strong homeostasis perturbations and are directly associated with several pathological conditions, including congenital neuromyopathies and heart diseases (Rahman, 2020), diabetes (Las; Oliveira; Shirihai, 2020), and psychiatric (Martins-de-Souza et al., 2011; Allen et al., 2018) and neurological disorders (Ghirotto et al., 2022; Cabral-Costa; Kowaltowski, 2020; Pereira et al., 2021).

Indeed, the central nervous system strongly relies on mitochondrial function for major processes that are involved in pathophysiological mechanisms. In **Chapter 1 – Neurological Disorders and Mitochondria**, we highlight the relevance of mitochondrial dysfunctions in adult-onset neurological diseases, such as Alzheimer's, Huntington's, and Parkinson's disease, Amyotrophic Lateral Sclerosis, and stroke. By focusing on how processes such as  $\text{Ca}^{2+}$  homeostasis, cell death regulation, redox balance, mitochondrial dynamics, and oxidative phosphorylation contribute to these pathologies, we demonstrate that mitochondrial physiology is deeply rooted in brain pathophysiology.

One of these processes, mitochondrial  $\text{Ca}^{2+}$  handling, is of particularly great interest. The ability of mitochondria to take up and release  $\text{Ca}^{2+}$  has been known since the 1960s (Lehninger; Rossi; Greenawalt, 1963; Vasington; Murphy, 1962; Drahota; Lehninger, 1965). However, it was only in the last decade, after the major components of the mitochondrial  $\text{Ca}^{2+}$  handling system were identified (Palty et al., 2010; Perocchi et al., 2010; Baughman et al., 2011; De Stefani et al., 2011; Plovanich et al., 2013; Sancak et al., 2013), that the mechanisms and interactions with other cellular pathways were better dissected. In **Chapter 2 – Mitochondrial  $\text{Ca}^{2+}$  handling as a cell signaling hub: lessons from astrocyte function**, we review the composition of the mitochondrial  $\text{Ca}^{2+}$  handling system, digging into its influence

on astrocyte homeostasis and brain function. Of note, we discuss the function of the mitochondrial  $\text{Na}^+/\text{Ca}^{2+}$  exchanger (NCLX) controlling mitochondrial  $\text{Ca}^{2+}$  efflux, and how little is known about its influence on astrocytic homeostasis.

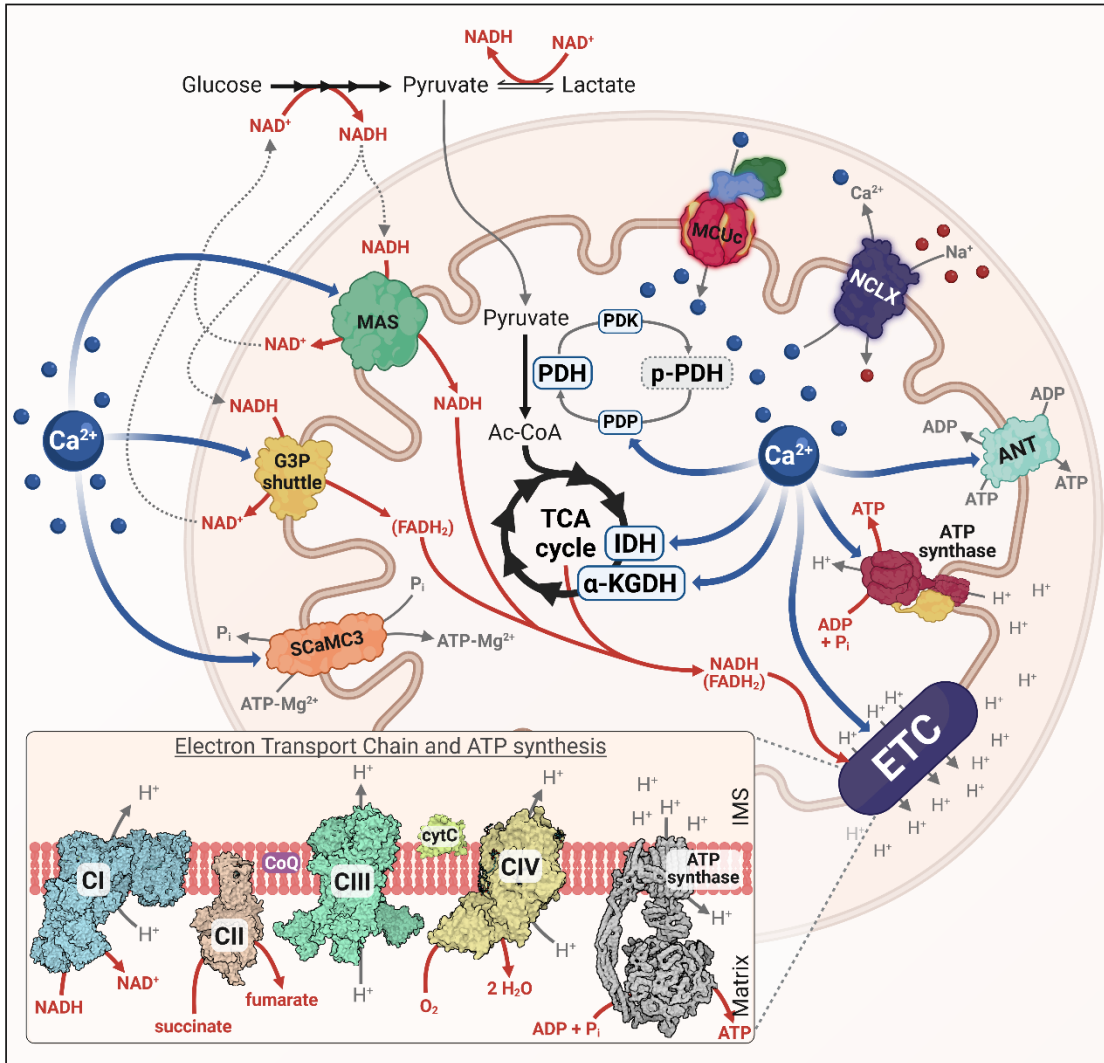


**Figure 3. Mitochondria,  $\text{Ca}^{2+}$ , and metabolic integration.** Schematic illustration of mitochondrial metabolic aspects of importance to this thesis. Glycolytic pyruvate is transported into the mitochondrial matrix, where it is converted into Ac-CoA and oxidized through the TCA cycle. NADH/ $\text{FADH}_2$  equivalents produced in the TCA cycle, as well as NADH from MAS and GP3 shuttles, are oxidized through the ETC, contributing toward proton pumping by ETC complexes. ATP synthase then synthesizes ATP driven by this protonmotive force. Synthesized ATP can then be exported in exchange for ADP by the ANT. The total adenine nucleotide pool may also be influenced by ATP- $\text{Mg}^{2+}$  transport by SCaMC3. Mitochondria can take up  $\text{Ca}^{2+}$  through the MCUc and export matrix free  $\text{Ca}^{2+}$  in exchange for cytosolic  $\text{Na}^+$  through the NCLX. Both cytosolic and matrix  $\text{Ca}^{2+}$  can positively modulate these steps, culminating in metabolic pathway activation. This figure was adapted from Llorente-Folch et al. (2015), and mitochondrial ETC complexes were designed from crystalized structures from complex I (Agip et al., 2018; PDB 6G2J); complex II (Sun et al., 2005; PDB 1ZOY); complex III (Solmaz; Hunte, 2008; PDB 3CX5); cytochrome C (Berghuis et al., 1994; PDB: 1CRH); complex IV (Koepke et al., 2009; PDB: 3HB3); and ATP synthase (Guo; Rubinstein, 2022; PDB: 7TK4). (MCU: mitochondrial calcium uniporter complex; NCLX: mitochondrial  $\text{Na}^+/\text{Ca}^{2+}$  exchanger; ANT: adenine nucleotide translocator; ETC: electron transport chain; CI-IV: ETC complexes; CoQ: coenzyme-Q; cytC: cytochrome C; (p)-PDH: (phospho)-pyruvate dehydrogenase; PDK: pyruvate dehydrogenase kinase; PDP: pyruvate dehydrogenase phosphatase; Ac-CoA: acetyl-Coenzyme A; TCA: tricarboxylic acid; IDH: isocitrate dehydrogenase;  $\alpha$ -KGDH:  $\alpha$ -ketoglutarate dehydrogenase; SCaMC3: mitochondrial ATP- $\text{Mg}/\text{Pi}$  carrier; G3P: glycerol 3-phosphate; MAS: malate-aspartate shuttle).

Astrocytes are star-shaped macroglial cells and one of the most abundant cell types in the brain (Khakh; Deneen, 2019). Apart from controlling extracellular  $K^+$  levels, neurotransmitter recycling, and structuring the blood-brain barrier, astrocytes play a key role supporting neuronal energy metabolism (Oheim; Schmidt; Hirrlinger, 2018; Bonvento; Bolaños, 2021). Thus, considering that  $Ca^{2+}$  is a strong modulator of energy metabolism (Llorente-Folch et al., 2015; Juaristi et al., 2019; Bonvento; Bolaños, 2021), we hypothesized that NCLX could act as regulatory point of control for astrocytic metabolism and, consequently, neuronal homeostasis. We then delineated an experimental design to tackle this question. In **Chapter 3 – *In vivo* and *in vitro* manipulation of the mitochondrial  $Na^+/Ca^{2+}$  (NCLX) exchanger: general methodological approaches**, we give an overview of this experimental design. In addition, we discuss how an odd observation on experimental controls from a pilot study opened a path to further study the regulation of NCLX gene expression.

Then, in **Chapter 4 – NCLX fine-tunes glycolysis and lactate secretion in astrocytes**, we pursue our hypothesis and test the functional implications of hampering NCLX activity in astrocytes *in vivo* and *in vitro*, mainly focusing on its metabolic outcomes. This way, these four chapters are tightly connected. Thus, finally, in the last section **Concluding remarks**, we summarize our major findings, connect them with the current understanding of the literature, and pinpoint future perspectives of this research area.

## References<sup>1</sup>

- Agip A-NA, Blaza JN, Bridges HR, Viscomi C, Rawson S, Muench SP, et al. Cryo-EM structures of complex I from mouse heart mitochondria in two biochemically defined states. *Nat Struct Mol Biol* 2018;25:548–56. <https://doi.org/10.1038/s41594-018-0073-1>.
- Allen J, Romay-Tallon R, Brymer KJ, Caruncho HJ, Kalynchuk LE. Mitochondria and mood: mitochondrial dysfunction as a key player in the manifestation of depression. *Front Neurosci* 2018;12:386. <https://doi.org/10.3389/fnins.2018.00386>.
- Baughman JM, Perocchi F, Girgis HS, Plovanich M, Belcher-Timme CA, Sancak Y, et al. Integrative genomics identifies MCU as an essential component of the mitochondrial calcium uniporter. *Nature* 2011;476:341–5. <https://doi.org/10.1038/nature10234>.
- Berghuis AM, Guillemette JG, McLendon G, Sherman F, Smith M, Brayer GD. The role of a conserved internal water molecule and its associated hydrogen bond network in Cytochrome c. *J Mol Biol* 1994;236:786–99. <https://doi.org/10.1006/jmbi.1994.1189>.
- Bonvento G, Bolaños JP. Astrocyte-neuron metabolic cooperation shapes brain activity. *Cell Metab* 2021;33:1546–64. <https://doi.org/10.1016/j.cmet.2021.07.006>.
- Cabral-Costa JV, Kowaltowski AJ. Neurological disorders and mitochondria. *Mol Aspects Med* 2020;71:100826. <https://doi.org/10.1016/j.mam.2019.10.003>.
- De Stefani D, Raffaello A, Teardo E, Szabò I, Rizzuto R. A forty-kilodalton protein of the inner membrane is the mitochondrial calcium uniporter. *Nature* 2011;476:336–40. <https://doi.org/10.1038/nature10230>.
- Drahota Z, Lehninger AL. Movements of H<sup>+</sup>, K<sup>+</sup>, and Na<sup>+</sup> during energy-dependent uptake and retention of Ca<sup>++</sup> in rat liver mitochondria. *Biochem Biophys Res Commun* 1965;19:351–6. [https://doi.org/10.1016/0006-291X\(65\)90467-5](https://doi.org/10.1016/0006-291X(65)90467-5).
- Dupré J, O'Malley MA. Varieties of living things: life at the intersection of lineage and metabolism. *Philos Theor Biol* 2009;1. <https://doi.org/10.3998/ptb.6959004.0001.003>.
- Ferree A, Shirihai O. Mitochondrial dynamics: the intersection of form and function. In: Kadenbach B, editor. *Mitochondrial Oxidative Phosphorylation*, vol. 748, New York, NY: Springer New York; 2012, p. 13–40. [https://doi.org/10.1007/978-1-4614-3573-0\\_2](https://doi.org/10.1007/978-1-4614-3573-0_2).
- Funaro VMB de O, Pestana MC, Dziabas MCC, Garcia EM, Santos MF dos, Nascimento MM, et al. Diretrizes para apresentação de dissertações e teses da USP: parte IV (Vancouver). vol. IV. 3rd ed. Universidade de São Paulo. Sistema Integrado de Bibliotecas; 2016.
- Ghirotto B, Oliveira DF, Cipelli M, Basso PJ, Lima J, Breda CNS, et al. MS-driven metabolic alterations are recapitulated in iPSC-derived astrocytes. *Ann Neurol* 2022;91:652–69. <https://doi.org/10.1002/ana.26336>.
- Guo H, Rubinstein JL. Structure of ATP synthase under strain during catalysis. *Nat Commun* 2022;13:2232. <https://doi.org/10.1038/s41467-022-29893-2>.
- Juaristi I, Contreras L, González-Sánchez P, Pérez-Liévana I, González-Moreno L, Pardo B, et al. The response to stimulation in neurons and astrocytes. *Neurochem Res* 2019;44:2385–91. <https://doi.org/10.1007/s11064-019-02803-7>.

---

<sup>1</sup> Following the Vancouver system, in accordance with the *Diretrizes para apresentação de dissertações e teses da USP – Parte IV* (Funaro et al., 2016).

- Khakh BS, Deneen B. The emerging nature of astrocyte diversity. *Annu Rev Neurosci* 2019;42:187–207. <https://doi.org/10.1146/annurev-neuro-070918-050443>.
- Koepke J, Olkhova E, Angerer H, Müller H, Peng G, Michel H. High resolution crystal structure of *Paracoccus denitrificans* cytochrome c oxidase: New insights into the active site and the proton transfer pathways. *Biochim Biophys Acta Bioenerg* 2009;1787:635–45. <https://doi.org/10.1016/j.bbabi.2009.04.003>.
- Las G, Oliveira MF, Shirihai OS. Emerging roles of  $\beta$ -cell mitochondria in type-2-diabetes. *Mol Aspects Med* 2020;71:100843. <https://doi.org/10.1016/j.mam.2019.100843>.
- Lehninger AL, Rossi CS, Greenawalt JW. Respiration-dependent accumulation of inorganic phosphate and  $\text{Ca}^{++}$  by rat liver mitochondria. *Biochem Biophys Res Commun* 1963;10:444–8. [https://doi.org/10.1016/0006-291X\(63\)90377-2](https://doi.org/10.1016/0006-291X(63)90377-2).
- Llorente-Folch I, Rueda CB, Pardo B, Szabadkai G, Duchen MR, Satrustegui J. The regulation of neuronal mitochondrial metabolism by calcium: regulation of neuronal mitochondrial metabolism. *J Physiol* 2015;593:3447–62. <https://doi.org/10.1113/JP270254>.
- Loussouarn C, Pers Y-M, Bony C, Jorgensen C, Noël D. Mesenchymal stromal cell-derived extracellular vesicles regulate the mitochondrial metabolism via transfer of miRNAs. *Front Immunol* 2021;12:623973. <https://doi.org/10.3389/fimmu.2021.623973>.
- Martins-de-Souza D, Harris LW, Guest PC, Bahn S. The role of energy metabolism dysfunction and oxidative stress in schizophrenia revealed by proteomics. *Antiox Redox Signal* 2011;15:2067–79. <https://doi.org/10.1089/ars.2010.3459>.
- Nascimento M, Brant F. Bola de meia, bola de gude. *Discos CBS*; 1988.
- Nunnari J, Suomalainen A. Mitochondria: in sickness and in health. *Cell* 2012;148:1145–59. <https://doi.org/10.1016/j.cell.2012.02.035>.
- Oheim M, Schmidt E, Hirrlinger J. Local energy on demand: Are ‘spontaneous’ astrocytic  $\text{Ca}^{2+}$ -microdomains the regulatory unit for astrocyte-neuron metabolic cooperation? *Brain Res Bull* 2018;136:54–64. <https://doi.org/10.1016/j.brainresbull.2017.04.011>.
- Palty R, Silverman WF, Hershinkel M, Caporale T, Sensi SL, Parnis J, et al. NCLX is an essential component of mitochondrial  $\text{Na}^+/\text{Ca}^{2+}$  exchange. *Proc Natl Acad Sci USA* 2010;107:436–41. <https://doi.org/10.1073/pnas.0908099107>.
- Pereira OR, Ramos VM, Cabral-Costa JV, Kowaltowski AJ. Changes in mitochondrial morphology modulate LPS-induced loss of calcium homeostasis in BV-2 microglial cells. *J Bioenerg Biomembr* 2021;53:109–18. <https://doi.org/10.1007/s10863-021-09878-4>.
- Perocchi F, Gohil VM, Girgis HS, Bao XR, McCombs JE, Palmer AE, et al. MICU1 encodes a mitochondrial EF hand protein required for  $\text{Ca}^{2+}$  uptake. *Nature* 2010;467:291–6. <https://doi.org/10.1038/nature09358>.
- Plovanich M, Bogorad RL, Sancak Y, Kamer KJ, Strittmatter L, Li AA, et al. MICU2, a paralog of MICU1, resides within the Mitochondrial Uniporter Complex to regulate calcium handling. *PLoS ONE* 2013;8:e55785. <https://doi.org/10.1371/journal.pone.0055785>.
- Rahman S. Mitochondrial disease in children. *J Intern Med* 2020;287:609–33. <https://doi.org/10.1111/joim.13054>.
- Sancak Y, Markhard AL, Kitami T, Kovács-Bogdán E, Kamer KJ, Udeshi ND, et al. EMRE is an essential component of the mitochondrial calcium uniporter complex. *Science* 2013;342:1379–82. <https://doi.org/10.1126/science.1242993>.

Schrödinger E. What is life?: the physical aspect of the living cell ; with Mind and matter ; & Autobiographical sketches. Cambridge: Cambridge University Press; 1992.

Solmaz SRN, Hunte C. Structure of Complex III with bound Cytochrome c in reduced state and definition of a minimal core interface for electron transfer. *J Biol Chem* 2008;283:17542–9. <https://doi.org/10.1074/jbc.M710126200>.

Spinelli JB, Haigis MC. The multifaceted contributions of mitochondria to cellular metabolism. *Nat Cell Biol* 2018;20:745–54. <https://doi.org/10.1038/s41556-018-0124-1>.

Sun F, Huo X, Zhai Y, Wang A, Xu J, Su D, et al. Crystal structure of mitochondrial respiratory membrane protein Complex II. *Cell* 2005;121:1043–57. <https://doi.org/10.1016/j.cell.2005.05.025>.

Vasington FD, Murphy JV. Ca<sup>++</sup> uptake by rat kidney mitochondria and its dependence on respiration and phosphorylation. *J Biol Chem* 1962;237:2670–7. [https://doi.org/10.1016/S0021-9258\(19\)73805-8](https://doi.org/10.1016/S0021-9258(19)73805-8).

Voet D, Voet JG. *Biochemistry*. 4th ed. Hoboken, NJ: John Wiley & Sons; 2011.



# CHAPTER 1

## Neurological disorders and mitochondria

“Anxiety is never irrational, Geralt thought to himself. Aside from psychological disturbances. It was one of the first things novice witchers were taught. It’s good to feel fear. If you feel fear it means there’s something to be feared, so be vigilant. Fear doesn’t have to be overcome. Just don’t yield to it. And you can learn from it.”

(Sapkowski, 2018, ch. 10, §9)<sup>1</sup>

---

<sup>1</sup> Sapkowski A. Season of storms. First U.S. edition. New York: Orbit; 2018.

## Summary

In this first chapter, we highlight the importance of studying mitochondrial physiology to better understand interactions between this organelle and cellular functions in the brain, ultimately unveiling mitochondrial relevance in pathophysiological mechanisms. To attain this, we reviewed the literature on the role of mitochondrial homeostasis as hallmark of neurological disorders.

As summarized by Cabral-Costa and Kowaltowski (2020)<sup>2</sup>

The brain is highly dependent on mitochondrial energy metabolism. As a result, mitochondrial dysfunction is a central aspect of many adult-onset neurological diseases, including stroke, ALS, Alzheimer's, Huntington's, and Parkinson's diseases. We review here how different mitochondrial functions, including oxidative phosphorylation, mitochondrial dynamics, oxidant generation, cell death regulation, Ca<sup>2+</sup> homeostasis, and proteostasis are involved in these disorders.

This chapter is a full reproduction of the original published review “Neurological disorders and mitochondria” published in *Molecular Aspects of Medicine* in February 2020 (Cabral-Costa; Kowaltowski, 2020)<sup>2</sup>, that can also be accessed at <https://doi.org/10.1016/j.mam.2019.10.003>, in accordance with the publisher’s copyright policy (Elsevier, 2022)<sup>3</sup>.

---

<sup>2</sup> Cabral-Costa JV, Kowaltowski AJ. Neurological disorders and mitochondria. *Mol Aspects Med* 2020;71:100826. <https://doi.org/10.1016/j.mam.2019.10.003>.

<sup>3</sup> Elsevier. Copyright Policy 2022. <https://www.elsevier.com/about/policies/copyright> (accessed August 23, 2022).



## Neurological disorders and mitochondria

J.V. Cabral-Costa, A.J. Kowaltowski\*

Departamento de Bioquímica, Instituto de Química, Universidade de São Paulo, Av. Prof. Lineu Prestes, 748, São Paulo, SP, 05508-000, Brazil

### ARTICLE INFO

#### Keywords:

Neurodegeneration  
Mitochondria  
Mitophagy  
Calcium  
Reactive oxygen species

### ABSTRACT

The brain is highly dependent on mitochondrial energy metabolism. As a result, mitochondrial dysfunction is a central aspect of many adult-onset neurological diseases, including stroke, ALS, Alzheimer's, Huntington's, and Parkinson's diseases. We review here how different mitochondrial functions, including oxidative phosphorylation, mitochondrial dynamics, oxidant generation, cell death regulation,  $\text{Ca}^{2+}$  homeostasis, and proteostasis are involved in these disorders.

### 1. Introduction

Mitochondria are mostly remembered within their fundamental role as energy metabolism hubs, or the organelles in which the citric acid cycle,  $\beta$  oxidation and oxidative phosphorylation happen, generating most of the ATP used by our cells. While these are undoubtedly central functions, knowledge regarding the participation of these organelles in cell physiology and pathology has expanded largely over the last decades. Today many changes in mitochondrial functions beyond loss of ATP synthesis (Fig. 1) are associated with neurological disorders, and have in fact become promising targets for therapeutic interventions in these diseases. Here, we will present an overview of mitochondrial involvement in some important adult neurological diseases, including changes in non-canonical mitochondrial functions such as the regulation of cell death, production of oxidants, calcium buffering and organelle dynamics (Fig. 2).

Mitochondria have long been associated with cell death due to energetic failure, but in the 1990s were also found to participate actively in programmed cell death (for reviews, see Lemasters et al., 1998; Wang and Youle, 2009; Parsons and Green, 2010; Tait and Green, 2013; Vakifahmetoglu-Norberg et al., 2017). This participation involves the release of pro-apoptotic proteins (including cytochrome c, Smac/DIABLO, Omi/HtrA2, EndoG and AIF) from mitochondria to the cytosol, where they initiate the cell death program. The release is often mediated by Bcl-2 family member proteins, although it may also occur secondarily to less selective forms of mitochondrial membrane permeabilization.

One form of inner membrane permeabilization that promotes loss of mitochondrial content and is associated with cell death is the mitochondrial permeability transition (MPT, reviewed in Lemasters et al., 1998; Brookes et al., 2004; Biasutto et al., 2016; Vercesi et al., 2018).

MPT is a loss of inner mitochondrial membrane impermeability due to the opening of a wide proteinaceous pore with debated molecular composition. Irrespective of the composition of this pore, its sustained opening results in loss of inner mitochondrial membrane potentials (due to permeabilization to protons) and, thus, impaired oxidative phosphorylation. Additionally, MPT leads to the release of mitochondrial pro-apoptotic proteins. Causes for opening of MPT pores are multiple, but include supra-physiological quantities of mitochondrial  $\text{Ca}^{2+}$ , production of mitochondrial free radicals/oxidants, and membrane protein thiol oxidation.

The production of free radicals and other mitochondrial oxidants is another non-canonical mitochondrial function of relevance in neurological disease. Because of the abundance of electron-transfer reactions that occur in mitochondria, this organelle can produce free radicals due to occasional one electron transfers to oxygen, generating superoxide radicals, which then can originate other oxidants such as  $\text{H}_2\text{O}_2$ , the hydroxyl radical, and peroxynitrite (reviewed in Dröge, 2002; Murphy, 2009; Figueira et al., 2013; Zorov et al., 2014; Wong et al., 2017; Kowaltowski, 2019). Although this production could be viewed as "accidental", mitochondrial oxidants have evolved for so long with life that they have also developed a rich role in cell signaling. Mitochondrial oxidants are thus not always undesirable, but participate actively in intracellular physiology.

The generation of mitochondrial oxidants has many tissue-specific characteristics (Tahara et al., 2009; Cardoso et al., 2012; Figueira et al., 2013). In the brain, mitochondrial oxidant production is significantly attributed to reverse electron transfer, or the transfer of electrons from coenzyme Q back to complex I, where they reduce oxygen to superoxide radicals (Tahara et al., 2009). Another quantitatively relevant source of oxidants in brain mitochondria is  $\alpha$ -ketoglutarate dehydrogenase

\* Corresponding author.

E-mail addresses: [joao.victor.costa@usp.br](mailto:joao.victor.costa@usp.br) (J.V. Cabral-Costa), [alicia@iq.usp.br](mailto:alicia@iq.usp.br) (A.J. Kowaltowski).

<https://doi.org/10.1016/j.mam.2019.10.003>

Received 21 August 2019; Received in revised form 13 October 2019; Accepted 13 October 2019

Available online 17 October 2019

0098-2997/© 2019 Elsevier Ltd. All rights reserved.

(Starkov et al., 2004; Tretter and Adam-Vizi, 2004) – indeed, mitochondrial flavoenzymes are quantitatively relevant, but often overlooked, oxidant sources. Brain mitochondrial oxidant generation is strongly regulated by the mitochondrial inner membrane potentials, with high membrane potentials increasing oxidant production, and lower membrane potentials preventing it (Starkov and Fiskum, 2003; Tahara et al., 2009). Finally, brain mitochondrial oxidant generation under conditions of high inner membrane potentials is stimulated by  $\text{Ca}^{2+}$  ions, an effect related to the release of pro-apoptotic cytochrome c, which impairs electron flow, facilitating superoxide radical formation (Starkov et al., 2002).

Indeed, another non-canonical mitochondrial function which is relevant in neurological disease is  $\text{Ca}^{2+}$  transport. Mitochondria express an intricate Mitochondrial Calcium Uniporter complex (MCUc), in the inner membrane (Baughman et al., 2011; De Stefani et al., 2011) that mediates  $\text{Ca}^{2+}$  transport from the cytosol into the matrix, using the driving force of the mitochondrial inner membrane potential (the negative matrix charge favors accumulation of these ions; reviewed in Gunter et al., 1994; Duchen, 2000; Williams et al., 2013; De Stefani et al., 2016; Belosludtsev et al., 2019). MCUc gating is mediated by sensor components (MICU-2 and MICU-3) that change the conformation of the complex when  $\text{Ca}^{2+}$  concentrations reach a threshold (De Stefani et al., 2016). The expression profile of MICUs varies according to cell type and cellular compartments, granting pre-synaptic mitochondria greater sensitivity to  $\text{Ca}^{2+}$  oscillations, a key feature to guarantee ATP supply under neuronal activation (Ashrafi et al., 2019).  $\text{Ca}^{2+}$  extrusion from mitochondria in the presence of physiological inner membrane potentials occurs in exchange for  $\text{Na}^+$  or  $\text{H}^+$ . Physiologically, mitochondrial  $\text{Ca}^{2+}$  efflux is mostly carried out by the mitochondrial  $\text{Na}^+/\text{Ca}^{2+}/\text{Li}^+$  exchanger (NCLX), in favor of both  $\text{Na}^+$  and  $\text{H}^+$  electrochemical gradients (De Marchi et al., 2014). The  $\text{Ca}^{2+}$  concentration threshold necessary to activate mitochondrial  $\text{Ca}^{2+}$  uptake by the MCUc is much higher than that of the sarco/endoplasmic reticulum  $\text{Ca}^{2+}$ -ATPase (SERCA), which mediates endoplasmic reticulum (ER)  $\text{Ca}^{2+}$  uptake. However, mitochondrial  $\text{Ca}^{2+}$  uptake capacity is much higher, so these organelles are important buffers under conditions of cellular  $\text{Ca}^{2+}$  overload. Indeed, there is ample recent evidence that  $\text{Ca}^{2+}$  uptake by this organelle has important roles in physiological and pathological changes in cellular  $\text{Ca}^{2+}$  homeostasis (Favaro et al., 2019;

Grossmann et al., 2019; Kowaltowski et al., 2019).

Mitochondrial  $\text{Ca}^{2+}$  signaling, although important on its own, is not completely unrelated to ER  $\text{Ca}^{2+}$  handling. ER-mitochondria communication is one of the most extensively characterized inter-organelle interactions, and is key to a plethora of functions, from energy metabolism to cell survival (reviewed by López-Crisosto et al., 2015). ER-mitochondria tethers are mostly maintained through homo or heterotypic interactions between Mitofusins (Mfn)-1 and -2, which allow close coupling between inositol 1,4,5-trisphosphate receptor (IP<sub>3</sub>R), in the ER, with the MCUc in mitochondria. This proximity allows the mitochondrial  $\text{Ca}^{2+}$  uptake threshold to be reached more easily, independent of average cytosolic  $\text{Ca}^{2+}$  concentrations (López-Crisosto et al., 2015). Defects in this communication have been described in the context of neurodegenerative diseases and were linked to loss of  $\text{Ca}^{2+}$  homeostasis and increase in cell death susceptibility (Grossmann et al., 2019).

Interestingly, recent data suggests that mitochondrial  $\text{Ca}^{2+}$  uptake may be physiologically regulated by mitochondrial morphology and dynamics. Artificially hyperfused mitochondria possess increased  $\text{Ca}^{2+}$  uptake capacity (Favaro et al., 2019; Kowaltowski et al., 2019), while inducing mitochondrial fission culminates in decreased  $\text{Ca}^{2+}$  uptake speed and capacity (Kowaltowski et al., 2019). Indeed, dynamic changes in mitochondrial morphology and location over time have been increasingly recognized as important regulators of metabolism and determinants in cellular resistance to stresses (reviewed in Okamoto and Shaw, 2005; Liesa et al., 2009; Liesa and Shirihai, 2013; Mishra and Chan, 2016; Pernas and Scorrano, 2016).

Mitochondria have a complex array of signals and morphology-determining proteins that make them change size and shape continuously within the cell, undergoing both fission and fusion. These changes are often correlated with alterations in oxidative phosphorylation, as well as other mitochondrial functional parameters. Additionally, dynamic mitochondrial fission and fusion are essential for segregation and elimination of these organelles by autophagy (mitophagy, Twig et al., 2008), and therefore maintain mitochondrial quality-control. Mitochondrial morphology and dynamics are also of importance in trafficking the organelles, in particular within the long distances present in neurons (reviewed by Flannery and Trushina, 2019). The central importance of mitochondrial dynamics in neurological disease is illustrated by the fact that proteins that regulate this process were first described within the context of neurological disorders autosomal dominant optic atrophy and axonal Charcot-Marie-Tooth disease type 2A (reviewed in Burté et al., 2015). More recent studies are increasingly identifying changes in mitochondrial dynamics and morphology involved in adult neurological disorders, as described below.

## 2. Ischemic stroke

Stroke is a leading cause of death and disability worldwide. It is the result of lack of oxygen and nutrient delivery to the brain, and thus involves changes in energy metabolism, and specifically mitochondria, in its pathogenesis (reviewed in Lin and Beal, 2006; Nizuma et al., 2010; Russo et al., 2018; Yang et al., 2018; Liu et al., 2018).

Ischemia/reperfusion in the brain leads to complex I inhibition, and compromised function, due to oxidation of thiol residues within the complex that are central for normal enzymatic activity (Kahl et al., 2018). Furthermore, lack of oxygen during ischemia leads to accumulation of mitochondrial succinate, secondarily to the reversal of succinate dehydrogenase, which forms succinate from fumarate under these conditions. As we saw above, brain mitochondria have substantial production of superoxide radicals due to reverse electron transfer to complex I (Tahara et al., 2009). Consequently, succinate accumulation results in high generation of oxidants in brain mitochondria under ischemic conditions (Chouchani et al., 2014). This is an important cause of tissue damage, as indicated by the fact that either preventing succinate accumulation or use of mitochondria-targeted antioxidants significantly protects against stroke-induced damage (Chouchani et al.,

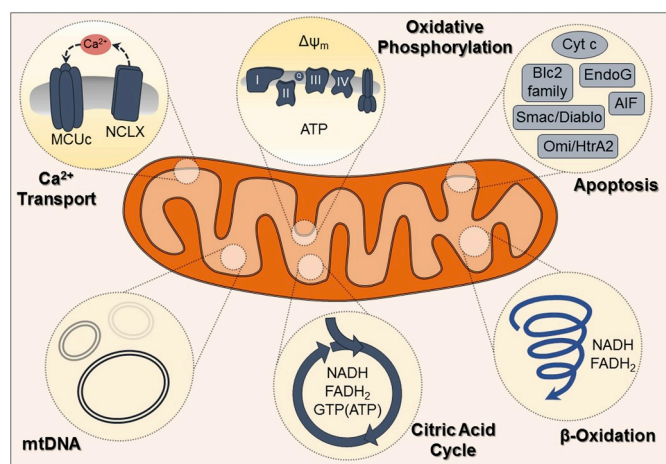


**Fig. 1. Many facets of the mitochondrion.** Mitochondria are very complex organelles that partially express local proteins from circular DNA (mtDNA) located within the matrix, where catabolic reactions of the tricarboxylic acid (TCA) cycle and  $\beta$ -oxidation also take place. Within the inner membrane, proteins responsible for mitochondrial  $\text{Ca}^{2+}$  handling (e.g., influx and efflux through MCUc and NCLX, respectively) as well as membrane potential ( $\Delta\Psi$ )-dependent oxidative phosphorylation are embedded. Mitochondria also act as an important hub that participates in signaling pathways of cell survival and apoptosis.

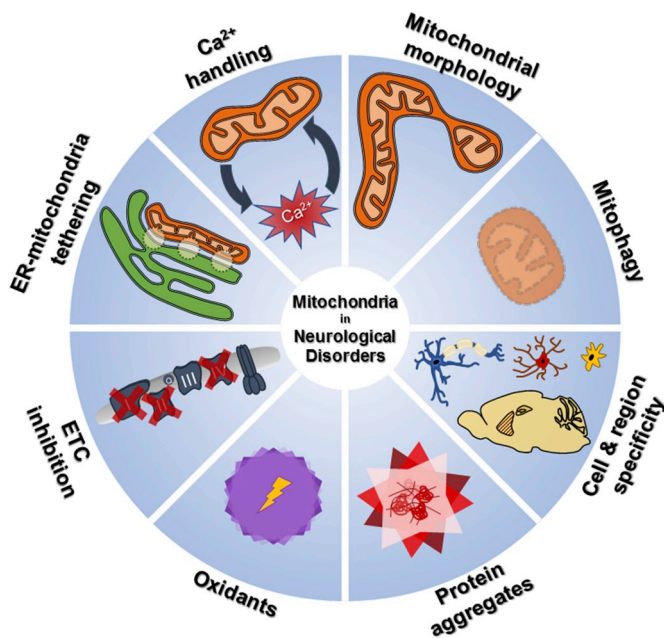


**Fig. 2.** Major aspects of the interface between mitochondria and pathophysiology in neurological disorders. All neurological disorders discussed in this review – ischemic stroke, Alzheimer's, Parkinson's and Huntington's diseases, and amyotrophic lateral sclerosis – have mitochondrial defects described within their mechanisms. Whether these effects (e.g., increase in oxidants production, electron transport chain (ETC) inhibition, and impairment in ER-mitochondria tethering, mitochondrial  $\text{Ca}^{2+}$  handling, morphology and mitophagy) are direct consequences of well-described pathological markers (e.g., protein aggregates) or participate directly into the genesis of the disease often remains to be elucidated. Either way, a better understanding of particularities of cell-type and brain region specificities regarding metabolic and protein expression profiles will be key to reveal new targets for novel therapeutic approaches.

2014; Silachev et al., 2018; Zhang et al., 2019). Indeed, use of mitochondria-targeted antioxidants is an interesting strategy for acute disease management related to mitochondrial oxidative imbalance overall, with many successes in animal models and some clinical trials underway (reviewed in Smith et al., 2011).

Interestingly, levels of mitochondrial DNA (which can be used as a marker for mitochondrial mass) do not decrease substantially with stroke, but increase significantly in the hours after the ischemic insult (Yin et al., 2008). This could indicate that mitochondrial biogenesis is part of the post-stroke repair mechanisms in the brain (Yang et al., 2018). Indeed, because mitochondria are a target of extensive damage generated by locally-produced oxidants during stroke, it seems logical to assume that they may be a specific target for effective endogenous repair strategies. In this sense, intriguing recent studies suggest mitochondrial pools in damaged cells may be repopulated by mitochondrial transfer from other cells, such as astrocytes, mesenchymal stem cells or even extracellular vesicles (Hayakawa et al., 2016; Liu et al., 2018, 2019; Russell et al., 2019). How morphology, dynamics and organelle traffic (Bastian et al., 2018) in both donor and recipient cells affect mitochondrial transfer, as well as how this affects the neuronal mitochondrial population long-term, remains to be fully understood.

Mitochondrial morphological changes affect stroke outcome, as inhibition of fission is neuroprotective (Zhang et al., 2013; Flipppo et al., 2018; Bastian et al., 2018). This may be because of the higher  $\text{Ca}^{2+}$  buffering capacity and resistance against MPT of more fused mitochondria (Kowaltowski et al., 2019). Indeed, caloric restriction, which protects against stroke, also leads to increased mitochondrial respiratory capacity and  $\text{Ca}^{2+}$  uptake, by inhibiting MPT (Cerqueira et al., 2012; Amigo et al., 2017).

Increased cellular and mitochondrial  $\text{Ca}^{2+}$  uptake occur in stroke for two chronologically separate reasons: primary loss of cellular  $\text{Ca}^{2+}$  homeostasis due to lack of ATP production, and secondary excitotoxic cellular  $\text{Ca}^{2+}$  uptake (reviewed in Lai et al., 2014; Khoshnam et al., 2017). Excitotoxicity occurs due to extensive glutamate release in the brain, triggered by energetic deficiency. Excessive glutamate overactivates neurons, leading to pathological quantities of  $\text{Ca}^{2+}$  in their cytosol. Under these conditions, mitochondria act as important  $\text{Ca}^{2+}$  buffering systems, but excess of the ion in these organelles comes at the price of loss of oxidative phosphorylation, excessive oxidant production and MPT. Indeed, preventing mitochondrial  $\text{Ca}^{2+}$  uptake, decreasing mitochondrial susceptibility to MPT or use of mitochondria-targeted antioxidants in excitotoxicity is neuroprotective (Stout et al., 1998; Nicholls, 2004; Arundine and Tymianski, 2003; Amigo et al., 2017; Yang et al., 2018; Zhang et al., 2019). Overall, mitochondrial functional preservation is an attractive manner to prevent many different aspects of stroke-induced neuronal loss, due to the multifactorial role of these organelles in stroke.

### 3. Alzheimer's disease

Alzheimer's is an unfortunately common neurological disorder in aging, which involves progressive cognitive impairment and behavioral changes. It is characterized by the formation of amyloid plaques, composed of agglomerated amyloid beta peptides, which are fragments of amyloid precursor proteins, as well as neurofibrillary tangles, composed of abnormally aggregated tau protein, a component of the neuronal cytoskeleton. Mitochondria are involved in many aspects of the pathogenesis of the disease (reviewed in Reddy and Beal, 2005; Yin et al., 2016; Panchal and Tiwari, 2019), including inhibited electron transport, especially at the level of cytochrome c oxidase, in both the brain and other cells (Parker et al., 1994; Hirai et al., 2001; Bosetti et al., 2002; Aliev et al., 2003). This may be due to mitochondrial DNA alterations and decreased repair activity, inhibiting transcription and replication (Cavalier et al., 2001; Lin et al., 2002; Coskun et al., 2004; Soltys et al., 2019). Oxidative imbalance, which is widely reported in Alzheimer's disease brains (Markesbery and Carney, 1999; Smith et al., 2000; Reddy and Beal, 2005), may be the result of this electron transport inhibition and associated increase in mitochondrial oxidant generation.

Reasons for impaired mitochondrial function are still under investigation. Tau accumulation in axons has been shown to affect mitochondrial trafficking (Mandelkow et al., 2003), an essential process for bioenergetic maintenance in neurons. Disease-associated tau has also been shown to impair mitophagy, and thus hamper quality-control systems (Cummins et al., 2019). Amyloid beta and accumulated amyloid beta precursor protein seem to cause direct mitochondrial damage (Askanas et al., 1996; Casley et al., 2002; Kim et al., 2002; Anandatheerthavarada et al., 2003; Crouch et al., 2005). Enhancing mitochondrial proteostasis in animal models can reduce amyloid beta toxicity, suggesting this is a key step in the pathogenesis of the disease (Sorrentino et al., 2017). Additionally, mitochondrial  $\text{Ca}^{2+}$  efflux transporter NCLX expression was shown to be reduced in brains of patients, inversely correlating with disease progression (Jadiya et al., 2019). Interestingly, NCLX was also reduced in a mouse model, and disease phenotype was hampered by rescuing its expression (Jadiya et al., 2019), reinforcing the importance of mitochondrial  $\text{Ca}^{2+}$  efflux as a potential pharmacological target in Alzheimer's disease.

Taken together, evidence linking mitochondrial dysfunction and mitochondrial abnormalities in late-onset sporadic Alzheimer's disease is vast. However, a clear indication that mitochondrial dysfunction is a trigger for neuronal loss rather than a more general response to stress is still lacking.

### 4. Amyotrophic lateral sclerosis (ALS)

Amyotrophic Lateral Sclerosis (ALS) is a motor neuron disease characterized by progressive neurodegeneration of brain and spinal



cord cells. Approximately 90% of cases are sporadic, while the remaining ~10% are familial cases (Brown and Al-Chalabi, 2017). Mutations in a plethora of genes, including C9orf72, SOD1, Fused in Sarcoma (FUS), TDP43 and Coiled-helix coiled-helix domain containing protein 10 (CHCHD10), have been correlated with the occurrence of both familial and sporadic cases (Carrì et al., 2017). Though they may play multiple roles in distinct physiological cellular processes, the majority of them can be clustered in three major categories: cytoskeleton dynamics, RNA trafficking and homeostasis, and protein homeostasis. Their disruption may cause ER stress, Ca<sup>2+</sup> signaling disruption, protein aggregation, disturbed axonal transport, mitochondrial dysfunction, and apoptosis (Prell et al., 2013; Brown and Al-Chalabi, 2017; Carrì et al., 2017). Post-mortem samples of spinal cords from sporadic ALS patients showed an impairment in complex IV activity and an aberrant profile of mitochondrial distribution throughout motor neurons (Delic et al., 2018), which is compatible with widespread mitochondrial integrity loss in the disease. Indeed, both familial and sporadic ALS patients show widespread mitochondrial alterations in fibroblasts (Walczak et al., 2019).

Recent studies have found mechanistic connections between mitochondrial dysfunction and ALS. Neurons differentiated from mouse embryonic stem cells with mutated (R495X) FUS show disruption in translation efficiency of genes associated with mitochondrial function, and display processes with smaller mitochondria (Nakaya and Maragkakis, 2018). R495X binds to mature mRNAs, in contrast to the wild-type protein, that acts through binding to precursor mRNAs (Nakaya and Maragkakis, 2018). CHCHD10 is important for mitochondrial cristae organization, acting at cristae junctions at the mitochondrial contact site and cristae organizing systems (Genin et al., 2016). It might also be involved in the control of mitochondrial iron metabolism (Burstein et al., 2018). CHCHD10 mutations are associated with an impairment in the mitochondrial genome (Genin et al., 2016). Fibroblasts obtained from patients carrying an ALS-associated variant of the CHCHD10 gene have hyperfused mitochondria and a shift toward dependence on anaerobic glycolysis, effects linked to a disruption in Complex I assembly (Straub et al., 2018). When forced to produce energy through oxidative metabolism by incubation in galactose, cells present an increase in levels of CHCHD2, a protein associated with the regulation of electron transport chain complexes and oxidative phosphorylation (Aras et al., 2015, 2013; Baughman et al., 2009) and that has been shown to interact with CHCHD10 (Burstein et al., 2018; Straub et al., 2018). Therefore, it is possible that the complexation of CHCHD10-CHCHD2 is central in the maintenance of metabolic homeostasis during changes in ATP demands (Straub et al., 2018). However, a study has shown that homozygote CHCHD10 knockout mice do not show any remarkable phenotype, while cells expressing mutant (S59L, R15L) CHCHD10 present dysfunctional mitochondrial energy metabolism (Burstein et al., 2018), indicating that the effect observed in ALS patients might be associated with a gain-of-function mutation rather than to a simple loss-of-function (Burstein et al., 2018).

Overall, ALS causes are multifactorial, a clear mechanism in the disease as a whole still remains to be understood, but many of the uncovered mechanisms involve changes in mitochondrial function (reviewed in MUYDERMAN and CHEN, 2014; SMITH et al., 2018), which may both be causative and secondary to the trigger pathways in the disease.

## 5. Huntington's disease

Huntington's disease is caused by excess CAG repeat expansion within the gene encoding the huntingtin protein. It results in neuronal loss and consequent motor and cognitive disturbances in young to middle aged adults. This neuronal damage is linked to many mitochondrial abnormalities (reviewed in Beal, 2005; Lin and Beal, 2006; Chen and Chan, 2009; Panchal and Tiwari, 2019).

The huntingtin protein is essential for the maintenance of mitochondrial bioenergetics (Ismailoglu et al., 2014). Interestingly,

Huntington's disease has not only been linked to reduced mitochondrial electron transport activity (Panchal and Tiwari, 2019), but can also be modelled in cells and animals by inhibiting Complex II with 3-nitropropionic acid (Borlongan et al., 1995; Brouillet et al., 2005; Hariharan et al., 2014). This demonstrates that mitochondrial abnormalities not only accompany Huntington's disease, but are a cause of striatal lesions central towards its pathology. Impaired mitochondrial Ca<sup>2+</sup> uptake capacity has also been observed in Huntington's (Panov et al., 2002; Milakovic et al., 2006; Gellerich et al., 2008; Lim et al., 2008; Damiano et al., 2010; Naia et al., 2017), as well as altered mitochondrial iron homeostasis (Agrawal et al., 2018). Furthermore, there is ample evidence of mitochondrial oxidative imbalance in this disease (reviewed by Browne and Beal, 2006). Changes in mitochondrial morphology and turnover have also been reported (Joshi et al., 2019).

Many questions still remain, such as exact mechanisms in which the modified huntingtin promotes neurodegeneration, and why this disease and the striatum are specifically sensitive to Complex II inhibition. This last effect may be due to specific changes in striatum astrocyte metabolism, which oxidize high quantities of lipids and generate more oxidants (Polyzos et al., 2019). Additionally, both striatal neurons and astrocytes possess smaller Ca<sup>2+</sup> buffering capacity and increased MPT sensitivity in comparison to their cortical counterparts (Oliveira and Gonçalves, 2008). Overall, the causal effects of mitochondrial respiratory inhibition in Huntington's strongly suggest this is an attractive target for therapeutic advances.

## 6. Parkinson's disease

Parkinson's disease involves progressive loss of dopaminergic neurons in the *substantia nigra*, resulting in motor symptoms (including resting tremor and rigidity) and non-motor symptoms (including depression and dementia). A plethora of different experimental approaches indicate that mitochondrial abnormalities are triggers of neuronal loss generating the symptoms of this disease (reviewed in Sherer et al., 2002; Beal, 2003; Schapira, 2008; Jin et al., 2014).

A landmark finding relating mitochondria to Parkinson's disease was the description of four young patients who quickly developed symptoms of the disease after using illicit intravenous drug preparations containing 1-methyl-4-phenyl-1,2,5,6-tetrahydropyridine (MPTP – Langston et al., 1983). MPTP very effectively causes parkinsonism in animal models (Sedelis et al., 2001; Jackson-Lewis and Przedborski, 2007), and MPTP and its metabolites are potent inhibitors of mitochondrial complex I (McNaught et al., 1995; Richardson et al., 2007). Interestingly, spontaneous Parkinson's disease patients were also found to have impairments in Complex I activity (Parker et al., 1989; Krige et al., 1992). Finally, Parkinson's disease symptoms can be mirrored by treating laboratory animals with a classical Complex I inhibitor, rotenone (Panov et al., 2005; Tanner et al., 2011). Together, these different lines of evidence strongly indicate that Complex I deficiency is a cause of neuronal loss in the *substantia nigra* leading to parkinsonism.

Inhibited Complex I activity in neurons leads to depolarization, altered mitochondrial Ca<sup>2+</sup> homeostasis and oxidative imbalance (Sheehan et al., 1997; Alam et al., 1997; Chinopoulos and Adam-Vizi, 2001; Sousa et al., 2003; Lu et al., 2016; Umeno et al., 2017; Ludtmann et al., 2018). Indeed, mitochondria-targeted antioxidants have been explored as neuroprotective agents in this disease, with mixed results (Ghosh et al., 2010; Snow et al., 2011; Jin et al., 2014).

Another seminal link between mitochondria and the etiology of Parkinson's disease is the role of Parkin, an E3 ubiquitin ligase which ubiquitinates outer mitochondrial membrane proteins, promoting damaged mitochondrial clearance (reviewed in Mizuno et al., 2001; Kim et al., 2007; Chen and Chan, 2009; Youle and Narendra, 2011; Seirafi et al., 2015; Pinto et al., 2018). Parkin receives its name from the finding that it has different mutations in patients with early onset Parkinson's (Hedrich et al., 2004; Kahle and Haass, 2004; Dawson and Dawson, 2010). Overall, this suggests that defective removal of

damaged mitochondria and mitochondrial proteostasis are involved in the pathogenesis of the disease. Indeed, mutations in PTEN-induced kinase 1 (PINK1), which is also part of the mitophagic machinery, cause autosomal recessive Parkinson's disease, as well as mitochondrial dysfunction (Pickrell and Youle, 2015; Zhi et al., 2019). Interestingly, PINK1 knockdown inhibits NCLX activity (Kostic et al., 2015). Impairment in leucine-rich repeat kinase 2 (LRRK2), commonly associated with Parkinson's, also affects NCLX function (Ludtmann et al., 2019), highlighting the potential role of mitochondrial  $\text{Ca}^{2+}$  efflux in pathology of the disease.

Altogether, there is strong evidence of a central mitochondrial dysfunction involving Complex I inhibition and defective turnover as causative in Parkinson's disease. However, these mechanistic findings have not yet been translated into effective therapeutic approaches.

## 7. Conclusions

Given the high energetic demands of the brain, which accounts for 20% of resting state oxygen consumption despite representing only 2% of a human's body weight (Mink et al., 1981), it is not surprising that mitochondria are involved in the pathogenesis of many neurological diseases.

In ischemic stroke, mitochondria are intuitively downstream of the cause of the disorder – both decreases in oxygen and substrate perfusion, added to metabolite accumulation, are associated with the initial hits that culminate in mitochondrial impairment and cell death. In the context of neurodegenerative diseases, however, the distinction between cause and consequence when it comes to the role of mitochondria in pathophysiology is often unclear (Fig. 2). Although mitochondrial interventions have been shown to have the potential to rescue disease phenotype, the respective effects may still be downstream of the causative mechanisms. Either way, both when mitochondria are triggers for neurodegeneration and when they are collaterally involved in damage progression, mitochondrial protective interventions should be promising new therapeutic strategies. Further research should yet clarify what are the determinants that define cell- and region-specificity of disease markers and cell death, key parameters in mitochondrial physiology for the development of novel therapeutic approaches.

## Funding

J.V.C.-C. is supported by *Fundação de Amparo à Pesquisa no Estado de São Paulo* (FAPESP) grant #2017/14713-0 and by the *Coordenação de Aperfeiçoamento de Pessoal de Nível Superior* (CAPES) – Finance Code 001.

A.J.K. is supported by the *Conselho Nacional de Desenvolvimento Científico e Tecnológico* (CNPq) and FAPESP grant #2013/07937-8, *Centro de Pesquisa, Inovação e Difusão de Processos Redox em Biomedicina*.

## Abbreviations

AIF	apoptosis inducing factor
ALS	amyotrophic lateral sclerosis
CHCHD10	coiled-helix coiled-helix domain containing protein 10
CHCHD10	coiled-helix coiled-helix domain containing protein 2
ER	endoplasmic reticulum
FUS:	fused in sarcoma
MCUC	mitochondrial calcium uniporter complex
MICU	mitochondrial calcium uptake
Mfn	mitofusin
MPT	mitochondrial permeability transition
MPTP	1-methyl-4-phenyl-1,2,5,6-tetrahydropyridine
NCLX	mitochondrial $\text{Na}^+/\text{Ca}^{2+}/\text{Li}^+$ exchanger
PINK1	PTEN-induced kinase 1
SERCA	sarco/endoplasmic reticulum $\text{Ca}^{2+}$ -ATPase

## Appendix A. Supplementary data

Supplementary data to this article can be found online at <https://doi.org/10.1016/j.mam.2019.10.003>.

## References

- Agrawal, S., Fox, J., Thyagarajan, B., Fox, J.H., 2018. Brain mitochondrial iron accumulates in Huntington's disease, mediates mitochondrial dysfunction, and can be removed pharmacologically. *Free Radic. Biol. Med.* <https://doi.org/10.1016/j.freeradbiomed.2018.04.002>.
- Alam, Z.I., Jenner, A., Daniel, S.E., Lees, A.J., Cairns, N., Marsden, C.D., Jenner, P., Halliwell, B., 1997. Oxidative DNA damage in the parkinsonian brain: an apparent selective increase in 8-hydroxyguanine levels in substantia nigra. *J. Neurochem.* 69, 1196–1203. <https://doi.org/10.1046/j.1471-4159.1997.69031196.x>.
- Aliiev, G., Seyidova, D., Lamb, B.T., Obrenovich, M.E., Siedlak, S.L., Vinters, H.V., Friedland, R.P., LaManna, J.C., Smith, M.A., Perry, G., 2003. Mitochondria and vascular lesions as a central target for the development of Alzheimer's disease and Alzheimer disease-like pathology in transgenic mice. *Neurol. Res.* 25, 665–674. <https://doi.org/10.1179/016164103101201977>.
- Amigo, I., Menezes-Filho, S.L., Luévano-Martínez, L.A., Chausse, B., Kowaltowski, A.J., 2017. Caloric restriction increases brain mitochondrial calcium retention capacity and protects against excitotoxicity. *Aging Cell* 16, 73–81. <https://doi.org/10.1111/acel.12527>.
- Anandatheerthavarada, H.K., Biswas, G., Robin, M.A., Avadhani, N.G., 2003. Mitochondrial targeting and a novel transmembrane arrest of Alzheimer's amyloid precursor protein impairs mitochondrial function in neuronal cells. *J. Cell Biol.* 161, 41–54. <https://doi.org/10.1083/jcb.200207030>.
- Aras, S., Bai, M., Lee, I., Springett, R., Hüttemann, M., Grossman, L.I., 2015. MNRR1 (formerly CHCHD2) is a bi-organellar regulator of mitochondrial metabolism. *Mitochondrion* 20, 43–51. <https://doi.org/10.1016/j.mito.2014.10.003>.
- Aras, S., Pak, O., Sommer, N., Finley, R., Hü Ttemann, M., Weissmann, N., Grossman, L.I., 2013. Oxygen-dependent expression of cytochrome c oxidase subunit 4-2 gene expression is mediated by transcription factors RBPJ, CXXC5 and CHCHD2. *Nucleic Acids Res.* 41, 2255–2266. <https://doi.org/10.1093/nar/gks1454>.
- Arundine, M., Tymianski, M., 2003. Molecular mechanisms of calcium-dependent neurodegeneration in excitotoxicity. *Cell Calcium* 34, 325–337. [https://doi.org/10.1016/s0143-4160\(03\)00141-6](https://doi.org/10.1016/s0143-4160(03)00141-6).
- Ashrafi, G., de Juan-Sanz, J., Farrell, R.J., Ryan, T.A., 2019. Molecular Tuning of the Axonal Mitochondrial  $\text{Ca}^{2+}$  Uniporter Ensures Metabolic Flexibility of Neurotransmission. *bioRxiv*.
- Askanas, V., McFerrin, J., Baqué, S., Alvarez, R.B., Sarkozi, E., Engel, W.K., 1996. Transfer of beta-amyloid precursor protein gene using adenovirus vector causes mitochondrial abnormalities in cultured normal human muscle. *Proc. Natl. Acad. Sci. U. S. A.* 93, 1314–1319. <https://doi.org/10.1073/pnas.93.3.1314>.
- Bastian, C., Zaleski, J., Stahon, K., Parr, B., McCray, A., Day, J., Brunet, S., Baltan, S., 2018. NOS3 inhibition confers post-ischemic protection to young and aging white matter integrity by conserving mitochondrial dynamics and Miro-2 levels. *J. Neurosci.* 38, 6247–6266. <https://doi.org/10.1523/JNEUROSCI.3017-17.2018>.
- Baughman, J.M., Nilsson, R., Gohil, V.M., Arlow, D.H., Gauhar, Z., Mootha, V.K., 2009. A computational screen for regulators of oxidative phosphorylation implicates SLRP in mitochondrial RNA homeostasis. *PLoS Genet.* 5. <https://doi.org/10.1371/journal.pgen.1000590>.
- Baughman, J.M., Perocchi, F., Girgis, H.S., Plovanich, M., Belcher-Timme, C.A., Sancak, Y., Bao, X.R., Strittmatter, L., Goldberger, O., Bogorad, R.L., Kotliansky, V., Mootha, V.K., 2011. Integrative genomics identifies MCU as an essential component of the mitochondrial calcium uniporter. *Nature* 476 (7360), 341–345. <https://doi.org/10.1038/nature10234>.
- Beal, M.F., 2003. Mitochondria, oxidative damage, and inflammation in Parkinson's disease. *Ann. N. Y. Acad. Sci.* 991, 120–131. <https://doi.org/10.1111/j.1749-6632.2003.tb07470.x>.
- Beal, M.F., 2005. Mitochondria take center stage in aging and neurodegeneration. *Ann. Neurol.* 58, 495–505. <https://doi.org/10.1002/ana.20624>.
- Belosludtsev, K.N., Dubinin, M.V., Belosludtseva, N.V., Mironova, G.D., 2019. Mitochondrial  $\text{Ca}^{2+}$  transport: mechanisms, molecular structures, and role in cells. *Biochemistry (Mosc.)* 84, 593–607. <https://doi.org/10.1134/S0006297919060026>.
- Biasutto, L., Azzolini, M., Szabò, I., Zoratti, M., 2016. The mitochondrial permeability transition pore in AD 2016: an update. *Biochim. Biophys. Acta* 1863, 2515–2530. <https://doi.org/10.1016/j.bbamcr.2016.02.012>.
- Borlongan, C.V., Koutouzis, T.K., Randall, T.S., Freeman, T.B., Cahill, D.W., Sanberg, P.R., 1995. Systemic 3-nitropropionic acid: behavioral deficits and striatal damage in adult rats. *Brain Res. Bull.* 36, 549–556. [https://doi.org/10.1016/0361-9230\(94\)00242-8](https://doi.org/10.1016/0361-9230(94)00242-8).
- Bosetti, F., Brizzi, F., Barogi, S., Mancuso, M., Siciliano, G., Tendi, E.A., Murri, L., Rappoport, S.I., Solaini, G., 2002. Cytochrome c oxidase and mitochondrial F1F0-ATPase (ATP synthase) activities in platelets and brain from patients with Alzheimer's disease. *Neurobiol. Aging* 23, 371–376. [https://doi.org/10.1016/s0197-4580\(01\)00314-1](https://doi.org/10.1016/s0197-4580(01)00314-1).
- Brookes, P.S., Yoon, Y., Robotham, J.L., Anders, M.W., Sheu, S.S., 2004. Calcium, ATP, and ROS: a mitochondrial love-hate triangle. *Am. J. Physiol. Cell Physiol.* 287, C817–C833. <https://doi.org/10.1152/ajpcell.00139.2004>.
- Brouillet, E., Jacquard, C., Bizat, N., Blum, D., 2005. 3-Nitropropionic acid: a mitochondrial toxin to uncover physiopathological mechanisms underlying striatal degeneration in Huntington's disease. *J. Neurochem.* 95, 1521–1540. <https://doi.org/10.1111/j.1471-4159.2005.03515.x>.

- Brown, R., Al-Chalabi, A., 2017. Amyotrophic lateral sclerosis. *N. Engl. J. Med.* 377, 162–172. <https://doi.org/10.1056/NEJMra1603471>.
- Browne, S.E., Beal, M.F., 2006. Oxidative damage in Huntington's disease pathogenesis. *Antioxidants Redox Signal.* 8, 2061–2073. <https://doi.org/10.1089/ars.2006.8.2061>.
- Burstein, S.R., Valsecchi, F., Kawamata, H., Bourens, M., Zeng, R., Zuberi, A., Milner, T.A., Cloonan, S.M., Lutz, C., Barrientos, A., Manfredi, G., 2018. In vitro and in vivo studies of the ALS-FTLD protein CHCHD10 reveal novel mitochondrial topology and protein interactions. *Hum. Mol. Genet.* 27, 160–177. <https://doi.org/10.1093/hmg/ddx397>.
- Burté, F., Carelli, V., Chinnery, P.F., Yu-Wai-Man, P., 2015. Disturbed mitochondrial dynamics and neurodegenerative disorders. *Nat. Rev. Neurol.* 11, 11–24. <https://doi.org/10.1038/nrneuro.2014.228>.
- Cardoso, A.R., Chausse, B., da Cunha, F.M., Luévano-Martínez, L.A., Marazzi, T.B., Pessoa, P.S., Queliconi, B.B., Kowaltowski, A.J., 2012. Mitochondrial compartmentalization of redox processes. *Free Radic. Biol. Med.* 52, 2201–2208. <https://doi.org/10.1016/j.freeradbiomed.2012.03.008>.
- Carrí, M.T., D'Ambrosi, N., Cozzolino, M., 2017. Pathways to mitochondrial dysfunction in ALS pathogenesis. *Biochem. Biophys. Res. Commun.* 483, 1187–1193. <https://doi.org/10.1016/j.bbrc.2016.07.055>.
- Casley, C.S., Canevari, L., Land, J.M., Clark, J.B., Sharpe, M.A., 2002. Beta-amyloid inhibits integrated mitochondrial respiration and key enzyme activities. *J. Neurochem.* 80, 91–100. <https://doi.org/10.1046/j.0022-3042.2001.00681.x>.
- Cavelier, L., Erikson, L., Tammi, M., Jalonen, P., Lindholm, E., Jazin, E., Smith, P., Luthman, H., Gyllenstein, U., 2001. MtDNA mutations in maternally inherited diabetes: presence of the 3397 ND1 mutation previously associated with Alzheimer's and Parkinson's disease. *Hereditas* 135, 65–70. <https://doi.org/10.1111/j.1601-5223.2001.00065.x>.
- Cerqueira, F.M., Cunha, F.M., Laurindo, F.R., Kowaltowski, A.J., 2012. Calorie restriction increases cerebral mitochondrial respiratory capacity in a NO-mediated mechanism: impact on neuronal survival. *Free Radic. Biol. Med.* 52, 1236–1241. <https://doi.org/10.1016/j.freeradbiomed.2012.01.011>.
- Chen, H., Chan, D.C., 2009. Mitochondrial dynamics—fusion, fission, movement, and mitophagy—in neurodegenerative diseases. *Hum. Mol. Genet.* 18, R169–R176. <https://doi.org/10.1093/hmg/ddp326>.
- Chinopoulos, C., Adam-Vizi, V., 2001. Mitochondria deficient in complex I activity are depolarized by hydrogen peroxide in nerve terminals: relevance to Parkinson's disease. *J. Neurochem.* 76, 302–306. <https://doi.org/10.1046/j.1471-4159.2001.00060.x>.
- Chouchani, E.T., Pell, V.R., Gaudé, E., Aksentijević, D., Sundier, S.Y., Robb, E.L., Logan, A., Nadochiy, S.M., Ord, E.N.J., Smith, A.C., Eyassu, F., Shirley, R., Hu, C.H., Dare, A.J., James, A.M., Rogatti, S., Hartley, R.C., Eaton, S., Costa, A.S.H., Brookes, P.S., Davidson, S.M., Duchon, M.R., Saeb-Parsy, K., Shattock, M.J., Robinson, A.J., Work, L.M., Frezza, C., Krieg, T., Murphy, M.P., 2014. Ischaemic accumulation of succinate controls reperfusion injury through mitochondrial ROS. *Nature* 515, 431–435. <https://doi.org/10.1038/nature13909>.
- Coskun, P.E., Beal, M.F., Wallace, D.C., 2004. Alzheimer's brains harbor somatic mtDNA control-region mutations that suppress mitochondrial transcription and replication. *Proc. Natl. Acad. Sci. U. S. A.* 101, 10726–10731. <https://doi.org/10.1073/pnas.0403649101>.
- Crouch, P.J., Blake, R., Duce, J.A., Ciccotosto, G.D., Li, Q.X., Barnham, K.J., Curtain, C.C., Cherny, R.A., Cappai, R., Dyrks, T., Masters, C.L., Trounce, I.A., 2005. Copper-dependent inhibition of human cytochrome c oxidase by a dimeric conformer of amyloid-beta1-42. *J. Neurosci.* 25, 672–679. <https://doi.org/10.1523/JNEUROSCI.4276-04.2005>.
- Cummins, N., Tweedie, A., Zuryin, S., Bertran-Gonzalez, J., Götz, J., 2019. Disease-associated tau impairs mitophagy by inhibiting Parkin translocation to mitochondria. *EMBO J.* 38, e99360. <https://doi.org/10.15252/emboj.201899360>.
- Damiano, M., Galvan, L., Déglon, N., Brault, E., 2010. Mitochondria in Huntington's disease. *Biochim. Biophys. Acta* 1802, 52–61. <https://doi.org/10.1016/j.bbdis.2009.07.012>.
- Dawson, T.M., Dawson, V.L., 2010. The role of parkin in familial and sporadic Parkinson's disease. *Mov. Disord.* 25, S32–S39. <https://doi.org/10.1002/mds.22798>.
- De Marchi, U., Santo-Domingo, J., Castelbou, C., Sekler, I., Wiederkehr, A., Demareux, N., 2014. NCLX protein, but not LETM1, mediates mitochondrial Ca<sup>2+</sup> extrusion, thereby limiting Ca<sup>2+</sup>-induced NAD(P)H production and modulating matrix redox state. *J. Biol. Chem.* 289, 20377–20385. <https://doi.org/10.1074/jbc.M113.540898>.
- De Stefani, D., Raffaello, A., Teardo, E., Szabó, L., Rizzuto, R., 2011. A forty-kilodalton protein of the inner membrane is the mitochondrial calcium uniporter. *Nature* 476, 336–340. <https://doi.org/10.1038/nature10230>.
- De Stefani, D., Rizzuto, R., Pozzan, T., 2016. Enjoy the trip: calcium in mitochondria back and forth. *Annu. Rev. Biochem.* 85, 161–192. <https://doi.org/10.1146/annurev-biochem-060614-034216>.
- Delic, V., Kurién, C., Cruz, J., Zivkovic, S., Barretta, J., Thomson, A., Hennessey, D., Joseph, J., Ehrhart, J., Willing, A.E., Bradshaw, P., Garbuzova-Davis, S., 2018. Discrete mitochondrial aberrations in the spinal cord of sporadic ALS patients. *J. Neurosci. Res.* 96, 1353–1366. <https://doi.org/10.1002/jnr.24249>.
- Dröge, W., 2002. Free radicals in the physiological control of cell function. *Physiol. Rev.* 82, 47–95. <https://doi.org/10.1152/physrev.00018.2001>.
- Duchen, M.R., 2000. Mitochondria and calcium: from cell signalling to cell death. *J. Physiol.* 529, 57–68. <https://doi.org/10.1111/j.1469-7793.2000.00057.x>.
- Favaro, G., Romanello, V., Varaniti, T., Andrea Desbats, M., Morbidoni, V., Tezze, C., Albiero, M., Canato, M., Gherardi, G., De Stefani, D., Mammucari, C., Blaauw, B., Boncompagni, S., Protasi, F., Reggiani, C., Scorrano, L., Salviati, L., Sandri, M., 2019. DRP1-mediated mitochondrial shape controls calcium homeostasis and muscle mass. *Nat. Commun.* 10, 2576. <https://doi.org/10.1038/s41467-019-10226-9>.
- Figueira, T.R., Barros, M.H., Camargo, A.A., Castilho, R.F., Ferreira, J.C., Kowaltowski, A.J., Sluse, F.E., Souza-Pinto, N.C., Vercesi, A.E., 2013. Mitochondria as a source of reactive oxygen and nitrogen species: from molecular mechanisms to human health. *Antioxidants Redox Signal.* 18, 2029–2074. <https://doi.org/10.1089/ars.2012.4729>.
- Flannery, P.J., Trushina, E., 2019. Mitochondrial dynamics and transport in Alzheimer's disease. *Mol. Cell. Neurosci.* 98, 109–120. <https://doi.org/10.1016/j.mcn.2019.06.009>.
- Flippo, K.H., Gnanasekaran, A., Perkins, G.A., Ajmal, A., Merrill, R.A., Dickey, A.S., Taylor, S.S., McKnight, G.S., Chauhan, A.K., Usachev, Y.M., Strack, S., 2018. AKAP1 protects from cerebral ischemic stroke by inhibiting Drp1-dependent mitochondrial fission. *J. Neurosci.* 38, 8233–8242. <https://doi.org/10.1523/JNEUROSCI.0649-18.2018>.
- Gellerich, F.N., Gizatullina, Z., Nguyen, H.P., Trumbeckaite, S., Vielhaber, S., Seppet, E., Zierz, S., Landwehrmeyer, B., Riess, O., von Hörsten, S., Striggow, F., 2008. Impaired regulation of brain mitochondria by extramitochondrial Ca<sup>2+</sup> in transgenic Huntington disease rats. *J. Biol. Chem.* 283, 30715–30724. <https://doi.org/10.1074/jbc.M709555200>.
- Genin, E.C., Plutino, M., Bannwarth, S., Villa, E., Cisneros-Barroso, E., Roy, M., Ortega-Vila, B., Fragaki, K., Lespinaise, F., Pinero-Martos, E., Auge, G., Moore, D., Burte, F., Lacas-Gervais, S., Kageyama, Y., Itoh, K., Yu-Wai-Man, P., Sesaki, H., Ricci, J.-E., Vives-Bauza, C., Paquis-Fluckinger, V., 2016. CHCHD10 mutations promote loss of mitochondrial cristae junctions with impaired mitochondrial genome maintenance and inhibition of apoptosis. *EMBO Mol. Med.* 8, 58–72. <https://doi.org/10.15252/emmm.201505496>.
- Ghosh, A., Chandran, K., Kalivendi, S.V., Joseph, J., Antholine, W.E., Hillard, C.J., Kanthasamy, A., Kanthasamy, A., Kalyanaram, B., 2010. Neuroprotection by a mitochondrial-targeted drug in a Parkinson's disease model. *Free Radic. Biol. Med.* 49, 1674–1684. <https://doi.org/10.1016/j.freeradbiomed.2010.08.028>.
- Grossmann, D., Berenguer-Escuder, C., Bellet, M.E., Scheibner, D., Bohler, J., Massart, F., Rapaport, D., Skupin, A., Fouquier d'Hérouël, A., Sharma, M., Ghelfi, J., Rakovic, A., Lichtner, P., Antony, P., Glaab, E., May, P., Dimmer, K.S., Fitzgerald, J.C., Gruenewald, A., Krüger, R., 2019. Mutations in RHOT1 disrupt ER-mitochondria contact sites interfering with calcium homeostasis and mitochondrial dynamics in Parkinson's disease. *Antioxidants Redox Signal.* <https://doi.org/10.1089/ars.2018.7718>. [Epub ahead of print].
- Gunter, T.E., Gunter, K.K., Sheu, S.S., Gavin, C.E., 1994. Mitochondrial calcium transport: physiological and pathological relevance. *Am. J. Physiol.* 267, C313–C339. <https://doi.org/10.1152/ajpcell.1994.267.2.C313>.
- Hariharan, A., Shetty, S., Shirole, T., Jagtap, A.G., 2014. Potential of protease inhibitor in 3-nitropropionic acid induced Huntington's disease like symptoms: mitochondrial dysfunction and neurodegeneration. *Neurotoxicology (Little Rock)* 45, 139–148. <https://doi.org/10.1016/j.neuro.2014.10.004>.
- Hayakawa, K., Esposito, E., Wang, X., Terasaki, Y., Liu, Y., Xing, C., Ji, X., Lo, E.H., 2016. Transfer of mitochondria from astrocytes to neurons after stroke. *Nature* 535, 551–555. <https://doi.org/10.1038/nature18928>.
- Hedrich, K., Eskelson, C., Wilmut, B., Marder, K., Harris, J., Garrels, J., Mejia-Santana, H., Vieregge, P., Jacobs, H., Bressnan, S.B., Lang, A.E., Kapp, M., Abbruzzese, G., Martinielli, P., Schwinger, E., Ozelius, L.J., Pramstaller, P.P., Klein, C., Kramer, P., 2004. Distribution, type, and origin of Parkin mutations: review and case studies. *Mov. Disord.* 19, 1146–1157.
- Hirai, K., Aliev, G., Nunomura, A., Fujioka, H., Russell, R.L., Atwood, C.S., Johnson, A.B., Kress, Y., Vinters, H.V., Tabaton, M., Shimohama, S., Cash, A.D., Siedlak, S.L., Harris, P.L., Jones, P.K., Petersen, R.B., Perry, G., Smith, M.A., 2001. Mitochondrial abnormalities in Alzheimer's disease. *J. Neurosci.* 21, 3017–3023.
- Ismailoglu, I., Chen, Q., Popowski, M., Yang, L., Gross, S.S., Brivanlou, A.H., 2014. Huntingtin protein is essential for mitochondrial metabolism, bioenergetics and structure in murine embryonic stem cells. *Dev. Biol.* 391, 230–240. <https://doi.org/10.1016/j.ydbio.2014.04.005>.
- Jackson-Lewis, V., Przedborski, S., 2007. Protocol for the MPTP mouse model of Parkinson's disease. *Nat. Protoc.* 2, 141–151. <https://doi.org/10.1038/nprot.2006.342>.
- Jadiya, P., Kolmetzky, D.W., Tomar, D., Di Meco, A., Lombardi, A.A., Lambert, J.P., Luongo, T.S., Ludtmann, M.H., Praticò, D., Elrod, J.W., 2019. Impaired mitochondrial calcium efflux contributes to disease progression in models of Alzheimer's disease. *Nat. Commun.* 10, 3885. <https://doi.org/10.1038/s41467-019-11813-6>.
- Jin, H., Kanthasamy, A., Ghosh, A., Anantharam, V., Kalyanaram, B., Kanthasamy, A.G., 2014. Mitochondria-targeted antioxidants for treatment of Parkinson's disease: preclinical and clinical outcomes. *Biochim. Biophys. Acta* 1842, 1282–1294. <https://doi.org/10.1016/j.bbdis.2013.09.007>.
- Joshi, A.U., Ebert, A.E., Haileselassie, B., Mochly-Rosen, D., 2019. Drp1/Fis1-mediated mitochondrial fragmentation leads to lysosomal dysfunction in cardiac models of Huntington's disease. *J. Mol. Cell. Cardiol.* 127, 125–133. <https://doi.org/10.1016/j.yjmcc.2018.12.004>.
- Kahl, A., Stepanova, A., Konrad, C., Anderson, C., Manfredi, G., Zhou, P., Iadecola, C., Galkin, A., 2018. Critical role of flavin and glutathione in complex I-mediated bioenergetic failure in brain ischemia/reperfusion injury. *Stroke* 49, 1223–1231. <https://doi.org/10.1161/STROKEAHA.117.019687>.
- Kahle, P.J., Haass, C., 2004. How does parkin ligate ubiquitin to Parkinson's disease? *EMBO Rep.* 5, 681–685. <https://doi.org/10.1038/sj.embo.7400188>.
- Khoshnam, S.E., Winlow, W., Farzaneh, M., Farbood, Y., Moghaddam, H.F., 2017. Pathogenic mechanisms following ischemic stroke. *Neurol. Sci.* 38, 1167–1186. <https://doi.org/10.1007/s10072-017-2938-1>.
- Kim, H.S., Lee, J.H., Lee, J.P., Kim, E.M., Chang, K.A., Park, C.H., Jeong, S.J., Wittendorp, M.C., Seo, J.H., Choi, S.H., Suh, Y.H., 2002. Amyloid beta peptide induces cytochrome C release from isolated mitochondria. *Neuroreport* 13, 1989–1993.
- Kim, I., Rodriguez-Enriquez, S., Lemasters, J.J., 2007. Selective degradation of mitochondria by mitophagy. *Arch. Biochem. Biophys.* 462, 245–253. <https://doi.org/10.1016/j.ab.2007.05.011>.



- 10.1016/j.abb.2007.03.034.
- Kostic, M., Ludtmann, M.H.R., Bading, H., Hershinkel, M., Steer, E., Chu, C.T., Abramov, A.Y., Sekler, I., 2015. PKA phosphorylation of NCLX reverses mitochondrial calcium overload and depolarization, promoting survival of PINK1-deficient dopaminergic neurons. *Cell Rep.* 13, 376–386. <https://doi.org/10.1016/j.celrep.2015.08.079>.
- Kowaltowski, A.J., 2019. Strategies to detect mitochondrial oxidants. *Redox Biol.* 21, 101065. <https://doi.org/10.1016/j.redox.2018.101065>.
- Kowaltowski, A.J., Menezes-Filho, S.L., Assali, E.A., Gonçalves, I.G., Cabral-Costa, J.V., Abreu, P., Miller, N., Nolasco, P., Laurindo, F.R.M., Bruni-Cardoso, A., Shirihai, O., 2019. Mitochondrial morphology regulates organellar Ca<sup>2+</sup> uptake and changes cellular Ca<sup>2+</sup> homeostasis. *FASEB J* (in press).
- Krige, D., Carroll, M.T., Cooper, J.M., Marsden, C.D., Schapira, A.H., 1992. Platelet mitochondrial function in Parkinson's disease. *Ann. Neurol.* 32, 782–788. <https://doi.org/10.1002/ana.410320612>.
- Lai, T.W., Zhang, S., Wang, Y.T., 2014. Excitotoxicity and stroke: identifying novel targets for neuroprotection. *Prog. Neurobiol.* 115, 157–188. <https://doi.org/10.1016/j.pneurobio.2013.11.006>.
- Langston, J.W., Ballard, P., Tetrud, J.W., Irwin, I., 1983. Chronic Parkinsonism in humans due to a product of meperidine-analog synthesis. *Science* 219, 979–980. <https://doi.org/10.1126/science.6823561>.
- Lemasters, J.J., Nieminen, A.L., Qian, T., Trost, L.C., Elmore, S.P., Nishimura, Y., Crowe, R.A., Cascio, W.E., Bradham, C.A., Brenner, D.A., Herman, B., 1998. The mitochondrial permeability transition in cell death: a common mechanism in necrosis, apoptosis and autophagy. *Biochim. Biophys. Acta* 10 (1366), 177–196. [https://doi.org/10.1016/s0005-2728\(98\)00112-1](https://doi.org/10.1016/s0005-2728(98)00112-1).
- Liesa, M., Palacin, M., Zorzano, A., 2009. Mitochondrial dynamics in mammalian health and disease. *Physiol. Rev.* 89, 799–845. <https://doi.org/10.1152/physrev.00030.2008>.
- Liesa, M., Shirihai, O.S., 2013. Mitochondrial dynamics in the regulation of nutrient utilization and energy expenditure. *Cell Metabol.* 17, 491–506. <https://doi.org/10.1016/j.cmet.2013.03.002>.
- Lim, D., Fedrizzi, L., Tartari, M., Zuccato, C., Cattaneo, E., Brini, M., Carafoli, E., 2008. Calcium homeostasis and mitochondrial dysfunction in striatal neurons of Huntington disease. *J. Biol. Chem.* 283, 5780–5789. <https://doi.org/10.1074/jbc.M704704200>.
- Lin, M.T., Beal, M.F., 2006. Mitochondrial dysfunction and oxidative stress in neurodegenerative diseases. *Nature* 443, 787–795. <https://doi.org/10.1038/nature05292>.
- Lin, M.T., Simon, D.K., Ahn, C.H., Kim, L.M., Beal, M.F., 2002. High aggregate burden of somatic mtDNA point mutations in aging and Alzheimer's disease brain. *Hum. Mol. Genet.* 11, 133–145. <https://doi.org/10.1093/hmg/11.2.133>.
- Liu, F., Lu, J., Manaenko, A., Tang, J., Hu, Q., 2018. Mitochondria in ischemic stroke: new insight and implications. *Aging Dis* 9, 924–937. <https://doi.org/10.14336/AD.2017.11.26>.
- Liu, K., Guo, L., Zhou, Z., Pan, M., Yan, C., 2019. Mesenchymal stem cells transfer mitochondria into cerebral microvasculature and promote recovery from ischemic stroke. *Microvasc. Res.* 123, 74–80. <https://doi.org/10.1016/j.mvr.2019.01.001>.
- López-Crisosto, C., Bravo-Sagua, R., Rodríguez-Peña, M., Mera, C., Castro, P.F., Quest, A.F.G., Rothermel, B.A., Cifuentes, M., Lavandero, S., 2015. ER-to-mitochondria Miscommunication and Metabolic Diseases.
- Lu, M., Su, C., Qiao, C., Bian, Y., Ding, J., Hu, G., 2016. Metformin prevents dopaminergic neuron death in MPTP/P-induced mouse model of Parkinson's disease via autophagy and mitochondrial ROS clearance. *Int. J. Neuropsychopharmacol.* 19, pyw047. <https://doi.org/10.1093/ijnp/pyw047>.
- Ludtmann, M.H.R., Angelova, P.R., Horrocks, M.H., Choi, M.L., Rodrigues, M., Baev, A.Y., Berezhnov, A.V., Yao, Z., Little, D., Banushi, B., Al-Menhali, A.S., Ranasinghe, R.T., Whitten, D.R., Yapom, R., Dolt, K.S., Devine, M.J., Gissen, P., Kunath, T., Jaganjac, M., Pavlov, E.V., Klenerman, D., Abramov, A.Y., Gandhi, S., 2018.  $\alpha$ -synuclein oligomers interact with ATP synthase and open the permeability transition pore in Parkinson's disease. *Nat. Commun.* 9, 2293. <https://doi.org/10.1038/s41467-018-04422-2>.
- Ludtmann, M.H.R., Kostic, M., Horne, A., Gandhi, S., Sekler, I., Abramov, A.Y., 2019. LRRK2 deficiency induced mitochondrial Ca<sup>2+</sup> efflux inhibition can be rescued by Na<sup>+</sup>/Ca<sup>2+</sup>/Li<sup>+</sup> exchanger upregulation. *Cell Death Dis.* 10, 265. <https://doi.org/10.1038/s41419-019-1469-5>.
- Mandelkow, E.M., Stamer, K., Vogel, R., Thies, E., Mandelkow, E., 2003. Clogging of axons by tau, inhibition of axonal traffic and starvation of synapses. *Neurobiol. Aging* 24, 1079–1085. <https://doi.org/10.1016/j.neurobiolaging.2003.04.007>.
- Markesbery, W.R., Carney, J.M., 1999. Oxidative alterations in Alzheimer's disease. *Brain Pathol.* 9, 133–146.
- McNaught, K.S., Thull, U., Carrupt, P.A., Altomare, C., Cellamare, S., Carotti, A., Testa, B., Jenner, P., Marsden, C.D., 1995. Inhibition of complex I by isoquinoline derivatives structurally related to 1-methyl-4-phenyl-1,2,3,6-tetrahydropyridine (MPTP). *Biochem. Pharmacol.* 50, 1903–1911. [https://doi.org/10.1016/0006-2952\(95\)02086-1](https://doi.org/10.1016/0006-2952(95)02086-1).
- Milakov, T., Quintanilla, R.A., Johnson, G.V., 2006. Mutant huntingtin expression induces mitochondrial calcium handling defects in clonal striatal cells: functional consequences. *J. Biol. Chem.* 281, 34785–34795. <https://doi.org/10.1074/jbc.M603845200>.
- Mink, J.W., Blumenshine, R.J., Adams, D.B., 1981. Ratio of central nervous system to body metabolism in vertebrates: its constancy and functional basis. *Am. J. Physiol.* 241, R203–R212. <https://doi.org/10.1152/ajpregu.1981.241.3.R203>.
- Mishra, P., Chan, D.C., 2016. Metabolic regulation of mitochondrial dynamics. *J. Cell Biol.* 212, 379–387. <https://doi.org/10.1083/jcb.201511036>.
- Mizuno, Y., Hattori, N., Mori, H., Suzuki, T., Tanaka, K., 2001. Parkin and Parkinson's disease. *Curr. Opin. Neurol.* 14, 477–482.
- Murphy, M.P., 2009. How mitochondria produce reactive oxygen species. *Biochem. J.* 417, 1–13. <https://doi.org/10.1042/BJ20081386>.
- Muyderman, H., Chen, T., 2014. Mitochondrial dysfunction in amyotrophic lateral sclerosis - a valid pharmacological target? *Br. J. Pharmacol.* 171, 2191–2205. <https://doi.org/10.1111/bph.12476>.
- Naia, L., Ferreira, I.L., Ferreira, E., Rego, A.C., 2017. Mitochondrial Ca<sup>2+</sup> handling in Huntington's and Alzheimer's diseases - role of ER-mitochondria crosstalk. *Biochem. Biophys. Res. Commun.* 483, 1069–1077. <https://doi.org/10.1016/j.bbrc.2016.07.122>.
- Nakaya, T., Maragkakis, M., 2018. Amyotrophic Lateral Sclerosis associated FUS mutation shortens mitochondria and induces neurotoxicity. *Sci. Rep.* 8, 1–15. <https://doi.org/10.1038/s41598-018-33964-0>.
- Nicholls, D.G., 2004. Mitochondrial dysfunction and glutamate excitotoxicity studied in primary neuronal cultures. *Curr. Mol. Med.* 4, 149–177. <https://doi.org/10.2174/1566524043479239>.
- Niizuma, K., Yoshioka, H., Chen, H., Kim, G.S., Jung, J.E., Katsu, M., Okami, N., Chan, P.H., 2010. Mitochondrial and apoptotic neuronal death signaling pathways in cerebral ischemia. *Biochim. Biophys. Acta* 1802, 92–99. <https://doi.org/10.1016/j.bbadis.2009.09.002>.
- Okamoto, K., Shaw, J.M., 2005. Mitochondrial morphology and dynamics in yeast and multicellular eukaryotes. *Annu. Rev. Genet.* 39, 503–536. <https://doi.org/10.1146/annurev.genet.38.072902.093019>.
- Oliveira, J.M., Gonçalves, J., 2008. In situ mitochondrial Ca<sup>2+</sup> buffering differences of intact neurons and astrocytes from cortex and striatum. *J. Biol. Chem.* 284, 5010–5020. <https://doi.org/10.1074/jbc.M807459200>.
- Panchal, K., Tiwari, A.K., 2019. Mitochondrial dynamics, a key executioner in neurodegenerative diseases. *Mitochondrion* 47, 151–173. <https://doi.org/10.1016/j.mito.2018.11.002>.
- Panov, A., Dikalov, S., Shalbuyeva, N., Taylor, G., Sherer, T., Greenamyre, J.T., 2005. Rotenone model of Parkinson disease: multiple brain mitochondria dysfunctions after short term systemic rotenone intoxication. *J. Biol. Chem.* 280, 42026–42035. <https://doi.org/10.1074/jbc.M508628200>.
- Panov, A.V., Gutekunst, C.A., Leavitt, B.R., Hayden, M.R., Burke, J.R., Strittmatter, W.J., Greenamyre, J.T., 2002. Early mitochondrial calcium defects in Huntington's disease are a direct effect of polyglutamines. *Nat. Neurosci.* 5, 731–736. <https://doi.org/10.1038/nm884>.
- Parker Jr., W.D., Boyson, S.J., Parks, J.K., 1989. Abnormalities of the electron transport chain in idiopathic Parkinson's disease. *Ann. Neurol.* 26, 719–723. <https://doi.org/10.1002/ana.410260606>.
- Parker Jr., W.D., Parks, J., Filley, C.M., Kleinschmidt-DeMasters, B.K., 1994. Electron transport chain defects in Alzheimer's disease brain. *Neurology* 44, 1090–1096. <https://doi.org/10.1212/wnl.44.6.1090>.
- Parsons, M.J., Green, D.R., 2010. Mitochondria in cell death. *Essays Biochem.* 47, 99–114. <https://doi.org/10.1042/bse0470099>.
- Pernas, L., Scorrano, L., 2016. Mito-morphosis: mitochondrial fusion, fission, and cristae remodeling as key mediators of cellular function. *Annu. Rev. Physiol.* 78, 505–531. <https://doi.org/10.1146/annurev-physiol-021115-105011>.
- Pickrell, A.M., Youle, R.J., 2015. The roles of PINK1, parkin, and mitochondrial fidelity in Parkinson's disease. *Neuron* 85, 257–273. <https://doi.org/10.1016/j.neuron.2014.12.007>.
- Pinto, M., Nissanka, N., Moraes, C.T., 2018. Lack of Parkin anticipates the phenotype and affects mitochondrial morphology and mtDNA levels in a mouse model of Parkinson's disease. *J. Neurosci.* 38, 1042–1053. <https://doi.org/10.1523/JNEUROSCI.1384-17.2017>.
- Polyzos, A.A., Lee, D.Y., Datta, R., Hauser, M., Budworth, H., Holt, A., Mihalik, S., Goldschmidt, P., Frankel, K., Trego, K., Bennett, M.J., Vockley, J., Xu, K., Gratton, E., McMurray, C.T., 2019. Metabolic reprogramming in astrocytes distinguishes region-specific neuronal susceptibility in huntington mice. *Cell Metabol.* 29, 1258–1273. <https://doi.org/10.1016/j.cmet.2019.03.004>. e11.
- Prell, T., Lautenschläger, J., Grosskreutz, J., 2013. Calcium-dependent protein folding in amyotrophic lateral sclerosis. *Cell Calcium* 54, 132–143. <https://doi.org/10.1016/j.ceca.2013.05.007>.
- Reddy, P.H., Beal, M.F., 2005. Are mitochondria a critical in the pathogenesis of Alzheimer's disease? *Brain Res. Rev.* 49, 618–632. <https://doi.org/10.1016/j.brainresrev.2005.03.004>.
- Richardson, J.R., Caudle, W.M., Guillot, T.S., Watson, J.L., Nakamaru-Ogiso, E., Seo, B.B., Sherer, T.B., Greenamyre, J.T., Yagi, T., Matsuno-Yagi, A., Miller, G.W., 2007. Obligatory role for complex I inhibition in the dopaminergic neurotoxicity of 1-methyl-4-phenyl-1,2,3,6-tetrahydropyridine (MPTP). *Toxicol. Sci.* 95, 196–204. <https://doi.org/10.1093/toxsci/kfl133>.
- Russell, A.E., Jun, S., Sarkar, S., Geldenhuys, W.J., Lewis, S.E., Rellick, S.L., Simpkins, J.W., 2019. Extracellular vesicles secreted in response to cytokine exposure increase mitochondrial oxygen consumption in recipient cells. *Front. Cell. Neurosci.* 13, 51. <https://doi.org/10.3389/fncel.2019.00051>.
- Russo, E., Napoli, E., Borlongan, C.V., 2018. Healthy mitochondria for stroke cells. *Brain Circ.* 4, 95–98. <https://doi.org/10.4103/bc.bc.20.18>.
- Schapira, A.H., 2008. Mitochondria in the aetiology and pathogenesis of Parkinson's disease. *Lancet Neurol.* 7, 97–109. [https://doi.org/10.1016/S1474-4422\(07\)70327-7](https://doi.org/10.1016/S1474-4422(07)70327-7).
- Sedelis, M., Schwarting, R.K., Huston, J.P., 2001. Behavioral phenotyping of the MPTP mouse model of Parkinson's disease. *Behav. Brain Res.* 125, 109–125. [https://doi.org/10.1016/s0166-4328\(01\)00309-6](https://doi.org/10.1016/s0166-4328(01)00309-6).
- Seirafi, M., Kozlov, G., Gehring, K., 2015. Parkin structure and function. *FEBS J.* 282, 2076–2088. <https://doi.org/10.1111/febs.13249>.
- Sheehan, J.P., Swerdlow, R.H., Parker, W.D., Miller, S.W., Davis, R.E., Tuttle, J.B., 1997. Altered calcium homeostasis in cells transformed by mitochondria from individuals with Parkinson's disease. *J. Neurochem.* 68, 1221–1233. <https://doi.org/10.1046/j.1471-4159.1997.68031221.x>.

- Sherer, T.B., Betarbet, R., Greenamyre, J.T., 2002. Environment, mitochondria, and Parkinson's disease. *The Neuroscientist* 8, 192–197. <https://doi.org/10.1177/1073858402008003004>.
- Silachev, D.N., Plotnikov, E.Y., Pevzner, I.B., Zorova, L.D., Balakireva, A.V., Gulyaev, M.V., Pirogov, Y.A., Skulachev, V.P., Zorov, D.B., 2018. Neuroprotective effects of mitochondria-targeted plastoquinone in a rat model of neonatal hypoxic ischemic brain injury. *Molecules* 23, E1871. <https://doi.org/10.3390/molecules23081871>.
- Smith, M.A., Nunomura, A., Zhu, X., Takeda, A., Perry, G., 2000. Metabolic, metallic, and mitotic sources of oxidative stress in Alzheimer disease. *Antioxidants Redox Signal* 2, 413–420. <https://doi.org/10.1089/15230860050192198>.
- Smith, E.F., Shaw, P.J., De Vos, K.J., 2018. The role of mitochondria in amyotrophic lateral sclerosis. *Neurosci. Lett.* S0304–3940 (17), 30544–X. <https://doi.org/10.1016/j.neulet.2017.06.052>.
- Smith, R.A., Hartley, R.C., Murphy, M.P., 2011. Mitochondria-targeted small molecule therapeutics and probes. *Antioxidants Redox Signal* 5, 3021–3038. <https://doi.org/10.1089/ars.2011.3969>.
- Snow, B.J., Rolfe, F.L., Lockhart, M.M., Frampton, C.M., O'Sullivan, J.D., Fung, V., Smith, R.A., Murphy, M.P., Taylor, K.M., Protect Study Group, 2010. A double-blind, placebo-controlled study to assess the mitochondria-targeted antioxidant MitoQ as a disease-modifying therapy in Parkinson's disease. *Mov. Disord.* 25, 1670–1674. <https://doi.org/10.1002/mds.23148>.
- Soltys, D.T., Pereira, C.P.M., Rowies, F.T., Farfel, J.M., Grinberg, L.T., Suemoto, C.K., Leite, R.E.P., Rodriguez, R.D., Ericson, N.G., Bielas, J.H., Souza-Pinto, N.C., 2019. Lower mitochondrial DNA content but not increased mutagenesis associates with decreased base excision repair activity in brains of AD subjects. *Neurobiol. Aging* 73, 161–170. <https://doi.org/10.1016/j.neurobiolaging.2018.09.015>.
- Sorrentino, V., Romani, M., Mouchiroud, L., Beck, J.S., Zhang, H., D'Amico, D., Moullan, N., Potenza, F., Schmid, A.W., Rietsch, S., Counts, S.E., Auwerx, J., 2017. Enhancing mitochondrial proteostasis reduces amyloid- $\beta$  proteotoxicity. *Nature* 552, 187–193. <https://doi.org/10.1038/nature25143>.
- Sousa, S.C., Maciel, E.N., Vercesi, A.E., Castilho, R.F., 2003. Ca<sup>2+</sup>-induced oxidative stress in brain mitochondria treated with the respiratory chain inhibitor rotenone. *FEBS Lett.* 543, 179–183. [https://doi.org/10.1016/s0014-5793\(03\)00421-6](https://doi.org/10.1016/s0014-5793(03)00421-6).
- Starkov, A.A., Fiskum, G., 2003. Regulation of brain mitochondrial H<sub>2</sub>O<sub>2</sub> production by membrane potential and NAD(P)H redox state. *J. Neurochem.* 86, 1101–1107. <https://doi.org/10.1046/j.1471-4159.2003.01908.x>.
- Starkov, A.A., Fiskum, G., Chinopoulos, C., Lorenzo, B.J., Browne, S.E., Patel, M.S., Beal, M.F., 2004. Mitochondrial alpha-ketoglutarate dehydrogenase complex generates reactive oxygen species. *J. Neurosci.* 24, 7779–7788. <https://doi.org/10.1523/JNEUROSCI.1899-04.2004>.
- Starkov, A.A., Polster, B.M., Fiskum, G., 2002. Regulation of hydrogen peroxide production by brain mitochondria by calcium and Bax. *J. Neurochem.* 83, 220–228. <https://doi.org/10.1046/j.1471-4159.2002.01153.x>.
- Stout, A.K., Raphael, H.M., Kanterewicz, B.I., Klann, E., Reynolds, I.J., 1998. Glutamate-induced neuron death requires mitochondrial calcium uptake. *Nat. Neurosci.* 1, 366–373. <https://doi.org/10.1038/1577>.
- Straub, I.R., Janer, A., Weraarpachai, W., Zinman, L., Robertson, J., Rogava, E., Shoubridge, E.A., 2018. Loss of CHCHD10-CHCHD2 complexes required for respiration underlies the pathogenicity of a CHCHD10 mutation in ALS. *Hum. Mol. Genet.* 27, 178–189. <https://doi.org/10.1093/hmg/ddx393>.
- Tahara, E.B., Navarete, F.D., Kowaltowski, A.J., 2009. Tissue-, substrate-, and site-specific characteristics of mitochondrial reactive oxygen species generation. *Free Radic. Biol. Med.* 46, 1283–1297. <https://doi.org/10.1016/j.freeradbiomed.2009.02.008>.
- Tait, S.W., Green, D.R., 2013. Mitochondrial regulation of cell death. *Cold Spring Harb. Perspect Biol.* 5, a008706. <https://doi.org/10.1101/cshperspect.a008706>.
- Tanner, C.M., Kamel, F., Ross, G.W., Hoppin, J.A., Goldman, S.M., Korell, M., Marras, C., Bhudhikanok, G.S., Kasten, M., Chade, A.R., Comyns, K., Richards, M.B., Meng, C., Priestley, B., Fernandez, H.H., Cambi, F., Umbach, D.M., Blair, A., Sandler, D.P., Langston, J.W., 2011. Rotenone, paraquat, and Parkinson's disease. *Environ. Health Perspect.* 119, 866–872. <https://doi.org/10.1289/ehp.1002839>.
- Tretter, L., Adam-Vizi, V., 2004. Generation of reactive oxygen species in the reaction catalyzed by alpha-ketoglutarate dehydrogenase. *J. Neurosci.* 24, 7771–7778. <https://doi.org/10.1523/JNEUROSCI.1842-04.2004>.
- Twig, G., Elorza, A., Molina, A.J., Mohamed, H., Wikstrom, J.D., Walzer, G., Stiles, L., Haigh, S.E., Katz, S., Las, G., Alroy, J., Wu, M., Py, B.F., Yuan, J., Deeney, J.T., Corkey, B.E., Shirihai, O.S., 2008. Fission and selective fusion govern mitochondrial segregation and elimination by autophagy. *EMBO J.* 27, 433–446. <https://doi.org/10.1038/sj.emboj.7601963>.
- Umeno, A., Biju, V., Yoshida, Y., 2017. In vivo ROS production and use of oxidative stress-derived biomarkers to detect the onset of diseases such as Alzheimer's disease, Parkinson's disease, and diabetes. *Free Radic. Res.* 51, 413–427. <https://doi.org/10.1080/10715762.2017.1315114>.
- Vakifahmetoglu-Norberg, H., Ouchida, A.T., Norberg, E., 2017. The role of mitochondria in metabolism and cell death. *Biochem. Biophys. Res. Commun.* 482, 426–431. <https://doi.org/10.1016/j.bbrc.2016.11.088>.
- Vercesi, A.E., Castilho, R.F., Kowaltowski, A.J., de Oliveira, H.C.F., de Souza-Pinto, N.C., Figueira, T.R., Busanello, E.N.B., 2018. Mitochondrial calcium transport and the redox nature of the calcium-induced membrane permeability transition. *Free Radic. Biol. Med.* 129, 1–24. <https://doi.org/10.1016/j.freeradbiomed.2018.08.034>.
- Walczak, J., Dębska-Vielhaber, G., Vielhaber, S., Szymański, J., Charzyńska, A., Duszyński, J., Szczepanowska, J., 2019. Distinction of sporadic and familial forms of ALS based on mitochondrial characteristics. *FASEB J.* 33, 4388–4403. <https://doi.org/10.1096/fj.201801843r>.
- Wang, C., Youle, R.J., 2009. The role of mitochondria in apoptosis. *Annu. Rev. Genet.* 43, 95–118. <https://doi.org/10.1146/annurev-genet-102108-134850>.
- Williams, G.S., Boyman, L., Chikando, A.C., Khairallah, R.J., Lederer, W.J., 2013. Mitochondrial calcium uptake. *Proc. Natl. Acad. Sci. U. S. A.* 110, 10479–10486. <https://doi.org/10.1073/pnas.1300410110>.
- Wong, H.S., Dighe, P.A., Mezera, V., Montemier, P.A., Brand, M.D., 2017. Production of superoxide and hydrogen peroxide from specific mitochondrial sites under different bioenergetic conditions. *J. Biol. Chem.* 292, 16804–16809. <https://doi.org/10.1074/jbc.R117.789271>.
- Yang, J.L., Mukda, S., Chen, S.D., 2018. Diverse roles of mitochondria in ischemic stroke. *Redox Biol.* 16, 263–275. <https://doi.org/10.1016/j.redox.2018.03.002>.
- Yin, F., Sancheti, H., Patil, I., Cadenas, E., 2016. Energy metabolism and inflammation in brain aging and Alzheimer's disease. *Free Radic. Biol. Med.* 100, 108–122. <https://doi.org/10.1016/j.freeradbiomed.2016.04.200>.
- Yin, W., Signore, A.P., Iwai, M., Cao, G., Gao, Y., Chen, J., 2008. Rapidly increased neuronal mitochondrial biogenesis after hypoxic-ischemic brain injury. *Stroke* 39, 3057–3063. <https://doi.org/10.1161/STROKEAHA.108.520114>.
- Youle, R.J., Narendra, D.P., 2011. Mechanisms of mitophagy. *Nat. Rev. Mol. Cell Biol.* 12, 9–14. <https://doi.org/10.1038/nrm3028>.
- Zhang, N., Wang, S., Li, Y., Che, L., Zhao, Q., 2013. A selective inhibitor of Drp1, mdivi-1, acts against cerebral ischemia/reperfusion injury via an anti-apoptotic pathway in rats. *Neurosci. Lett.* 535, 104–109. <https://doi.org/10.1016/j.neulet.2012.12.049>.
- Zhang, T., Wu, P., Budbazar, E., Zhu, Q., Sun, C., Mo, J., Peng, J., Gospodarev, V., Tang, J., Shi, H., Zhang, J.H., 2019. Mitophagy reduces oxidative stress via Keap1 (kelch-like epichlorohydrin-associated protein 1)/Nrf2 (nuclear factor-E2-related factor 2)/PHB2 (prohibitin 2) pathway after subarachnoid hemorrhage in rats. *Stroke* 50, 978–988. <https://doi.org/10.1161/STROKEAHA.118.021590>.
- Zhi, L., Qin, Q., Muqem, T., Seifert, E.L., Liu, W., Zheng, S., Li, C., Zhang, H., 2019. Loss of PINK1 causes age-dependent decrease of dopamine release and mitochondrial dysfunction. *Neurobiol. Aging* 75, 1–10. <https://doi.org/10.1016/j.neurobiolaging.2018.10.025>.
- Zorov, D.B., Juhaszova, M., Sollott, S.J., 2014. Mitochondrial reactive oxygen species (ROS) and ROS-induced ROS release. *Physiol. Rev.* 94, 909–950. <https://doi.org/10.1152/physrev.00026.2013>.

## CHAPTER 2

### **Mitochondrial Ca<sup>2+</sup> handling as a cell signaling hub: lessons from astrocyte function**

*“Finally, a thought. He who has never sinned is less reliable than he who has only sinned once. And someone who has made plenty of errors – though never the same error more than once – is more reliable than someone who has never made any.”*

(Taleb, 2012, p. 74)<sup>1</sup>

---

<sup>1</sup> Taleb NN. Antifragile: things that gain from disorder. 1st ed. New York: Random House; 2012.

## Summary

Considering the importance of mitochondrial homeostasis in brain pathophysiology, as discussed in Chapter 1, we focused on one of the major hallmarks of mitochondrial function: the Ca<sup>2+</sup> handling. We further deepened our literature review on the composition of the mitochondrial Ca<sup>2+</sup> handling system and its functional impacts on astrocyte physiology and brain function.

As summarized by Cabral-Costa and Kowaltowski (2022)

Astrocytes are a heterogenous population of macroglial cells spread throughout the central nervous system with diverse functions, expression signatures, and intricate morphologies. Their subcellular compartments contain a distinct range of mitochondria, with functional microdomains exhibiting widespread activities, such as controlling local metabolism and Ca<sup>2+</sup> signaling. Ca<sup>2+</sup> is an ion of utmost importance, both physiologically and pathologically, and participates in critical central nervous system processes, including synaptic plasticity, neuron-astrocyte integration, excitotoxicity, and mitochondrial physiology and metabolism. The mitochondrial Ca<sup>2+</sup> handling system is formed by the mitochondrial Ca<sup>2+</sup> uniporter complex (MCUc), which mediates Ca<sup>2+</sup> influx, and the mitochondrial Na<sup>+</sup>/Ca<sup>2+</sup> exchanger (NCLX), responsible for most mitochondrial Ca<sup>2+</sup> efflux, as well as additional components, including the mitochondrial permeability transition pore (mtPTP). Over the last decades, mitochondrial Ca<sup>2+</sup> handling has been shown to be key for brain homeostasis, acting centrally in physiopathological processes such as astrogliosis, astrocyte-neuron activity integration, energy metabolism control, and neurodegeneration. In this review we discuss the current state of knowledge of the mitochondrial Ca<sup>2+</sup> handling system molecular composition, highlighting its impact on astrocytic homeostasis.

This chapter is a full reproduction of the review “Mitochondrial Ca<sup>2+</sup> handling as a cell signaling hub: lessons from astrocyte function”, deposited in MitoFit Preprints in September 2022 and currently under revision in *Essays in Biochemistry* (Cabral-Costa; Kowaltowski, 2022)<sup>2</sup>, that can also be accessed at <https://doi.org/10.26124/mitofit:2022-0027>, in accordance with the publishers’ copyright policies (Portland Press, 2022<sup>3</sup>; Creative Commons, 2022<sup>4</sup>).

---

<sup>2</sup> Cabral-Costa JV, Kowaltowski AJ. Mitochondrial Ca<sup>2+</sup> handling as a cell signaling hub: lessons from astrocyte function. *MitoFit Preprints* 2022;2022.27. <https://doi.org/10.26124/mitofit:2022-0027>.

<sup>3</sup> Portland Press. Copyright and Permissions 2022. [https://portlandpress.com/pages/copyright\\_and\\_permissions](https://portlandpress.com/pages/copyright_and_permissions) (accessed August 23, 2022).

<sup>4</sup> Creative Commons. Creative Commons — Attribution-Non-Commercial-No Derivatives 4.0 International — CC BY-NC-ND 4.0 2022. <https://creativecommons.org/licenses/by-nc-nd/4.0/> (accessed September 12, 2022).

## Review

### Cite

Cabral-Costa JV, Kowaltowski AJ (2022) Mitochondrial Ca<sup>2+</sup> handling as a cell signaling hub: lessons from astrocyte function. MitoFit Preprints 2022.27. <https://doi.org/10.26124/mitofit:2022-0027>

### Author contributions

JVCC contributed with the conceptualization, investigation, visualization, writing, reviewing, and editing; AJK contributed with the conceptualization, supervision, writing, reviewing, and editing.

### Conflicts of interest

The authors declare no conflict of interests.

Received 2022-09-23

Accepted 2022-09-27

Online 2022-09-27

### Keywords

astrocytes;  
mitochondria;  
calcium signalling;  
MCU;  
NCLX;  
metabolism

# Mitochondrial Ca<sup>2+</sup> handling as a cell signaling hub: lessons from astrocyte function

 João Victor Cabral-Costa<sup>1,\*</sup>,

 Alicia J. Kowaltowski<sup>1</sup>

<sup>1</sup> Departamento de Bioquímica, Instituto de Química, Universidade de São Paulo, São Paulo, Brazil.

\* Corresponding author: [joao.victor.costa@usp.br](mailto:joao.victor.costa@usp.br)

## Abstract

**Astrocytes are a heterogenous population of macroglial cells spread throughout the central nervous system with diverse functions, expression signatures, and intricate morphologies. Their subcellular compartments contain a distinct range of mitochondria, with functional microdomains exhibiting widespread activities, such as controlling local metabolism and Ca<sup>2+</sup> signaling. Ca<sup>2+</sup> is an ion of utmost importance, both physiologically and pathologically, and participates in critical central nervous system processes, including synaptic plasticity, neuron-astrocyte integration, excitotoxicity, and mitochondrial physiology and metabolism. The mitochondrial Ca<sup>2+</sup> handling system is formed by the mitochondrial Ca<sup>2+</sup> uniporter complex (MCUc), which mediates Ca<sup>2+</sup> influx, and the mitochondrial Na<sup>+</sup>/Ca<sup>2+</sup> exchanger (NCLX), responsible for most mitochondrial Ca<sup>2+</sup> efflux, as well as additional components, including the mitochondrial permeability transition pore (mtPTP). Over the last decades, mitochondrial Ca<sup>2+</sup> handling has been shown to be key for brain homeostasis, acting centrally in physiopathological processes such as astrogliosis, astrocyte-neuron activity integration, energy metabolism control, and neurodegeneration. In this review we discuss the current state of knowledge of the mitochondrial Ca<sup>2+</sup> handling system molecular composition, highlighting its impact on astrocytic homeostasis.**



## 1. Introduction

Astrocytes are a macroglial cell and one of the most abundant cell types in the brain. They consist of a heterogeneous population spread throughout the central nervous system with specific morphologies, functions, and expression signatures (Khakh, Deneen 2019). These star-shaped cells are morphologically intricate, consisting of a cell soma that forms branches, branchlets, leaflets and, ultimately, endfeet (Aboufares El Alaoui et al 2021). Each of which subcellular compartments contributes toward particular cellular functions and interactions with the extracellular space and other cells, and has specific structures and organelle distributions (Aboufares El Alaoui et al 2021). Of note, astrocytes present diverse mitochondrial populations distributed throughout (Aboufares El Alaoui et al 2021), in functional microdomains with distinct activities, such as controlling local metabolism and Ca<sup>2+</sup> signaling (Agarwal et al 2017) (Fig. 1).

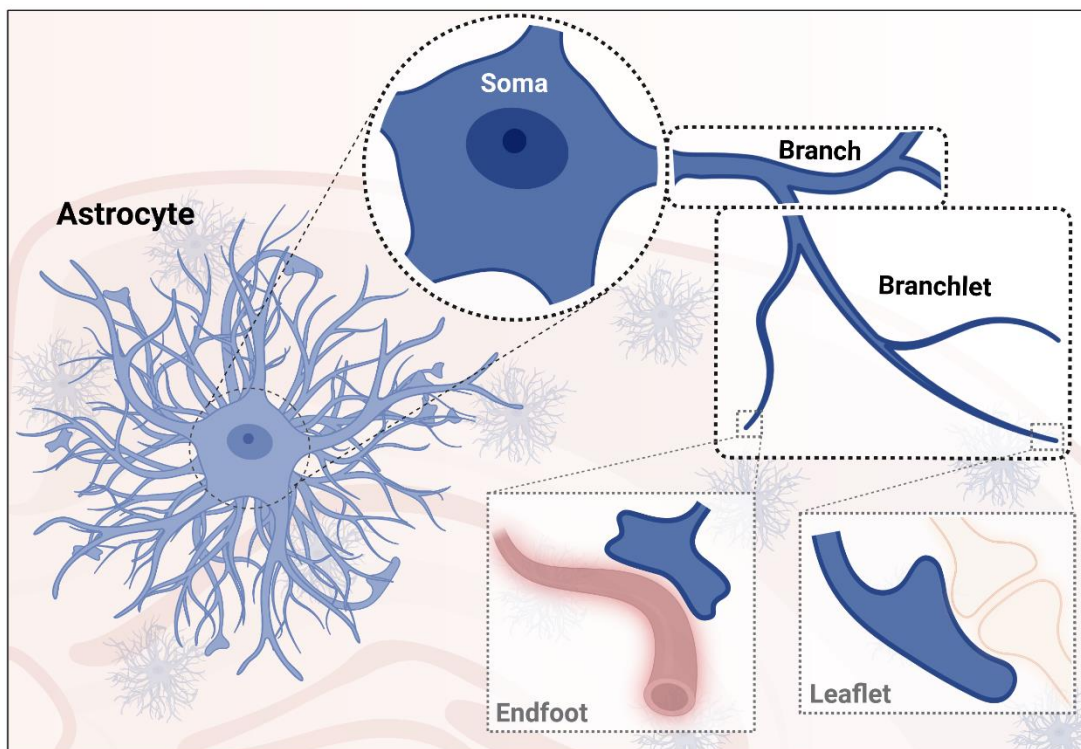


**Figure 1. Astrocyte morphology and subcellular compartments.** General schematic illustration of a protoplasmic astrocyte, depicting its cell body (soma) ramifying into branches, branchlets and, ultimately, endfeet and leaflets in close contact with brain vessels and synapses, respectively (further discussed by Khakh, Deneen 2019).

Ca<sup>2+</sup> is an ion of seminal importance in cellular homeostasis, both physiologically (Kawamoto et al 2012) and pathologically (Cabral-Costa, Kowaltowski 2020). It is a critical second messenger of key processes in the central nervous system, such as neurovascular coupling (Lourenço, Laranjinha 2021), synaptic plasticity (Kawamoto et al 2012), and neuron-astrocyte integration between excitability and function (Oliveira, Araque 2022). Ca<sup>2+</sup> is also involved in mitochondrial redox balance and the development of mitochondrial permeability transition (Vercesi et al 2018), participating in the induction of excitotoxicity (Amigo et al 2017) and cell death (Vercesi et al 2018).

$\text{Ca}^{2+}$  also evolved as an indicator for energetic demands. Increases in intramitochondrial  $\text{Ca}^{2+}$  levels can boost tricarboxylic acid cycle dehydrogenase affinity, regulate the activity of oxidative phosphorylation complexes, and, indirectly, activate pyruvate dehydrogenase (Llorente-Folch et al 2015). In addition, cytosolic  $\text{Ca}^{2+}$  also positively modulates mitochondrial energy metabolism through activation of malate-aspartate and glycerol-phosphate shuttles (Juaristi et al 2019a). Globally, these  $\text{Ca}^{2+}$  effects modulate mitochondrial metabolism, coupling metabolic needs dictated by cellular activity with ATP production.

This interaction between mitochondria and  $\text{Ca}^{2+}$  is not passive, as mitochondrial and cytosolic  $\text{Ca}^{2+}$  levels are tightly coupled, well controlled (Nicholls 2017), and prone to be regulated by brain activity, influencing both information processing and bioenergetic output (Lin et al 2019), with great relevance for the pathophysiology of neurodegenerative diseases (Cabral-Costa, Kowaltowski 2020). In this review, we discuss the importance of the mitochondrial  $\text{Ca}^{2+}$  handling system, highlighting its impact on astrocytic homeostasis and current questions and gaps in the literature in this field.

## 2. Mitochondrial $\text{Ca}^{2+}$ homeostasis

The first descriptions of mitochondrial  $\text{Ca}^{2+}$  uptake were from experiments conducted more than 6 decades ago in isolated kidney and liver mitochondria (DeLuca and Engstrom 1961; Lehninger et al 1963; Vasington and Murphy 1962). In 1965, Drahotka and Lehninger (1965) described what appeared then to be a minor effect of  $\text{Na}^+$  on mitochondrial  $\text{Ca}^{2+}$  homeostasis, which may have been the first description of the equilibrium between mitochondrial  $\text{Ca}^{2+}$  influx and its  $\text{Na}^+$ -dependent efflux. Other phenomena associated with mitochondrial  $\text{Ca}^{2+}$  homeostasis were described in the following years, including an extensive and time-tested description of the mitochondrial permeability transition (Haworth, Hunter 1979; Hunter, Haworth 1979a, 1979b), characterizing this form of non-selective inner membrane permeabilization caused by high  $\text{Ca}^{2+}$  loads.

However, at that time the endoplasmic reticulum (ER) was identified as a major  $\text{Ca}^{2+}$ -storage hub in skeletal muscle contraction/relaxation (Endo et al 1970), effectively overshadowing the role of mitochondrial  $\text{Ca}^{2+}$  handling in cellular homeostasis. Indeed, mitochondrial  $\text{Ca}^{2+}$  uptake was thought to be irrelevant physiologically until the 1990's, due to the low affinity of mitochondria for this cation, below the average intracellular concentration range. This view changed in 1991, when mitochondrially-targeted apoaequorin was used to measure the ion in this organelle *in situ*, and membrane-potential dependent mitochondrial  $\text{Ca}^{2+}$  transients were observed in parallel to cytosolic increases in  $\text{Ca}^{2+}$  (Rizzuto et al 1992). This was later shown to be possible due to specific increases in  $\text{Ca}^{2+}$  concentrations in the microdomain around these organelles (Rizzuto et al 1993). Subsequent studies demonstrated that mitochondrial  $\text{Ca}^{2+}$  uptake and release indeed participated in a myriad of physiological and biological phenomena (Arieli et al 2004; Arnaudeau et al 2001; Chinopoulos et al 2005; Collins et al 2001; Doczi et al 2011; Kowaltowski et al 1996; Murphy et al 1996; Rudolf et al 2004), although the field exhibited experimental difficulties due to the challenge of identifying the molecular composition of mitochondrial transport pathways. This was achieved beginning in 2010, when the genes for the major components of the mitochondrial  $\text{Ca}^{2+}$  handling system began to be identified with the characterization of the mitochondrial  $\text{Na}^+/\text{Ca}^{2+}$  exchanger

(NCLX) and the mitochondrial Ca<sup>2+</sup> uniporter (MCU) (Baughman et al 2011; De Stefani et al 2011; Palty et al 2010), allowing for a new era of mechanistic discoveries related to mitochondrial Ca<sup>2+</sup> homeostasis.

## 2.1. Mitochondrial Ca<sup>2+</sup> influx

An instructive way to describe the mitochondrial Ca<sup>2+</sup> handling system is to separately focus on its influx and efflux components (Fig. 2). Virtually all mitochondrial Ca<sup>2+</sup> influx is mediated by the inner mitochondrial membrane mitochondrial calcium uniporter complex (MCUc), thoroughly reviewed by Feno et al (2021). In metazoans, the MCUc has the Ca<sup>2+</sup>-selective pore-forming component MCU (Baughman et al 2011; De Stefani et al 2011) arranged in tetramers, intercalated and stabilized by the essential MCU regulator (EMRE) (Sancak et al 2013), and regulatory subunits containing EF-hand Ca<sup>2+</sup>-binding domains – the mitochondrial calcium uptake proteins (MICUs). Additionally, MCUb, a protein with extensive sequence similarity to MCU, may form heteromers with MCU, acting as a dominant-negative agent and suppressing mitochondrial Ca<sup>2+</sup> uptake (Feno et al 2021; Raffaello et al 2013). MCUc activity may also rely on the putative assembly factor MCU regulator 1 (MCUR1), although this is still under dispute (Giorgi et al 2018). Apart from the composition of the MCUc itself and the direct influence of its regulatory components, post-translational modifications (phosphorylation, Joiner et al 2012; and oxidation, Dong et al 2017) may also be key in modulating the activity of the MCU.

Regarding the regulatory subunits, MICU-1 (Perocchi et al 2010) acts as a seal, directly interacting with the MCU tetramer at the region facing the intermembrane space and restricting ion movement through the channel pore when in its closed state. MICU-2 and MICU-3 (Plovanich et al 2013) have a gatekeeping function and may act as Ca<sup>2+</sup> sensors, contributing toward the cooperativity observed in MCUc activity. Interestingly enough, MICU-1 may also mediate the cooperative activation of the channel independently (Payne et al 2017), and sense extramitochondrial Ca<sup>2+</sup> levels (Kamer, Mootha 2014). The stoichiometry of MICU-1 to MCU alone appears to be sufficient to influence mitochondrial Ca<sup>2+</sup> uptake (Paillard et al 2017). This suggests potential non-redundant functions of MICU-1 that may be related to the origins of its paralogs (Feno et al 2021). The expression profile of MICU-2 and MICU-3 also reinforces their intrinsic regulatory role as Ca<sup>2+</sup> sensors. While MICU-2 is more ubiquitous, MICU-3 is highly expressed in the brain, specifically in neurons (Patron et al 2019). Removal of MICU-3 from neurons significantly decreases their mitochondrial response to lower Ca<sup>2+</sup> levels, whereas expression of MICU-3 in non-neuronal cells is sufficient to increase mitochondrial sensitivity to Ca<sup>2+</sup> (Ashrafi et al 2020). Therefore, MICU-3 grants axonal mitochondria greater Ca<sup>2+</sup> sensitivity, triggering pre-synaptic Ca<sup>2+</sup> uptake by mitochondria at a lower Ca<sup>2+</sup> threshold, which may justify its crucial importance in the maintenance of neuronal function and homeostasis (Patron et al 2019).

## 2.2. Mitochondrial Ca<sup>2+</sup> efflux

The major player in mitochondrial Ca<sup>2+</sup> efflux activity is the NCLX (Palty et al 2010), which can exchange either Na<sup>+</sup> or Li<sup>+</sup> for Ca<sup>2+</sup>. Li<sup>+</sup> exchange is used to experimentally confirm activity as mediated by this exchanger, but Na<sup>+</sup>/Ca<sup>2+</sup> activity is evidently predominant *in vivo* (Katoshevski et al 2021; Serna et al 2022). NCLX transport culminates in Ca<sup>2+</sup> efflux from the mitochondrial matrix in exchange for the entrance of



$\text{Na}^+$  from the intermembrane space, a direction which was only shown to be reversible under non-physiological conditions (Samanta et al 2018). NCLX activity follows an electroneutral ( $2 \text{Na}^+ : 1 \text{Ca}^{2+}$ ) or electrophoretic ( $3-4 \text{Na}^+ : 1 \text{Ca}^{2+}$ ) stoichiometry that is still under debate (Giorgi et al 2018; Katoshevski et al 2021). Either way, NCLX activity can be allosterically inhibited by mild mitochondrial membrane depolarization, unless when protected by PKA phosphorylation of its regulatory site (Kostic et al 2015). Therefore, mitochondrial  $\text{Ca}^{2+}$  efflux through NCLX may be controlled by intra- and extra-mitochondrial  $\text{Na}^+$  and  $\text{Ca}^{2+}$  levels, and the mitochondrial membrane potential, while also being influenced by PKA-dependent signaling.

Apart from NCLX, there are additional putative  $\text{Ca}^{2+}$  efflux components. Leucine zipper EF-hand containing transmembrane 1 protein (LETM1) was initially proposed to be a  $\text{K}^+/\text{H}^+$  transporter (Dimmer et al 2007), but later pointed out to be a possible  $\text{Ca}^{2+}/\text{H}^+$  exchanger (Jiang et al 2009; Tsai et al 2014), although this is still intensely debated (De Marchi et al 2014; Giorgi et al 2018). More recently, the transmembrane BAX Inhibitor-1 Motif 5 (TMBIM5, also known as MICS1) was suggested to be the mitochondrial  $\text{Ca}^{2+}/\text{H}^+$  exchanger (Austin et al 2021; Patron et al 2022), in addition to presenting a regulatory role in mitochondrial proteostasis (Patron et al 2022). However, we still require strong

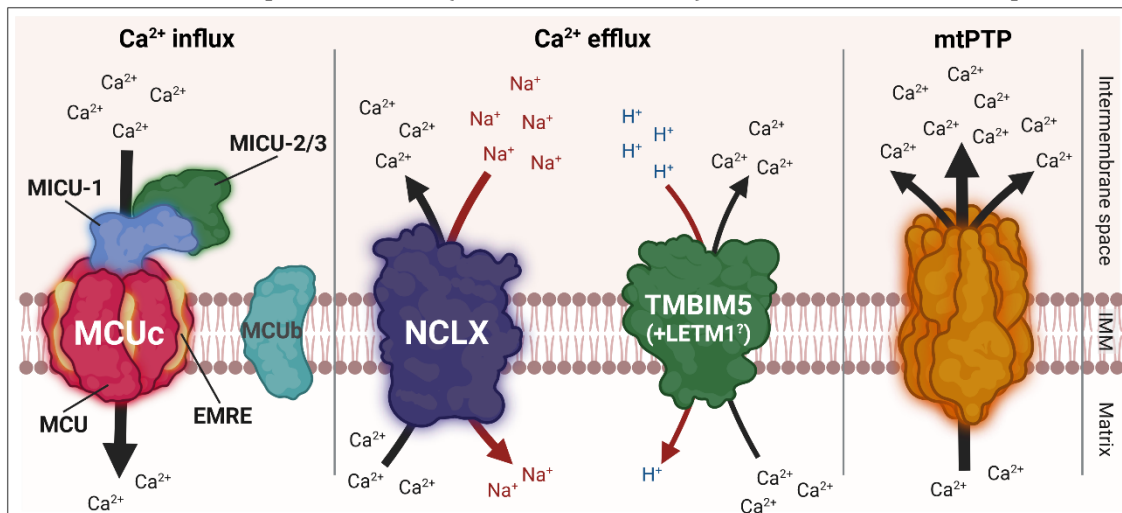


**Figure 2. Mitochondrial  $\text{Ca}^{2+}$  handling system.** Mitochondrial  $\text{Ca}^{2+}$  influx is mediated by the mitochondrial calcium uniporter (MCU) complex (MCUc), formed by a tetramer of MCU subunits intercalated by the essential MCU regulator (EMRE). The channel is gated by the mitochondrial calcium uptake protein (MICU-)1, which is bound to MICU-2 or MICU-3, acting as an extramitochondrial  $\text{Ca}^{2+}$  sensor; MCUB is a regulatory dominant-negative agent that can suppress MCUc activity. Most mitochondrial  $\text{Ca}^{2+}$  efflux activity is mediated by the mitochondrial  $\text{Na}^+/\text{Ca}^{2+}$  exchanger (NCLX), which moves  $\text{Ca}^{2+}$  from the mitochondrial matrix out to the intermembrane space in exchange for extramitochondrial  $\text{Na}^+$ . Alternatively, a  $\text{Ca}^{2+}/\text{H}^+$  exchanger may also contribute to a minor, slower mitochondrial  $\text{Ca}^{2+}$  efflux; it has been recently identified as the transmembrane BAX Inhibitor-1 Motif 5 (TMBIM5), although the leucine zipper EF-hand containing transmembrane 1 protein (LETM1) has previously been associated with this activity, which is still under dispute. Besides  $\text{Ca}^{2+}$  cycling through these transporters, the opening of the mitochondrial permeability transition pore (mtPTP) can also contribute to a significant release of  $\text{Ca}^{2+}$  from the mitochondrial matrix, although through a less specific pathway. (IMM: inner mitochondrial membrane).

data to confirm and validate the molecular identity of the mitochondrial Ca<sup>2+</sup>/H<sup>+</sup> exchanger.

### 2.3. Mitochondrial permeability transition pore (mtPTP)

In addition to canonical mitochondrial Ca<sup>2+</sup> influx and efflux pathways that act similarly to other membrane uniporters and exchangers, we must also emphasize the importance of the mitochondrial membrane permeability transition, a complex and variable process that leads to the opening of the mitochondrial permeability transition pore (mtPTP), a non-selective membrane pathway that allows movement of ions and small molecules (please refer to Vercesi et al 2018 for further details). While its structure and activation mechanisms are diverse and still debated (Bernardi et al 2021; Vercesi et al 2018), mitochondrial Ca<sup>2+</sup> overload and oxidative imbalance are undoubtedly strong triggers for mtPTP opening (Vercesi et al 2018). In addition, while mtPTP activation mostly culminates in an irreversible activation of the pore – leading to mitochondrial swelling, Ca<sup>2+</sup> extrusion, and possible cell death (Vercesi et al 2018) – it may also present a fast reversible opening state, called flickering (Bernardi et al 2021), that can shape cytosolic Ca<sup>2+</sup> signaling by promoting intermittent mitochondrial Ca<sup>2+</sup> release.

## 3. Astrocytic Ca<sup>2+</sup> signaling

In 1986, Pearce et al. (Pearce et al 1986) presented one of the first descriptions in astrocytes of functional glutamate receptors, which relied on Ca<sup>2+</sup> as a signal transducer. Cornell-Bell and colleagues soon after observed that this astrocytic activation induced Ca<sup>2+</sup> waves, which not only shaped intracellular Ca<sup>2+</sup> levels over time within a given astrocyte, but also had the ability to propagate from cell to cell (Cornell-Bell et al 1990; Cornell-Bell, Finkbeiner 1991). These seminal works paved the way for investigations of the functional role of astrocytic Ca<sup>2+</sup> signaling (Fig. 3).

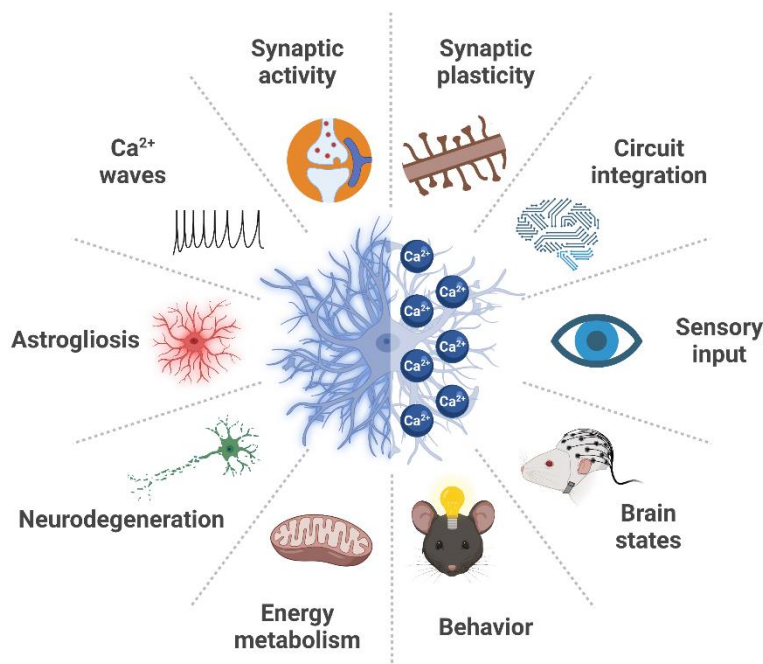


**Figure 3. Astrocytic Ca<sup>2+</sup> signaling and brain function.** Astrocytes are one of the most abundant cell types in the brain, integrated in a plethora of physiopathological processes, many of them relying on astrocytic Ca<sup>2+</sup> signaling. By controlling neuronal and astrocyte survival, synaptic plasticity, neuronal coupling and circuit integration, astrocytic Ca<sup>2+</sup> signaling culminates in the control of superior brain function, including brain states and animal behavior.

Since then, temporal and spatial properties of astrocytic  $\text{Ca}^{2+}$  signaling have been linked to many brain processes (thoroughly reviewed and discussed by Guerra-Gomes et al 2018 and Oliveira and Araque 2022), including integration of sensory inputs and synaptic activity, synaptic plasticity, regulation of neuronal rhythmical activity and brain states, and several behavioral parameters (Guerra-Gomes et al 2018; Oliveira, Araque 2022). Interestingly, astrocytes may act as a redundant layer in brain circuit integration by activation by neurotransmitters – either inhibitory or excitatory – and release of modulatory gliotransmitters that exert a feedback control over synapses (Guerra-Gomes et al 2018).

All these  $\text{Ca}^{2+}$ -dependent effects may arise from a plethora of cytosolic  $\text{Ca}^{2+}$  control mechanisms, including G-protein-coupled receptors (GPCRs, mostly Gq-, but also Gi-mediated), transient receptor potential (TRP) channels, store-operated  $\text{Ca}^{2+}$  entry (SOCE), and, particularly, mitochondrial  $\text{Ca}^{2+}$  handling (Guerra-Gomes et al 2018).

### 3.1. Astrocytic mitochondrial $\text{Ca}^{2+}$ handling

Astrocytic  $\text{Ca}^{2+}$  waves are spatially controlled by mitochondria (Simpson et al 1998), which, apart from the soma, are distributed through most of the astrocytic subcompartments, although found at higher density in branches (Aboufares El Alaoui et al 2021). Mitochondria are frequently found in association with the ER (Aboufares El Alaoui et al 2021) which may tightly interact with mitochondria through  $\text{IP}_3$  receptor-mediated (Wu et al 2007; Zheng et al 2013) or independent  $\text{Ca}^{2+}$  exchanges in local microdomains (Okubo et al 2019). While  $\text{Ca}^{2+}$  is a crucial messenger during astrocytic activation, only 45% of perisynaptic astrocytic processes – as the astrocytic structures are called when wrapping around a synaptic region – displayed ER content. This suggests a strong importance of alternative pools for  $\text{Ca}^{2+}$  exchange in these cells (Aboufares El Alaoui et al 2021) to achieve physiological mitochondrial  $\text{Ca}^{2+}$  handling. In line with this, astrocytic mitochondria were shown to be recruited to and confined in regions near to active synaptic signaling, in a  $\text{Ca}^{2+}$ -dependent manner (Jackson et al 2014; Jackson, Robinson 2015; Stephen et al 2015).

Astrocytes show a greater mitochondrial  $\text{Ca}^{2+}$  buffering capacity when compared to neurons (Oliveira, Gonçalves 2009), in keeping with the expected resilience of this cell type when facing diverse stimuli and stresses. Interestingly however, astrocytes and neurons of cortical origin have increased  $\text{Ca}^{2+}$  buffering capacity in comparison to the same cell types in the striatum (Oliveira, Gonçalves 2009). In this line, striatal astrocytes show increased mitochondrial  $\text{Ca}^{2+}$  influx compared to hippocampal astrocytes (Huntington, Srinivasan 2021). Although this may be due to a difference in local baseline activity and, consequently, in  $\text{Ca}^{2+}$  transients and energetic demand (Huntington, Srinivasan 2021), it could also indicate that components and/or regulation of the mitochondrial  $\text{Ca}^{2+}$  handling system may be tightly controlled not only in a cell-specific manner, but also according to tissue region. Some brain areas are more prone to mitochondrial damage, and, consequently, associated with neurodegenerative processes (Cabral-Costa, Kowaltowski 2020). Therefore, many pathological models in which a general susceptibility to insult of a brain area is observed may not be related only to neuronal-specific mechanisms, but also rely on astrocytic targeting (Oliveira, Gonçalves 2009).

In fact, incubation of astrocytes with tau protein was able to inhibit mitochondrial  $\text{Ca}^{2+}$  efflux (Britti et al 2020), which points to an interesting potential mechanism involved

in tauopathies-associated neurodegeneration. In addition, in an amyotrophic lateral sclerosis (ALS) mouse model, astrocytes displayed increased Ca<sup>2+</sup> transients in astrocytic microdomains, which were formed independently of neurotransmitter release and the ER, and relied on mitochondrial Ca<sup>2+</sup> handling and mPTP flickering (Agarwal et al 2017). Furthermore, astrocyte-derived extracellular vesicles in the plasma derived from patients with resolved acute COVID-19 showed an increase in MCU and NCLX levels, also pointing to a potential effect of SARS-CoV-2 infection over astrocytic mitochondrial Ca<sup>2+</sup> handling (Peluso et al 2022).

Mitochondrial Ca<sup>2+</sup> uptake is relevant in physiological protective contexts as well. Cerebrovascular damage-induced neovascularization requires mitochondrial-ER interaction in astrocytic perivascular processes, in a mechanism that depends on mitochondrial Ca<sup>2+</sup> uptake to allow for the control of Ca<sup>2+</sup> transients (Göbel et al 2020). In addition, MCU Ca<sup>2+</sup> uptake was demonstrated to be seminal for mitochondrial-associated type-1 cannabinoid receptor (mtCB1) signaling, independently of cytosolic Ca<sup>2+</sup> (Serrat et al 2021). Astrocytic mitochondrial Ca<sup>2+</sup> uptake was also shown to contribute toward protective effects in brain damage (Zheng et al 2013), hypoxia (Smith et al 2004), and aging (Wu et al 2007).

But astrocytic Ca<sup>2+</sup> is not a simple readout of a second messenger. As discussed above, glutamate activation was the background for the characterization of astrocytic Ca<sup>2+</sup> signaling (Cornell-Bell et al 1990; Cornell-Bell, Finkbeiner 1991; Pearce et al 1986). And although glutamate stimuli are known to enhance ATP production in astrocytes, they induce an increase in ATP production mostly due to cytosolic Na<sup>+</sup> uptake: glutamate uptake in astrocytes occurs through co-transport with Na<sup>+</sup>, thus activating the Na<sup>+</sup>/K<sup>+</sup>-ATPase to reestablish ionic homeostasis (Juaristi et al 2019b). Although this explains the glutamate-induced increase in ATP demand, Na<sup>+</sup> signaling may also play an additional role in mitochondrial function, including implications in mitochondrial Ca<sup>2+</sup> transport. The major mechanism for mitochondrial Ca<sup>2+</sup> efflux, NCLX, is coupled with mitochondrial Na<sup>+</sup> influx, which was previously shown to be central in mitochondrial respiratory chain-linked signaling in hypoxia (Hernansanz-Agustín et al 2020). Thus, glutamate-dependent Na<sup>+</sup> effects on metabolism may not be restricted to cytosolic ATP depletion, but may also include mitochondrial Na<sup>+</sup> and, indirectly, Ca<sup>2+</sup>-mediated effects. This is an interesting critical point for astrocytic function, as it is tightly coupled – both functionally and energetically – to neuronal activity (Bonvento, Bolaños 2021).

Parnis et al. (Parnis et al 2013) were the first to modulate NCLX activity in astrocytes. NCLX silencing, as expected, increased basal mitochondrial Ca<sup>2+</sup> influx and total content, while significantly decreasing efflux activity, culminating in increased cytosolic Ca<sup>2+</sup> clearance after a purinergic-induced Ca<sup>2+</sup> wave (Parnis et al 2013). This was shown to also decrease store-operated Ca<sup>2+</sup> entry (SOCE) and Ca<sup>2+</sup> wave propagation between astrocytes. Functionally, NCLX silencing inhibited astrocytic proliferation.

NCLX knockdown also induced neurodegeneration and a decrease in astrocyte numbers, both *in vitro* and *in vivo* (Hagenston et al 2022). In this experimental design, both neurons and astrocytes were affected by the shRNA, in mixed cultures and in the intact brain, so the authors correlated these results with astrodegeneration induced by NCLX silencing (Hagenston et al 2022). Nonetheless, NCLX silencing could have also hampered astrogliosis induced by the viral stereotaxic injection, as NCLX knockdown may inhibit astrocyte proliferation (Parnis et al 2013). Therefore, even though NCLX-linked neurodegeneration (Jadiya et al 2019) and cognitive impairment (Stavsky et al 2021) may



be primarily associated with an intrinsic neuronal NCLX activity impairment (Hagenston et al 2022), astrocytic NCLX function may also hold a relevant homeostatic role.

In fact, further NCLX activity implications in cellular function have been explored in  $\beta$ -cells (Kostic et al 2018; Nita et al 2015, 2014, 2012), brown adipose tissue (Assali et al 2020), colorectal cancer (Pathak et al 2020), cardiovascular cells (De La Fuente et al 2018; Garbincius et al 2022; Hernansanz-Agustín et al 2020; Luongo et al 2017), and neurons (Britti et al 2021, 2020; Hagenston et al 2022; Jadiya et al 2019; Kostic et al 2015, 2018; Ludtmann et al 2019; Sharma et al 2017; Stavsky et al 2021). However, there little understood regarding NCLX functional roles in astrocytes. Thus, considering the importance of  $\text{Ca}^{2+}$  signaling for brain activity and astrocyte homeostasis, a deeper comprehension of astrocytic mitochondrial  $\text{Ca}^{2+}$  handling mechanisms and regulation could shed a light on the pathophysiology and potential pharmacological targets of the central nervous system and respective diseases (Cabral-Costa, Kowaltowski 2020) (Fig. 4).

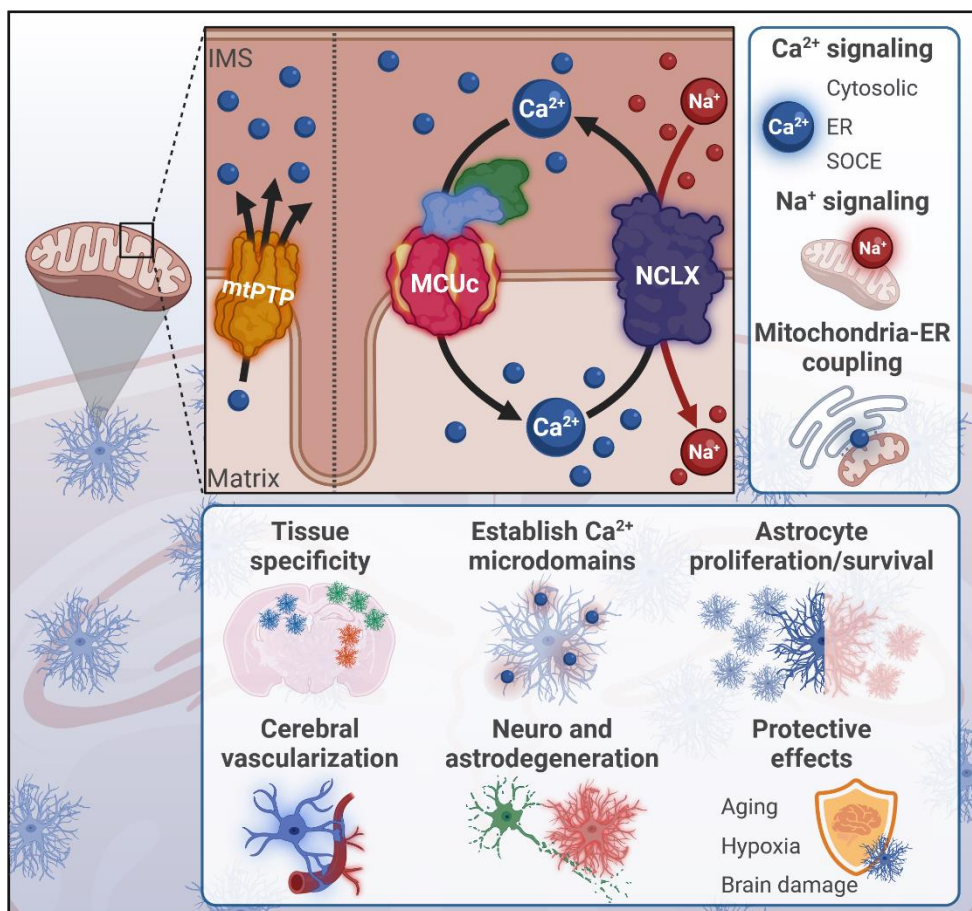


**Figure 4. Astrocytic mitochondrial  $\text{Ca}^{2+}$  handling.** Apart from directly controlling cellular  $\text{Ca}^{2+}$  – and, indirectly,  $\text{Na}^{+}$  – signaling, the mitochondrial  $\text{Ca}^{2+}$  handling system is tightly coupled with many astrocytic functions, from defining  $\text{Ca}^{2+}$  microdomains in astrocytic processes through controlling astrocyte proliferation and survival, with distinct tissue-specific profiles. This contributes to key astrocyte outputs in brain physiology, such as neovascularization and survival of brain cells, and protective effects under diverse challenges.

## 4. Open questions

- What are the underlying mechanisms and implications behind the composition and functional heterogeneity of the mitochondrial Ca<sup>2+</sup> handling system in astrocytes throughout different brain areas?
- How is the mitochondrial Ca<sup>2+</sup> handling system (mainly MCUc and NCLX activities) physiologically controlled in astrocytes – at transcriptional, assembly, and post-translational levels?
- How does mitochondrial Ca<sup>2+</sup> efflux through NCLX control astrocytic proliferation and cell death?
- Are there other physiological roles of NCLX activity in astrocytic function?

## 5. Summary

- Astrocytic Ca<sup>2+</sup> signaling temporally and spatially controls a plethora of brain processes, including synaptic plasticity, electrophysiological brain states, and behavior. Ca<sup>2+</sup> levels are influenced by many transporters and channels, including the mitochondrial Ca<sup>2+</sup> handling system, which is key in controlling several pathways, such as cell survival, ionic balance, and metabolism.
- Ca<sup>2+</sup> signaling events, even those more focused on cytosolic Ca<sup>2+</sup> transients, must also be interpreted in light of mitochondrial Ca<sup>2+</sup> handling and its potential consequences.
- Mitochondrial Ca<sup>2+</sup> handling shapes astrocytic function and is key toward brain homeostasis. Further mechanistic studies, as well as dissection of available single cell omic datasets, may allow for the investigation of the processes behind the heterogeneity of astrocytic mitochondrial Ca<sup>2+</sup> handling molecular composition.
- There is still much to be understood regarding the role of the mitochondrial Ca<sup>2+</sup> handling system (especially the mitochondrial Ca<sup>2+</sup> efflux transporter NCLX), on astrocytic function, which could further advance the understanding of brain pathophysiological mechanisms.

## Abbreviations

ALS	amyotrophic lateral sclerosis	mtCB1	mitochondrial-associated type-1 cannabinoid receptor
EMRE	essential MCU regulator	mtPTP	mitochondrial permeability transition pore mitochondrial Na <sup>+</sup> /Ca <sup>2+</sup> exchanger
ER	endoplasmic reticulum	NCLX	store-operated Ca <sup>2+</sup> entry transmembrane BAX Inhibitor-1 Motif 5
GPCR	G-protein-coupled receptors	SOCE	transient receptor potential
IMM	inner mitochondrial membrane	TMBIM5	
LETM1	leucine zipper EF-hand containing transmembrane 1	TRP	
MCU	mitochondrial Ca <sup>2+</sup> uniporter		
MCUc	MCU complex		
MCUR1	MCU regulator 1		
MICU	mitochondrial calcium uptake protein		

## Acknowledgements

The authors would like to acknowledge the illustration comments and revisions by Juçara Guiçardi Vercelino. Figures were created with Biorender.com. This manuscript is currently under review in *Essays in Biochemistry* (Online ISSN 1744-1358 / Print ISSN 0071-1365, special issue “Astrocytes in Higher Central Nervous System Functions: Facts and Questions”) and has been deposited in MitoFit Preprints with the publisher’s authorization.

## References

- Aboufares El Alaoui A, Jackson M, Fabri M, de Vivo L, Bellesi M (2021). Characterization of subcellular organelles in cortical perisynaptic astrocytes. *Front Cell Neurosci*14:573944. <https://doi.org/10.3389/fncel.2020.573944>.
- Agarwal A, Wu PH, Hughes EG, Fukaya M, Tischfield MA, Langseth AJ, et al (2017). Transient opening of the mitochondrial permeability transition pore induces microdomain calcium transients in astrocyte processes. *Neuron* 93:587-605.e7. <https://doi.org/10.1016/j.neuron.2016.12.034>.
- Amigo I, Menezes-Filho SL, Luévano-Martínez LA, Chausse B, Kowaltowski AJ (2017) Caloric restriction increases brain mitochondrial calcium retention capacity and protects against excitotoxicity. *Aging Cell* 16:73–81. <https://doi.org/10.1111/accel.12527>.
- Arieli Y, Hemamalini G, Eaton M, Hernandez L, Schaefer S. Gender modulation of Ca<sup>2+</sup> uptake in cardiac mitochondria (2004) *J Mol Cell Cardiol* 37:507–13. <https://doi.org/10.1016/j.yjmcc.2004.04.023>.
- Arnaudeau S, Kelley WL, Walsh JV, Demaurex N (2001) Mitochondria recycle Ca<sup>2+</sup> to the endoplasmic reticulum and prevent the depletion of neighboring endoplasmic reticulum regions. *J Biol Chem* 276:29430–9. <https://doi.org/10.1074/jbc.M103274200>.
- Ashrafi G, de Juan-Sanz J, Farrell RJ, Ryan TA (2020) Molecular tuning of the axonal mitochondrial Ca<sup>2+</sup> uniporter ensures metabolic flexibility of neurotransmission. *Neuron* 105:678-687.e5. <https://doi.org/10.1016/j.neuron.2019.11.020>.
- Assali EA, Jones AE, Veliova M, Acín-Pérez R, Taha M, Miller N, et al. (2020) NCLX prevents cell death during adrenergic activation of the brown adipose tissue. *Nat Commun* 11:3347. <https://doi.org/10.1038/s41467-020-16572-3>.
- Austin S, Mekis R, Mohammed SEM, Scalise M, Pfeiffer C, Galluccio M, et a (2021). MICS1 is the Ca<sup>2+</sup>/H<sup>+</sup> antiporter of mammalian mitochondria. *BioRxiv* <https://doi.org/10.1101/2021.11.11.468204>.
- Baughman JM, Perocchi F, Girgis HS, Plovanich M, Belcher-Timme CA, Sancak Y, et al (2011) Integrative genomics identifies MCU as an essential component of the mitochondrial calcium uniporter. *Nature* 476:341–5. <https://doi.org/10.1038/nature10234>.
- Bernardi P, Carraro M, Lippe G (2021) The mitochondrial permeability transition: Recent progress and open questions. *The FEBS Journal* febs.16254. <https://doi.org/10.1111/febs.16254>.
- Bonvento G, Bolaños JP. Astrocyte-neuron metabolic cooperation shapes brain activity (2021) *Cell Metab* 33:1546–64. <https://doi.org/10.1016/j.cmet.2021.07.006>.
- Britti E, Delaspre F, Tamarit J, Ros J (2021) Calpain-inhibitors protect frataxin-deficient dorsal root ganglia neurons from loss of mitochondrial Na<sup>+</sup>/Ca<sup>2+</sup> exchanger, NCLX, and apoptosis. *Neurochem Res* 46:108–19. <https://doi.org/10.1007/s11064-020-03020-3>.
- Britti E, Ros J, Esteras N, Abramov AY (2020) Tau inhibits mitochondrial calcium efflux and makes neurons vulnerable to calcium-induced cell death. *Cell Calcium* 86:102150. <https://doi.org/10.1016/j.ceca.2019.102150>.
- Cabral-Costa JV, Kowaltowski AJ (2020) Neurological disorders and mitochondria. *Mol Aspects Med* 71:100826. <https://doi.org/10.1016/j.mam.2019.10.003>.

- Chinopoulos C, Starkov AA, Grigoriev S, Dejean LM, Kinnally KW, Liu X, et al (2005) Diacylglycerols activate mitochondrial cationic channel(s) and release sequestered Ca<sup>2+</sup>. *J Bioenerg Biomembr* 37:237–47. <https://doi.org/10.1007/s10863-005-6634-0>.
- Collins TJ, Lipp P, Berridge MJ, Bootman MD (2001) Mitochondrial Ca<sup>2+</sup> uptake depends on the spatial and temporal profile of cytosolic Ca<sup>2+</sup> signals. *J Biol Chem* 276:26411–20. <https://doi.org/10.1074/jbc.M101101200>.
- Cornell-Bell AH, Finkbeiner SM (1991) Ca<sup>2+</sup> waves in astrocytes. *Cell Calcium* 12:185–204. [https://doi.org/10.1016/0143-4160\(91\)90020-f](https://doi.org/10.1016/0143-4160(91)90020-f).
- Cornell-Bell AH, Finkbeiner SM, Cooper MS, Smith SJ (1990) Glutamate induces calcium waves in cultured astrocytes: long-range glial signaling. *Science* 247:470–3. <https://doi.org/10.1126/science.1967852>.
- De La Fuente S, Lambert JP, Nichtova Z, Fernandez Sanz C, Elrod JW, Sheu S-S, et al (2018) Spatial separation of mitochondrial calcium uptake and extrusion for energy-efficient mitochondrial calcium signaling in the heart. *Cell Rep* 24:3099–3107.e4. <https://doi.org/10.1016/j.celrep.2018.08.040>.
- De Marchi U, Santo-Domingo J, Castelbou C, Sekler I, Wiederkehr A, Demaurex N (2014) NCLX protein, but not LETM1, mediates mitochondrial Ca<sup>2+</sup> extrusion, thereby limiting Ca<sup>2+</sup>-induced NAD(P)H production and modulating matrix redox state. *J Biol Chem* 289:20377–85. <https://doi.org/10.1074/jbc.M113.540898>.
- De Stefani D, Raffaello A, Teardo E, Szabò I, Rizzuto R (2011) A forty-kilodalton protein of the inner membrane is the mitochondrial calcium uniporter. *Nature* 476:336–40. <https://doi.org/10.1038/nature10230>.
- DeLuca HF, Engstrom GW (1961) Calcium uptake by rat kidney mitochondria. *Proc Natl Acad Sci USA* 47:1744–50. <https://doi.org/10.1073/pnas.47.11.1744>.
- Dimmer KS, Navoni F, Casarin A, Trevisson E, Endeles S, Winterpacht A, et al (2007) LETM1, deleted in Wolf Hirschhorn syndrome is required for normal mitochondrial morphology and cellular viability. *Hum Mol Genet* 17:201–14. <https://doi.org/10.1093/hmg/ddm297>.
- Doczi J, Turiák L, Vajda S, Mándi M, Töröcsik B, Gerencsér AA, et al (2011) Complex contribution of cyclophilin D to Ca<sup>2+</sup>-induced permeability transition in brain mitochondria, with relation to the bioenergetic state. *J Biol Chem* 286:6345–53. <https://doi.org/10.1074/jbc.M110.196600>.
- Dong Z, Shanmughapriya S, Tomar D, Siddiqui N, Lynch S, Nemani N, et al (2017) Mitochondrial Ca<sup>2+</sup> Uniporter is a mitochondrial luminal redox sensor that augments MCU channel activity. *Mol Cell* 65:1014–1028.e7. <https://doi.org/10.1016/j.molcel.2017.01.032>.
- Drahota Z, Lehninger AL (1965) Movements of H<sup>+</sup>, K<sup>+</sup>, and Na<sup>+</sup> during energy-dependent uptake and retention of Ca<sup>++</sup> in rat liver mitochondria. *Biochem Biophys Res Commun* 19:351–6. [https://doi.org/10.1016/0006-291X\(65\)90467-5](https://doi.org/10.1016/0006-291X(65)90467-5).
- Endo M, Tanaka M, Ogawa Y (1970) Calcium induced release of calcium from the sarcoplasmic reticulum of skinned skeletal muscle fibres. *Nature* 228:34–6. <https://doi.org/10.1038/228034a0>.
- Feno S, Rizzuto R, Raffaello A, Vecellio Reane D (2021) The molecular complexity of the Mitochondrial Calcium Uniporter. *Cell Calcium* 93:102322. <https://doi.org/10.1016/j.ceca.2020.102322>.
- Garbincius JF, Luongo TS, Jadiya P, Hildebrand AN, Kolmetzky DW, Mangold AS, et al (2022) Enhanced NCLX-dependent mitochondrial Ca<sup>2+</sup> efflux attenuates pathological remodeling in heart failure. *J Mol Cell Cardiol* 167:52–66. <https://doi.org/10.1016/j.yjmcc.2022.03.001>.
- Giorgi C, Marchi S, Pinton P (2018) The machineries, regulation and cellular functions of mitochondrial calcium. *Nat Rev Mol Cell Biol* 19:713–30. <https://doi.org/10.1038/s41580-018-0052-8>.
- Guerra-Gomes S, Sousa N, Pinto L, Oliveira JF (2018) Functional roles of astrocyte calcium elevations: from synapses to behavior. *Front Cell Neurosci* 11:427. <https://doi.org/10.3389/fncel.2017.00427>.



- Göbel J, Engelhardt E, Pelzer P, Sakthivelu V, Jahn HM, Jevtic M, et al (2020) Mitochondria-endoplasmic reticulum contacts in reactive astrocytes promote vascular remodeling. *Cell Metab* 31:791-808.e8. <https://doi.org/10.1016/j.cmet.2020.03.005>.
- Hagenston AM, Yan J, Bas-Orth C, Tan Y, Sekler I, Bading H (2022) Disrupted expression of mitochondrial NCLX sensitizes neuroglial networks to excitotoxic stimuli and renders synaptic activity toxic. *J Biol Chem* 298:101508. <https://doi.org/10.1016/j.jbc.2021.101508>.
- Haworth RA, Hunter DR (1979) The Ca<sup>2+</sup>-induced membrane transition in mitochondria: II. Nature of the Ca<sup>2+</sup> trigger site. *Arch Biochem Biophys* 195:460-7. [https://doi.org/10.1016/0003-9861\(79\)90372-2](https://doi.org/10.1016/0003-9861(79)90372-2).
- Hernansanz-Agustín P, Choya-Foces C, Carregal-Romero S, Ramos E, Oliva T, Villa-Piña T, et al (2020) Na<sup>+</sup> controls hypoxic signalling by the mitochondrial respiratory chain. *Nature* 586:287-91. <https://doi.org/10.1038/s41586-020-2551-y>.
- Hunter DR, Haworth RA (1979a) The Ca<sup>2+</sup>-induced membrane transition in mitochondria: I. The protective mechanisms. *Arch Biochem Biophys* 195:453-9. [https://doi.org/10.1016/0003-9861\(79\)90371-0](https://doi.org/10.1016/0003-9861(79)90371-0).
- Hunter DR, Haworth RA (1979b) The Ca<sup>2+</sup>-induced membrane transition in mitochondria: III. Transitional Ca<sup>2+</sup> release. *Arch Biochem Biophys* 195:468-77. [https://doi.org/10.1016/0003-9861\(79\)90373-4](https://doi.org/10.1016/0003-9861(79)90373-4).
- Huntington TE, Srinivasan R (2021) Astrocytic mitochondria in adult mouse brain slices show spontaneous calcium influx events with unique properties. *Cell Calcium* 96:102383. <https://doi.org/10.1016/j.ceca.2021.102383>.
- Jackson JG, O'Donnell JC, Takano H, Coulter DA, Robinson MB (2014) Neuronal activity and glutamate uptake decrease mitochondrial mobility in astrocytes and position mitochondria near glutamate transporters. *J Neurosci* 34:1613-24. <https://doi.org/10.1523/JNEUROSCI.3510-13.2014>.
- Jackson JG, Robinson MB (2015) Reciprocal regulation of mitochondrial dynamics and calcium signaling in astrocyte processes. *J Neurosci* 35:15199-213. <https://doi.org/10.1523/JNEUROSCI.2049-15.2015>.
- Jadiya P, Kolmetzky DW, Tomar D, Di Meco A, Lombardi AA, Lambert JP, et al (2019) Impaired mitochondrial calcium efflux contributes to disease progression in models of Alzheimer's disease. *Nat Commun* 10:3885. <https://doi.org/10.1038/s41467-019-11813-6>.
- Jiang D, Zhao L, Clapham DE (2009) Genome-wide RNAi screen identifies Letm1 as a mitochondrial Ca<sup>2+</sup>/H<sup>+</sup> antiporter. *Science* 326:144-7. <https://doi.org/10.1126/science.1175145>.
- Joiner MA, Koval OM, Li J, He BJ, Allamargot C, Gao Z, et al (2012) CaMKII determines mitochondrial stress responses in heart. *Nature* 491:269-73. <https://doi.org/10.1038/nature11444>.
- Juaristi I, Contreras L, González-Sánchez P, Pérez-Liévana I, González-Moreno L, Pardo B, et al (2019a) The response to stimulation in neurons and astrocytes. *Neurochem Res* 44:2385-91. <https://doi.org/10.1007/s11064-019-02803-7>.
- Juaristi I, Llorente-Folch I, Satrustegui J, del Arco A (2019b) Extracellular ATP and glutamate drive pyruvate production and energy demand to regulate mitochondrial respiration in astrocytes. *Glia* 67:759-74. <https://doi.org/10.1002/glia.23574>.
- Kamer KJ, Mootha VK (2014) MICU1 and MICU2 play nonredundant roles in the regulation of the mitochondrial calcium uniporter. *EMBO Rep* 15:299-307. <https://doi.org/10.1002/embr.201337946>.
- Katoshevski T, Ben-Kasus Nissim T, Sekler I (2021) Recent studies on NCLX in health and diseases. *Cell Calcium* 94:102345. <https://doi.org/10.1016/j.ceca.2020.102345>.
- Kawamoto EM, Vivar C, Camandola S (2012) Physiology and pathology of calcium signaling in the brain. *Front Pharmacol* 3. <https://doi.org/10.3389/fphar.2012.00061>.
- Khakh BS, Deneen B (2019) The emerging nature of astrocyte diversity. *Annu Rev Neurosci* 42:187-207. <https://doi.org/10.1146/annurev-neuro-070918-050443>.

- Kostic M, Katoshevski T, Sekler I (2018) Allosteric regulation of NCLX by mitochondrial membrane potential links the metabolic state and Ca<sup>2+</sup> signaling in mitochondria. *Cell Rep* 25:3465–3475.e4. <https://doi.org/10.1016/j.celrep.2018.11.084>.
- Kostic M, Ludtmann MHR, Bading H, Hershinkel M, Steer E, Chu CT, et al (2015) PKA Phosphorylation of NCLX Reverses Mitochondrial Calcium Overload and Depolarization, Promoting Survival of PINK1-Deficient Dopaminergic Neurons. *Cell Reports* 13:376–86. <https://doi.org/10.1016/j.celrep.2015.08.079>.
- Kowaltowski AJ, Castilho RF, Vercesi AE (1996) Opening of the mitochondrial permeability transition pore by uncoupling or inorganic phosphate in the presence of Ca<sup>2+</sup> is dependent on mitochondrial-generated reactive oxygen species. *FEBS Letters* 378:150–2. [https://doi.org/10.1016/0014-5793\(95\)01449-7](https://doi.org/10.1016/0014-5793(95)01449-7).
- Lehninger AL, Rossi CS, Greenawalt JW (1963) Respiration-dependent accumulation of inorganic phosphate and Ca<sup>++</sup> by rat liver mitochondria. *Biochem Biophys Res Commun* 10:444–8. [https://doi.org/10.1016/0006-291X\(63\)90377-2](https://doi.org/10.1016/0006-291X(63)90377-2).
- Lin Y, Li L-L, Nie W, Liu X, Adler A, Xiao C, et al (2019) Brain activity regulates loose coupling between mitochondrial and cytosolic Ca<sup>2+</sup> transients. *Nat Commun* 10:5277. <https://doi.org/10.1038/s41467-019-13142-0>.
- Llorente-Folch I, Rueda CB, Pardo B, Szabadkai G, Duchen MR, Satrustegui J (2015) The regulation of neuronal mitochondrial metabolism by calcium: regulation of neuronal mitochondrial metabolism. *J Physiol* 593:3447–62. <https://doi.org/10.1113/jp270254>.
- Lourenço CF, Laranjinha J (2021). Nitric oxide pathways in neurovascular coupling under normal and stress conditions in the brain: strategies to rescue aberrant coupling and improve cerebral blood flow. *Front Physiol* 12:729201. <https://doi.org/10.3389/fphys.2021.729201>.
- Ludtmann MHR, Kostic M, Horne A, Gandhi S, Sekler I, Abramov AY (2019) LRRK2 deficiency induced mitochondrial Ca<sup>2+</sup> efflux inhibition can be rescued by Na<sup>+</sup>/Ca<sup>2+</sup>/Li<sup>+</sup> exchanger upregulation. *Cell Death Dis* 10:265. <https://doi.org/10.1038/s41419-019-1469-5>.
- Luongo TS, Lambert JP, Gross P, Nwokedi M, Lombardi AA, Shanmughapriya S, et al (2017) The mitochondrial Na<sup>+</sup>/Ca<sup>2+</sup> exchanger is essential for Ca<sup>2+</sup> homeostasis and viability. *Nature* 545:93–7. <https://doi.org/10.1038/nature22082>.
- Murphy AN, Bredesen DE, Cortopassi G, Wang E, Fiskum G (1996) Bcl-2 potentiates the maximal calcium uptake capacity of neural cell mitochondria. *Proc Natl Acad Sci USA* 93:9893–8. <https://doi.org/10.1073/pnas.93.18.9893>.
- Nicholls DG (2017) Brain mitochondrial calcium transport: origins of the set-point concept and its application to physiology and pathology. *Neurochem Int* 109:5–12. <https://doi.org/10.1016/j.neuint.2016.12.018>.
- Nita II, Hershinkel M, Fishman D, Ozeri E, Rutter GA, Sensi SL, et al (2012) The mitochondrial Na<sup>+</sup>/Ca<sup>2+</sup> exchanger upregulates glucose dependent Ca<sup>2+</sup> signalling linked to insulin secretion. *PLoS ONE* 7:e46649. <https://doi.org/10.1371/journal.pone.0046649>.
- Nita II, Hershinkel M, Kantor C, Rutter GA, Lewis EC, Sekler I (2014) Pancreatic β-cell Na<sup>+</sup> channels control global Ca<sup>2+</sup> signaling and oxidative metabolism by inducing Na<sup>+</sup> and Ca<sup>2+</sup> responses that are propagated into mitochondria. *FASEB J* 28:3301–12. <https://doi.org/10.1096/fj.13-248161>.
- Nita II, Hershinkel M, Lewis EC, Sekler I (2015) A crosstalk between Na<sup>+</sup> channels, Na<sup>+</sup>/K<sup>+</sup> pump and mitochondrial Na<sup>+</sup> transporters controls glucose-dependent cytosolic and mitochondrial Na<sup>+</sup> signals. *Cell Calcium* 57:69–75. <https://doi.org/10.1016/j.ceca.2014.12.007>.
- Okubo Y, Kanemaru K, Suzuki J, Kobayashi K, Hirose K, Iino M (2019) Inositol 1,4,5-trisphosphate receptor type 2-independent Ca<sup>2+</sup> release from the endoplasmic reticulum in astrocytes. *Glia* 67:113–24. <https://doi.org/10.1002/glia.23531>.
- Oliveira JF, Araque A (2022) Astrocyte regulation of neural circuit activity and network states. *Glia* 67:24178. <https://doi.org/10.1002/glia.24178>.

- Oliveira JMA, Gonçalves J (2009) In situ mitochondrial  $\text{Ca}^{2+}$  buffering differences of intact neurons and astrocytes from cortex and striatum. *J Biol Chem* 284:5010–20. <https://doi.org/10.1074/jbc.M807459200>.
- Paillard M, Csordás G, Szanda G, Golenár T, Debattisti V, Bartok A, et al (2017) Tissue-specific mitochondrial decoding of cytoplasmic  $\text{Ca}^{2+}$  signals is controlled by the stoichiometry of MICU1/2 and MCU. *Cell Reports* 18:2291–300. <https://doi.org/10.1016/j.celrep.2017.02.032>.
- Palty R, Silverman WF, Hershfinkel M, Caporale T, Sensi SL, Parnis J, et al (2010) NCLX is an essential component of mitochondrial  $\text{Na}^+/\text{Ca}^{2+}$  exchange. *Proc Natl Acad Sci USA* 107:436–41. <https://doi.org/10.1073/pnas.0908099107>.
- Parnis J, Montana V, Delgado-Martinez I, Matyash V, Parpura V, Kettenmann H, et al (2013) Mitochondrial exchanger NCLX plays a major role in the intracellular  $\text{Ca}^{2+}$  signaling, gliotransmission, and proliferation of astrocytes. *J Neurosci* 33:7206–19. <https://doi.org/10.1523/JNEUROSCI.5721-12.2013>.
- Pathak T, Gueguinou M, Walter V, Delierneux C, Johnson MT, Zhang X, et al (2020) Dichotomous role of the human mitochondrial  $\text{Na}^+/\text{Ca}^{2+}/\text{Li}^+$  exchanger NCLX in colorectal cancer growth and metastasis. *ELife* 9:e59686. <https://doi.org/10.7554/eLife.59686>.
- Patron M, Granatiero V, Espino J, Rizzuto R, De Stefani D (2019). MICU3 is a tissue-specific enhancer of mitochondrial calcium uptake. *Cell Death Differ* 26:179–95. <https://doi.org/10.1038/s41418-018-0113-8>.
- Patron M, Tarasenko D, Nolte H, Kroczeck L, Ghosh M, Ohba Y, et al (2022) Regulation of mitochondrial proteostasis by the proton gradient. *EMBO J* 41:e110476 <https://doi.org/10.15252/embj.2021110476>.
- Payne R, Hoff H, Roskowski A, Foskett JK (2017) MICU2 restricts spatial crosstalk between  $\text{InsP}_3$  R and MCU channels by regulating threshold and gain of MICU1-mediated inhibition and activation of MCU. *Cell Rep* 21:3141–54. <https://doi.org/10.1016/j.celrep.2017.11.064>.
- Pearce B, Albrecht J, Morrow C, Murphy S (1986) Astrocyte glutamate receptor activation promotes inositol phospholipid turnover and calcium flux. *Neurosci Lett* 72:335–40. [https://doi.org/10.1016/0304-3940\(86\)90537-9](https://doi.org/10.1016/0304-3940(86)90537-9).
- Peluso MJ, Deeks SG, Mustapic M, Kapogiannis D, Henrich TJ, Lu S, et al (2022) SARS-CoV-2 and mitochondrial proteins in neural-derived exosomes of COVID-19. *Ann Neurol* 91:772–781. <https://doi.org/10.1002/ana.26350>.
- Perocchi F, Gohil VM, Girgis HS, Bao XR, McCombs JE, Palmer AE, et al (2010) MICU1 encodes a mitochondrial EF hand protein required for  $\text{Ca}^{2+}$  uptake. *Nature* 467:291–6. <https://doi.org/10.1038/nature09358>.
- Plovanich M, Bogorad RL, Sancak Y, Kamer KJ, Strittmatter L, Li AA, et al (2013) MICU2, a paralog of MICU1, resides within the Mitochondrial Uniporter Complex to regulate calcium handling. *PLoS ONE* 8:e55785. <https://doi.org/10.1371/journal.pone.0055785>.
- Raffaello A, De Stefani D, Sabbadin D, Teardo E, Merli G, Picard A, et al (2013) The mitochondrial calcium uniporter is a multimer that can include a dominant-negative pore-forming subunit. *EMBO J* 32:2362–76. <https://doi.org/10.1038/emboj.2013.157>.
- Rizzuto R, Brini M, Murgia M, Pozzan T (1993) Microdomains with high  $\text{Ca}^{2+}$  close to IP<sub>3</sub>-sensitive channels that are sensed by neighboring mitochondria. *Science* 262:744–7. <https://doi.org/10.1126/science.8235595>.
- Rizzuto R, Simpson AWM, Brini M, Pozzan T (1992) Rapid changes of mitochondrial  $\text{Ca}^{2+}$  revealed by specifically targeted recombinant aequorin. *Nature* 358:325–7. <https://doi.org/10.1038/358325a0>.
- Rudolf R, Mongillo M, Magalhães PJ, Pozzan T (2004) In vivo monitoring of  $\text{Ca}^{2+}$  uptake into mitochondria of mouse skeletal muscle during contraction. *J Cell Biol* 166:527–36. <https://doi.org/10.1083/jcb.200403102>.
- Samanta K, Mirams GR, Parekh AB (2018) Sequential forward and reverse transport of the  $\text{Na}^+/\text{Ca}^{2+}$  exchanger generates  $\text{Ca}^{2+}$  oscillations within mitochondria. *Nat Commun* 9:156. <https://doi.org/10.1038/s41467-017-02638-2>.

- Sancak Y, Markhard AL, Kitami T, Kovács-Bogdán E, Kamer KJ, Udeshi ND, et al (2013) EMRE is an essential component of the mitochondrial calcium uniporter complex. *Science* 342:1379–82. <https://doi.org/10.1126/science.1242993>.
- Serna JDC, de Miranda Ramos V, Cabral-Costa JV, Vilas-Boas EA, Amaral AG, Ohya G, et al (2022) Measuring mitochondrial Ca<sup>2+</sup> efflux in isolated mitochondria and permeabilized cells. *Bioenerg Comm* 2022.7. <https://doi.org/10.26124/BEC:2022-0007>.
- Serrat R, Covelo A, Kouskoff V, Delcasso S, Ruiz-Calvo A, Chenouard N, et al (2021) Astroglial ER-mitochondria calcium transfer mediates endocannabinoid-dependent synaptic integration. *Cell Rep* 37:110133. <https://doi.org/10.1016/j.celrep.2021.110133>.
- Sharma V, Roy S, Sekler I, O'Halloran DM (2017) The NCLX-type Na<sup>+</sup>/Ca<sup>2+</sup> exchanger NCX-9 is required for patterning of neural circuits in *Caenorhabditis elegans*. *J Biol Chem* 292:5364–77. <https://doi.org/10.1074/jbc.M116.758953>.
- Simpson PB, Mehotra S, Langley D, Sheppard CA, Russell JT (1998) Specialized distributions of mitochondria and endoplasmic reticulum proteins define Ca<sup>2+</sup> wave amplification sites in cultured astrocytes. *J Neurosci Res* 52:672–83. [https://doi.org/10.1002/\(SICI\)1097-4547\(19980615\)52:6<672::AID-JNR6>3.0.CO;2-5](https://doi.org/10.1002/(SICI)1097-4547(19980615)52:6<672::AID-JNR6>3.0.CO;2-5).
- Smith IF, Boyle JP, Kang P, Rome S, Pearson HA, Peers C (2004) Hypoxic regulation of Ca<sup>2+</sup> signaling in cultured rat astrocytes. *Glia* 49:153–7. <https://doi.org/10.1002/glia.20083>.
- Stavsky A, Stoler O, Kostic M, Katoshevsky T, Assali EA, Savic I, et al (2021) Aberrant activity of mitochondrial NCLX is linked to impaired synaptic transmission and is associated with mental retardation. *Commun Biol* 4:666. <https://doi.org/10.1038/s42003-021-02114-0>.
- Stephen T-L, Higgs NF, Sheehan DF, Al Awabdh S, López-Doménech G, Arancibia-Carcamo IL, et al (2015) Miro1 regulates activity-driven positioning of mitochondria within astrocytic processes apposed to synapses to regulate intracellular calcium signaling. *J Neurosci* 35:15996–6011. <https://doi.org/10.1523/JNEUROSCI.2068-15.2015>.
- Tsai M-F, Jiang D, Zhao L, Clapham D, Miller C (2014) Functional reconstitution of the mitochondrial Ca<sup>2+</sup>/H<sup>+</sup> antiporter Letm1. *J Gen Physiol* 143:67–73. <https://doi.org/10.1085/jgp.201311096>.
- Vasington FD, Murphy JV (1962) Ca<sup>++</sup> uptake by rat kidney mitochondria and its dependence on respiration and phosphorylation. *J Biol Chem* 237:2670–7. [https://doi.org/10.1016/S0021-9258\(19\)73805-8](https://doi.org/10.1016/S0021-9258(19)73805-8).
- Vercesi AE, Castilho RF, Kowaltowski AJ, de Oliveira HCF, de Souza-Pinto NC, Figueira TR, et al (2018) Mitochondrial calcium transport and the redox nature of the calcium-induced membrane permeability transition. *Free Rad Biol Med* 129:1–24. <https://doi.org/10.1016/j.freeradbiomed.2018.08.034>.
- Wu J, Holstein JD, Upadhyay G, Lin D-T, Conway S, Muller E, et al (2007) Purinergic receptor-stimulated IP3-mediated Ca<sup>2+</sup> release enhances neuroprotection by increasing astrocyte mitochondrial metabolism during aging. *J Neurosci* 27:6510–20. <https://doi.org/10.1523/JNEUROSCI.1256-07.2007>.
- Zheng W, Talley Watts L, Holstein DM, Wewer J, Lechleiter JD (2013) P2Y1R-initiated, IP3R-dependent stimulation of astrocyte mitochondrial metabolism reduces and partially reverses ischemic neuronal damage in mouse. *J Cereb Blood Flow Metab* 33:600–11. <https://doi.org/10.1038/jcbfm.2012.214>.

**Copyright:** © 2022 The authors. This is an Open Access preprint (not peer-reviewed) distributed under the terms of the Creative Commons Attribution License, which permits unrestricted use, distribution, and reproduction in any medium, provided the original authors and source are credited. © remains with the authors, who have granted MitoFit Preprints an Open Access publication license in perpetuity.



## CHAPTER 3

### ***In vivo* and *in vitro* manipulation of the mitochondrial Na<sup>+</sup>/Ca<sup>2+</sup> (NCLX) exchanger: general methodological approaches**

*“A ciência é mais do que o conhecimento acumulado do mundo natural. É uma visão de mundo, um estilo de vida, uma aspiração coletiva de crescermos como espécie em um cosmos repleto de mistérios, de medos e de encantos. A ciência é o cobertor com que cobrimos os pés à noite, a luz que ligamos no fim do corredor, o mentor paciente que nos lembra do que somos capazes quando trabalhamos juntos. Que a ciência é usada tanto para o bem quanto para o mal não reflete a ciência em si, mas a precariedade da natureza humana, a tendência que temos tanto para criar quanto para destruir.”*

(Gleiser, 2014, p. 326)

### 3.1 Summary

Given the significance of mitochondrial homeostasis for central nervous system pathophysiology (reviewed in the Chapter 1) and the importance of the mitochondrial Ca<sup>2+</sup> handling system for brain function (reviewed in the Chapter 2), we sought to characterize the role of the mitochondrial Na<sup>+</sup>/Ca<sup>2+</sup> exchanger (NCLX) in astrocyte physiology, focusing on its metabolic effects. We hypothesized that NCLX activity could directly influence metabolic balance and pathways in astrocytes, acting as a regulatory point of control that could ultimately integrate astrocytic physiology with neuronal homeostasis.

In this chapter, we delineate our experimental design, from the *in vivo* functional, behavioral approach through the *in vitro* assessment of the influence of NCLX activity on astrocytic metabolism. We introduce the scientific reasoning behind this design and key methodological validations. Additionally, we discuss the influence of stressful stimuli on NCLX expression, observed in pilot experiments, which led to a parallel initial investigation on the regulation of NCLX expression.



### 3.2 *In vivo* NCLX deletion and behavioral assessment

Given our hypothesis that the mitochondrial  $\text{Na}^+/\text{Ca}^{2+}$  exchanger (NCLX) may have an important role in astrocytic metabolism and function, we aimed to assess this question through both *in vivo* and *in vitro* approaches. To tackle NCLX function *in vivo*, we used of a Cre-loxP system based on a mouse model carrying a floxed *Nclx* gene (*Nclx*<sup>loxP/loxP</sup>, originally denoted *Slc8b1*<sup>loxP/loxP</sup>, constructed and described by Luongo et al. 2017, Fig. 1A), kindly provided by Dr. John W. Elrod (Temple University, Philadelphia, USA) and supplied by Dr. Antonio Martínez-Ruiz (Hospital de La Princesa, Madrid, Spain). Under the activity of Cre recombinase, the loci containing the *Nclx* exons 5-7 is recombined, interrupting NCLX expression.

Cre expression was controlled by an astrocyte-specific (GFAP(0.7)) promoter. In parallel, to allow for the assessment of cell-type specific effects, neuronal deletion (controlled through the CaMKII(0.4) promoter) was also promoted. Cre expression was induced by adeno-associated viral (AAV) vectors that were stereotaxically delivered to *Nclx*<sup>loxP/loxP</sup> mouse brain hippocampi (for further details, please refer to Chapter 4, Material and Methods/Viral Transduction and /Stereotaxic surgery sections). The hippocampus is an important hub connecting many brain areas (including cortical areas and amygdala), involved in information processing such as spatial and recognition learning, and memory consolidation and recall (Opitz, 2014). Therefore, we aimed to assess both behavioral- and tissue-level effects of NCLX deletion *in vivo* using the hippocampus as proxy.

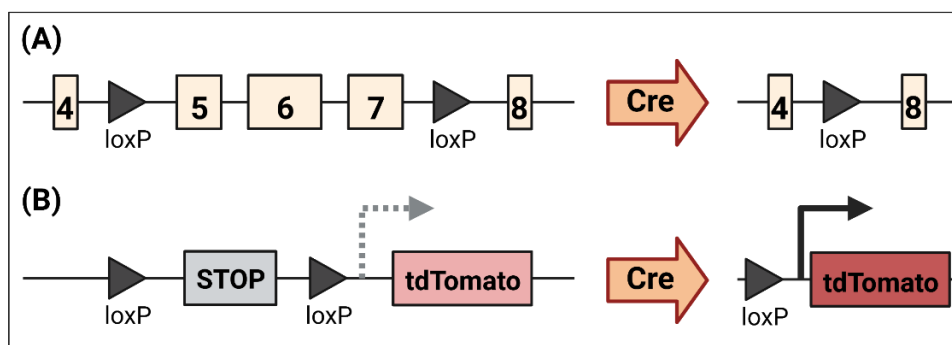


**Figure 1.** *Nclx*<sup>loxP/loxP</sup> and Ai9 Cre reporter constructs. Illustration of (A) *Nclx* floxed gene (adapted from Luongo et al. (2017)), highlighting Cre-mediated recombination that hampers NCLX expression; and (B) Ai9 tdTomato reporter system. Cre-mediated recombination of a stop codon releases the inhibition of tdTomato expression, allowing for the fluorescent reporting of time- and site-specific Cre expression.

Methods for stereotaxical surgery and hippocampal astrocyte viral transduction were previously validated (Jimenez-Blasco et al., 2020; Lapresa et al., 2022). Hippocampal neuronal transduction was validated through a fluorescent reporter mouse line Ai9 (B6.Cg-Gt(ROSA)26Sortm9(CAG-tdTomato)Hze/J, strain #007909, The Jackson Laboratory, Bar

Harbor, USA). These animals carry a *tdTomato* gene, in which expression is limited by a floxed stop codon (Fig. 1B). Thus, in cells that express Cre recombinase – in this case, transduced neurons that activate the CaMKII(0.4) promoter – the stop codon is deleted, allowing for the expression of the fluorescent tdTomato protein. This fluorescence pattern can then be assessed and interpreted as an indicator of cellular and area specificity for Cre recombination (Fig. 2, 3).

Three weeks after transduction, animals were euthanized and had their brains dissected. Samples were post-fixed in 4% PFA, dehydrated in 10-30% sucrose in phosphate-buffered saline (PBS), and stored at 4°C. Cryoprotected brains were cut into slices (20 µm) with a freezing-sliding cryostat (CM1950 AgProtect, Leica, USA), DAPI-stained, and mounted with Fluoromount-G (#0100-01, SouthernBiotech, Birmingham, EUA). Slides were then imaged in a High Content Screening Operetta CLS apparatus (Perkin Elmer, Waltham, USA).

Viral titration (Fig1A,  $1.1 \times 10^{13}$  genome copies (GC)/mL; Fig. 1B,  $5.5 \times 10^{12}$  GC/mL; and Fig. 1C,  $2.75 \times 10^{12}$  GC/mL) was evaluated to assess the minimal dose sufficient to achieve broad hippocampal Cre expression. The two lowest doses showed a more specific profile, staining cells with the expected neuronal morphology and strongly covering the CA1 and CA2 regions of the dorsal hippocampus (Fig. 3A-D), an area that is involved with cognitive functions such as locomotion, exploration, and navigation (Fanselow; Dong, 2010).

Minimal spillage to other brain areas was observed (Fig. 2B,C), mostly covering surrounding frontoparietal cortical and thalamic areas and the contralateral CA1. In addition, to further control for Cre-independent tdTomato expression, we assessed spontaneous reporter expression in mouse testis, a tissue that shares a significant expression profile with the brain (Matos et al., 2021), and found no detectable tdTomato leakage (Fig. 3E-F).

Therefore, we opted to follow through using the lowest dose ( $2.75 \times 10^{12}$  GC/mL), to avoid undesirable off-target effects. The experiment was then replicated in *Nclx*<sup>loxP/loxP</sup> adult mice (~12-week-old). Following stereotaxic surgery, animals were monitored for 3 weeks, to allow for surgery recovery and virally-mediated Cre combination. Functional effects of hippocampal astrocytic or neuronal NCLX deletion were then assessed through three behavioral assays: Open Field, Novel Object Recognition, and Y-maze (further details in Chapter 4/Behavioral assays). All experiments were conducted in a behavior assessment room inside the animal facility (Fig. 4A-C), in which animals were previously familiarized for 5 to 7 days prior to the beginning of experiments, always under controlled temperature, humidity, and lighting.



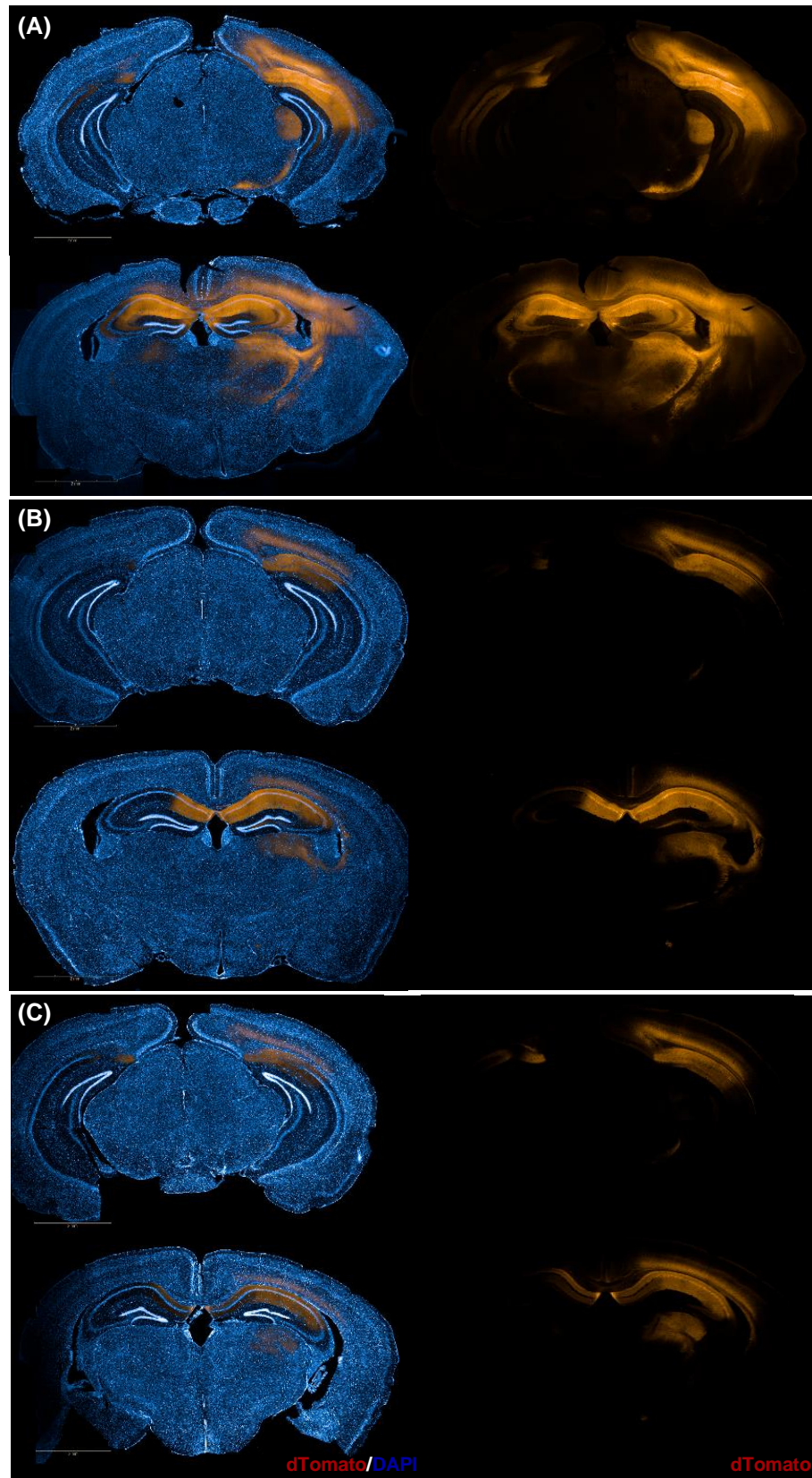


**Figure 2. Dosage validation of AAV/rh10-CamKII(0.4)-eGFP-T2A-Cre virus.** Ai9 mice were stereotaxically injected in a single hemisphere with three viral titers, (A)  $1.1 \times 10^{13}$  GC/mL, (B)  $5.5 \times 10^{12}$  GC/mL, (C)  $2.75 \times 10^{12}$  GC/mL. Neuronal Cre expression induces tdTomato expression, which was followed after three weeks by fluorescence (right side of panels). Nuclei were stained by DAPI and are shown in blue; tdTomato expression was assessed through a dTomato filter and shown in red. (GC: genome copies).

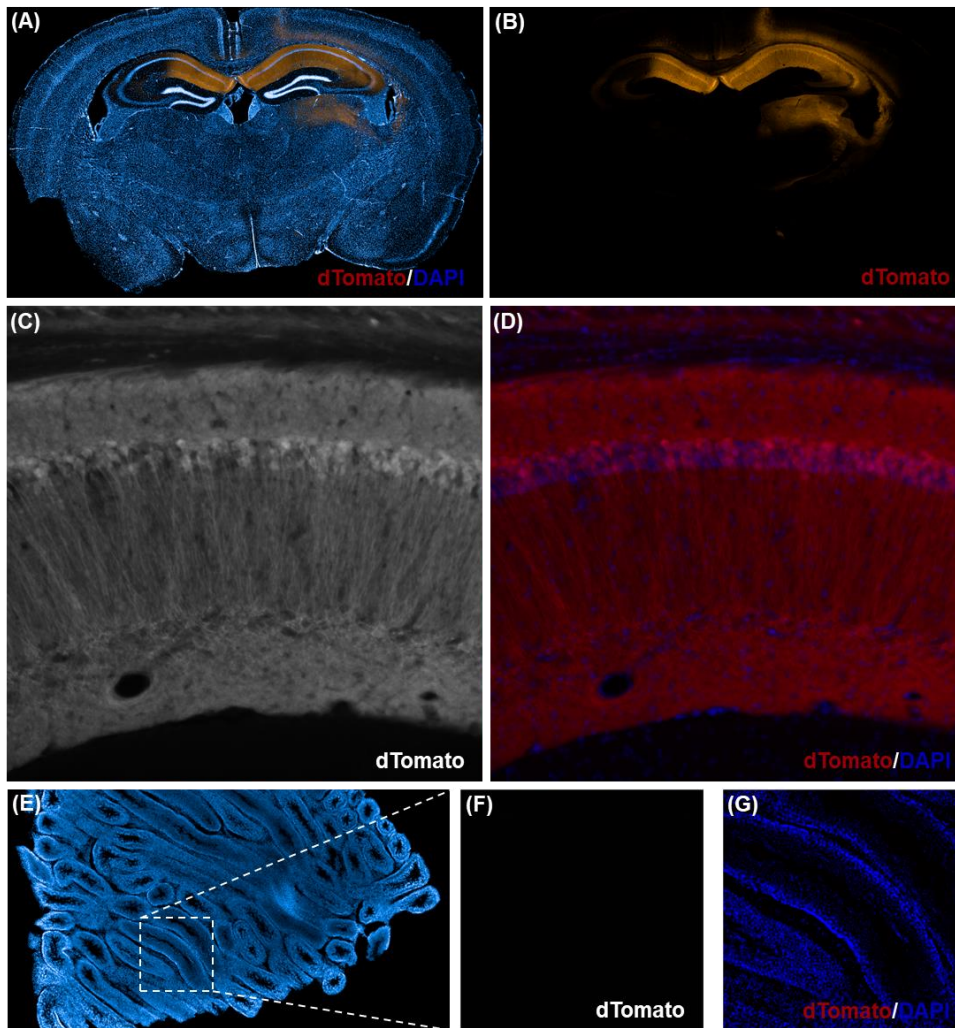


**Figure 3. Expression pattern validation of AAV/rh10-CamKII-eGFP-T2A-iCre virus.** Ai9 mice were stereotaxically injected in a single hemisphere ( $2.75 \times 10^{12}$  GC/mL) and tissue was collected after 3 weeks. tdTomato expression driven by neuronal Cre can be observed as shown in (A) and (B), in a coronal slice. (C, D) Representative image of the CA1 region of a hippocampus, showing a spread expression of tdTomato, with a typically neuronal morphology. (E-G) Testis slice as an additional negative control for spontaneous recombination and expression of tdTomato. Nuclei were stained by DAPI and are shown in blue; tdTomato expression was assessed through a dTomato filter and shown in gray or red, as indicated.

In the Open Field (OF) test, animals are allowed to freely explore the arena, and mobility and exploratory behaviors are assessed. In addition, the exploratory pattern (*e.g.*, avoidance of the central area of the arena) can also be analyzed to evaluate fear- and anxiety-related behaviors (Cabral-Costa et al., 2018). In the Novel Object Recognition (NOR) test, mice are individually exposed to two equal objects in the same arena. Then, after spending time back in their home cages, animals are reintroduced to the arena, now with one of the familiar objects substituted by a novel one (Fig. B). This task relies on mouse innate preference for novelty (Vogel-Ciernia; Wood, 2014; Denninger; Smith; Kirby, 2018). Their recognition memory can thus be indirectly

calculated by their proportional preference for the novel object. Lastly, in the Y-maze, animals are positioned in the center of a three-armed maze. Mice have the tendency to spontaneously alternate their choices between these arms on subsequent entries (Hughes, 2004). Therefore, by calculating the percentage of spontaneous alternation over total arm exploration, we can indirectly infer their spatial working memory performance (Hughes, 2004).

Open Field and Novel Object Recognition (NOR) tests were conducted using two ANY-box cores connected with a AMi-maze photo-beam interface and monitored by digital cameras connected to a computer (Fig. 4A,B). Y-maze assays were conducted in an adapted radial maze that had all but three of its arms closed by a plastic sheet, leaving these three arms, separated by a 120° angle, open to be explored (Fig. 4C,D). Experiments were tracked using the same cameras, which were positioned over the apparatus (Fig. 4C).

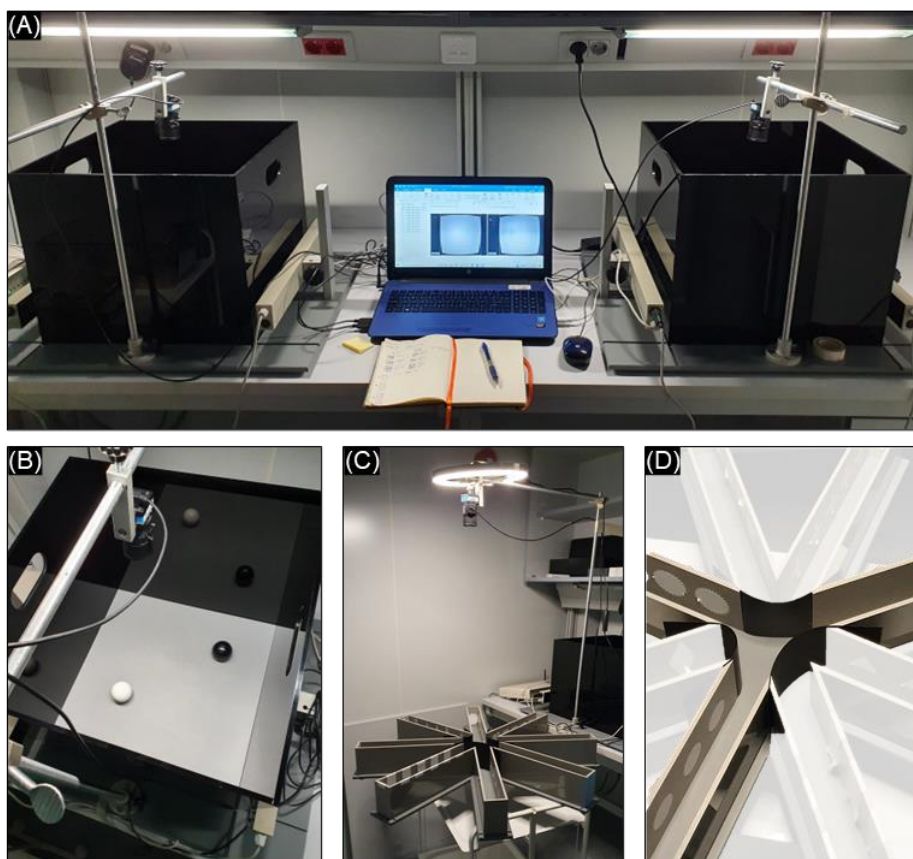


**Figure 4. Behavioral assessment set up.** General view of the behavioral assessment room. For the Open Field and Novel Object Recognition tests, experiments were monitored in parallel by (A) two sets AMi-maze photo-beam interface cores and digital cameras connected to a computer, which tracked the animal movement in a (B) 40 x 40 cm ANY-box arena. For the (C) Y-maze tests, animals were individually tracked using the same camera, which was positioned over a radial maze that was (D) adapted to perform the 3-arm assay.



### 3.3 Mouse astrocyte primary cultures

While *in vivo* deletion of NCLX allows the assessment of complex outputs (such as behavioral performance), *in vitro* approaches offer greater flexibility and sensitivity to dissect the metabolic effects affected by NCLX activity. In this sense, primary astrocyte cultures are a reliable alternative to model astrocyte function, as they maintain several astrocytic physiological and pathological signatures, including energy metabolism (Lange et al., 2012). There are, however, a variety of cultivation protocols available, that vary according to the laboratory of origin and aim of the study (Lange et al., 2012). Here, we followed a well-established protocol that had been extensively validated (Herrero-Mendez et al., 2009; Vicente-Gutierrez et al., 2019; Jimenez-Blasco et al., 2020), kindly made available by Dr. Juan Pedro Bolaños and his team.

In this protocol (Fig. 5), brains are obtained from neonatal mice, usually a litter of 6-8 neonates, from between postnatal day P0-P1, optimally within their first 24 h. Animals are promptly euthanized by decapitation with a sharp razor, in accordance with the bioethical and animal care regulations. Brains are removed with a round-tip curved tweezer or surgical spatula and both hemispheres are dissected, isolating the cortex. The whole isolating process, unless denoted otherwise, is conducted in freshly prepared isolation buffer, consisted of Earle's balanced salt solution (EBSS) – or, alternatively, Hank's balanced salt solution (HBSS) – supplemented with 0.3% bovine serum albumin (BSA) and 24 µg/mL DNase type I.

Meningeal tissue is an important source of contamination with other cell types, and is frequently manually dissected under a stereoscopic binocular microscope (Fig. 6). However, this is a time-consuming process that can compromise tissue quality and, ultimately, cell survival and culture yield, if not tightly controlled. Thus, alternatively, meninges and blood vessels can be removed by gently rolling the isolated tissue over a piece of fine filter paper, with the help of a round-tip, curved tweezer.

Using a scalpel, each hemisphere cortex is cut into four fragments, transferred to a 50 mL conical tube and isolation medium is substituted by digestion buffer, consisted of EBSS (or HBSS) supplemented with 0.3% BSA, 60 µg/mL DNase type I, and 0.1% trypsin (the latter added right before using). Volume of digestion medium varies in accordance with the number of collected brains: 1 mL plus 1 mL per pair of cortex hemispheres. The tube is then incubated in a water bath at 37°C for 10-15 min. To maximize trypsin activity, it is advisable to shake the

tube every 2-3 min, thus avoiding tissue sedimentation. Digestion is interrupted by the addition of pure fetal bovine serum (FBS) to a final concentration of 10% v/v.

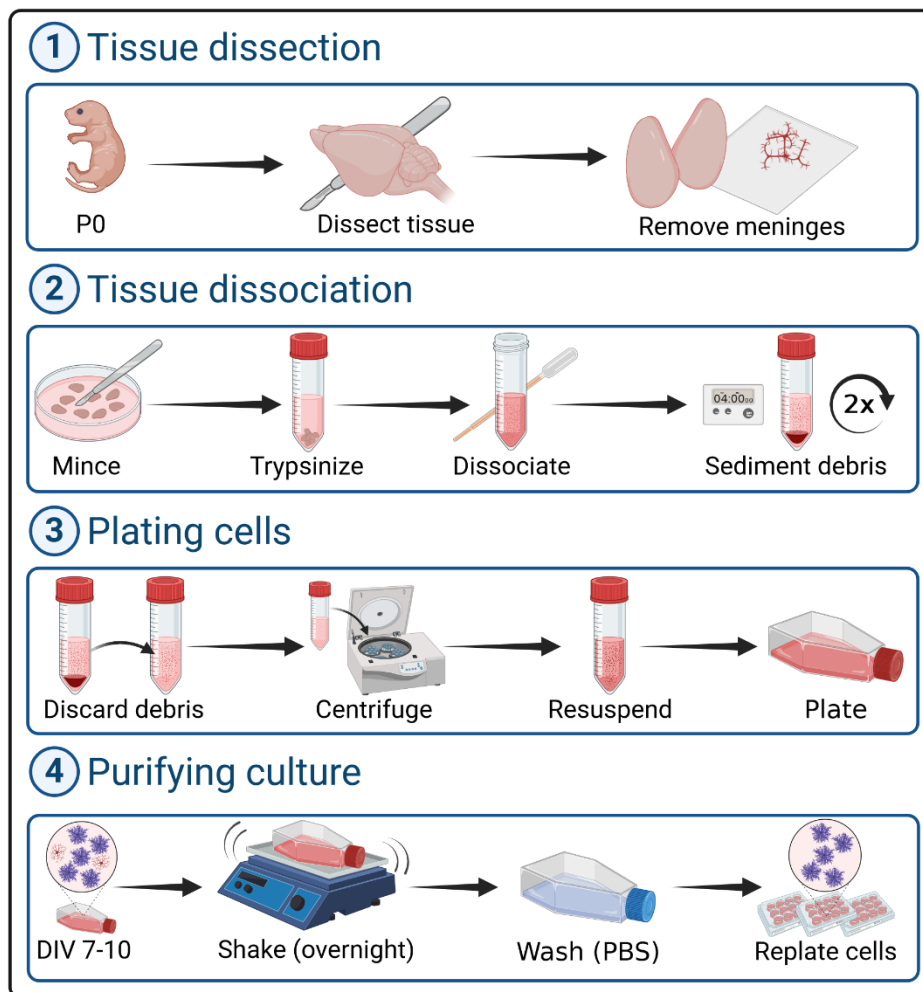


**Figure 5. Mouse astrocyte primary cultures.** Schematic illustration of the protocol used to obtain pure primary astrocyte cultures from mouse cortex. (1) Mouse neonates from up to 24 h of age (P0) are euthanized by decapitation with a sharp blade, and have their brains dissected to isolate the cortex; meninges and blood vessels are removed by gentle movements over a filter paper. (2) Tissue is minced with a sharp scalpel and digested with trypsin to facilitate cell dissociation; cells are dissociated using a fire-polished, silanized, glass Pasteur pipette, and the suspension is partially sedimented to separate tissue debris. (3) This cell suspension is then transferred to a new tube, centrifuged, resuspended in growth medium, and plated. (4) After 7 to 10 days *in vitro* (DIV), plates are shaken overnight to detach microglial cells; growth media (enriched with microglia) is separated or discarded, plates are washed with sterile PBS, and then trypsinized and resuspended; finally, pure astrocytes are plated under the desired experimental conditions, and grown to the desired confluence and/or morphology (~DIV10-15).

Tissue suspension is then centrifuged at 600 x g for 5 min, and the supernatant is carefully removed by aspiration using a glass pipette. Cells are resuspended in 12 mL isolation buffer and gently dissociated by passing 10 times through a silanized fire-polished, sterile glass pipette. This suspension is sedimented for 4 min to separate cellular debris and undissociated tissue, and then the supernatant is transferred to a clean 50 mL tube. This process is repeated by adding 8 mL of isolation buffer over the sedimented debris followed again by 10

resuspensions and the sedimentation step. The resultant supernatant is mixed with the previous step's, and centrifuged at 600 x g for 5 min.

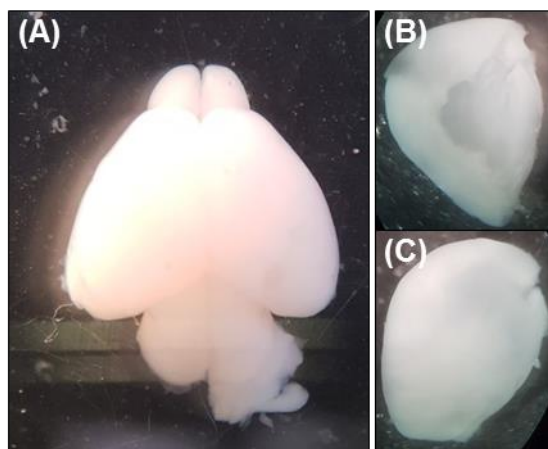


**Figure 6. Representative photograph of a neonatal brain dissection.** Stereoscopic binocular microscope-amplified view of the (A) mouse neonatal brain and dissected cortex, from both (B) medio-lateral and (C) lateromedial perspectives. Samples were obtained from P1 mice and were already devoid of meningeal tissue.

This pellet is gently resuspended in 1 mL warm cultivating medium (Dulbecco's modified Eagle's medium, DMEM, low glucose, supplemented with 10% FBS, 1% penicillin, and 1% streptomycin) with a plastic pipette and by flicking the tube, then finally diluted to the desired, plating density. In general, 3-4 brains are plated on a T175 plate (*i.e.*, 6-10 mL plating suspension per dissected brain).

Plates are maintained in humidified incubators at 37°C and 5% CO<sub>2</sub>, and medium is exchanged every 3-4 days. After 7-10 days *in vitro* (DIV), a confluent culture is expected, with astrocytes covering most, if not all, the plate surface, along with sparse colonies of other cell types (*e.g.*, oligodendrocyte progenitors) and some microglial cells resting over the astrocyte layer. To obtain an enriched, purer primary astrocyte culture, plates are shaken at 150-200 rpm in an incubator overnight. While astrocytes are strongly attached to the plate surface, other contaminant cell types detach more easily. Thus, when medium is removed, the plate is washed with PBS, and astrocytes are trypsinized (0.25% trypsin/EDTA, 10 mL per T175 plate) for 3-4 min. This suspension is transferred to a new 50 mL conical tube, and the plate washed with 10 mL PBS to collect cells that might have remained attached (here, the experimenter may gently slap the side of the plate to facilitate astrocyte detachment). Cells are then centrifuged at 600 x g for 5 min, resuspended in 1-5 mL cultivating medium, counted, diluted, and plated into the desired culture plates. Common plating density is 50.10<sup>3</sup> cells/cm<sup>2</sup>, but this may vary according to the experimental design and desired confluence. Astrocytes will be fully detached and reach

mature morphology from 24-48 h after plating, but it may be advisable to pursue longer cultivation (around DIV15) to achieve an even more mature and/or confluent culture.

As an example, Fig. 7 shows a representative purified astrocytic culture, visualized through immunofluorescence with GFAP (glial fibrillary acidic protein, a fibrous astrocyte marker) staining. Purified astrocytes were grown over glass coverslips, fixed with 4% PFA, permeabilized with 0.25% Triton X-100 in PBS, and blocked in PBS supplemented with 10% BSA and 0.01 Triton X-100. The primary antibody (1:1000 in tris-buffered saline with 0.1% Tween 20, TTBS, anti-GFAP, #3670, Cell Signaling, Danvers, USA) was incubated overnight at 4 °C, followed by three 5 min PBS washes. The secondary antibody was incubated in a similar buffer, for 2 h, followed by a similar washing step. Nuclei were then stained with DAPI (1:20,000) for 30 min in PBS containing 3% BSA and 0.01% Triton X-100. Coverslips were mounted with Fluoromount-G, imaged through a fluorescence microscope (Nikon Eclipse 80i, Nikon Instruments, Melville, USA) and visualized through FIJI ImageJ 1.52p (Schindelin et al., 2012).

Here, we observe confluent astrocytes in culture, covering basically the whole plate surface and exhibiting the expected astrocytic morphology – from more oblong to wide, spread-out cells (Fig. 7). From this point on, astrocytes were ready for treatments, stimuli, and experiments.

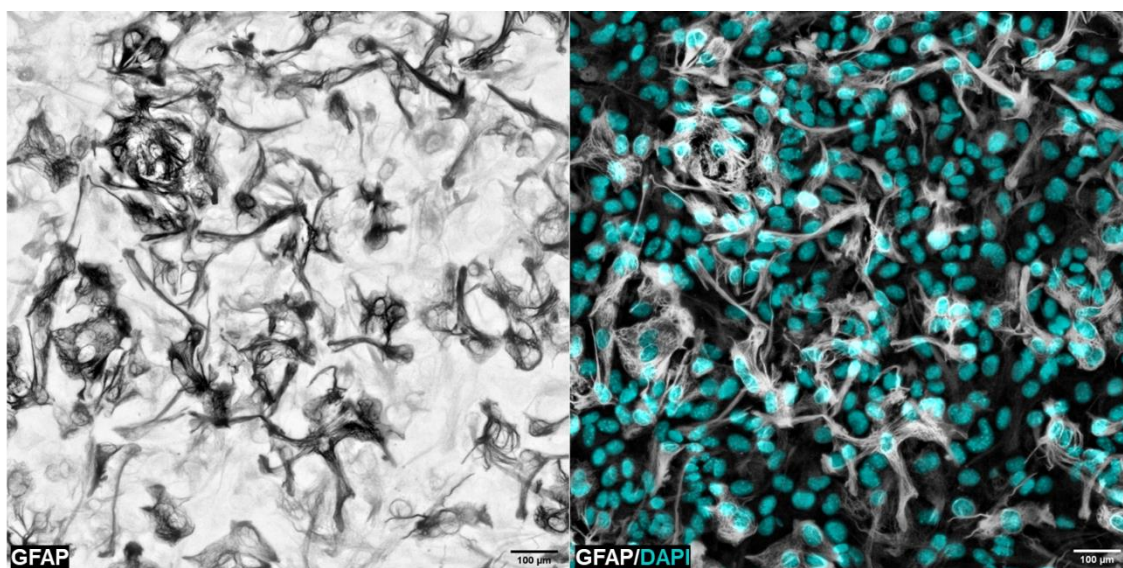


**Figure 7. Characterization of the mouse astrocyte primary cultures.** Representative immunofluorescence photomicrographs of the astrocytes, immunostained with anti-GFAP (in gray or white, as described). Nuclei were stained with DAPI (cyan).

In this thesis, we assessed the importance of NCLX for astrocytic metabolism by modulating its activity with the benzothiazepine CGP-37157, a well-known, widely-used

inhibitor of NCLX (Palty et al., 2010; Parnis et al., 2013; Assali; Sekler, 2021; Serna et al., 2022). Pharmacological inhibition is an interesting tool as it allows for controlled acute modulation of NCLX activity. However, additional approaches, such as silencing or knocking-out NCLX, can complement and validate observed effects. To attain this, we standardized a NCLX knockout model *in vitro*. Brains of neonates from *Nclx*<sup>loxP/loxP</sup> mice were used to obtain primary astrocytes as described above (Fig. 5). Purified cells were re-plated at DIV7, grown for 1 day, and incubated for 24h with an adenoviral vector carrying a Cre recombinase gene under a strong promoter (Ad5-CMV-Cre-eGFP, lot# Ad4334 13D6, University of Iowa Viral Vector Core, Iowa City, IA, USA). As a control, astrocytes were incubated with an empty vector (Ad5-CMV-GFP, lot# Ad4415 13D3, University of Iowa Viral Vector Core).

First, cultures were maintained for 5 days after transduction with different viral multiplicity of infection (MOI; 5, 10, 15, and 20). Total RNA was then extracted and purified from astrocytes using the RNeasy kit (#74004, Qiagen, Germantown, USA). Quantitative reverse transcription polymerase chain reaction (RT-qPCR) was conducted as described by Sánchez-Morán et al. (2020), using a Power SYBR Green RNA-to-CT™ 1-step kit (#4389986, Applied Biosystems, Foster City, USA). Reverse transcription was performed at 48°C for 30 min, followed by PCR amplification (10 min at 95°C followed by 40 cycles of 15 s at 95°C and 1 min at 60°C). Primers used for *Nclx* amplification were 5'-TGTCACCTTCCTGGCCTTTG-3' (forward) and 5'-CACCCCTGCACCAAACAGA-3' (reverse), and for *Actb* (to normalize expression data), 5'-AGAGTCATGAGCTGCCTGAC-3' (forward) and 5'-AGAGTCATGAGCT GCCTGAC-3' (reverse).

We observed that MOI greater than 10 showed similar results, inducing a maximal relative decrease of  $0.69 \pm 0.01$  (fold *Actb*  $\Delta\Delta Ct$ ) (Fig. 8A). Thus, we chose the second smallest dose (15 MOI), to avoid toxic effects, and proceeded with a time-course analysis of *Nclx* mRNA expression following transduction (Fig. 8B). NCLX knockout induced a stable decrease in mRNA levels from day 3 through 7 after viral transduction ( $0.76 \pm 0.04$  fold *Actb*  $\Delta\Delta Ct$ ) (Fig. 8B). To confirm how this effect translated to NCLX protein levels, we cultivated cells under this same condition and followed with a Western blot analysis (Cabral-Costa et al., 2018; Jimenez-Blasco et al., 2020).

Proteins were extracted with RIPA buffer (pH 7.0, 1% sodium dodecyl sulfate, 10 mM EDTA, 1% Triton X-100, 150 mM NaCl, and 10 mM Na<sub>2</sub>HPO<sub>4</sub>) supplemented with phosphatase and protease inhibitors (100  $\mu$ M phenylmethylsulfonyl fluoride, 50  $\mu$ g/mL antipain, 50  $\mu$ g/mL pepstatin, 50  $\mu$ g/mL amastatin, 50  $\mu$ g/mL leupeptin, 50  $\mu$ g/mL bestatin,



1 mM orthovanadate, 50 mM NaF and 50  $\mu$ g/ml soybean trypsin inhibitor). Samples were prepared and loaded into a 10% acrylamide gel, electrophoretically resolved, and transferred to a nitrocellulose membrane. After blocking (5% low-fat milk in TTBS buffer), membranes were incubated with primary anti-NCLX antibodies (overnight at 4°C, 1:1,000 in blocking buffer; #ab136975, Abcam, Cambridge, United Kingdom) and anti- $\beta$ -actin antibodies (1 h at room temperature, 1:30,000 in blocking buffer; #A5441, Sigma-Aldrich, Saint Louis, MO, USA), and then with secondary, horseradish peroxidase-conjugated, goat anti-rabbit and goat anti-mouse antibodies (1:10,000 in blocking buffer; Santa Cruz Biotechnology, Dallas, USA). Membranes were washed 5 times for 5 min with TTBS after each incubation, and then developed by chemiluminescence in a Vilber Fusion Fx imaging system (Vilber, Collégien, France), using WesternBright ECL (#K-12045, Advansta, San Jose, USA) or a SuperSignal West Femto Maximum Sensitivity Substrate (#34095, Thermo Fisher Scientific, Rockford, USA) kits. Images were then quantified by densitometric analysis through FIJI ImageJ 1.52p (Schindelin et al., 2012).

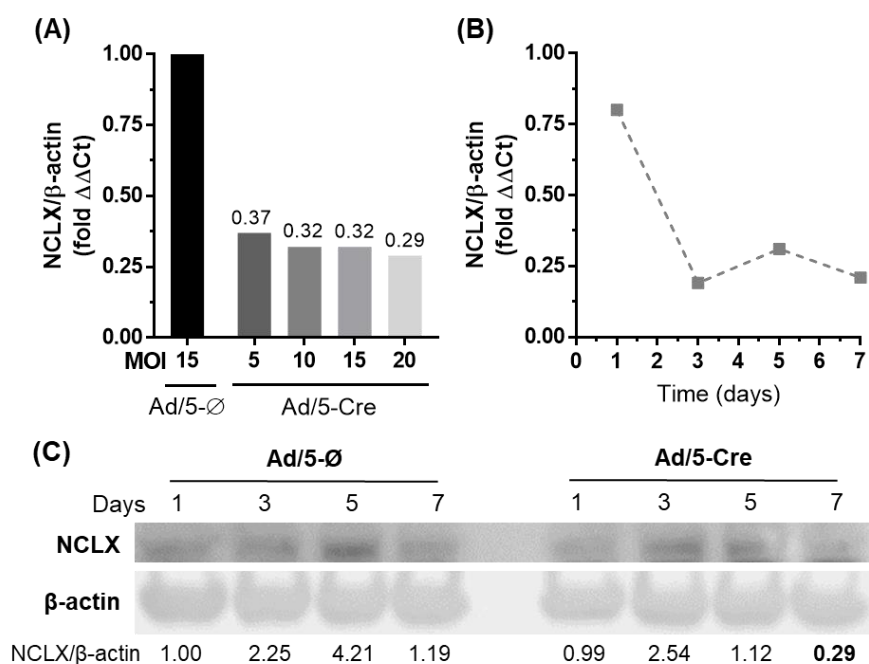


**Figure 8. Validation of NCLX knockout induced by adenoviral-mediated Cre recombinase expression.** Representative experiments. (A) Multiplicity of infection (MOI) optimization of Ad/5-CMV-Cre necessary for NCLX deletion. NCLX expression was assessed 5 days after transduction; (B) NCLX expression time-course after viral transduction with a MOI of 15; (C) NCLX protein levels time-course after viral transduction with a MOI of 15.

Western blot analysis showed that NCLX levels were only reduced 7 days after transduction (~71% reduction in comparison with control on day 1, Fig. 8C). Therefore, experiments with astrocytes were conducted on the seventh day after transduction. Interestingly, NCLX levels appeared to increase on the first days (Fig. 8C, most noticeable on

control group). This did not affect our experimental design, as NCLX expression was normalized at day 7. Yet this result caught our attention, as it could indicate that NCLX expression may be modulated by stressful stimuli, motivating us to explore the regulatory background of NCLX expression in parallel (section 3.5).

### 3.4 *In vitro* metabolic assessment

Astrocytic metabolic function was assessed through complementary approaches, both under NCLX pharmacological inhibition and genetic knockout (Fig. 9). Pharmacological modulation of NCLX activity was conducted by incubation with 10  $\mu$ M CGP-37157 for 4 h (glycolytic flux, glucose consumption, lactate secretion), 1 h or acutely during experiments (Seahorse assays, live imaging). Astrocytes with NCLX deletion were used 7 days after viral transduction, or earlier, during standardization steps.

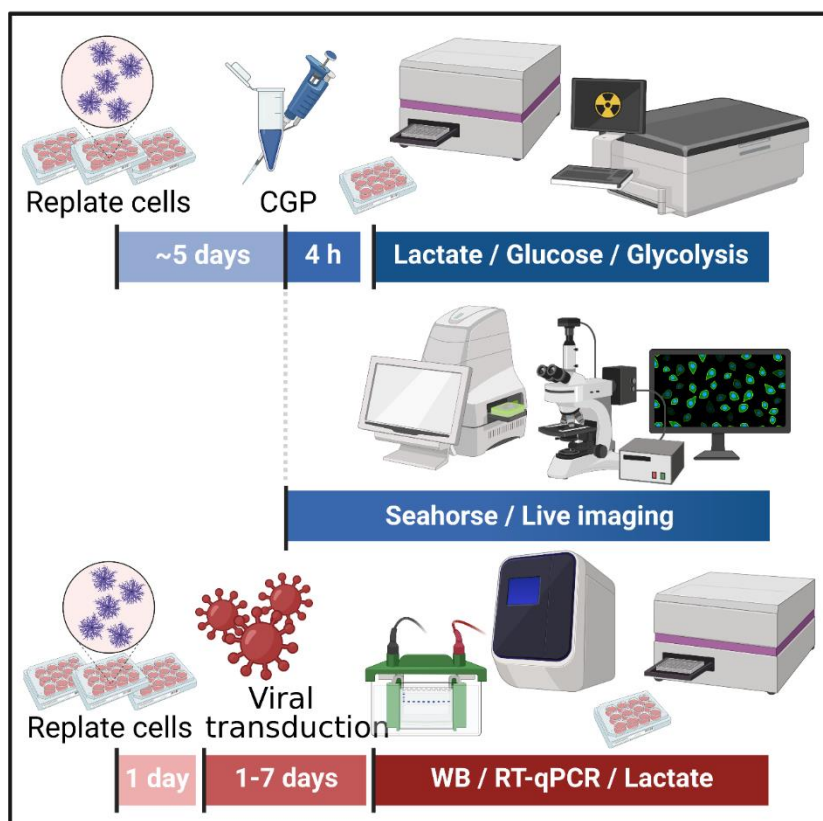


**Figure 9. *In vitro* experimental design.** General depiction of *in vitro* approaches to assess the metabolic effects of NCLX activity modulation through pharmacological inhibition or genetic deletion.

First, we assessed astrocyte ATP production rates through a Seahorse XFe24 analyzer, an apparatus that allows real-time, sensitive measurement of cell media pH and oxygen concentrations (Fig. 10A, further refer to 4.5.4 Seahorse assays for further details). Thus, it is possible to calculate oxygen consumption (OCR) and extracellular acidification (ECAR) rates.

Mookerjee et al. (2017) previously validated a method to quantify intracellular mitochondrial and glycolytic ATP production rates, based on OCRs and ECARs under basal and stimulated conditions, followed by inhibition of mitochondrial ATP synthesis and electron transport chain activity. This method is well established using Seahorse devices (Romero et al., 2018, Fig. 10B). ATP production rates are estimated based on the proton efflux rate (PER), *i.e.*, the number of protons extruded by the cells over time, which is proportional to glycolytic flux. However, mitochondrial ATP production also indirectly contributes to media acidification, as CO<sub>2</sub> (produced by the reactions catalyzed by pyruvate, isocitrate and α-ketoglutarate dehydrogenases) can be hydrated and dissociated into HCO<sub>3</sub><sup>-</sup> and H<sup>+</sup> (Mookerjee et al., 2017). This mitochondrial contribution to PER can be accounted for by quantifying mitochondrial-dependent oxygen consumption and calculating the CO<sub>2</sub>-contribution factor (CCF) to the pH variation. Therefore, considering the medium buffer factor, it is possible to calculate the glycolytic ATP production rate (glycoATP, Fig. 10B). Finally, by finding the oxygen consumption rate associated with ATP synthesis (OCR<sub>ATP</sub>) and associating the expected stoichiometry of ATP produced by O<sub>2</sub> reduced (P/O ratio), it is possible to calculate mitochondrial, as well as total, ATP production rates (Fig. 10B).

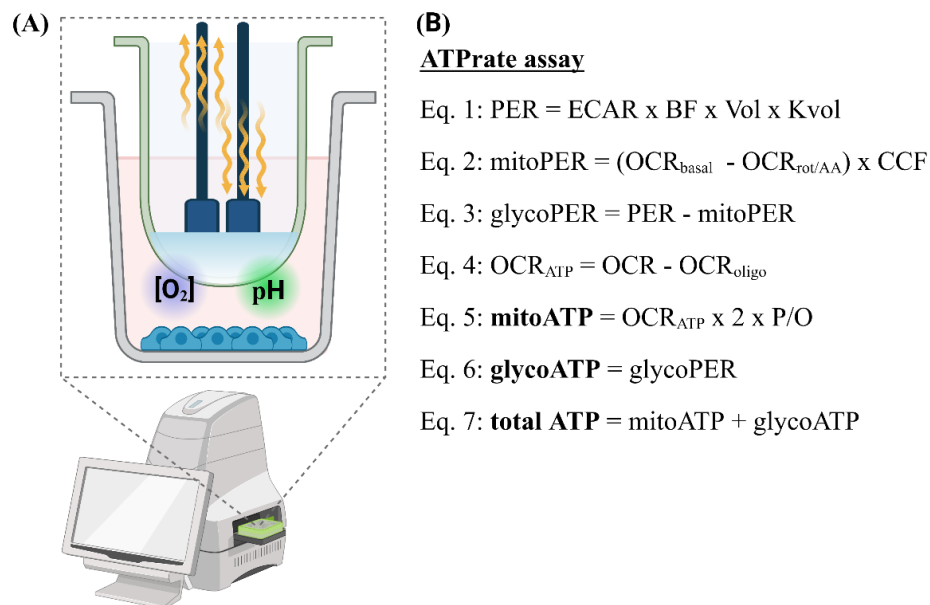


**Figure 10. Seahorse apparatus.** Schematic depiction of a Seahorse XFe24 apparatus and the principle behind ATPrate measurement. (A) After the mixing and waiting stages, that allows for equilibration between atmospheric and media oxygen concentrations, the cartridge sensors are lowered and form a microchamber with 7 μL media surrounding the surface of attached cells; optic fibers connected to the equipment excite and measure the fluorescence of O<sub>2</sub> and pH sensors dispersed through the base of the probe, thus allowing for the measurement of the oxygen consumption rate (OCR) and extracellular acidification rate (ECAR). In the (B) ATPrate assay, by assessing OCRs and ECARs under basal and inhibited conditions (oligo: oligomycin, ATP synthase inhibitor; rot: rotenone, complex I inhibitor; AA: antimycin A, complex III inhibitor) conditions, it is possible to estimate the total ATP production rate, as well as the partitioning between mitochondrial and glycolytic ATP production rates. (PER: proton exchange rate; BF: buffer factor; Vol: microchamber geometric volume; Kvol: volume scaling factor; CCF: CO<sub>2</sub> contribution factor; P/O: stoichiometry of ATP phosphorylated per atoms of oxygen reduced).

Seahorse analyses were conducted with adherent cells, mimicking the most physiological condition possible. To control for cell number variations, which may arise from plating errors, cell death, and treatment effects, it is highly advisable to normalize results afterwards. This can be done by extracting the proteins from each well and individually calculating the total protein content, for instance using a BCA kit (Thermo Fisher Scientific, Rockford, USA). Nonetheless, due to the low amount of material (usually 1,000-50,000 cells per well), this technique may not have the experimental sensitivity to account for intraexperimental variations. To avoid this issue, we validated a method to quantify the total cell number per well after each experiment, based on Assali et al. (2020). Plates were gently washed with PBS at the end of each assay and fixed with 4% PFA in methanol, at 4°C, overnight. Nuclei were stained with DAPI and imaged on a High Content Screening Operetta CLS apparatus (Fig. 11).

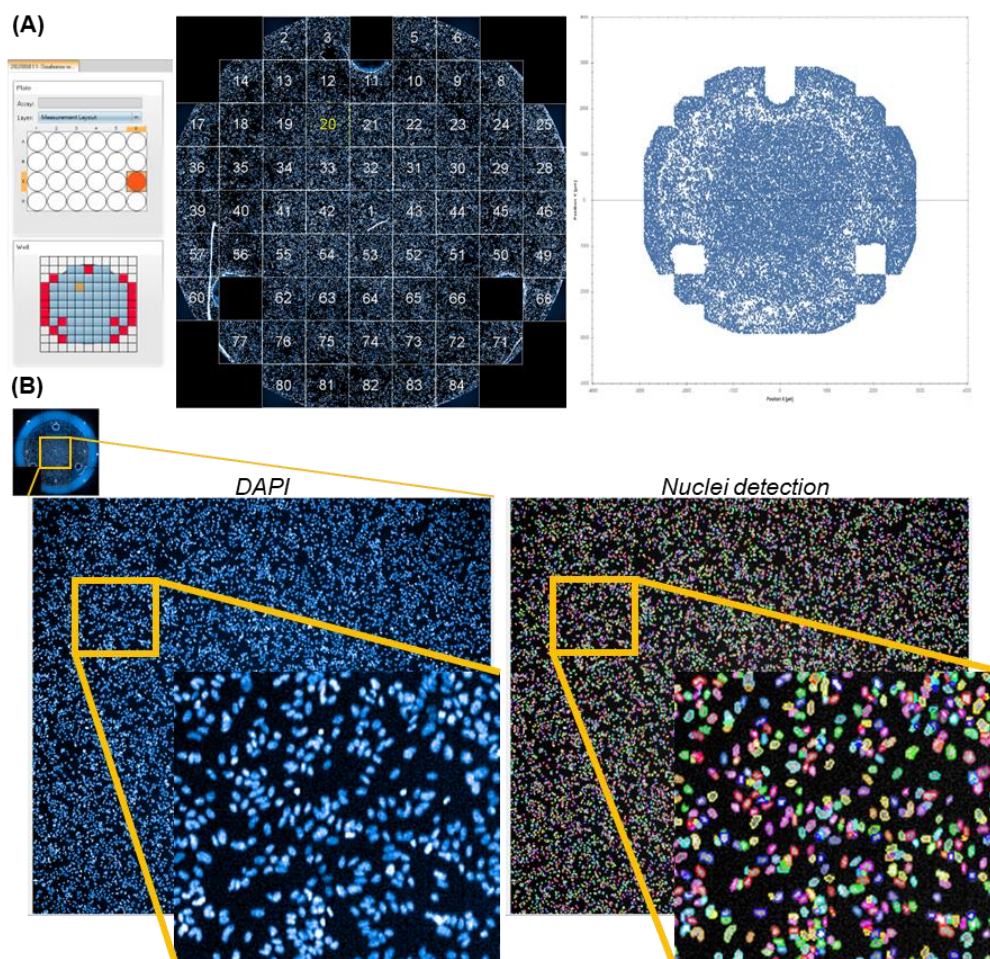


**Figure 11. Representative figure of nuclei detection for Seahorse assay normalization.** Astrocytes were fixed and stained with DAPI, then submitted to a high-content imaging in an Operetta High-Content Imaging System. Automated parameters for cell imaging (left) and nuclei detection (right) were standardized to provide high accuracy in cell count.



Manufacturer's plate measurements were considered as a start point, and then calibrated to guarantee proper alignment of the microscope lens with each well: A) distance of the plate's first row, first well center to plate's left side: 19.00 mm; B) distance of plate's first row, first well center to plate's upper side: 15.74 mm; C) plate length: 127.76 mm; D) plate width: 85.47 mm; E) distance of plate's first row, last well center to plate's left side: 109.00 mm; F) distance of plate's last row, first well center to plate's upper side: 69.73 mm; G) plate height: 20.32 mm; H) plate base-to-well bottom distance: 0.51 mm; I) well bottom thickness: 0.89 mm; J) well diameter: 6.00 mm. We then developed a custom workflow to proceed with the nuclei detection protocol (Fig. 11B), which then allowed us to calculate the total cell number per well in each plate assessed, allowing for a high throughput, precise normalization.

Then, we proceeded to estimate astrocyte glycolytic flux by evaluating glucose-to-glycolysis metabolism (for further details, please refer to Jimenez-Blasco et al., 2020 and Chapter 4, Material and methods/Glycolytic flux section). Cells were incubated with [3-<sup>3</sup>H]-glucose, which only releases its <sup>3</sup>H as <sup>3</sup>H<sub>2</sub>O through glycolysis (at the level of the triosephosphate isomerase, Chapter 1 – Fig. 2 and Chapter 4 – Fig. 4A). Thus, by assessing <sup>3</sup>H<sub>2</sub>O production, we can analyze glucose metabolism through glycolysis under NCLX inhibition. In parallel, we also measured media glucose consumption and, finally, the endpoint of glycolysis, lactate secretion.

### 3.5 Influence of stressful stimuli on NCLX expression

As previously discussed, viral transduction induced a transient increase in NCLX protein levels, including – and most noticeably – in control cells (Fig. 8C). Interestingly, we observed the same phenomenon in a standardization siRNA experiment. Astrocytes were transfected with Lipofectamine RNAiMAX transfection reagent (4.58 μL/500 μL cell medium, #13778150, Invitrogen, Waltham, MA, USA) to deliver 2 nM double-stranded siRNA targeted to silence *Nclx* (siNCLX, #10147724, Ambion, Austin, USA) or the negative control (siCtrl, Silencer Negative Control N° 1 siRNA, #AM4635, Invitrogen, Waltham, MA, USA). While the siNCLX transfection induced the expected drop in *Nclx* mRNA levels (Fig. 12A, 48 h), the siCtrl astrocytes showed a transient greater than 2-fold increase in comparison to the first 24 h (Fig. 12A). To confirm that this was not a phenomenon limited to primary astrocytes, we did the same experiment in primary mouse embryonic fibroblasts (MEFs, Fig. 12B) and in mouse primary cortical neurons (Fig. 12C). Again, in both MEFs and neurons, siCtrl also induced an increase in *Nclx* expression.

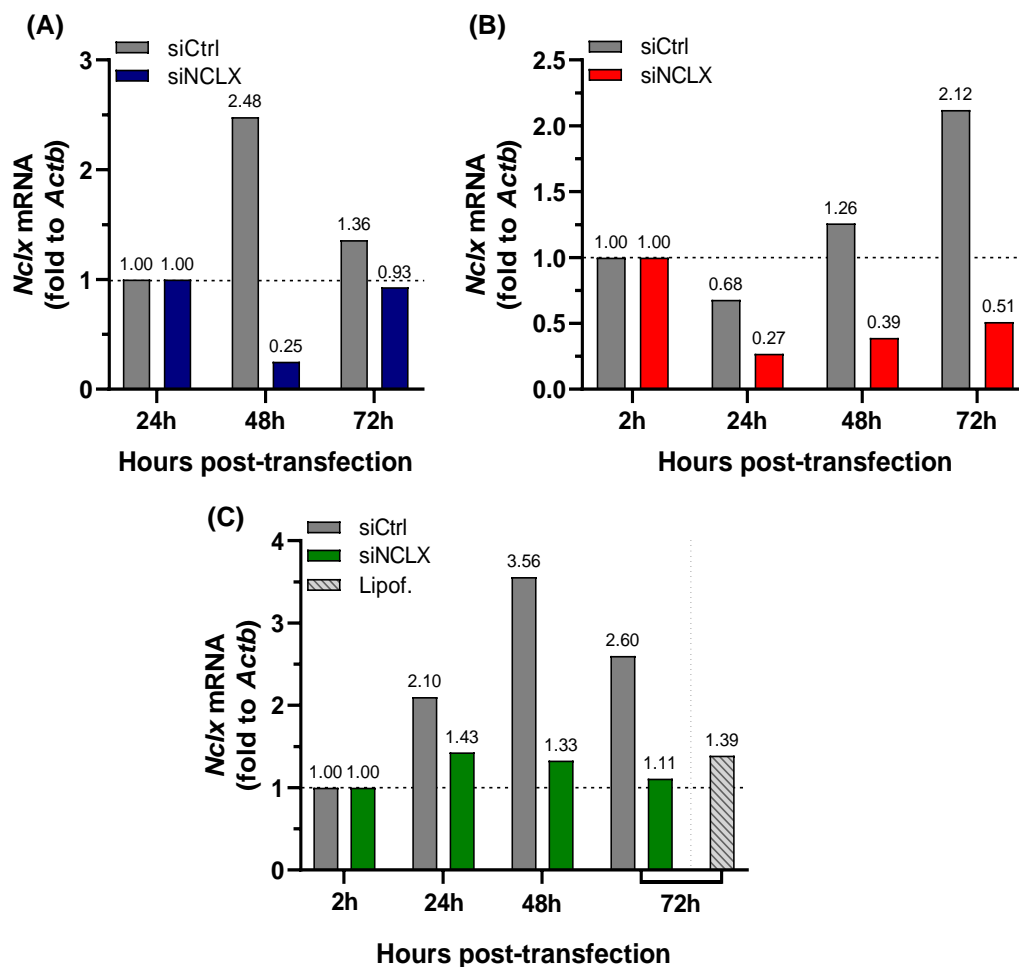


**Figure 12. Knock-out and silencing experiments in primary mouse cells show NCLX modulation by scrambled siRNA.** Time-course assessment of *Nclx* mRNA levels, assessed through RT-qPCR, normalized to *Actb*, of (A) astrocytes, (B) mouse embryonic fibroblasts (MEFs), and neurons (C) transfected with Lipofectamine RNAiMAX carrying a scrambled siRNA (siCtrl) or siNCLX.

This led us to hypothesize that NCLX expression might be controlled by some signalling pathway that is sensitive to stressful stimuli (Fig. 13). This would be of great interest, as decreased NCLX activity or expression is involved in pathophysiological mechanisms, such as cancer (Pathak et al., 2020), and Alzheimer’s (Jadiya et al., 2019) and Parkinson’s diseases (Kostic et al., 2015; Ludtmann et al., 2019). We observed that both transfection with a scrambled siRNA and an empty adenoviral vector were sufficient to induce NCLX expression. The pathways that could lead to such regulation, however, have not been described in the literature yet. We then began an investigation to clarify mechanisms behind the control of NCLX expression (Fig. 13).

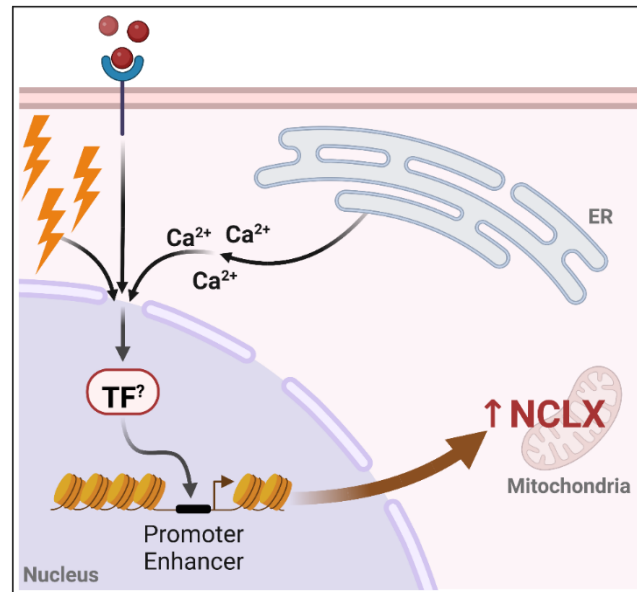


**Figure 13. Working hypothesis – modulation of NCLX expression.** *Nclx* expression is sensitive to extra and/or intracellular stimuli (*e.g.*, viral infection, growth factors, signaling molecules, oxidants), that may trigger the activation of conserved pathways leading to either activator activation or repressor inhibition. NCLX is a well-known controller of mitochondrial  $\text{Ca}^{2+}$  efflux, playing a key role in many cellular functions (*e.g.*, proliferation, survival, oxidant production, metabolism), and its expression level is centrally involved in pathophysiological mechanisms. Therefore, a strict, stress-sensitive, conserved transcriptional control of *Nclx* expression may exist; it may be explored as a pharmacological target. (TF: transcription factor).

First, to confirm the reproducibility of the observed phenomena following other stressful stimuli, we treated astrocytes and MEFs with an inhibitor of the sarco/endoplasmic reticulum  $\text{Ca}^{2+}$ -ATPase (SERCA), thapsigargin, to induce a strong increase in intracellular  $\text{Ca}^{2+}$  levels; and with  $\text{H}_2\text{O}_2$ , to induce redox imbalance. These treatments were performed in the absence of serum, to avoid the interference of growth factors (Fig. 14).

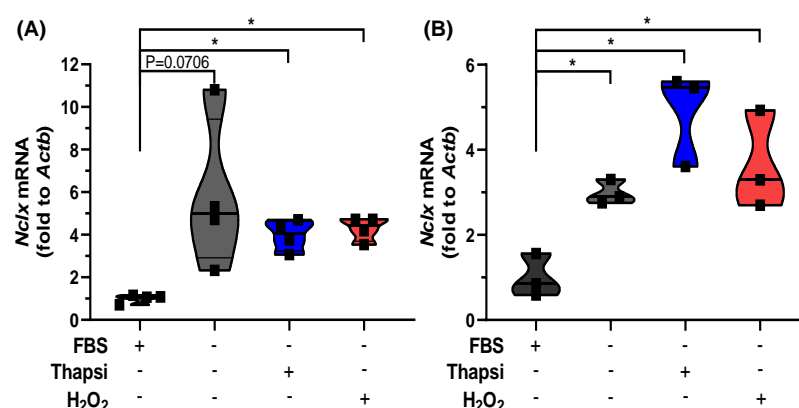


**Figure 14. Primary C57Bl/6NTac mouse astrocytes and MEFs stimulated by mild stress present higher *Nclx* mRNA levels.** (A) astrocytes and (B) mouse embryonic fibroblasts (MEFs) were incubated for 4 h under control conditions (DMEM supplemented 10% fetal bovine serum), or in media without serum with DMSO (vehicle), thapsigargin (astrocytes: 300 nM; MEFs: 1  $\mu\text{M}$ ), or  $\text{H}_2\text{O}_2$  (500  $\mu\text{M}$ ). mRNAs were extracted and assessed through RT-qPCR. \* $P < 0.05$ , paired one-way ANOVA followed by Holm-Šidak's post-hoc test,  $n = 3-4$ .

Curiously, serum deprivation was sufficient to induce an increase in *Nclx* mRNA levels in both astrocytes (Fig. 14A) and MEFs (Fig. 14B). Although the individual thapsigargin and



H<sub>2</sub>O<sub>2</sub> contributions were not totally clear, they appeared to have an additive effect on MEFs (Fig. 14B). This further confirms that NCLX expression indeed appears to be sensitive to external, environmental signalling.

We then analyzed the *Nclx* gene structure and epigenetic signature to look for potential regulatory regions. The mouse *Nclx* gene is located in chromosome 5 (fragment 5qF). We proceeded with an integrated analysis with epigenetic data from the Encyclopedia of DNA Elements (ENCODE) project, containing Chromatin Immunoprecipitation Sequencing (ChIP-seq), Assay for Transposase-Accessible Chromatin using Sequencing (ATAC-seq), and DNase-seq data from the ENCODE Consortium Phase 3 from mouse neonatal forebrain at P0, performed by the laboratory of Dr. Bing Ren (Kent, 2002; Pruitt; Tatusova; Maglott, 2005; Pruitt et al., 2014; Gardiner-Garden; Frommer, 1987; Gorkin et al., 2017; Sloan et al., 2016; Shen et al., 2012; Buenrostro et al., 2013; Kent et al., 2002). The resulting Genome Browser view is available at [https://genome.ucsc.edu/s/jvccosta/Slc8b1\\_regulatory\\_view1](https://genome.ucsc.edu/s/jvccosta/Slc8b1_regulatory_view1).

We observed that the *Nclx* gene only has two CpG islands, regions in the genome containing a large number of CpG repeats (Gardiner-Garden; Frommer, 1987), that locate right over the first exon and in a position around 5kb upstream of the transcription initiation site. Both regions presented DNase-seq and ATAC-seq peaks, reinforcing that these might constitute regulatory regions with accessible chromatin. Accordingly, we found that these putative regulatory regions presented typical epigenetic signatures. The first upstream region showed a histone H3 lysine (K) trimethylation (me3) and acetylation (ac) pattern (H3K4me3, H3K27ac, H3K9ac) that may be interpreted as a distant enhancer-like signature (dELS; The ENCODE Project Consortium et al., 2020). On the other hand, the second region presented a pattern (H3K4me3, H3K27me3, H3K9ac) typical of a promoter-like signature (PLS; The ENCODE Project Consortium et al., 2020), thus emphasizing the potential regulatory role of these two regions over *Nclx* gene expression.

To pursue further validation of the functional relevance of these dELS and PLS regions, we conducted an analysis of regulatory motif over-representation across the *Nclx* gene and dELS and PLS sequences, looking for potential transcription factor binding sites (TFBS). We then followed with an *in silico* analysis using the oPOSSUM-3 software (Kwon et al., 2012), collecting transcription factor-binding profile data from the JASPAR database (Fornes et al., 2019) (Fig. 15B,C). Several candidate transcription factors were found with the potential to bind to dELS and PLS regions (Fig. 15C). In fig. 15B we show the top four candidates for each region, with their respective binding motifs, which included: POU5F1 (also known as Oct4,

critical for embryonic development, and stem cell self-renewal and pluripotency; Pan et al., 2002), ELK4 (also known as serum response factor accessory protein 1; Kaikkonen et al., 2010), GATA1 (important for hematopoiesis; Ferreira et al., 2005), REST (associated with synaptic plasticity and neuronal survival; Baldelli; Meldolesi, 2015), EVI1 (involved in cell cycle regulation and myeloid malignancies; Glass et al., 2014), ESR2 (estrogen receptor  $\beta$ , involved in a plethora of functions, including reproduction and behavior; Deroo; Korach, 2006), NF- $\kappa$ B1 (associated with a plethora of functions, including inflammation, aging, and synaptic plasticity; Cartwright; Perkins; Wilson, 2016; De Bosscher et al., 1997).

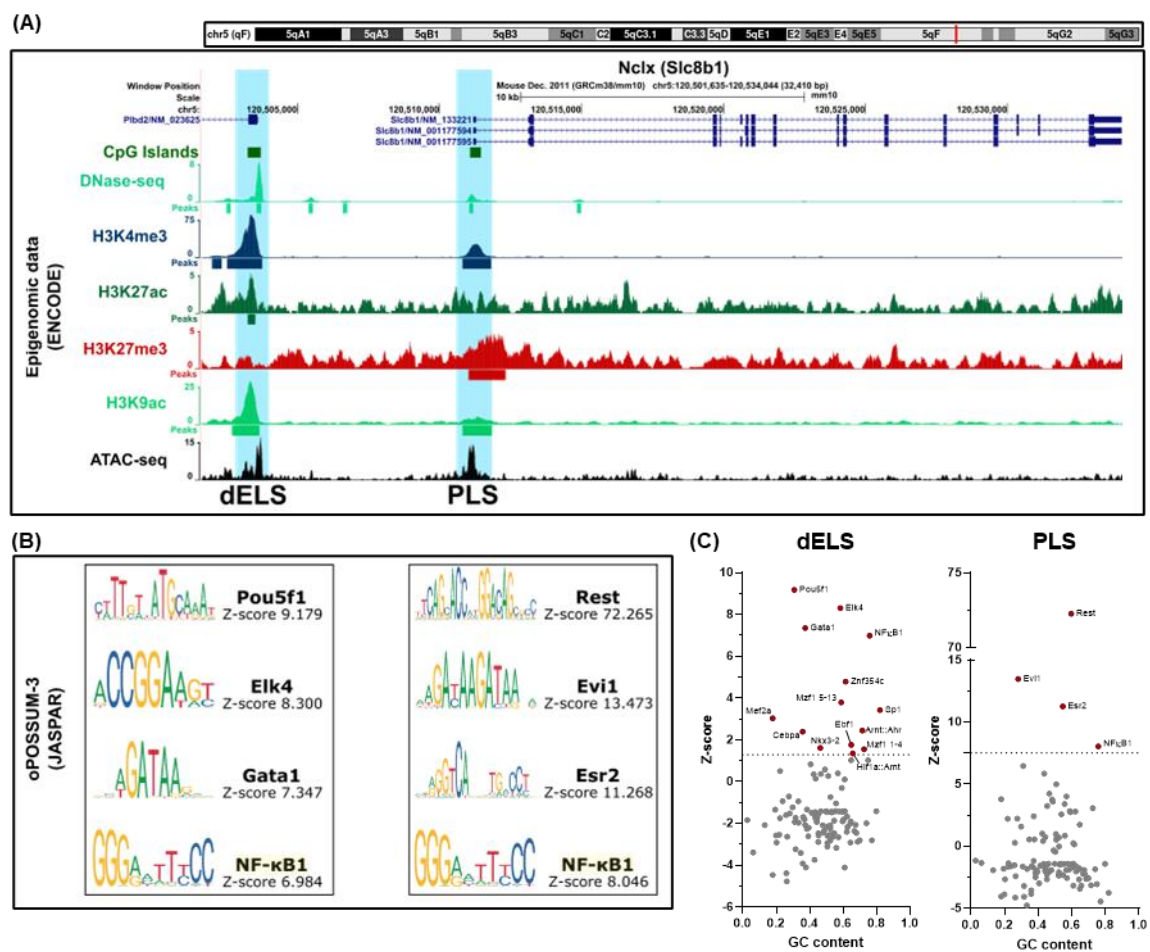


**Figure 15. Possible regulatory regions and transcription factor over-enriched motifs in the *Nclx* locus.** (A) UCSC genome browser figure depicting a simplified scheme for the *Nclx* locus, indicating representative DNase-seq, ChIP-seq (H3K4me3, H3K27ac, H3K24me3, H3K9ac), and ATAC-seq tracks retrieved from the ENCODE GSE91978 public dataset (*M. musculus*, strain B6NCR1, forebrain tissue from postnatal day 0). Sequence tag plots per million read values for nucleotide position -10000 upstream of the TSS to the transcription termination site, highlighting the identification of two regulatory regions: a distant enhancer-like signature (dELS) and a promoter-like signature (PLS). (B, C) Sequence-based single site analysis for over-represented enriched elements identified by *de novo* motif analysis of the dELS and the PLS regions, using the web-based tool oPOSSUM-3 and the JASPAR database. (B) Z-score scatter plot of over-represented enriched elements dispersed according to GC content; transcription factors with Z-scores above the threshold of average + 1 SD (dotted line) were highlighted. (C) Sequence logo corresponding to the top 4 over-represented enriched motifs of dELS (left) and PLS (right) regions. Data extracted from the UCSC Genome Browser on Mouse (GRCm38/mm10; Kent et al., 2002) and ENCODE project (The ENCODE Project Consortium et al., 2020). Source session available at [https://genome.ucsc.edu/s/jvccosta/Slc8b1\\_regulatory\\_view1](https://genome.ucsc.edu/s/jvccosta/Slc8b1_regulatory_view1).

Of note, NF-κB1 appeared as a candidate transcription factor in all analyses (whole gene, dELS, and PLS), highlighting that it may be involved in *Nclx* expression regulation. This is particularly interesting, since NF-κB signaling has been extensively associated with the pathophysiology of Alzheimer's disease (Sun et al., 2022), a condition that is linked to decreased cortical NCLX levels, both in mice and humans (Jadiya et al., 2019).

### 3.6 Concluding remarks

In this chapter, we conducted a narrative discussion of the major experimental design characteristics of this project (further explored on Chapter 4), presenting and validating the methodological basis that was used to test our hypothesis, including the *in vitro* and *in vivo* pharmacological and genetic modulation of NCLX activity, as well as approaches to assess metabolic effects.

In addition, we initiated the characterization of two *Nclx* gene regulatory regions that will be further validated to allow for the investigation of putative transcription factors involved in the modulation of NCLX expression, with the potential to impact research on pathophysiological mechanisms and treatments.

### 3.7 References<sup>1</sup>

- Assali EA, Jones AE, Veliova M, Acín-Pérez R, Taha M, Miller N, et al. NCLX prevents cell death during adrenergic activation of the brown adipose tissue. *Nat Commun* 2020;11:3347. <https://doi.org/10.1038/s41467-020-16572-3>.
- Assali EA, Sekler I. Sprinkling salt on mitochondria: the metabolic and pathophysiological roles of mitochondrial Na<sup>+</sup> signaling mediated by NCLX. *Cell Calcium* 2021;97:102416. <https://doi.org/10.1016/j.ceca.2021.102416>.
- Baldelli P, Meldolesi J. The transcription repressor REST in adult neurons: physiology, pathology, and diseases. *Eneuro* 2015;2:ENEURO.0010-15.2015. <https://doi.org/10.1523/ENEURO.0010-15.2015>.
- Buenrostro JD, Giresi PG, Zaba LC, Chang HY, Greenleaf WJ. Transposition of native chromatin for fast and sensitive epigenomic profiling of open chromatin, DNA-binding proteins and nucleosome position. *Nat Methods* 2013;10:1213–8. <https://doi.org/10.1038/nmeth.2688>.
- Cabral-Costa JV, Andreotti DZ, Mello NP, Scavone C, Camandola S, Kawamoto EM. Intermittent fasting uncovers and rescues cognitive phenotypes in PTEN neuronal haploinsufficient mice. *Sci Rep* 2018;8:8595. <https://doi.org/10.1038/s41598-018-26814-6>.
- Cartwright T, Perkins ND, Wilson C. NFκB1: a suppressor of inflammation, ageing and cancer. *FEBS J* 2016;283:1812–22. <https://doi.org/10.1111/febs.13627>.
- De Bosscher K, Schmitz ML, Vanden Berghe W, Plaisance S, Fiers W, Haegeman G. Glucocorticoid-mediated repression of nuclear factor-κB dependent transcription involves direct interference with transactivation. *Proc Natl Acad Sci USA* 1997;94:13504–9. <https://doi.org/10.1073/pnas.94.25.13504>.
- Denninger JK, Smith BM, Kirby ED. Novel Object Recognition and Object Location behavioral testing in mice on a budget. *JoVE* 2018:58593. <https://doi.org/10.3791/58593>.
- Deroo B, Korach K. Estrogen receptors and human disease. *J Clin Investig* 2006;116:561–70. <https://doi.org/10.1172/JCI27987>.
- Fanselow MS, Dong H-W. Are the dorsal and ventral hippocampus functionally distinct structures? *Neuron* 2010;65:7–19. <https://doi.org/10.1016/j.neuron.2009.11.031>.
- Ferreira R, Ohneda K, Yamamoto M, Philipsen S. GATA1 function, a paradigm for transcription factors in hematopoiesis. *Mol Cell Biol* 2005;25:1215–27. <https://doi.org/10.1128/MCB.25.4.1215-1227.2005>.
- Fornes O, Castro-Mondragon JA, Khan A, van der Lee R, Zhang X, Richmond PA, et al. JASPAR 2020: update of the open-access database of transcription factor binding profiles. *Nucleic Acids Res* 2019;gkz1001. <https://doi.org/10.1093/nar/gkz1001>.
- Funaro VMB de O, Pestana MC, Dziabas MCC, Garcia EM, Santos MF dos, Nascimento MM, et al. Diretrizes para apresentação de dissertações e teses da USP: parte IV (Vancouver). vol. IV. 3rd ed. Universidade de São Paulo. Sistema Integrado de Bibliotecas; 2016.
- Gardiner-Garden M, Frommer M. CpG islands in vertebrate genomes. *J Mol Biol* 1987;196:261–82. [https://doi.org/10.1016/0022-2836\(87\)90689-9](https://doi.org/10.1016/0022-2836(87)90689-9).

---

<sup>1</sup> Following the Vancouver system, in accordance with the *Diretrizes para apresentação de dissertações e teses da USP – Parte IV* (Funaro et al., 2016).

- Glass C, Wilson M, Gonzalez R, Zhang Y, Perkins AS. The role of EVI1 in myeloid malignancies. *Blood Cells Mol Dis* 2014;53:67–76. <https://doi.org/10.1016/j.bcmd.2014.01.002>.
- Gleiser M. *A ilha do conhecimento: os limites da ciência e a busca por sentido*. 2nd ed. Rio de Janeiro (RJ): Record; 2014.
- Gorkin DU, Barozzi I, Zhang Y, Lee AY, Li B, Zhao Y, et al. Systematic mapping of chromatin state landscapes during mouse development. *Genomics*; 2017. <https://doi.org/10.1101/166652>.
- Herrero-Mendez A, Almeida A, Fernández E, Maestre C, Moncada S, Bolaños JP. The bioenergetic and antioxidant status of neurons is controlled by continuous degradation of a key glycolytic enzyme by APC/C–Cdh1. *Nat Cell Biol* 2009;11:747–52. <https://doi.org/10.1038/ncb1881>.
- Hughes RN. The value of spontaneous alternation behavior (SAB) as a test of retention in pharmacological investigations of memory. *Neuroscience & Biobehavioral Reviews* 2004;28:497–505. <https://doi.org/10.1016/j.neubiorev.2004.06.006>.
- Jadiya P, Kolmetzky DW, Tomar D, Di Meco A, Lombardi AA, Lambert JP, et al. Impaired mitochondrial calcium efflux contributes to disease progression in models of Alzheimer’s disease. *Nat Commun* 2019;10:3885. <https://doi.org/10.1038/s41467-019-11813-6>.
- Jimenez-Blasco D, Busquets-Garcia A, Hebert-Chatelain E, Serrat R, Vicente-Gutierrez C, Ioannidou C, et al. Glucose metabolism links astroglial mitochondria to cannabinoid effects. *Nature* 2020;583:603–8. <https://doi.org/10.1038/s41586-020-2470-y>.
- Kaikkonen S, Makkonen H, Rytinki M, Palvimo JJ. SUMOylation can regulate the activity of ETS-like transcription factor 4. *Biochim Biophys Acta Gene Regul Mechan* 2010;1799:555–60. <https://doi.org/10.1016/j.bbagr.2010.07.001>.
- Kent WJ. BLAT--the BLAST-like alignment tool. *Genome Res* 2002;12:656–64. <https://doi.org/10.1101/gr.229202>.
- Kent WJ, Sugnet CW, Furey TS, Roskin KM, Pringle TH, Zahler AM, et al. The Human Genome Browser at UCSC. *Genome Res* 2002;12:996–1006. <https://doi.org/10.1101/gr.229102>.
- Kostic M, Ludtmann MHR, Bading H, Hershinkel M, Steer E, Chu CT, et al. PKA phosphorylation of NCLX reverses mitochondrial calcium overload and depolarization, promoting survival of PINK1-deficient dopaminergic neurons. *Cell Rep* 2015;13:376–86. <https://doi.org/10.1016/j.celrep.2015.08.079>.
- Kwon AT, Arenillas DJ, Hunt RW, Wasserman WW. oPOSSUM-3: advanced analysis of regulatory motif over-representation across genes or ChIP-seq datasets. *G3 Genes Genomes Genet* 2012;2:987–1002. <https://doi.org/10.1534/g3.112.003202>.
- Lange SC, Bak LK, Waagepetersen HS, Schousboe A, Norenberg MD. Primary Cultures of Astrocytes: Their Value in Understanding Astrocytes in Health and Disease. *Neurochem Res* 2012;37:2569–88. <https://doi.org/10.1007/s11064-012-0868-0>.
- Lapresa R, Agulla J, Gonzalez-Guerrero S, Bolaños JP, Almeida A. Amyloid-β induces Cdh1-mediated Rock2 stabilization causing neurodegeneration. *Front Pharmacol* 2022;13:884470. <https://doi.org/10.3389/fphar.2022.884470>.

- Ludtmann MHR, Kostic M, Horne A, Gandhi S, Sekler I, Abramov AY. LRRK2 deficiency induced mitochondrial Ca<sup>2+</sup> efflux inhibition can be rescued by Na<sup>+</sup>/Ca<sup>2+</sup>/Li<sup>+</sup> exchanger upregulation. *Cell Death Dis* 2019;10:265. <https://doi.org/10.1038/s41419-019-1469-5>.
- Luongo TS, Lambert JP, Gross P, Nwokedi M, Lombardi AA, Shanmughapriya S, et al. The mitochondrial Na<sup>+</sup>/Ca<sup>2+</sup> exchanger is essential for Ca<sup>2+</sup> homeostasis and viability. *Nature* 2017;545:93–7. <https://doi.org/10.1038/nature22082>.
- Matos B, Publicover SJ, Castro LFC, Esteves PJ, Fardilha M. Brain and testis: more alike than previously thought? *Open Biol* 2021;11:200322. <https://doi.org/10.1098/rsob.200322>.
- Mookerjee SA, Gerencser AA, Nicholls DG, Brand MD. Quantifying intracellular rates of glycolytic and oxidative ATP production and consumption using extracellular flux measurements. *J Biol Chem* 2017;292:7189–207. <https://doi.org/10.1074/jbc.M116.774471>.
- Opitz B. Memory function and the hippocampus. *Front Neurol Neurosci* 2014;34:51–9. <https://doi.org/10.1159/000356422>.
- Palty R, Silverman WF, Hershinkel M, Caporale T, Sensi SL, Parnis J, et al. NCLX is an essential component of mitochondrial Na<sup>+</sup>/Ca<sup>2+</sup> exchange. *Proc Natl Acad Sci USA* 2010;107:436–41. <https://doi.org/10.1073/pnas.0908099107>.
- Pan GJ, Chang ZY, Schöler HR, Pei D. Stem cell pluripotency and transcription factor Oct4. *Cell Res* 2002;12:321–9. <https://doi.org/10.1038/sj.cr.7290134>.
- Parnis J, Montana V, Delgado-Martinez I, Matyash V, Parpura V, Kettenmann H, et al. Mitochondrial exchanger NCLX plays a major role in the intracellular Ca<sup>2+</sup> signaling, gliotransmission, and proliferation of astrocytes. *J Neurosci* 2013;33:7206–19. <https://doi.org/10.1523/JNEUROSCI.5721-12.2013>.
- Pathak T, Gueguinou M, Walter V, Delierneux C, Johnson MT, Zhang X, et al. Dichotomous role of the human mitochondrial Na<sup>+</sup>/Ca<sup>2+</sup>/Li<sup>+</sup> exchanger NCLX in colorectal cancer growth and metastasis. *ELife* 2020;9:e59686. <https://doi.org/10.7554/eLife.59686>.
- Pruitt KD, Brown GR, Hiatt SM, Thibaud-Nissen F, Astashyn A, Ermolaeva O, et al. RefSeq: an update on mammalian reference sequences. *Nucleic Acids Res* 2014;42:D756-763. <https://doi.org/10.1093/nar/gkt1114>.
- Pruitt KD, Tatusova T, Maglott DR. NCBI Reference Sequence (RefSeq): a curated non-redundant sequence database of genomes, transcripts and proteins. *Nucleic Acids Res* 2005;33:D501-504. <https://doi.org/10.1093/nar/gki025>.
- Romero N, Rogers G, Neilson A, Dranka B. Quantifying Cellular ATP Production Rate Using Agilent Seahorse XF Technology 2018.
- Sánchez-Morán I, Rodríguez C, Lapresa R, Agulla J, Sobrino T, Castillo J, et al. Nuclear WRAP53 promotes neuronal survival and functional recovery after stroke. *Sci Adv* 2020;6:eabc5702. <https://doi.org/10.1126/sciadv.abc5702>.
- Schindelin J, Arganda-Carreras I, Frise E, Kaynig V, Longair M, Pietzsch T, et al. Fiji: an open-source platform for biological-image analysis. *Nat Methods* 2012;9:676–82. <https://doi.org/10.1038/nmeth.2019>.
- Serna JDC, de Miranda Ramos V, Cabral-Costa JV, Vilas-Boas EA, Amaral AG, Ohya G, et al. Measuring mitochondrial Ca<sup>2+</sup> efflux in isolated mitochondria and permeabilized cells. *Bioenerg Comm* 2022. <https://doi.org/10.26124/BEC:2022-0007>.

Shen Y, Yue F, McCleary DF, Ye Z, Edsall L, Kuan S, et al. A map of the cis-regulatory sequences in the mouse genome. *Nature* 2012;488:116–20. <https://doi.org/10.1038/nature11243>.

Sloan CA, Chan ET, Davidson JM, Malladi VS, Strattan JS, Hitz BC, et al. ENCODE data at the ENCODE portal. *Nucleic Acids Res* 2016;44:D726-732. <https://doi.org/10.1093/nar/gkv1160>.

Sun E, Motolani A, Campos L, Lu T. The pivotal role of NF-κB in the pathogenesis and therapeutics of Alzheimer's disease. *Int J Mol Sci* 2022;23:8972. <https://doi.org/10.3390/ijms23168972>.

The ENCODE Project Consortium, Abascal F, Acosta R, Addleman NJ, Adrian J, Afzal V, et al. Expanded encyclopaedias of DNA elements in the human and mouse genomes. *Nature* 2020;583:699–710. <https://doi.org/10.1038/s41586-020-2493-4>.

Vicente-Gutierrez C, Bonora N, Bobo-Jimenez V, Jimenez-Blasco D, Lopez-Fabuel I, Fernandez E, et al. Astrocytic mitochondrial ROS modulate brain metabolism and mouse behaviour. *Nat Metab* 2019;1:201–11. <https://doi.org/10.1038/s42255-018-0031-6>.

Vogel-Ciernia A, Wood MA. Examining object location and object recognition memory in mice. *Curr Protoc Neurosci* 2014;69:8.31.1-17. <https://doi.org/10.1002/0471142301.ns0831s69>.



## CHAPTER 4

### **Mitochondrial sodium/calcium exchanger NCLX regulates glycolysis in astrocytes, impacting on cognitive performance**

*“Somos una especie en viaje  
No tenemos pertenencias sino equipaje  
Vamos con el polen en el viento  
Estamos vivos porque estamos en movimiento  
Nunca estamos quietos, somos trashumantes  
Somos padres, hijos, nietos y bisnietos de inmigrantes  
Es más mío le que sueño que lo que toco*

*Yo no soy de aquí  
Pero tú tampoco*

*De ningún lado del todo y  
De todos lados un poco”*

(Drexler, 2017)<sup>1</sup>

---

<sup>1</sup> Drexler J. Movimiento. Warner Music Spain; 2017.

**Summary**

Finally, to test our hypothesis that modulating NCLX activity could influence astrocyte function and metabolism, we followed the experimental design discussed in the Chapter 3, starting by screening for metabolic effects of NCLX pharmacological and genetic modulation *in vitro*, and followed by testing the functional effects of NCLX deletion *in vivo*.

As summarized by Cabral-Costa et al. (Cabral-Costa et al., 2022)<sup>2</sup>:

‘Intracellular  $\text{Ca}^{2+}$  concentrations are strictly controlled by plasma membrane transporters, the endoplasmic reticulum, and mitochondria, in which  $\text{Ca}^{2+}$  uptake is mediated by the mitochondrial calcium uniporter complex (MCUc), while efflux occurs mainly through the mitochondrial  $\text{Na}^+/\text{Ca}^{2+}$  exchanger (NCLX). RNAseq database repository searches led us to identify the *Nclx* transcript as highly enriched in astrocytes when compared to neurons. To assess the role of NCLX in mouse primary culture astrocytes, we inhibited its function both pharmacologically or genetically. This resulted in re-shaping of cytosolic  $\text{Ca}^{2+}$  signaling and a metabolic shift that increased glycolytic flux and lactate secretion in a  $\text{Ca}^{2+}$ -dependent manner. Interestingly, *in vivo* genetic deletion of NCLX in hippocampal astrocytes improved cognitive performance in behavioral tasks, whereas hippocampal neuron-specific deletion of NCLX impaired cognitive performance. These results unveil a role for NCLX as a novel modulator of astrocytic glucose metabolism, impacting on cognition.’

This chapter is a full reproduction of the preprint “Mitochondrial sodium/calcium exchanger NCLX regulates glycolysis in astrocytes, impacting on cognitive performance” deposited in bioRxiv in September 2022 (Cabral-Costa et al., 2022)<sup>2</sup>, that can also be accessed at <https://doi.org/10.1101/2022.09.16.507284>, in accordance with the published copyright license (CC-BY-NC-ND 4.0; Creative Commons, 2022)<sup>3</sup>.

---

<sup>2</sup> Cabral-Costa JV, Vicente-Gutierrez C, Agulla J, Lapresa R, Elrod JW, Almeida A, et al. Mitochondrial sodium/calcium exchanger NCLX regulates glycolysis in astrocytes, impacting on cognitive performance. BioRxiv 2022. <https://doi.org/10.1101/2022.09.16.507284>.

<sup>3</sup> Creative Commons. Creative Commons — Attribution-Non-Commercial-No Derivatives 4.0 International — CC BY-NC-ND 4.0 2022. <https://creativecommons.org/licenses/by-nc-nd/4.0/> (accessed September 12, 2022).

# Mitochondrial sodium/calcium exchanger NCLX regulates glycolysis in astrocytes, impacting on cognitive performance

João Victor Cabral-Costa<sup>1,2,\*</sup>, Carlos Vicente-Gutiérrez<sup>2,3,4</sup>, Jesús Agulla<sup>2,4</sup>, Rebeca Lapresa<sup>2,4</sup>, John W. Elrod<sup>5</sup>, Ángeles Almeida<sup>2,4</sup>, Juan P. Bolaños<sup>2,3,4,\*,#</sup>, Alicia J. Kowaltowski<sup>1,#</sup>

<sup>1</sup> Departamento de Bioquímica, Instituto de Química, Universidade de São Paulo, São Paulo, Brazil <sup>2</sup>

Institute of Functional Biology and Genomics, University of Salamanca, CSIC, Salamanca, Spain

<sup>3</sup> Centro de Investigación Biomédica en Red Sobre Fragilidad y Envejecimiento Saludable (CIBERFES), Instituto de Salud Carlos III, Madrid, Spain

<sup>4</sup> Institute of Biomedical Research of Salamanca, University Hospital of Salamanca, University of Salamanca, CSIC, Salamanca, Spain

<sup>5</sup> Center for Translational Medicine, Lewis Katz School of Medicine at Temple University, Philadelphia, PA, United States of America

#These authors jointly supervised this work

**\*Corresponding authors:**

**João Victor Cabral-Costa ([jvccosta@gmail.com](mailto:jvccosta@gmail.com))**

Departamento de Bioquímica, Instituto de Química, Universidade de São Paulo, Av. Prof. Lineu Prestes, 748, 05508-900, São Paulo, Brazil

**Juan Pedro Bolaños ([jbolanos@usal.es](mailto:jbolanos@usal.es))**

Institute of Functional Biology and Genomics, University of Salamanca-CSIC, Calle Zacarias Gonzalez, 2, 37007 Salamanca, Spain

**Running title:** NCLX fine-tunes astrocytic glycolysis

**Keywords:** brain metabolism; energy metabolism; mitochondrial metabolism; metabolic regulation; glycolysis; astrocyte; sodium-calcium exchange; calcium transport; sodium transport; NCLX; lactate.

## Abstract

Intracellular  $\text{Ca}^{2+}$  concentrations are strictly controlled by plasma membrane transporters, the endoplasmic reticulum, and mitochondria, in which  $\text{Ca}^{2+}$  uptake is mediated by the mitochondrial calcium uniporter complex (MCUc), while efflux occurs mainly through the mitochondrial  $\text{Na}^+/\text{Ca}^{2+}$  exchanger (NCLX). RNAseq database repository searches led us to identify the *Nclx* transcript as highly enriched in astrocytes when compared to neurons. To assess the role of NCLX in mouse primary culture astrocytes, we inhibited its function both pharmacologically or genetically. This resulted in reshaping of cytosolic  $\text{Ca}^{2+}$  signaling and a metabolic shift that increased glycolytic flux and lactate secretion in a  $\text{Ca}^{2+}$ -dependent manner. Interestingly, *in vivo* genetic deletion of NCLX in hippocampal astrocytes improved cognitive performance in behavioral tasks, whereas hippocampal neuron-specific deletion of NCLX impaired cognitive performance. These results unveil a role for NCLX as a novel modulator of astrocytic glucose metabolism, impacting on cognition.

## Introduction

$\text{Ca}^{2+}$  is an important second messenger which participates in a plethora of cell signaling pathways and brain functions, including membrane excitability, synaptic transmission, and plasticity (Kawamoto et al., 2012). Conversely,  $\text{Ca}^{2+}$  homeostasis disruption occurs under pathological conditions such as senescence and neurodegeneration (Cabral-Costa and Kowaltowski, 2020). Intracellular  $\text{Ca}^{2+}$  concentrations are tightly controlled by plasma membrane transporters (Kawamoto et al., 2012), the endoplasmic reticulum (Arruda and Parlakgöl, 2022), and mitochondria (Cabral-Costa and Kowaltowski, 2020).

We recently found that cerebral mitochondrial  $\text{Ca}^{2+}$  homeostasis is modulated by dietary calorie intake (Amigo et al., 2017), with strong protective effects against neuronal damage by excitotoxicity, a process that involves loss of cellular  $\text{Ca}^{2+}$  homeostasis (Arundine and Tymianski, 2003). This shows that these organelles, in addition to their canonical function generating most neuronal ATP, are also important regulators of intracellular  $\text{Ca}^{2+}$  responses, at least under pathological conditions. However, whether mitochondrial  $\text{Ca}^{2+}$  homeostasis has physiological impacts on the different cell types of the brain is unknown.

Mitochondrial  $\text{Ca}^{2+}$  uptake and release were first described in the 1960s (DeLuca and Engstrom, 1961; Vasington and Murphy, 1962; Lehninger et al., 1963; Drahota and Lehninger, 1965), but the major molecular components of the mitochondrial  $\text{Ca}^{2+}$  handling system were only recently identified (Palty et al., 2010; Perocchi et al., 2010; De Stefani et al., 2011; Baughman et al., 2011; Plovanich et al., 2013; Sancak et al., 2013).  $\text{Ca}^{2+}$  uptake is mediated by the Mitochondrial Calcium Uniporter (MCU) Complex (MCUc), comprised of a tetramer of MCUs, the structural stabilizer Essential MCU Regulator (EMRE), and gating and regulatory subunits Mitochondrial Calcium Uptake Protein (MICU)-1, -2 or -3 (thoroughly reviewed by Feno et al. (2021)). Cerebral mitochondrial  $\text{Ca}^{2+}$  efflux is mostly mediated by a  $\text{Na}^+/\text{Ca}^{2+}$  exchanger (NCLX, Fig. 1A), which removes  $\text{Ca}^{2+}$  from the

matrix in exchange for Na<sup>+</sup> from the intermembrane space (Palty et al., 2010; Assali and Sekler, 2021; Serna et al., 2022).

Apart from controlling mitochondrial and cytosolic ion fluxes, NCLX activity has been described to protect hearts against oxidative damage (De La Fuente et al., 2018; Luongo et al., 2017), modulate cardiac hypertrophy (Garbincius et al., 2022), and mediate cellular responses to hypoxia by modulating mitochondrial Na<sup>+</sup> levels (Hernansanz-Agustín et al., 2020). NCLX also prevents excess intramitochondrial Ca<sup>2+</sup> in brown adipocytes upon adrenergic activation (Assali et al., 2020), and modulates insulin secretion in β-cells (Nita et al., 2012, 2014, 2015), showing it has important physiological metabolic effects.

In neurons, NCLX integrates mitochondrial metabolism and Ca<sup>2+</sup> signaling responses (Kostic et al., 2015, 2018), prevents excitotoxicity (Hagenston et al., 2022), and participates in the pathogenesis of forms of Parkinson's and Alzheimer's disease (Ludtmann et al., 2019; Jadiya et al., 2019; Britti et al., 2020). Indeed, impaired NCLX activity is associated with reduced synaptic activity and mental retardation (Stavsky et al., 2021). Much less is known about NCLX in astrocytes, although it has been shown that its knockdown impairs proliferation *in vitro* (Parnis et al., 2013) and cell viability *in vivo* (Hagenston et al., 2022).

During search analyses of several public database repositories, we found that NCLX is highly expressed in astrocytes, the most abundant cell types of the brain (Khakh and Deneen, 2019) that participate in neurotransmitter uptake, glutamate recycling, neuronal energy metabolism, and redox balance (Oheim et al., 2018; Bonvento and Bolaños, 2021). Interestingly, we found that, while *in vivo* NCLX deletion in hippocampal astrocytes improves cognitive performance, it leads to cognitive impairment when deleted in hippocampal neurons. These findings correlated with an induction of the glycolytic flux and lactate secretion from astrocytes, revealing that this mitochondrial exchanger has a major impact on brain metabolism and function.

## Results

We were interested in studying the physiological role of mitochondrial  $\text{Ca}^{2+}$  transport in brain function. Interestingly, there is literature evidence that NCLX, the main mitochondrial  $\text{Ca}^{2+}$  extrusion pathway (involving exchange for  $\text{Na}^+$  ions, Fig. 1A), is specifically and strongly expressed in astrocytes. To quantify this astrocyte-specific *Nclx* expression, we mined public RNA-seq databases (Chai et al., 2017; Srinivasan et al., 2016; Zhang et al., 2014) and found that *Nclx* mRNA was indeed highly enriched in astrocytes in comparison to neurons (Fig. 1B). This > 5-fold level of enrichment of *Nclx* was a specific astrocytic signature, not associated with total mitochondrial protein, since astrocyte/neuron expression ratios for other mitochondrial proteins, such as those of the electron transport chain and mitochondrial  $\text{Ca}^{2+}$  transport, were not similarly enriched (Fig. 1C). The enrichment of *Nclx* in astrocytes was also consistent among different databases, and quite significant (8 to 11-fold) when analyzed as astrocyte versus total input tissue in the hippocampus (Fig. 1D,E) and cortex (Fig. 1F,G).

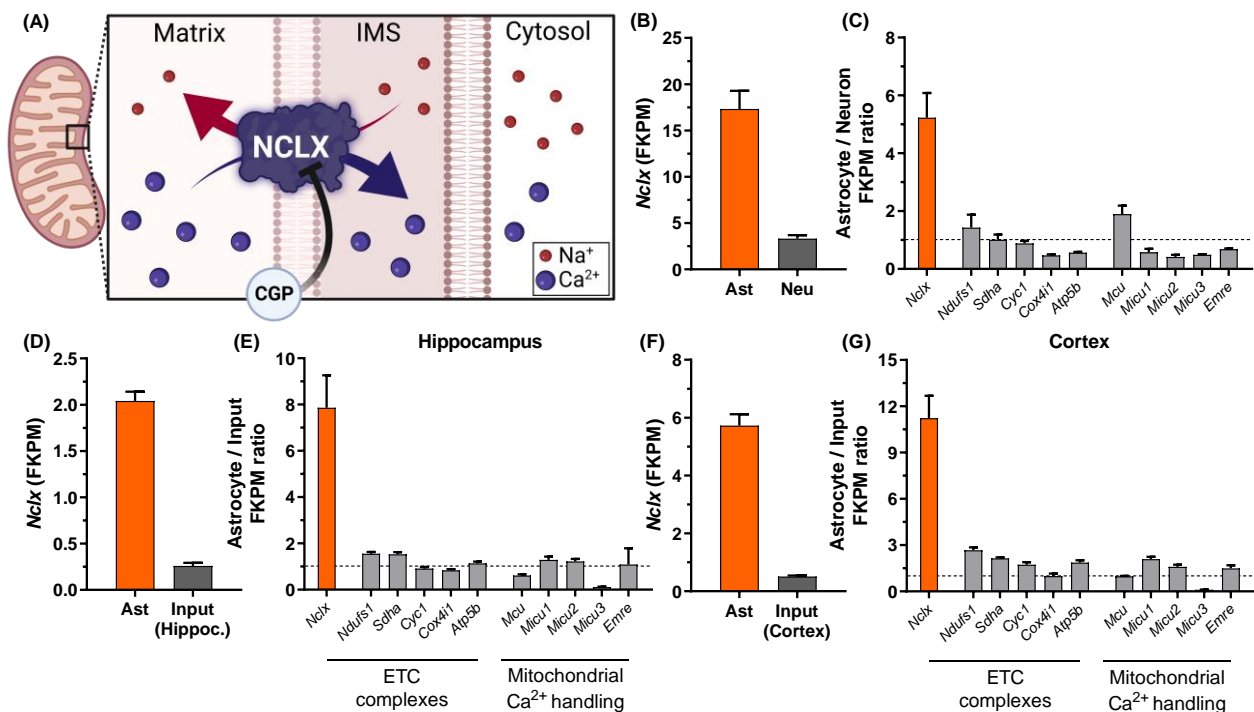


**Figure 1. *Nclx* (*Slc8b1*, *Slc24a6*) transcript is enriched in astrocytes.** (A) Schematic illustration of NCLX exchanging extramitochondrial  $\text{Na}^+$  with matrix  $\text{Ca}^{2+}$ , in a manner inhibited by its pharmacological modulator CGP-37157 (CGP). RNA-seq data extracted from Zhang et al. (2014) indicating (B) fragments per kilobase million (FPKM) values of *Nclx* transcript from astrocytes and neurons isolated from mouse cerebral cortex, and (C) FPKM value ratios between astrocytes



and neurons from selected transcripts, average  $\pm$  SD. RNA-seq data extracted from Chai et al. (2017) and Srinivasan et al. (2016) indicating FPKM values for the *Nclx* transcript from isolated astrocytes and respective hippocampal (D) or cortical (F) tissues, and ratio of FPKM values from selected transcripts between astrocytes and input tissue in the hippocampus (E) and (G) cortex. Bars indicate mean  $\pm$  SEM.

Based on this remarkable enrichment of NCLX specifically in astrocytes, we sought to investigate the effects of this exchanger on astrocytic function. To this end, we used an *in vitro* model of primary murine astrocyte cultures to assess the effects of NCLX inhibition. Parnis et al. (2013) demonstrated that *Nclx* silencing in astrocytes shaped stimulus-induced cytosolic  $\text{Ca}^{2+}$  responses. In good agreement with this, we observed that pharmacological NCLX inhibition with CGP-37157 (CGP) in cultured astrocytes also modified ATP-induced  $\text{Ca}^{2+}$  signaling (Fig. 2A,B). CGP-treated astrocytes showed a trend toward smaller ATP-induced  $\text{Ca}^{2+}$  peaks (Fig. 2C) and increased initial clearance slope (Fig. 2B,D). Indeed, NCLX inhibition significantly decreased the cumulative  $[\text{Ca}^{2+}]$  (area under the curve, AUC, Fig 2E). Our results therefore confirm that NCLX is active in astrocytes, and its activity impacts on cellular  $\text{Ca}^{2+}$  homeostasis.

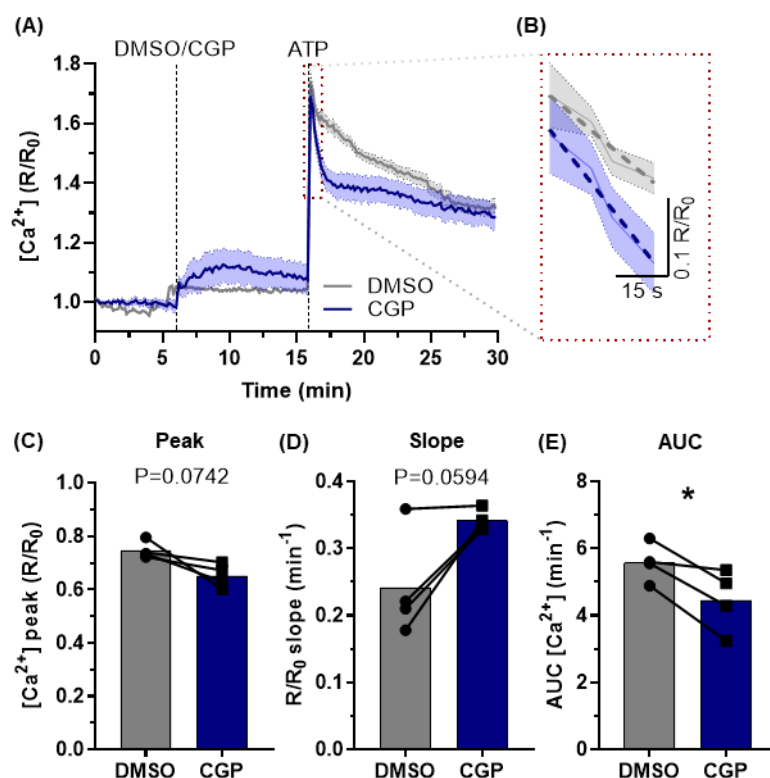


**Figure 2. NCLX inhibition changes intracellular  $\text{Ca}^{2+}$  homeostasis.** Primary mouse astrocytes were incubated with the membrane-permeable cytosolic  $\text{Ca}^{2+}$  probe Fura2-AM and imaged using a fluorescence microscope. (A) Representative

trace from a Fura2 imaging experiment (shadowed areas represent the confidence interval; continuous lines indicate mean value from 65 individual cells), indicating incubation with CGP-37157 (or DMSO as control) and ATP to induce a  $\text{Ca}^{2+}$  wave, and (B) an excerpt highlighting the slope after the peak (dashed lines). (C) Cytosolic  $[\text{Ca}^{2+}]$  peak, (D) slope after reaching peak, and (E) area under the curve (AUC) of the ATP peak. \* $P < 0.05$ , paired Student's t test,  $n = 4$  independent experiments with 55-125 cells each. Paired values are connected by lines, with a bar indicating the mean.

Since NCLX is a mitochondrial protein and modulates intracellular  $[\text{Ca}^{2+}]$ , a major metabolic regulator, we next sought to estimate ATP production rates in primary cortical astrocytes acutely stimulated with extracellular ATP with or without NCLX inhibition (Fig. 3), in order to uncover possible metabolic roles for this exchanger. Astrocytic oxygen consumption rates (OCR) and extracellular acidification rates (ECAR) were recorded using a Seahorse Extracellular Flux analysis system, and mitochondrial ATP production and electron transport chain activity were modulated by the addition of oligomycin (an ATP synthase inhibitor) and rotenone plus antimycin A (electron transport inhibitors) (Fig 3A,B). From these traces, the total ATP production rate, as well as its division between oxidative phosphorylation- and glycolysis-associated ATP production rates, were estimated as described by Mookerjee et al. (2017).

NCLX inhibition by CGP-37157 (CGP) induced a decrease in the total ATP production rate (Fig. 3C) both under basal and ATP-stimulated conditions. This was associated with a shift from oxidative phosphorylation to glycolysis (Fig. 3D,E). The increase in glycolysis observed with NCLX inhibition was not exclusive to primary astrocytes. In C6 glioblastoma cells, NCLX inhibition with CGP did not significantly alter overall mitochondrial respiratory parameters (Fig. 3 Suppl 1A-F), but significantly changed ECARs in response to oligomycin (Fig. 3 Suppl 1G), showing a similar metabolic profile to primary astrocytes, which suggests enhanced glycolytic flux. Of note, while the majority of basal ATP production in astrocytes came from mitochondrial respiration (88.9%, Fig. 3D), the effect size of the CGP-induced response was more substantial for glycolytic flux (Fig. 3E), *i.e.* the proportional increase in glycolysis appears to be of greater biological significance than mitochondrial ATP flux reduction.

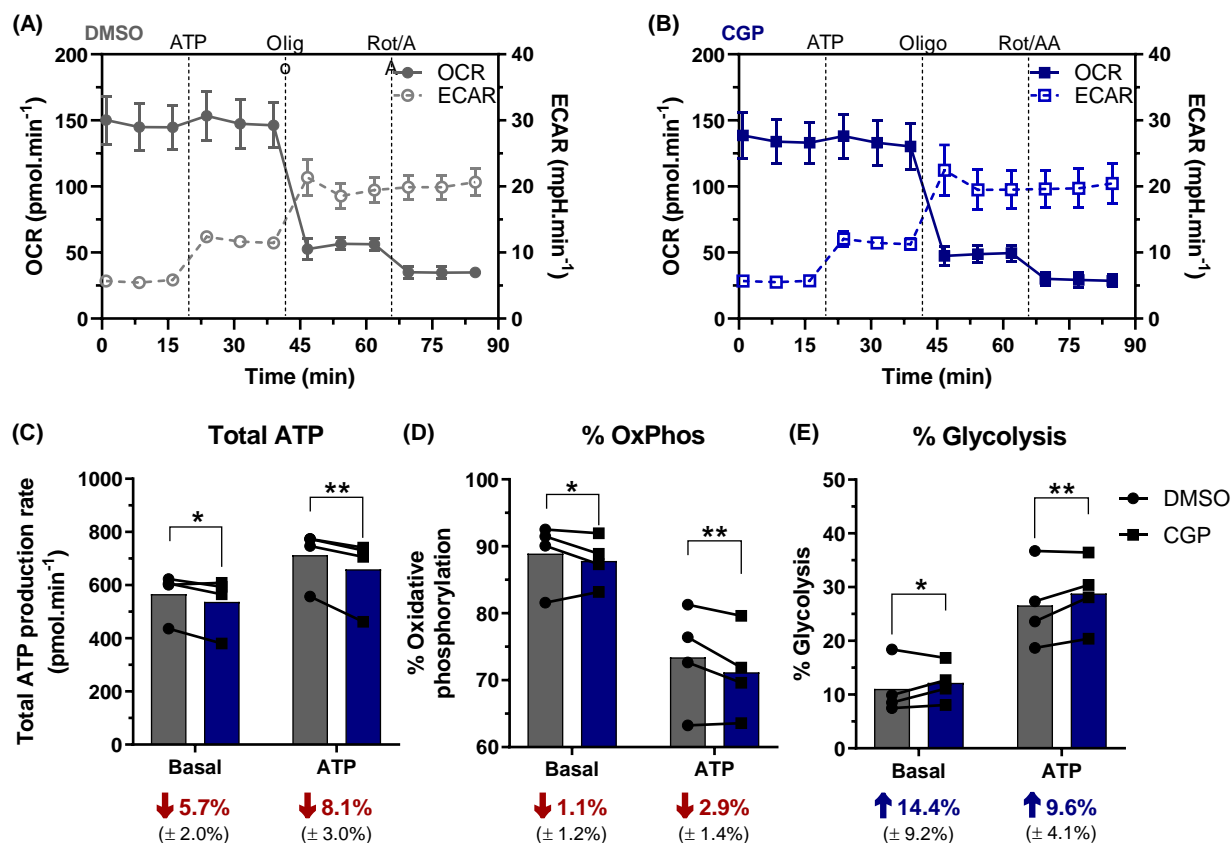


**Figure 3. NCLX inhibition increases glycolytic ATP production rates in primary mouse astrocytes.** Primary mouse astrocytes incubated with the NCLX inhibitor CGP-37157 (CGP) or DMSO had their oxygen consumption rates (OCR) and extracellular acidification rates (ECAR) monitored in a Seahorse ATP Production Rate assay. Representative traces of (A) DMSO- and (B) CGP-treated astrocytes, stimulated with ATP and followed by oligomycin (oligo) and rotenone plus antimycin A (Rot/AA) inhibition, average  $\pm$  SEM; Basal and ATP-induced (C) total ATP production rate, and proportional (D) oxidative phosphorylation (OxPhos)- and (E) glycolytic-associated ATP production rate. Average values ( $\pm$  SEM) of the proportional difference between CGP- and DMSO-treated groups were calculated and presented in their respective conditions (C-E). \* $P < 0.05$ , \*\* $P < 0.01$ , paired 2-way ANOVA followed by Holm-Šidak's post-hoc test,  $n = 4$  independent experiments. Lines and error bars indicate mean and SD, respectively (A,B); paired values are connected by lines, with a bar indicating the mean (C-E).

To further confirm the occurrence of a glycolytic shift promoted by NCLX inhibition, we assessed glucose metabolism through glycolysis by measuring tritiated water ( $^3\text{H}_2\text{O}$ ) production from radiolabeled glucose, which showed a trend toward an increased glycolytic flux in astrocytes with NCLX inhibition (Fig. 4A). This was paralleled by a significant increase in glucose consumption (Fig. 4B) and lactate secretion (Fig. 4C) under the same conditions, thus confirming that pharmacological inhibition of NCLX activity increases glycolysis and, ultimately, culminates in augmented lactate secretion. This same effect was observed in C6 cells, which presented increased lactate secretion when NCLX was inhibited (Fig. 3 Suppl. 1H).

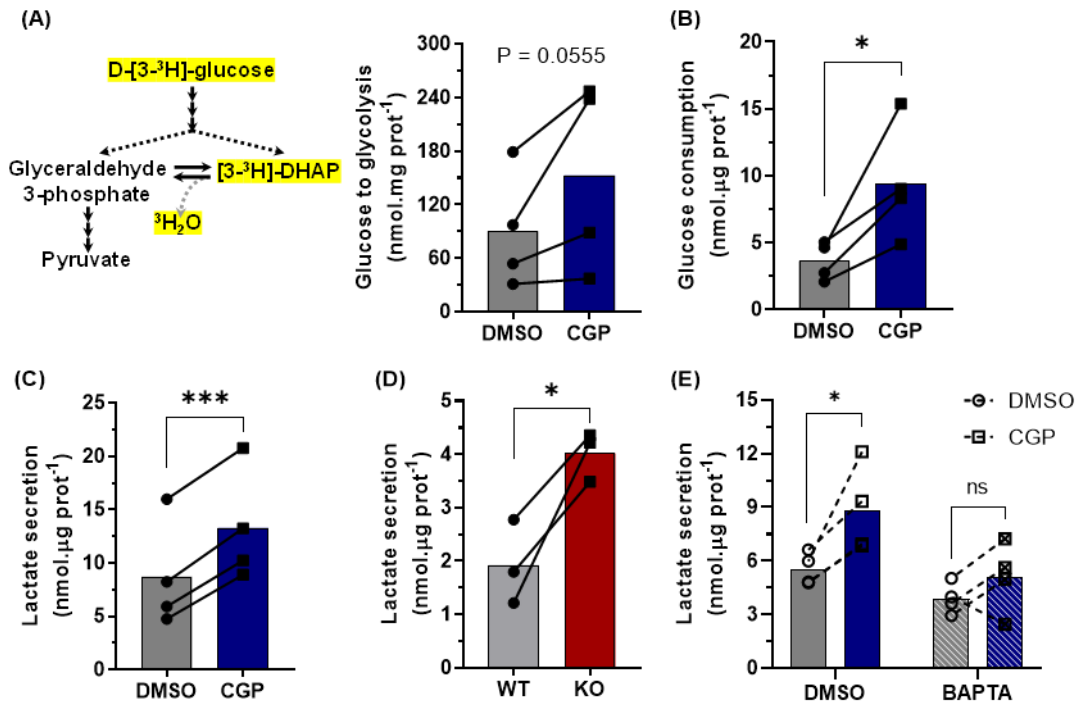


**Figure 4. NCLX inhibition increases astrocytic glycolytic flux in a Ca<sup>2+</sup>-dependent manner.** Primary mouse astrocytes were co-incubated with the NCLX inhibitor CGP-37157 (CGP) and marked D-[3-<sup>3</sup>H]-glucose for 4 h. Derived tritiated water was measured to estimate glucose metabolism through glycolysis. Glucose consumption (B) and lactate secretion (C) were assessed in parallel experiments. (D) Primary astrocytes derived from *Nclx*<sup>loxP/loxP</sup> mice were transduced with an adenoviral vector to express Cre-recombinase and achieve genetic deletion (NCLX KO); lactate secretion was measured during 1 h. Astrocytes were treated with the cytosolic Ca<sup>2+</sup> chelator BAPTA-AM, followed by incubation with CGP-37157 or DMSO as a control, similarly to Fig 3C. Lactate secretion (D) was then assessed. \*P < 0.05, \*\*\*P < 0.001, paired (B-D) or ratio-paired (A) Student's t test, or paired 2-way ANOVA followed by Holm-Šidak's post-hoc test (E), n = 3-4 independent experiments. Paired values are connected by lines, with a bar indicating the mean.

Pharmacological modulations, however, may be prone to undesired off-target effects. We therefore performed experiments in primary cultured astrocytes from *Nclx*<sup>loxP/loxP</sup> mice and induced *Nclx* deletion *in vitro* through adenoviral-mediated Cre expression. While CGP effects are acute (4 h incubations), NCLX knockout was achieved over the course of days, which could lead to compensatory mechanisms and dynamic changes in metabolic modulations observed. Notwithstanding, NCLX knockout induced a significant increase in lactate secretion during 1 h measurements (Fig. 4D), of similar magnitude to those observed in CGP-treated astrocytes.

Since the increased lactate production induced by NCLX inhibition does not involve significantly hampered oxidative phosphorylation or increased ATP demand (Fig. 3), we hypothesized it occurred secondarily to changes in cytosolic Ca<sup>2+</sup> handling. To investigate this possibility, we

verified the effects of NCLX inhibition in astrocytes pre-incubated with the cytosolic  $\text{Ca}^{2+}$  chelator BAPTA-AM. Again, NCLX inhibition induced a significant increase in lactate secretion in control cells but not in cells in which cytosolic  $\text{Ca}^{2+}$  was previously chelated by BAPTA (Fig. 4E), thus indicating that  $\text{Ca}^{2+}$  is necessary for this NCLX-mediated glycolysis modulation. Hence, glycolytic intensification and lactate secretion by NCLX inhibition is a specific,  $\text{Ca}^{2+}$ -dependent effect.

These findings suggest that NCLX has a key functional role in astrocytic metabolic homeostasis, regulating glycolytic flux and lactate secretion. As lactate is secreted from these cells and used as a substrate by neurons, with known effects on memory and synaptic plasticity (Suzuki et al., 2011; Yang et al., 2014; Roumes et al., 2021), we investigated the impact of these metabolic changes on brain function by promoting *Nclx* deletion *in vivo*. Adeno-associated viral vectors were stereotaxically delivered to the hippocampi of *Nclx<sup>loxP/loxP</sup>* adult mice (Fig. 5A) to selectively induce Cre recombinase expression in astrocytes or neurons (Fig. 5B). Behavioral assessment of these animals indicated that neither neuronal nor astrocytic *Nclx* deletion changed their exploratory profile (Fig. 5C,D; Fig. 5 Suppl. 1,2). Surprisingly, astrocytic NCLX KO animals showed improved novel object recognition performance (Fig. 5E; Fig. 5 Suppl. 4) and a similar trend in the Y-maze test (Fig. 5G; Fig. 5 Suppl. 6). In contrast, neuronal *Nclx* deletion negatively influenced the novel object recognition performance (Fig. 5F) without affecting the Y-maze test (Fig. 5H), a result compatible with previous results indicating that increased mitochondrial  $\text{Ca}^{2+}$  in neurons secondary to NCLX defects is linked to cognitive impairment (Jadiya et al., 2019; Stavsky et al., 2021). These results demonstrate that astrocytic NCLX activity influences cerebral function in a manner associated with enhanced glycolysis and lactate secretion by astrocytes.

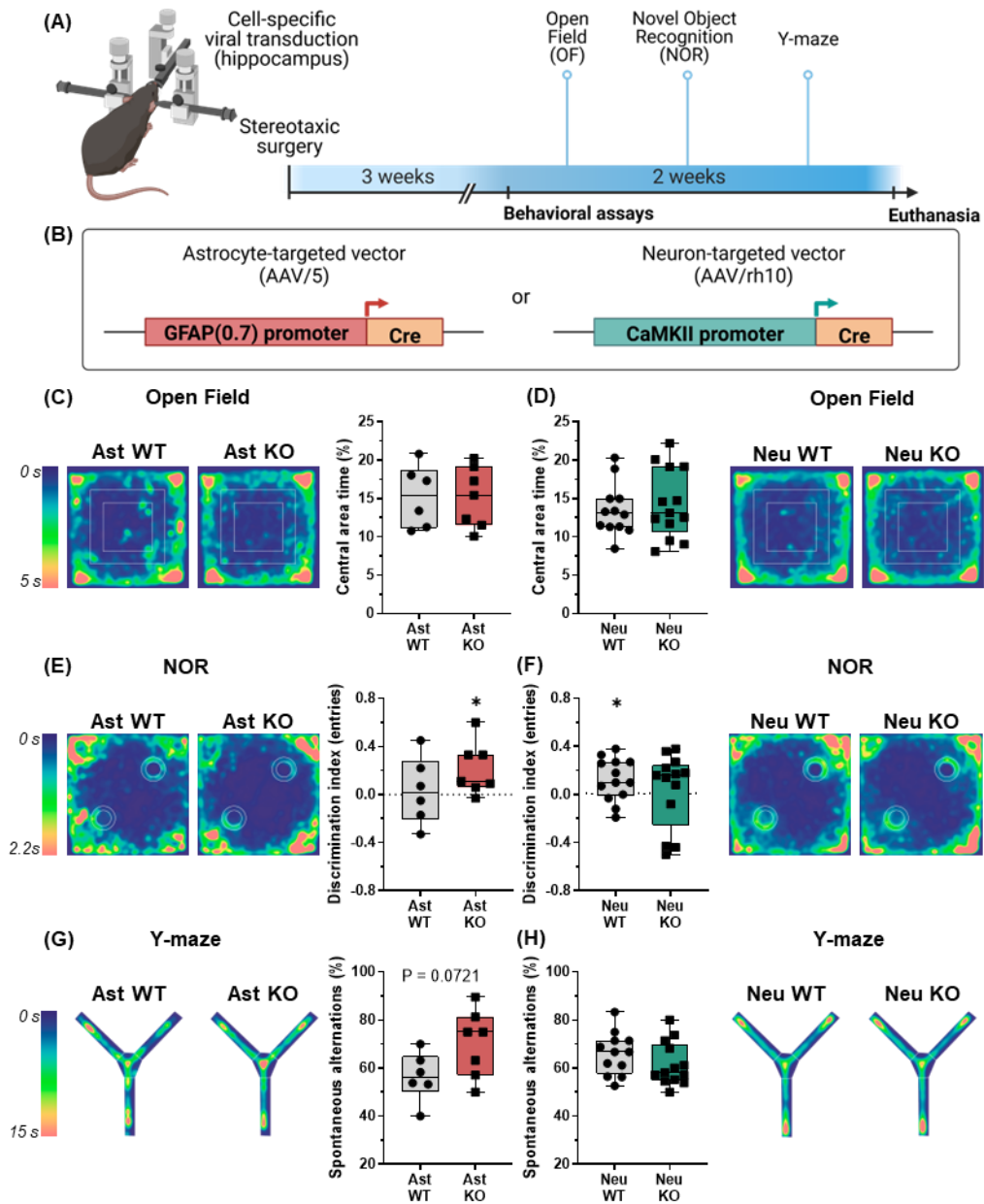


**Figure 5. *In vivo* cell-specific NCLX deletion in astrocytes or neurons has opposite behavioral effects.** (A) Schematic depiction of the experimental design: *Nclx<sup>loxP/loxP</sup>* mice were injected with cell-targeted vectors stereotaxically in the hippocampus to induce astrocytic or neuronal NCLX deletion, followed by behavioral assessment. (B) Illustration of the viral constructs used to induce astrocyte- (AAV/5) or neuron-specific (AAV/rh10) Cre recombinase expression. (C,D) Open field spatiotemporal quantitative heatmaps showing average occupation of the arena area, and calculation of proportional time in the central area. Not significant, unpaired Student's t test. (E,F) Novel object recognition spatiotemporal quantitative heatmaps, showing average occupation in the arena during the recognition test, and the discrimination index calculated from entries in novel and familiar object areas. \* $P < 0.05$ , one sample Wilcoxon test with theoretical mean = 0.0. (G,H) Y-maze spatiotemporal quantitative heatmaps, showing average occupation of the arena, and calculation of the proportion of spontaneous alternations in respect to total entries. Not significant, unpaired Student's t test,  $n = 6-13$  mice. Boxes indicate upper and lower quartiles and the median (line), whiskers represent min and max values.

## Discussion

NCLX, the  $\text{Na}^+/\text{Ca}^{2+}$  exchanger that promotes  $\text{Ca}^{2+}$  extrusion from mitochondria to the cytosol (Assali and Sekler, 2021; Serna et al., 2022), is highly enriched in astrocytes when compared to other cells in the brain or other mitochondrial proteins (Fig.1; Hagenston et al., 2022). Prior work in astrocytes demonstrated that NCLX silencing leads to impaired astrocyte proliferation *in vitro* (Parnis et al. 2013) and decreased astrocyte numbers *in vivo* (Hagenston et al. 2022). However, little was known about the influence of astrocytic NCLX activity on astrocytic function. NCLX activity in other cell types results mostly in changes in intra and extramitochondrial  $\text{Na}^+$  and  $\text{Ca}^{2+}$  levels, in a manner dependent on mitochondrial inner membrane potentials (Assali and Sekler, 2021). Indeed, we find that inhibiting NCLX activity significantly impacts on  $\text{Ca}^{2+}$  homeostasis in astrocytes (Fig. 2).

We also evaluated the effects of NCLX on astrocyte metabolic fluxes, given the known impact of mitochondrial ion transport and  $\text{Ca}^{2+}$  on metabolic regulation (Llorente-Folch et al., 2015; Juaristi et al., 2019; Ashrafi et al., 2020; Groten and MacVicar, 2022). Interestingly, we found that astrocytic ATP production through oxidative phosphorylation was only slightly decreased by inhibition of NCLX (Fig. 3). Accordingly, Hernansanz-Agustín et al. (2020) did not observe any effect of NCLX activity on mitochondrial respiration in endothelial cells. Furthermore, human colorectal cancer cells present lower maximal respiration in the absence of NCLX, but ATP-linked respiration is unaltered (Pathak et al., 2020). These mild effects of NCLX inhibition on mitochondrial respiration may be related to inhibition of metabolic shuttles secondarily to changes in cytosolic  $\text{Ca}^{2+}$ , since the mitochondrial isoform of glycerol-3-phosphate dehydrogenase (Gherardi et al., 2020) and the aspartate-glutamate exchanger, a component of the malate-aspartate shuttle, are both  $\text{Ca}^{2+}$ -sensitive; the latter is of great relevance for metabolic control in the brain (Llorente-Folch et al., 2015). Hampering the activity of these critical points for mitochondrial NADH uptake decreases maximal electron transport capacity in mitochondria and may also lead to enhanced cytosolic NADH levels (Wang et al., 2022) (Fig. 6).



Consistently, accumulation of  $\text{Ca}^{2+}$  in cerebral mitochondria leads to accumulation of NADH (Díaz-García et al., 2021).

While the effects of astrocyte NCLX inhibition on mitochondrial electron transport were small, glycolytic ATP fluxes were substantially increased, both in cells with pharmacologically-inhibited NCLX and in knockout cells (Figs. 3,4). Loss of NCLX activity in colorectal cells was also found to significantly increase glycolytic flux. Interestingly, NCLX is modulated by PKA (Assali et al., 2020; Kostic et al., 2015; Zhou et al., 2021), an important metabolic regulatory hub that also influences glycolysis (Rider et al., 2004), further supporting a role for this transporter in the regulatory network of glycolytic activity. Increased glycolytic flux, especially when in the presence of decreased oxidative phosphorylation and lower NADH oxidation (Rigoulet et al., 2020), typically promotes enhanced lactate production. Indeed, we find that astrocytes and C6 glioma cells secrete more lactate when NCLX is inhibited pharmacologically or knocked out (Fig. 5). This effect is a result of changes in cytosolic  $\text{Ca}^{2+}$  signaling promoted by NCLX, as it was abrogated by the presence of BAPTA as a cytosolic  $\text{Ca}^{2+}$  chelator.

Astrocytic lactate has long been characterized as a fundamental substrate for neurons (Pellerin and Magistretti, 1994; Herrero-Mendez et al., 2009; Rodriguez-Rodriguez et al., 2012; Mächler et al., 2016; Bonvento and Bolaños, 2021), which also acts as a gliotransmitter, promoting synaptic plasticity, and higher functions (Suzuki et al., 2011; Yang et al., 2014; Adamsky et al., 2018; Jimenez-Blasco et al., 2020; Roumes et al., 2021; Akther and Hirase, 2022). Our data show that NCLX can control lactate secretion and therefore potentially act as a modulator of the astrocyte-to-neuron lactate shuttle, by acting as a connection between cytosolic and mitochondrial  $\text{Ca}^{2+}$  signaling and glycolytic flux. Indeed, we observed that astrocyte-specific NCLX deletion in the hippocampus improves aspects of mouse cognitive performance (Fig. 5E,G), while hampering NCLX activity in neurons promotes deleterious effects (Kostic et al., 2015; Sharma et al., 2017; Jadiya et al., 2019; Stavsky et al., 2021; Britti et al., 2020, 2021; Hagenston et al., 2022).

In conclusion, we demonstrate that NCLX, which is over-enriched in astrocytes, modulates astrocytic glycolytic flux and lactate secretion secondarily to shaping cytosolic  $\text{Ca}^{2+}$  signaling (Fig. 6). By fine-tuning astrocytic glycolysis and lactate secretion, NCLX may act as a control check point in brain metabolism impacting on the astrocyte-to-neuron lactate shuttle and cerebral function.

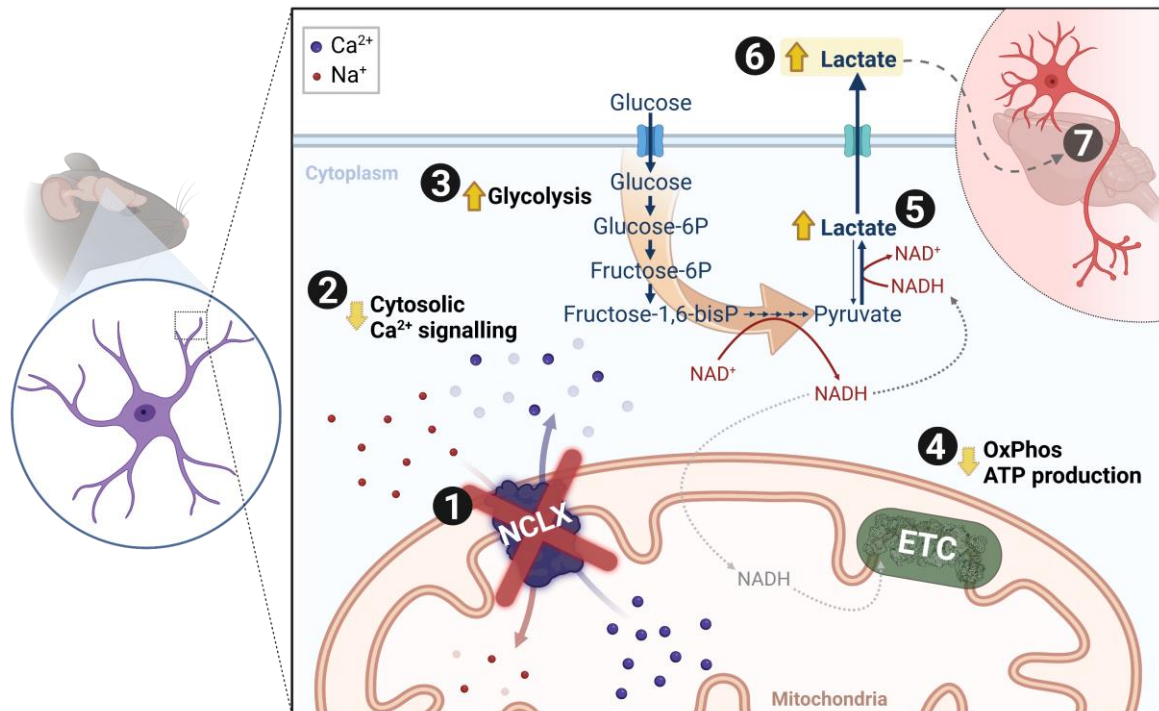


**Figure 6. Schematic overview.** In astrocytes, (1) inhibition/deletion of mitochondrial  $\text{Na}^+/\text{Ca}^{2+}$  exchanger (NCLX) activity leads to (2) augmented cytosolic  $\text{Ca}^{2+}$  clearance. This results in (3) increased glycolytic flux; and (4) slightly decreased mitochondrial oxidative phosphorylation, leading to (5) increased lactate dehydrogenase (LDH)-mediated reduction of pyruvate to lactate. The resulting increased lactate in astrocytes (6) is secreted (7) and may contribute to enhanced behavioral performance *in vivo*. (ETC: electron transport chain).

## Materials and methods

### RNAseq public databases

RNAseq data was mined from the public databases published by Zhang et al. (2014), accessed at <https://www.brainrnaseq.org/> (last access: 2021-11-01), GEO accession number [GSE52564](#); and by Chai et al. (2017) and Srinivasan et al. (2016), accessed at <http://astrocyternaseq.org/> (last access: 2021-11-01), GEO accession numbers [GSE84540](#) and [GSE94010](#), respectively.

### Animal care

Experimental design and animal care standards followed ARRIVE 2.0 guidelines (Percie du Sert et al., 2020). Animal procedures were performed according to Protocol #82/2017 from the *Comissão de Ética em Cuidado e Uso Animal do Instituto de Química da Universidade de São Paulo* and by the Bioethics Committee of the University of Salamanca (reference 449), following requirements described by the *Sociedade Brasileira de Ciência de Animais de Laboratório*, European Union Directive 86/609/EEC and Recommendation 2007/526/ EC, regarding the protection of animals used for experimental and other scientific purposes, and enforced under Spanish legislation directive RD1201/2005. Adult mice were maintained in groups of 4-5 animals per cage at the specific pathogen free Animal Experimentation Facility of the University of Salamanca (Biosafety Level 2 environments). Neonates (0-1 days-old) were obtained from breeding cages (1 male and 1-3 females per cage) from the specific pathogen free Animal Care Facility of the Institute of Chemistry and Faculty of Pharmaceutical Sciences at the University of São Paulo and from the Animal Experimentation Facility of the University of Salamanca. All animals were maintained in a light-dark cycle of 12 h, 45-65% humidity, 20-25 °C, with open and unlimited access to standard solid diet and water, in a microisolator system. Cages were changed and sanitized 1-2 times/week.

The number of neonates was determined by the demand of primary astrocyte cultures. Protocols and study design were optimized to yield the maximal cell count using the smallest numbers of animals, in accordance with the 3Rs principle (Percie du Sert et al., 2020). For *in vivo* experiments, a limited sample size was allocated, as the initial objective was to conduct an exploratory assessment in pursuit of evidence pointing out effects that may be of interest for further investigation. Experimental feasibility (surgery, recovery, behavioral assays, euthanasia) and operational limitations (processing capacity, total study duration and budget) were taken into account and adjusted as in a Fermi's approximation (Reynolds, 2019). Sample size range is specified in each figure legend and every animal is depicted as a symbol in graphical representations. Animals were allocated to each group haphazardly

and evenly through experimental and control groups, and cage order was counterbalanced through the course of experimental assays to avoid a time of the day bias. In total, 43 adult mice were used for *in vivo* experiments, 3 of which were excluded due to surgery issues.

*In vitro* pharmacological experiments with primary astrocytes were conducted in cells from C57Bl/6NTac mice. *Nclx*<sup>loxP/loxP</sup> (originally denoted *Slc8b1*<sup>fl/fl</sup>) mice were designed and produced at Dr. John Elrod's lab, as described by Luongo et al. (2017). Parental breeding pairs were kindly provided and shipped by Dr. Antonio Martínez-Ruiz (Hospital Universitario de La Princesa, Madrid, Spain) and maintained using a C57Bl/6J background.

## Cell cultures

Mouse cortical astrocyte primary cultures were conducted as previously described (Jimenez-Blasco et al., 2020). Briefly, brains of neonates (P0-1, both male and female) were dissected and digested with 0.1% trypsin (#T0134, Sigma-Aldrich, Saint Louis, MO, USA) in the presence of 60 µg/mL DNase I (#DN25, Sigma-Aldrich) in HBSS medium (#14175095, Gibco, Life Technologies, Carlsbad, CA, USA). The tissue was then dissociated in HBSS containing 24 µg/mL DNase I, decanted, and the resulting cell suspension was counted, plated, and maintained in Low Glucose DMEM (5.5 mM glucose, 1 mM pyruvate, 4 mM glutamine; #31600034, Gibco) supplemented with 10% fetal bovine serum (#12605729, Gibco) and 1% penicillin/streptomycin (#15140122, Gibco), in a 5% CO<sub>2</sub>, 37°C, humidified incubator. Cells were grown in a 75 cm<sup>2</sup> flask for 7 days and then shaken at 200 rpm in an incubator; the supernatant was discarded, and the remaining astrocyte-enriched culture was re-seeded at 50.10<sup>3</sup>/cm<sup>2</sup> and grown for 3-7 days for the experiments.

The C6 cell line stock (BCRJ Cat# 0057, RRID:CVCL\_0194) was kindly donated by Dr. Cristoforo Scavone (Institute of Biomedical Sciences, University of São Paulo, São Paulo, Brazil). C6 cells were grown and maintained in High Glucose DMEM (25 mM glucose, 1 mM pyruvate, 4 mM glutamine; #12800017, Gibco) supplemented with 10% fetal bovine serum and 1% penicillin/streptomycin, in a 5% CO<sub>2</sub>, 37°C, humidified incubator.

For the experiments, unless otherwise stated, all cell media were changed for a respective serum-free version and cells were allowed a 1 h equilibration period, after which 10 µM CGP-37157 (#1114, Tocris, Bio-Techne, Bristol, UK) or sterile DMSO, as a control, were added. When necessary, BAPTA-AM (10 µM, #A1076, Sigma) or DMSO, as a control, was incubated over the last 30 min of the equilibration period.

## **Seahorse assays**

Purified astrocytes or C6 cells were plated at a density of  $30 \cdot 10^3$  or  $72 \cdot 10^3$  cells per well, respectively, on XFe24 Seahorse plates (#100777-004, Agilent, Santa Clara, CA, USA) and experiments were conducted at day *in vitro* (DIV)  $15 \pm 1$ , either for acute pharmacological inhibition of NCLX or for NCLX knock-out (7 days after viral transduction). Cells were washed once with experimental medium – DMEM (phenol-free, lacking sodium bicarbonate; #D5030, Sigma-Aldrich) supplemented with 1 mM pyruvate, 4 mM glutamine, 10 mM HEPES, 1% penicillin/streptomycin, and 5.5 mM glucose (for astrocytes) or 25 mM glucose (for C6 cells) – and pre-incubated at 37°C, room atmosphere, for 1 h in 500  $\mu$ L experimental medium. Tests were conducted as described below, using pre-titrated inhibitor concentrations, and assessing respective oxygen consumption rates (OCR) and extracellular acidification rates (ECAR).

Astrocyte experiments were normalized by automated cell count, as described previously (Assali et al., 2020). Seahorse XFe24 plates were washed once with PBS right after ending the assay and fixed overnight at 4°C with PFA 4% in methanol, DAPI-stained and imaged and analyzed in a custom workflow on a High Content Screening Operetta CLS apparatus (Perkin Elmer, MA, USA). Alternatively, C6 cells were normalized by determination of total protein concentration through a BCA kit (Thermo Fisher Scientific, Rockford, USA).

### ***ATP rate test***

Total ATP production rates were estimated as previously described (Kakimoto et al., 2021; Mookerjee et al., 2017). Astrocytes were pre-incubated with 10  $\mu$ M CGP-37157 or DMSO for 1 h and then plates were inserted in a XFe24 Seahorse Analyzer apparatus (#102238-100, Agilent). Cells were stimulated with 100  $\mu$ M ATP, followed by ATP synthase inhibition with oligomycin (oligo, 2.5  $\mu$ M) and electron transport chain inhibition with rotenone (rot, 1.0  $\mu$ M) plus antimycin A (AA, 2.0  $\mu$ M). Total ATP production rates, as well as its partition between glycolytic and oxidative phosphorylation, were calculated according to the manufacturer's instructions (Romero et al., 2018), considering standard values of required constants and the buffer factor as 3.13 mM/pH.

### ***MitoStress test***

C6 cell metabolic assessment was conducted using a MitoStress test, as previously described (Amigo et al., 2017). Cell plates were inserted in an XFe24 Seahorse Analyzer apparatus (#102238-100, Agilent), acutely challenged with 10  $\mu$ M CGP-37157 or DMSO, followed by ATP synthase inhibition with oligomycin (oligo, 0.5  $\mu$ M), mitochondrial uncoupling with 2,4-dinitrophenol (DNP, 200  $\mu$ M),

and electron transport chain inhibition with rotenone (rot, 1  $\mu$ M) plus antimycin A (AA, 1  $\mu$ M). Non-mitochondrial respiration is defined as the Rot+AA-insensitive OCR and is subtracted from other parameters; OCR<sub>CGP</sub> was derived from the average between the last 3 OCR measurements; OCR<sub>proton-leak</sub> was calculated from the average between the last two oligomycin-insensitive OCR measurements; OCR<sub>ATP-linked</sub> was calculated from the difference between OCR<sub>CGP</sub> and OCR<sub>proton-leak</sub>;  $\Delta$ ECAR<sub>oligo</sub> was calculated as the difference between the first ECAR measurement right after and the one right before the oligomycin addition.

### **Glycolytic flux**

Glucose-to-glycolysis metabolism was assessed as described elsewhere (Jimenez-Blasco et al., 2020). In brief, astrocytes were washed and maintained in experimental medium at 37°C, room atmosphere, for 1 h to equilibrate. Then, cells were incubated with [3-<sup>3</sup>H]-glucose (2  $\mu$ Ci/well) and 10  $\mu$ M CGP-37157 or DMSO for 4 h, under gentle orbital rotation (60 rpm) at 37°C. Reactions were stopped by acidification with 20% perchloric acid, and cell media was collected and allowed to equilibrate with a separated tube containing 500  $\mu$ L deionized water, enclosed in a sealed glass vial, and maintained in a rotating incubator at 60 rpm, 37°C, room atmosphere, for 72 h. Produced <sup>3</sup>H<sub>2</sub>O was indirectly measured from these plastic vials through liquid scintillation counting (Tri-Carb 4810 TR, PerkinElmer).

### **Lactate secretion and glucose consumption**

In brief, cells were washed and maintained in serum-free culture medium for 1 h for equilibration, collected (baseline measurement), and followed by incubation with 10  $\mu$ M CGP-37157 or DMSO. Cell medium was collected right after CGP addition and after 1 or 4 h, and both glucose and lactate (Vicente-Gutierrez et al., 2019) levels were measured spectrophotometrically. Lactate concentrations were determined through assessment of NADH formation at  $\lambda = 340$  nm in a buffer (250 mM glycine, 500 mM hydrazine, 1 mM EDTA, pH 9.5) containing 1 mM NAD<sup>+</sup> and 22.5 U/mL lactate dehydrogenase, or using a commercial kit (#138, Labtest, Lagoa Santa, MG, Brazil). Glucose concentrations were determined by following NADPH production at  $\lambda = 340$  nm in a tris buffer (100 mM, pH 8.0), containing 0.5 mM MgCl<sub>2</sub>, 2 mM ATP, 1.5 mM NADP<sup>+</sup>, 2.5 U/mL hexokinase and 1.25 U/mL glucose-6-phosphate dehydrogenase.

### **Viral transduction**

Cre recombinase expression was induced *in vitro* through an adenoviral vector (Ad5-CMV-Cre-eGFP, lot# Ad4334 13D6, University of Iowa Viral Vector Core, Iowa City, IA, USA) or its respective empty vector as a control (Ad5-CMV-GFP, lot# Ad4415 13D3, University of Iowa Viral Vector Core).

Primary astrocytes were infected 2 days after being re-plated at 15 MOI (multiplicity of infection). Virus suspension was removed 24 h after transduction and experiments were conducted 7 days after beginning of infection.

For *in vivo* experiments (Fig. 5B), Cre recombinase expression was mediated by adeno-associated viral vectors (AAV, all from Vector Biolabs, Malvern, PA, USA) and driven by an astrocyte-specific GFAP promoter (AAV/5-GFAP(0.7)-GFP-2A-iCre, #VB1131, lot# 190527#25) or by a neuronal-specific CaMKII promoter (AAV/rh10-CaMKII(0.4)-eGFP-T2A-Cre, #VB1435, lot# 201123#1). Control groups were transduced with the empty vectors AAV/5-GFAP(0.7)-eGFP (#VB1149, lot# 190527#24) and AAV/rh10-CaMKII(0.4)-eGFP (#VB1435, lot# 201123#1), respectively.

### **Stereotaxic surgery**

Surgery was conducted as described by Lapresa et al. (2022). Male *Nclx<sup>loxP/loxP</sup>* mice ( $11.7 \pm 2.5$  weeks old) were briefly anesthetized with sevoflurane (4% for induction, 2.5% for maintenance) in a 30% O<sub>2</sub> and 70% N<sub>2</sub>O atmosphere (0.4 and 0.8 L/min, respectively). Animals were appropriately positioned in the stereotaxic apparatus (#1900, David Kopf Instruments, Tujunga, CA, USA) coupled with a digital readout (Wizard 550, Anilam, ACU-RITE/Heidenhain Corporation, Schaumburg, IL, USA), maintained under a heat lamp, and had their temperatures monitored by a rectal thermometer. Injections were controlled by a digitally-controlled pump (UltraMicroPump with a Micro4 UMC4 III controller, World Precision Instruments, Sarasota, FL, USA), in which 2  $\mu$ l containing  $1 \cdot 10^{10}$  PFU/ $\mu$ L of AAV/5 vectors (for astrocytic deletion, see constructs above) or  $2.75 \cdot 10^{12}$  viral genome copies/ $\mu$ L of AAV/rh10 vectors (for neuronal deletion, see constructs above) diluted in sterile PBS with 0.001% Pluronic F-68 were administered bilaterally in two depths (1  $\mu$ l each) at 500 nL/min. Hippocampi were targeted according to the following coordinates, based on Paxinos and Franklin atlas (Paxinos and Franklin, 2001) and previously validated (Jimenez-Blasco et al., 2020): AP = - 2 mm, ML =  $\pm$  1.5 mm, and DV = -2 mm (first injection) and -1.5 mm (second injection). Animals were kept in heated cages and closely monitored up to full recovery from anesthesia, and then were observed for the following days. Detection of unexpected recovery issues (*e.g.*, infection or excessive inflammation at suture site, inadequate wound healing) or cases when stereotaxic surgery was identified as unsuccessful by the surgeon (*e.g.*, syringe content overflowed injection site, death during surgery) were exclusion criteria, and animals were cared for to minimize suffering and euthanized.

### **Behavioral assays**

Behavioral assessment started 3 weeks after surgery (Fig. 5A), to allow proper recovery and gene recombination. Mice were acclimatized to the experimenter (male researcher) 1 week prior to the



beginning of the behavioral assays by daily soft manipulation, and to the experimental room for 1 h before each assay. Assays were tracked by ANY-maze software with the Ami-maze interface in an ANY-box core (40 x 40 cm; Stoelting Co., Wood Dale, IL, USA), except for the Y-maze test, which was conducted on a specific apparatus and manually scored. The experimenter was blinded to animal genotype through all behavioral experiments. Censoring was proceeded when justified by statistical outlier assessment or in the case of operational problems (*e.g.*, video recording issue), and properly reported when done.

### ***Open Field test***

Exploratory behavior was assessed through the Open Field test (Cabral-Costa et al., 2018; Lapresa et al., 2022). Animals were allowed to individually explore the experimental apparatus for 10 min. Total distance, mean speed, time freezing, number of rearings, and central area (defined as a virtual central 20 x 20 cm square) number of entries, and total time were measured.

### ***Novel Object Recognition test***

On the following day, animals were submitted to 2 sessions of 5 min each, separated by a 30 min interval. These sessions consisted of a training stage (two equal wooden objects on opposite symmetric sides of the arena, Fig. 5E,F) and novel object recognition (NOR, where a second, novel, object substituted one of the familiar ones, at the bottom left position). Total distance, time spent exploring and number of interactions (entries) with each object was measured. NOR discrimination indexes were assessed as an indicator of short-term recognition memory (Cabral-Costa et al., 2018; Vicente-Gutierrez et al., 2019), calculated as the difference in number of interactions (or time) between the novel and the familiar object divided by total number of entries (or total exploration time).

### ***Y-maze test***

Spontaneous alternation on a Y-maze was assessed as an indicator of working memory (Jimenez-Blasco et al., 2020). Animals were positioned in the central area of a Y-maze, facing the wall on the opposite side of the experimenter, and allowed to explore the maze for 5 min. Entrances on each arm (A, B, C) were manually scored from the recorded video by an independent researcher who was blinded for genotype. Spontaneous alternation was defined as the total number of triads of sequential entrances in three different arms and calculated in Rstudio (version 2022.02.0, PBC, Boston, MA, USA) using the script annotated at <https://github.com/jvccosta/NCLXAstMetab>.

## Calcium imaging

Calcium levels were live monitored in attached astrocytes through the ratiometric probe Fura-2-AM (#F1221, Invitrogen, Waltham, MA, USA) as done by Kowaltowski et al. (2019). Briefly, cells were plated in glass-bottom culture dishes (#627871, Greiner Bio-One, Kremsmünster, Austria), incubated with 5  $\mu\text{M}$  Fura-2-AM for 30 min at 37°C in experimental medium lacking FBS and supplemented with 1 mg/mL bovine serum albumin (BSA). Fluorescence was assessed at  $\lambda_{\text{ex}} = 340$  (F<sub>340</sub>) and 380 nm (F<sub>380</sub>) and  $\lambda_{\text{em}} = 510$  nm in a Leica DMI-8 microscope equipped with a Fura-2 filter (Leica Microsystems, Buffalo Grove, IL, USA). Cells were followed through additions of CGP (10  $\mu\text{M}$ ), ATP (100  $\mu\text{M}$ ), as well as ionomycin (20  $\mu\text{M}$ ) to allow calibration. Analyses were conducted through FIJI ImageJ 1.52p (Schindelin et al., 2012), in which individual cells (55-125/group per experiment) were identified as regions of interest (ROI) and  $[\text{Ca}^{2+}]$  variation was estimated as the ratio (R) between F<sub>340</sub>/F<sub>380</sub>. Data was calibrated by the maximal ratio induced by ionomycin, controlled for background fluorescence oscillations, and normalized by the initial ratio (R<sub>0</sub>).

## Statistical analyses

All raw data was organized and analyzed in Microsoft Excel (Microsoft 365 MSO, version 2207, Microsoft Corporation, Redmond, WA, USA), and statistical analyses were performed in GraphPad Prism 8 (version 8.4.3, GraphPad Software, San Diego, CA, USA), in which all figures were also plotted. According to the experimental design, as appropriately described in the figure legends, data was analyzed through unpaired, paired, or ratio-paired Student's t-test; one-sample Wilcoxon test with theoretical mean = 0.0, and paired two-way ANOVA, followed by Holm-Šidak's post-hoc test for parametric analyses; and through Mann-Whitney test for non-parametric analyses. A ROUT outlier test, with 5% sensitivity, was used to search for outliers.

## Data availability

All raw data will be made available as supplementary material.

## Acknowledgements

We would like to thank Camille C. Caldeira da Silva, Sirlei Mendes de Oliveira, and Monica Resch for the outstanding technical support; the IQ-FCF/USP and IBFG-USAL animal facilities staffs, in the name of Silvania Neves, Renata Spalutto Fontes, Flavia Ong, Monica Carabias-Carrasco, Lucia Martin, and Estefania Prieto-Garcia, for the exceptional animal care; André Costa Oliveira, for contributing with coding guidance; and Amanda Midori Matumoto, for contributing with animal behavior scoring. We are also deeply grateful to Dr. Antonio Martínez-Ruiz for kindly mediating the *Nclx*<sup>loxP/loxP</sup> mouse logistics, as well as to Dr. Pamela Kakimoto, Dr. Bruno Chausse, Dr. José Carlos de Lima Jr., Dr. Marcus F. Oliveira, Dr. Ruben Quintana-Cabrera, Dr. Marcel Vieira-Lara, Dr. Nathalia Dragano, Vitor M. Ramos, Paula Alonso-Batán, Dr. Daniel Jiménez-Blasco, and Dr. Pablo Hernansanz-Agustín for contributing with scientific discussions and inputs. Illustrations were created with Biorender.com. Electron transport chain scheme was constructed based on actual complex crystal structures (PDB #6G2J, 1ZOY, 3CX5, 3HB3, 1CRH, 7TK4).

## Funding

Authors were supported by grant #2020/06970–5 from *Fundação de Amparo à Pesquisa do Estado de São Paulo* (FAPESP); *Centro de Pesquisa, Inovação e Difusão de Processos Redox em Biomedicina* (CEPID Redoxoma, FAPESP grant #2013/07937–8); *Conselho Nacional de Desenvolvimento Científico e Tecnológico* (CNPq); and *Coordenação de Aperfeiçoamento de Pessoal de Nível Superior* (CAPES) line 001; *Agencia Estatal de Investigación* (PID2019-105699RB-I00/AEI/10.13039/501100011033, PDC2021-121013-I00 and RED2018-102576-T to JPB); *Plan Nacional de Drogas* (2020I028 to JPB); *Instituto de Salud Carlos III* (PI21/00727 and RD21/0006/0005 co-funded by the European Union FEDER/FSE+ and NextGenerationEU to AA); and *Junta de Castilla y León* (CS/151P20 co-funded by P.O. FEDER to AA; *Apoyo Regional a la Competitividad Empresarial*, ICE 04/18/LE/0017 to JPB, and *Escalera de Excelencia* CLU-2017-03 to JPB and AA). JVCC was also supported by FAPESP fellowships #2017/14713-0 and #2019/22178-2.

## Conflict of Interest

The authors declare that they have no conflicts of interest with the contents of this article.

## Author contributions

**Conceptualization:** JVCC, JPB, AJK. **Methodology:** JVCC, JWE. **Software:** JVCC. **Validation:** JVCC, CVG. **Investigation:** JVCC, CVG, JA, RL. **Formal Analysis:** JVCC, JA, RL. **Data Curation:** JVCC. **Visualization:** JVCC. **Writing – Original Draft:** JVCC. **Writing – Review:** JA, RL, JWE, AA, JPB, AJK. **Writing – Editing:** JVCC, AA, JPB, AJK. **Resources:** JWE, AA, JPB, AJK. **Funding Acquisition:** JVCC, AA, JPB, AJK. **Supervision:** CVG, JA, AA, JPB, AJK. **Project Administration:** JPB, AJK.

## References

- Adamsky A, Kol A, Kreisel T, Doron A, Ozeri-Engelhard N, Melcer T, Refaeli R, Horn H, Regev L, Groysman M, London M, Goshen I. 2018. Astrocytic activation generates de novo neuronal potentiation and memory enhancement. *Cell* **174**:59-71.e14. doi:10.1016/j.cell.2018.05.002
- Akther S, Hirase H. 2022. Assessment of astrocytes as a mediator of memory and learning in rodents. *Glia* **70**:1484–1505. doi:10.1002/glia.24099
- Amigo I, Menezes-Filho SL, Luévano-Martínez LA, Chausse B, Kowaltowski AJ. 2017. Caloric restriction increases brain mitochondrial calcium retention capacity and protects against excitotoxicity. *Aging Cell* **16**:73–81. doi:10.1111/ace.12527
- Arruda AP, Parlakgöl G. 2022. Endoplasmic reticulum architecture and inter-organelle communication in metabolic health and disease. *Cold Spring Harb Perspect Biol* a041261. doi:10.1101/cshperspect.a041261
- Arundine M, Tymianski M. 2003. Molecular mechanisms of calcium-dependent neurodegeneration in excitotoxicity. *Cell Calcium* **34**:325–337. doi:10.1016/S0143-4160(03)00141-6
- Ashrafi G, de Juan-Sanz J, Farrell RJ, Ryan TA. 2020. Molecular tuning of the axonal mitochondrial Ca<sup>2+</sup> uniporter ensures metabolic flexibility of neurotransmission. *Neuron* **105**:678-687.e5. doi:10.1016/j.neuron.2019.11.020
- Assali EA, Jones AE, Veliova M, Acín-Pérez R, Taha M, Miller N, Shum M, Oliveira MF, Las G, Liesa M, Sekler I, Shirihai OS. 2020. NCLX prevents cell death during adrenergic activation of the brown adipose tissue. *Nat Commun* **11**:3347. doi:10.1038/s41467-020-16572-3
- Assali EA, Sekler I. 2021. Sprinkling salt on mitochondria: the metabolic and pathophysiological roles of mitochondrial Na<sup>+</sup> signaling mediated by NCLX. *Cell Calcium* **97**:102416. doi:10.1016/j.ceca.2021.102416
- Baughman JM, Perocchi F, Girgis HS, Plovanich M, Belcher-Timme CA, Sancak Y, Bao XR, Strittmatter L, Goldberger O, Bogorad RL, Kotliansky V, Mootha VK. 2011. Integrative genomics identifies MCU as an essential component of the mitochondrial calcium uniporter. *Nature* **476**:341–345. doi:10.1038/nature10234
- Bonvento G, Bolaños JP. 2021. Astrocyte-neuron metabolic cooperation shapes brain activity. *Cell Metab* **33**:1546–1564. doi:10.1016/j.cmet.2021.07.006
- Britti E, Delaspre F, Tamarit J, Ros J. 2021. Calpain-inhibitors protect frataxin-deficient dorsal root ganglia neurons from loss of mitochondrial Na<sup>+</sup>/Ca<sup>2+</sup> exchanger, NCLX, and apoptosis. *Neurochem Res* **46**:108–119. doi:10.1007/s11064-020-03020-3
- Britti E, Ros J, Esteras N, Abramov AY. 2020. Tau inhibits mitochondrial calcium efflux and makes neurons vulnerable to calcium-induced cell death. *Cell Calcium* **86**:102150. doi:10.1016/j.ceca.2019.102150
- Cabral-Costa JV, Andreotti DZ, Mello NP, Scavone C, Camandola S, Kawamoto EM. 2018. Intermittent fasting uncovers and rescues cognitive phenotypes in PTEN neuronal haploinsufficient mice. *Sci Rep* **8**:8595. doi:10.1038/s41598-018-26814-6
- Cabral-Costa JV, Kowaltowski AJ. 2020. Neurological disorders and mitochondria. *Mol Aspects Med* **71**:100826. doi:10.1016/j.mam.2019.10.003
- Chai H, Diaz-Castro B, Shigetomi E, Monte E, Oceau JC, Yu X, Cohn W, Rajendran PS, Vondriska TM, Whitelegge JP, Coppola G, Khakh BS. 2017. Neural circuit-specialized astrocytes: transcriptomic, proteomic, morphological, and functional evidence. *Neuron* **95**:531-549.e9. doi:10.1016/j.neuron.2017.06.029
- De La Fuente S, Lambert JP, Nichtova Z, Fernandez Sanz C, Elrod JW, Sheu S-S, Csordás G. 2018. Spatial separation of mitochondrial calcium uptake and extrusion for energy-efficient mitochondrial calcium signaling in the heart. *Cell Rep* **24**:3099-3107.e4. doi:10.1016/j.celrep.2018.08.040

- De Stefani D, Raffaello A, Teardo E, Szabò I, Rizzuto R. 2011. A forty-kilodalton protein of the inner membrane is the mitochondrial calcium uniporter. *Nature* **476**:336–340. doi:10.1038/nature10230
- DeLuca HF, Engstrom GW. 1961. Calcium uptake by rat kidney mitochondria. *Proc Natl Acad Sci USA* **47**:1744–1750. doi:10.1073/pnas.47.11.1744
- Drahota Z, Lehninger AL. 1965. Movements of H<sup>+</sup>, K<sup>+</sup>, and Na<sup>+</sup> during energy-dependent uptake and retention of Ca<sup>++</sup> in rat liver mitochondria. *Biochem Biophys Res Commun* **19**:351–356. doi:10.1016/0006-291X(65)90467-5
- Feno S, Rizzuto R, Raffaello A, Vecellio Reane D. 2021. The molecular complexity of the Mitochondrial Calcium Uniporter. *Cell Calcium* **93**:102322. doi:10.1016/j.ceca.2020.102322
- Garbincius JF, Luongo TS, Jadiya P, Hildebrand AN, Kolmetzky DW, Mangold AS, Roy R, Ibetti J, Nwokedi M, Koch WJ, Elrod JW. 2022. Enhanced NCLX-dependent mitochondrial Ca<sup>2+</sup> efflux attenuates pathological remodeling in heart failure. *J Mol Cell Cardiol* **167**:52–66. doi:10.1016/j.yjmcc.2022.03.001
- Gherardi G, Monticelli H, Rizzuto R, Mammucari C. 2020. The mitochondrial Ca<sup>2+</sup> uptake and the fine-tuning of aerobic metabolism. *Front Physiol* **11**:554904. doi:10.3389/fphys.2020.554904
- Groten CJ, MacVicar BA. 2022. Mitochondrial Ca<sup>2+</sup> uptake by the MCU facilitates pyramidal neuron excitability and metabolism during action potential firing. *Commun Biol* **5**:900. doi:10.1038/s42003-022-03848-1
- Hagenston AM, Yan J, Bas-Orth C, Tan Y, Sekler I, Bading H. 2022. Disrupted expression of mitochondrial NCLX sensitizes neuroglial networks to excitotoxic stimuli and renders synaptic activity toxic. *J Biol Chem* **298**:101508. doi:10.1016/j.jbc.2021.101508
- Hernansanz-Agustín P, Choya-Foces C, Carregal-Romero S, Ramos E, Oliva T, Villa-Piña T, Moreno L, Izquierdo-Álvarez A, Cabrera-García JD, Cortés A, Lechuga-Vieco AV, Jadiya P, Navarro E, Parada E, Palomino-Antolín A, Tello D, Acín-Pérez R, Rodríguez-Aguilera JC, Navas P, Cogolludo Á, López-Montero I, Martínez-Del-Pozo Á, Egea J, López MG, Elrod JW, Ruíz-Cabello J, Bogdanova A, Enríquez JA, Martínez-Ruiz A. 2020. Na<sup>+</sup> controls hypoxic signalling by the mitochondrial respiratory chain. *Nature* **586**:287–291. doi:10.1038/s41586-020-2551-y
- Herrero-Mendez A, Almeida A, Fernández E, Maestre C, Moncada S, Bolaños JP. 2009. The bioenergetic and antioxidant status of neurons is controlled by continuous degradation of a key glycolytic enzyme by APC/C–Cdh1. *Nat Cell Biol* **11**:747–752. doi:10.1038/ncb1881
- Jadiya P, Kolmetzky DW, Tomar D, Di Meco A, Lombardi AA, Lambert JP, Luongo TS, Ludtmann MH, Praticò D, Elrod JW. 2019. Impaired mitochondrial calcium efflux contributes to disease progression in models of Alzheimer’s disease. *Nat Commun* **10**:3885. doi:10.1038/s41467-019-11813-6
- Jimenez-Blasco D, Busquets-Garcia A, Hebert-Chatelain E, Serrat R, Vicente-Gutierrez C, Ioannidou C, Gómez-Sotres P, Lopez-Fabuel I, Resch-Beusher M, Resel E, Arnouil D, Saraswat D, Varilh M, Cannich A, Julio-Kalajzic F, Bonilla-Del Río I, Almeida A, Puente N, Achicallende S, Lopez-Rodriguez M-L, Jollé C, Déglon N, Pellerin L, Josephine C, Bonvento G, Panatier A, Lutz B, Piazza P-V, Guzmán M, Bellocchio L, Bouzier-Sore A-K, Grandes P, Bolaños JP, Marsicano G. 2020. Glucose metabolism links astroglial mitochondria to cannabinoid effects. *Nature* **583**:603–608. doi:10.1038/s41586-020-2470-y
- Juaristi I, Contreras L, González-Sánchez P, Pérez-Liébana I, González-Moreno L, Pardo B, del Arco A, Satrústegui J. 2019. The response to stimulation in neurons and astrocytes. *Neurochem Res* **44**:2385–2391. doi:10.1007/s11064-019-02803-7
- Kakimoto PA, Serna JDC, de Miranda Ramos V, Zorzano A, Kowaltowski AJ. 2021. Increased glycolysis is an early consequence of palmitate lipotoxicity mediated by redox signaling. *Redox Biol* **45**:102026. doi:10.1016/j.redox.2021.102026
- Kawamoto EM, Vivar C, Camandola S. 2012. Physiology and pathology of calcium signaling in the brain. *Front Pharmacol* **3**. doi:10.3389/fphar.2012.00061

- Khakh BS, Deneen B. 2019. The emerging nature of astrocyte diversity. *Annu Rev Neurosci* **42**:187–207. doi:10.1146/annurev-neuro-070918-050443
- Kostic M, Katoshevski T, Sekler I. 2018. Allosteric regulation of NCLX by mitochondrial membrane potential links the metabolic state and Ca<sup>2+</sup> signaling in mitochondria. *Cell Rep* **25**:3465–3475.e4. doi:10.1016/j.celrep.2018.11.084
- Kostic M, Ludtmann MHR, Bading H, Hershinkel M, Steer E, Chu CT, Abramov AY, Sekler I. 2015. PKA phosphorylation of NCLX reverses mitochondrial calcium overload and depolarization, promoting survival of PINK1-deficient dopaminergic neurons. *Cell Rep* **13**:376–386. doi:10.1016/j.celrep.2015.08.079
- Kowaltowski AJ, Menezes-Filho SL, Assali EA, Gonçalves IG, Cabral-Costa JV, Abreu P, Miller N, Nolasco P, Laurindo FRM, Bruni-Cardoso A, Shirihai OS. 2019. Mitochondrial morphology regulates organellar Ca<sup>2+</sup> uptake and changes cellular Ca<sup>2+</sup> homeostasis. *FASEB J* **33**:13176–13188. doi:10.1096/fj.201901136R
- Lapresa R, Agulla J, Gonzalez-Guerrero S, Bolaños JP, Almeida A. 2022. Amyloid- $\beta$  induces Cdh1-mediated Rock2 stabilization causing neurodegeneration. *Front Pharmacol* **13**:884470. doi:10.3389/fphar.2022.884470
- Lehninger AL, Rossi CS, Greenawalt JW. 1963. Respiration-dependent accumulation of inorganic phosphate and Ca<sup>++</sup> by rat liver mitochondria. *Biochem Biophys Res Commun* **10**:444–448. doi:10.1016/0006-291X(63)90377-2
- Llorente-Folch I, Rueda CB, Pardo B, Szabadkai G, Duchen MR, Satrustegui J. 2015. The regulation of neuronal mitochondrial metabolism by calcium: regulation of neuronal mitochondrial metabolism. *J Physiol* **593**:3447–3462. doi:10.1113/JP270254
- Ludtmann MHR, Kostic M, Horne A, Gandhi S, Sekler I, Abramov AY. 2019. LRRK2 deficiency induced mitochondrial Ca<sup>2+</sup> efflux inhibition can be rescued by Na<sup>+</sup>/Ca<sup>2+</sup>/Li<sup>+</sup> exchanger upregulation. *Cell Death Dis* **10**:265. doi:10.1038/s41419-019-1469-5
- Luongo TS, Lambert JP, Gross P, Nwokedi M, Lombardi AA, Shanmughapriya S, Carpenter AC, Kolmetzky D, Gao E, van Berlo JH, Tsai EJ, Molkentin JD, Chen X, Madesh M, Houser SR, Elrod JW. 2017. The mitochondrial Na<sup>+</sup>/Ca<sup>2+</sup> exchanger is essential for Ca<sup>2+</sup> homeostasis and viability. *Nature* **545**:93–97. doi:10.1038/nature22082
- Mächler P, Wyss MT, Elsayed M, Stobart J, Gutierrez R, von Faber-Castell A, Kaelin V, Zuend M, San Martín A, Romero-Gómez I, Baeza-Lehnert F, Lengacher S, Schneider BL, Aebischer P, Magistretti PJ, Barros LF, Weber B. 2016. In vivo evidence for a lactate gradient from astrocytes to neurons. *Cell Metab* **23**:94–102. doi:10.1016/j.cmet.2015.10.010
- Mookerjee SA, Gerencser AA, Nicholls DG, Brand MD. 2017. Quantifying intracellular rates of glycolytic and oxidative ATP production and consumption using extracellular flux measurements. *J Biol Chem* **292**:7189–7207. doi:10.1074/jbc.M116.774471
- Nita II, Hershinkel M, Fishman D, Ozeri E, Rutter GA, Sensi SL, Khananshvili D, Lewis EC, Sekler I. 2012. The mitochondrial Na<sup>+</sup>/Ca<sup>2+</sup> exchanger upregulates glucose dependent Ca<sup>2+</sup> signalling linked to insulin secretion. *PLoS ONE* **7**:e46649. doi:10.1371/journal.pone.0046649
- Nita II, Hershinkel M, Kantor C, Rutter GA, Lewis EC, Sekler I. 2014. Pancreatic  $\beta$ -cell Na<sup>+</sup> channels control global Ca<sup>2+</sup> signaling and oxidative metabolism by inducing Na<sup>+</sup> and Ca<sup>2+</sup> responses that are propagated into mitochondria. *FASEB J* **28**:3301–3312. doi:10.1096/fj.13-248161
- Nita II, Hershinkel M, Lewis EC, Sekler I. 2015. A crosstalk between Na<sup>+</sup> channels, Na<sup>+</sup>/K<sup>+</sup> pump and mitochondrial Na<sup>+</sup> transporters controls glucose-dependent cytosolic and mitochondrial Na<sup>+</sup> signals. *Cell Calcium* **57**:69–75. doi:10.1016/j.ceca.2014.12.007
- Oheim M, Schmidt E, Hirrlinger J. 2018. Local energy on demand: Are ‘spontaneous’ astrocytic Ca<sup>2+</sup> - microdomains the regulatory unit for astrocyte-neuron metabolic cooperation? *Brain Res Bull* **136**:54–64. doi:10.1016/j.brainresbull.2017.04.011

- Palty R, Silverman WF, Hershfinkel M, Caporale T, Sensi SL, Parnis J, Nolte C, Fishman D, Shoshan-Barmatz V, Herrmann S, Khananshvil D, Sekler I. 2010. NCLX is an essential component of mitochondrial Na<sup>+</sup>/Ca<sup>2+</sup> exchange. *Proc Natl Acad Sci USA* **107**:436–441. doi:10.1073/pnas.0908099107
- Parnis J, Montana V, Delgado-Martinez I, Matyash V, Parpura V, Kettenmann H, Sekler I, Nolte C. 2013. Mitochondrial exchanger NCLX plays a major role in the intracellular Ca<sup>2+</sup> signaling, gliotransmission, and proliferation of astrocytes. *J Neurosci* **33**:7206–7219. doi:10.1523/JNEUROSCI.5721-12.2013
- Paxinos G, Franklin KBJ. 2001. The mouse brain in stereotaxic coordinates, 2nd ed. ed. San Diego: Academic Press.
- Pellerin L, Magistretti PJ. 1994. Glutamate uptake into astrocytes stimulates aerobic glycolysis: a mechanism coupling neuronal activity to glucose utilization. *Proc Natl Acad Sci USA* **91**:10625–10629. doi:10.1073/pnas.91.22.10625
- Percie du Sert N, Ahluwalia A, Alam S, Avey MT, Baker M, Browne WJ, Clark A, Cuthill IC, Dirnagl U, Emerson M, Garner P, Holgate ST, Howells DW, Hurst V, Karp NA, Lazic SE, Lidster K, MacCallum CJ, Macleod M, Pearl EJ, Petersen OH, Rawle F, Reynolds P, Rooney K, Sena ES, Silberberg SD, Steckler T, Würbel H. 2020. Reporting animal research: Explanation and elaboration for the ARRIVE guidelines 2.0. *PLoS Biol* **18**:e3000411. doi:10.1371/journal.pbio.3000411
- Perocchi F, Gohil VM, Girgis HS, Bao XR, McCombs JE, Palmer AE, Mootha VK. 2010. MICU1 encodes a mitochondrial EF hand protein required for Ca<sup>2+</sup> uptake. *Nature* **467**:291–296. doi:10.1038/nature09358
- Plovanich M, Bogorad RL, Sancak Y, Kamer KJ, Strittmatter L, Li AA, Girgis HS, Kuchimanchi S, De Groot J, Speciner L, Taneja N, OShea J, Koteliansky V, Mootha VK. 2013. MICU2, a paralog of MICU1, resides within the Mitochondrial Uniporter Complex to regulate calcium handling. *PLoS ONE* **8**:e55785. doi:10.1371/journal.pone.0055785
- Reynolds PS. 2019. When power calculations won't do: Fermi approximation of animal numbers. *Lab Anim* **48**:249–253. doi:10.1038/s41684-019-0370-2
- Rider MH, Bertrand L, Vertommen D, Michels PA, Rousseau GG, Hue L. 2004. 6-Phosphofructo-2-kinase/fructose-2,6-bisphosphatase: head-to-head with a bifunctional enzyme that controls glycolysis. *Biochem J* **381**:561–579. doi:10.1042/BJ20040752
- Rigoulet M, Bouchez CL, Paumard P, Ransac S, Cuvellier S, Duvezin-Caubet S, Mazat JP, Devin A. 2020. Cell energy metabolism: An update. *Biochimica et Biophysica Acta (BBA) - Bioenergetics* **1861**:148276. doi:10.1016/j.bbabi.2020.148276
- Rodriguez-Rodriguez P, Fernandez E, Almeida A, Bolaños JP. 2012. Excitotoxic stimulus stabilizes PFKFB3 causing pentose-phosphate pathway to glycolysis switch and neurodegeneration. *Cell Death Differ* **19**:1582–1589. doi:10.1038/cdd.2012.33
- Romero N, Rogers G, Neilson A, Dranka B. 2018. Quantifying Cellular ATP Production Rate Using Agilent Seahorse XF Technology.
- Roumes H, Jollé C, Blanc J, Benkhaled I, Chatain CP, Massot P, Raffard G, Bouchaud V, Biran M, Pythoud C, Déglon N, Zimmer ER, Pellerin L, Bouzier-Sore A-K. 2021. Lactate transporters in the rat barrel cortex sustain whisker-dependent BOLD fMRI signal and behavioral performance. *Proc Natl Acad Sci USA* **118**:e2112466118. doi:10.1073/pnas.2112466118
- Sancak Y, Markhard AL, Kitami T, Kovács-Bogdán E, Kamer KJ, Udeshi ND, Carr SA, Chaudhuri D, Clapham DE, Li AA, Calvo SE, Goldberger O, Mootha VK. 2013. EMRE is an essential component of the mitochondrial calcium uniporter complex. *Science* **342**:1379–1382. doi:10.1126/science.1242993
- Schindelin J, Arganda-Carreras I, Frise E, Kaynig V, Longair M, Pietzsch T, Preibisch S, Rueden C, Saalfeld S, Schmid B, Tinevez J-Y, White DJ, Hartenstein V, Eliceiri K, Tomancak P, Cardona A. 2012. Fiji: an open-source platform for biological-image analysis. *Nat Methods* **9**:676–682. doi:10.1038/nmeth.2019



- Serna JDC, de Miranda Ramos V, Cabral-Costa JV, Vilas-Boas EA, Amaral AG, Ohya G, da Silva CCC, Kowaltowski A. 2022. Measuring mitochondrial Ca<sup>2+</sup> efflux in isolated mitochondria and permeabilized cells. *Bioenerg Comm*. doi:10.26124/BEC:2022-0007
- Sharma V, Roy S, Sekler I, O'Halloran DM. 2017. The NCLX-type Na<sup>+</sup>/Ca<sup>2+</sup> exchanger NCX-9 is required for patterning of neural circuits in *Caenorhabditis elegans*. *J Biol Chem* **292**:5364–5377. doi:10.1074/jbc.M116.758953
- Srinivasan R, Lu T-Y, Chai H, Xu J, Huang BS, Golshani P, Coppola G, Khakh BS. 2016. New transgenic mouse lines for selectively targeting astrocytes and studying calcium signals in astrocyte processes in situ and in vivo. *Neuron* **92**:1181–1195. doi:10.1016/j.neuron.2016.11.030
- Stavsky A, Stoler O, Kostic M, Katoshevsky T, Assali EA, Savic I, Amitai Y, Prokisch H, Leiz S, Daumer-Haas C, Fleidervish I, Perocchi F, Gitler D, Sekler I. 2021. Aberrant activity of mitochondrial NCLX is linked to impaired synaptic transmission and is associated with mental retardation. *Commun Biol* **4**:666. doi:10.1038/s42003-021-02114-0
- Suzuki A, Stern SA, Bozdagi O, Huntley GW, Walker RH, Magistretti PJ, Alberini CM. 2011. Astrocyte-neuron lactate transport is required for long-term memory formation. *Cell* **144**:810–823. doi:10.1016/j.cell.2011.02.018
- Vasington FD, Murphy JV. 1962. Ca<sup>++</sup> uptake by rat kidney mitochondria and its dependence on respiration and phosphorylation. *J Biol Chem* **237**:2670–2677. doi:10.1016/S0021-9258(19)73805-8
- Vicente-Gutierrez C, Bonora N, Bobo-Jimenez V, Jimenez-Blasco D, Lopez-Fabuel I, Fernandez E, Josephine C, Bonvento G, Enriquez JA, Almeida A, Bolaños JP. 2019. Astrocytic mitochondrial ROS modulate brain metabolism and mouse behaviour. *Nat Metab* **1**:201–211. doi:10.1038/s42255-018-0031-6
- Wang Y, Stancliffe E, Fowle-Grider R, Wang R, Wang C, Schwaiger-Haber M, Shriver LP, Patti GJ. 2022. Saturation of the mitochondrial NADH shuttles drives aerobic glycolysis in proliferating cells. *Mol Cell* S1097276522007031. doi:10.1016/j.molcel.2022.07.007
- Yang J, Ruchti E, Petit J-M, Jourdain P, Grenningloh G, Allaman I, Magistretti PJ. 2014. Lactate promotes plasticity gene expression by potentiating NMDA signaling in neurons. *Proc Natl Acad Sci USA* **111**:12228–12233. doi:10.1073/pnas.1322912111
- Zhang Y, Chen K, Sloan SA, Bennett ML, Scholze AR, O'Keefe S, Phatnani HP, Guarnieri P, Caneda C, Ruderisch N, Deng S, Liddelow SA, Zhang C, Daneman R, Maniatis T, Barres BA, Wu JQ. 2014. An RNA-sequencing transcriptome and splicing database of glia, neurons, and vascular cells of the cerebral cortex. *J Neurosci* **34**:11929–11947. doi:10.1523/JNEUROSCI.1860-14.2014
- Zhou Q, Xie M, Zhu J, Yi Q, Tan B, Li Y, Ye L, Zhang X, Zhang Y, Tian J, Xu H. 2021. PINK1 contained in huMSC-derived exosomes prevents cardiomyocyte mitochondrial calcium overload in sepsis via recovery of mitochondrial Ca<sup>2+</sup> efflux. *Stem Cell Res Ther* **12**:269. doi:10.1186/s13287-021-02325-6

## Figure Supplements

[Fig2Suppl1\_FURA2videos.avi]

Figure 2 – Supplement 1. DMSO and CGP FURA-2 imaging representative videos.

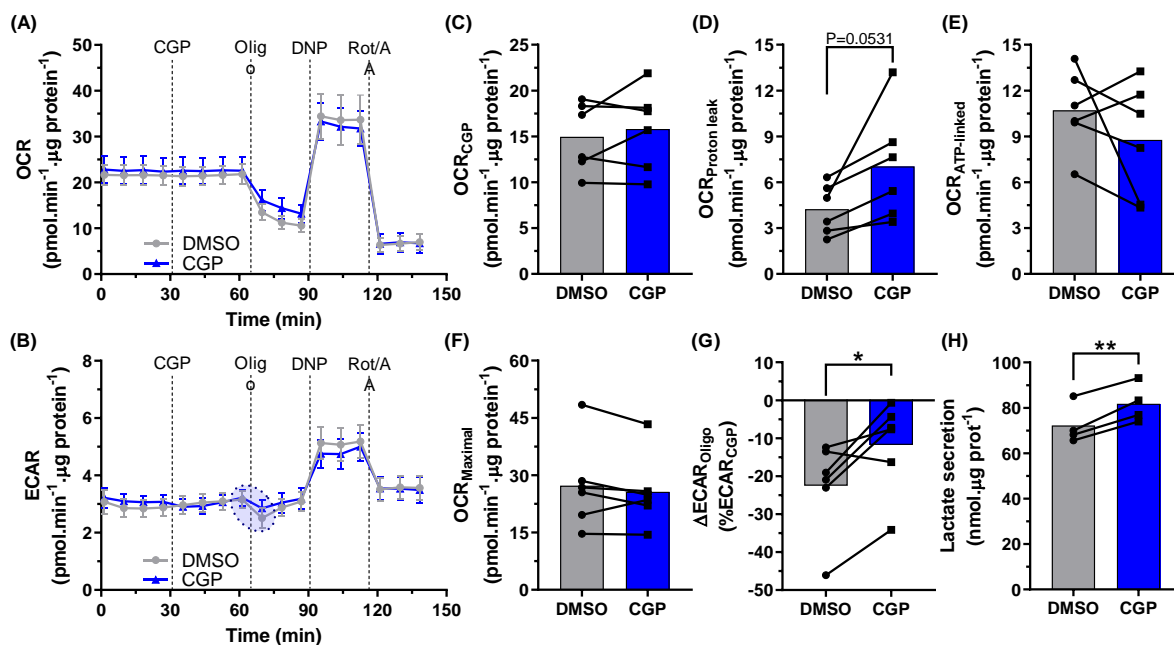


**Figure 3 – Supplement 1. C6 cells present increased lactate secretion upon NCLX inhibition.** C6 cells incubated with the NCLX inhibitor CGP-37157 (CGP) or DMSO had their oxygen consumption rate (OCR) and extracellular acidification rate (ECAR) monitored in a MitoStress Seahorse assay. Representative traces of (A) OCR and (B) ECAR from C6 cells acutely incubated with CGP, followed by oligomycin (oligo), 2,4-dinitrophenol (DNP), and rotenone plus antimycin A (Rot/AA) additions, average ± SEM; (C) CGP-induced, (D) proton leak-associated, (E) ATP-linked, and (F) maximal respirations; (G) ECAR variation after ATP synthase inhibition with oligomycin. Paired 2-way ANOVA followed by Holm-Šidak's post-hoc test, n = 6 independent experiments. (H) lactate secretion measured from C6 cells incubated with CGP or DMSO for 4 h. \*P < 0.05, Student's t test, n = 4 independent experiments, mean and SD (A,B) or mean and paired measurements (C-H).

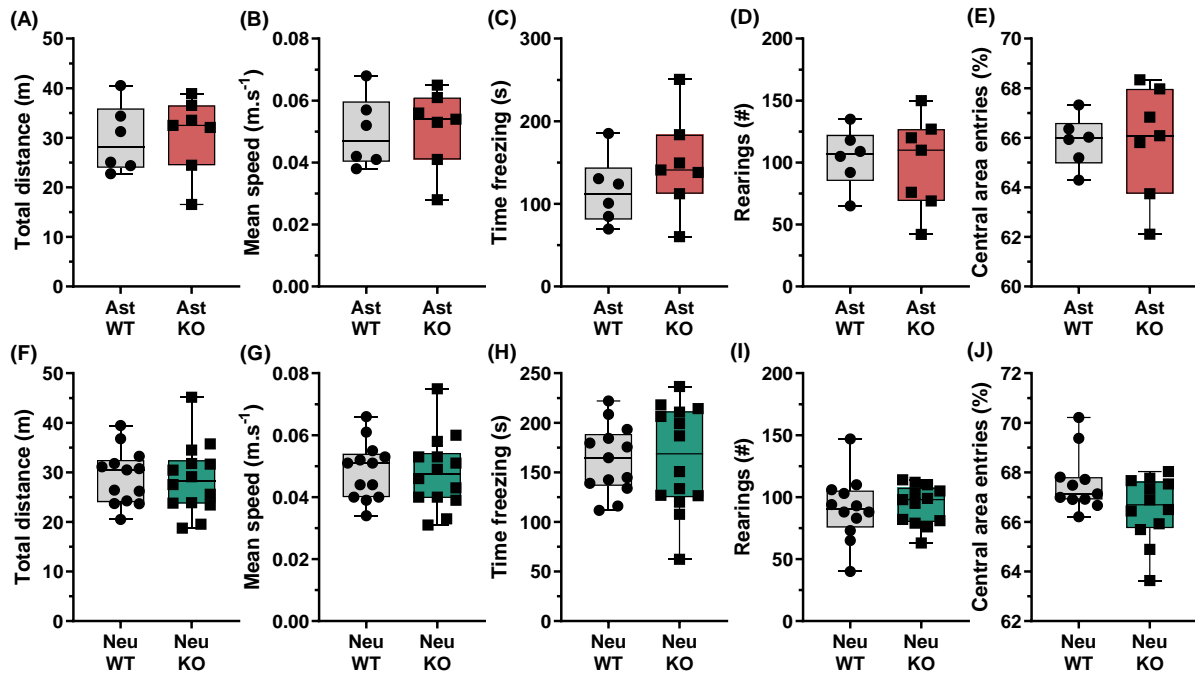


**Figure 5 – Supplement 1. Open Field test supplementary analyses.** Supplementary analyses from the Open Field test in mice with hippocampal astrocyte- (A-E) or neuronal-specific (F-J) NCLX deletion: (A,F) total distance; (B,G) mean speed; (C,H) total time in freezing behavior; (D,I) number of rearings; and (E,J) total entries in the central area. Not significant, unpaired Student's t test (A-C,F-H) or Mann-Whitney test (D,E,I,J), n = 6-14, box indicates upper and lower quartiles and the median (line), and whiskers represent min and max values.

[\[Fig5Suppl2\\_OF\\_videos.avi\]](#)

**Figure 5 – Supplement 2. Open Field test – *In vivo* hippocampal astrocyte- and neuronal-specific NCLX deletion representative videos.**

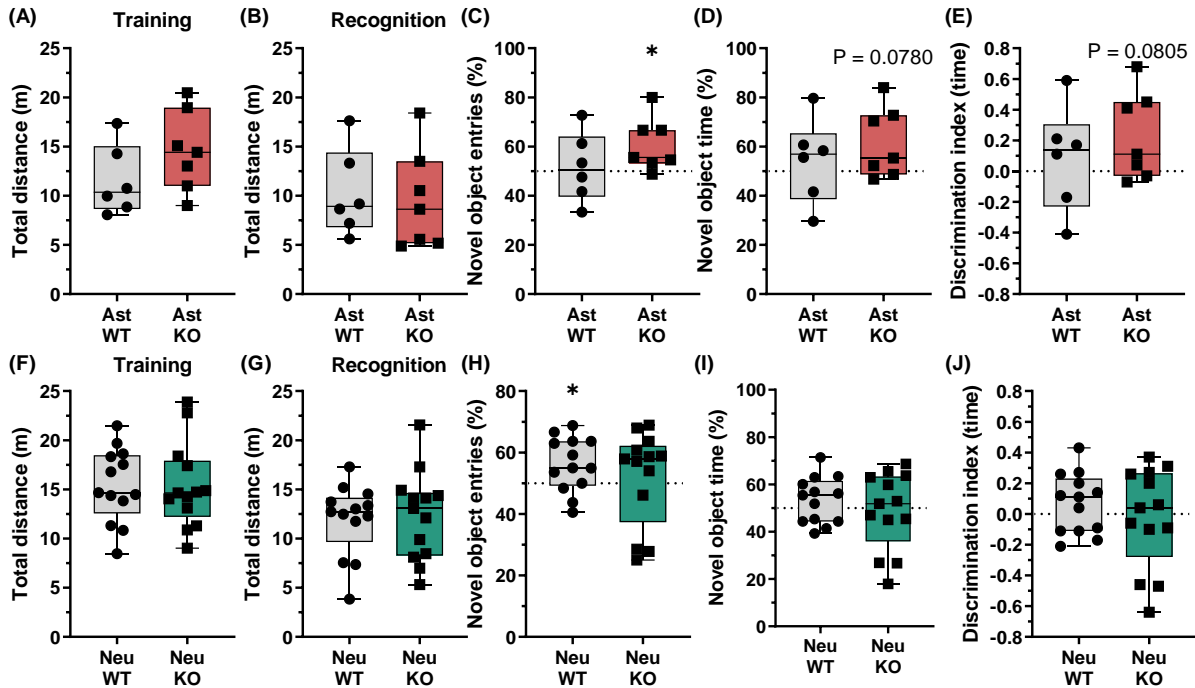


**Figure 5 – Supplement 3. Novel Object Recognition test supplementary analyses.** Supplementary analyses from the Novel Object Recognition test in mice with hippocampal astrocyte- (A-E) or neuronal-specific (F-J) NCLX deletion: (A,F) total distance in training and (B,G) recognition assay steps; (C,H) proportion of entries into and (D,I) time within the novel object area; and (E,J) discrimination index calculated from time in the novel and familiar object areas. \* $P < 0.05$ , unpaired Student's *t* test (A,B,D,E,F,G,H,I) or Mann-Whitney test (C,H),  $n = 6-14$ , box indicates upper and lower quartiles and the median (line), and whiskers represent min and max values.

[\[Fig5Suppl4 NOR videos.avi\]](#)

**Figure 5 – Supplement 4. Novel Object Recognition test – *In vivo* hippocampal astrocyte- and neuronal-specific NCLX deletion representative videos.**

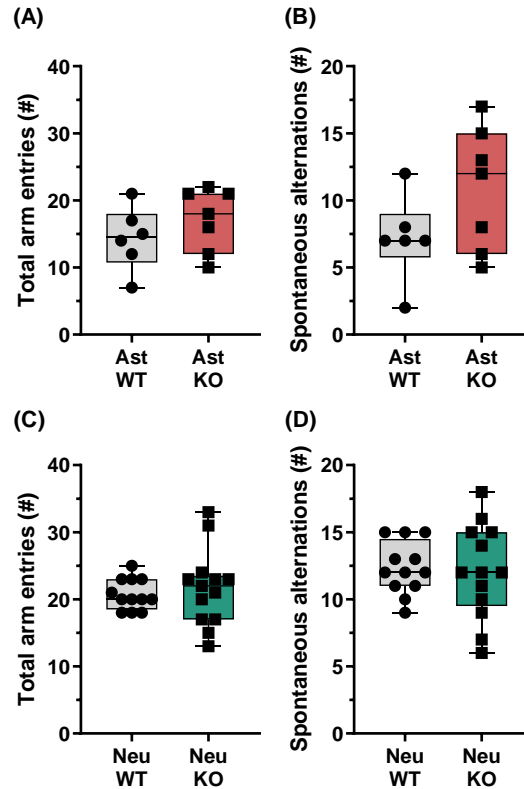


**Figure 5 – Supplement 5. Y-maze test supplementary analyses.** Supplementary analyses from the Y-maze test in mice with hippocampal astrocyte- (A,B) or neuronal-specific (C,D) NCLX deletion: (A,C) total number of arm entries; and (B,D) total number of spontaneous alternations. Not significant, Mann-Whitney test, n = 6-14, box indicates upper and lower quartiles and the median (line), and whiskers represent min and max values.

[\[Fig5Suppl6\\_Y-maze\\_videos.avi\]](#)

**Figure 5 – Supplement 6. Y-maze test – *In vivo* hippocampal astrocyte- and neuronal-specific NCLX deletion representative videos.**



## CONCLUDING REMARKS

Metabolism is an essential characteristic of life.  $\text{Ca}^{2+}$  is a key ion that participate as second messenger in a plethora of crucial cellular signalling processes, and many cell types have evolved mechanisms that couple  $\text{Ca}^{2+}$  levels with energetic demands. Thus, the mitochondrial  $\text{Ca}^{2+}$  handling system constitutes an important hub that contributes to both cytosolic and mitochondrial  $\text{Ca}^{2+}$  and  $\text{Na}^+$  signaling pathways, with a deep influence on mitochondrial physiology and cellular metabolism.

Our group recently found that mitochondrial and cellular  $\text{Ca}^{2+}$  handling are impacted by mitochondrial morphological changes (Kowaltowski et al., 2019; Annex B), with the potential to influence cellular functions, such as microglial activation (Pereira et al., 2021; Annex C). Additionally, we find that fine-tuning of mitochondrial and cytosolic  $\text{Ca}^{2+}$  levels is crucial to achieve optimal metabolic activation and meet cellular energetic demands appropriately (Vilas-Boas et al., 2022; Annex D), highlighting the importance of mitochondrial  $\text{Na}^+/\text{Ca}^{2+}$  exchanger (NCLX) activity (Serna et al., 2022; Annex E).

In this thesis, we reviewed the importance of mitochondrial physiology for brain function, reinforcing the central role of mitochondrial dysfunctions in the development and progress of neurological diseases, such as stroke and major neurodegenerative disorders, which also makes mitochondria an interesting pharmacological target (Cabral-Costa; Kowaltowski, 2020). Indeed, mitochondrial  $\text{Ca}^{2+}$  handling supports several brain functions, including synaptic activity, circuit integration, sensory inputs, behavioral outputs, and astrocytic homeostasis. (Cabral-Costa; Kowaltowski, 2022).

However, little was known to date regarding astrocytic mitochondrial  $\text{Ca}^{2+}$  handling through NCLX activity on cell physiology, apart from its influence on astrocyte proliferation (Parnis et al., 2013) and survival (Hagenston et al., 2022). Here we developed an experimental strategy to uncover the effects of pharmacologically or genetically inhibiting NCLX activity *in vitro* and *in vivo*. We found that astrocytic NCLX activity ablation leads to increased glycolytic flux and lactate secretion, with a minor influence on mitochondrial ATP production. This is associated with better performance at behavioral tasks, while the opposite effect is observed when NCLX is deleted in neurons (Cabral-Costa et al., 2022).

We have therefore identified NCLX as a modulator of glycolysis. In astrocytes, this is of utmost importance, since such a refined regulator of lactate secretion would have the



potential to act as a point-of-control of the astrocyte-to-neuron lactate shuttle. Further evaluations of the metabolic effects behind the behavioral improvement induced by NCLX deletion in astrocytes will, hopefully, contribute toward the understanding of the full role of NCLX in the astrocyte-to-neuron lactate shuttle. Moreover, we anticipate that a deeper assessment of the mechanisms associated with the glycolytic increase induced by hampered NCLX activity will shed light on the physiological regulation of NCLX function.

In conclusion, we highlight that mitochondrial  $\text{Na}^+/\text{Ca}^{2+}$  exchanger (NCLX) function goes well beyond controlling  $\text{Ca}^{2+}$  efflux from the mitochondrial matrix. NCLX activity controls glycolytic flux, adjusting astrocytic lactate secretion and, potentially, neuronal homeostasis. We hope our work leads to further exploration of NCLX activity as a potential pharmacological target, as well as its functional conservation in other cell types and organisms.

## References<sup>1</sup>

- Cabral-Costa JV, Kowaltowski AJ. Mitochondrial Ca<sup>2+</sup> handling as a cell signaling hub: lessons from astrocyte function. *Essays Biochem* 2022;Submitted.
- Cabral-Costa JV, Kowaltowski AJ. Neurological disorders and mitochondria. *Mol Aspects Med* 2020;71:100826. <https://doi.org/10.1016/j.mam.2019.10.003>.
- Cabral-Costa JV, Vicente-Gutierrez C, Agulla J, Lapresa R, Elrod JW, Almeida A, et al. Mitochondrial sodium/calcium exchanger NCLX regulates glycolysis in astrocytes, impacting on cognitive performance. *bioRxiv* 2022. <https://doi.org/10.1101/2022.09.16.507284>.
- Funaro VMB de O, Pestana MC, Dziabas MCC, Garcia EM, Santos MF dos, Nascimento MM, et al. *Diretrizes para apresentação de dissertações e teses da USP: parte IV (Vancouver)*. vol. IV. 3rd ed. Universidade de São Paulo. Sistema Integrado de Bibliotecas; 2016.
- Hagenston AM, Yan J, Bas-Orth C, Tan Y, Sekler I, Bading H. Disrupted expression of mitochondrial NCLX sensitizes neuroglial networks to excitotoxic stimuli and renders synaptic activity toxic. *J Biol Chem* 2022;298:101508. <https://doi.org/10.1016/j.jbc.2021.101508>.
- Kowaltowski AJ, Menezes-Filho SL, Assali EA, Gonçalves IG, Cabral-Costa JV, Abreu P, et al. Mitochondrial morphology regulates organellar Ca<sup>2+</sup> uptake and changes cellular Ca<sup>2+</sup> homeostasis. *FASEB J* 2019;33:13176–88. <https://doi.org/10.1096/fj.201901136R>.
- Parnis J, Montana V, Delgado-Martinez I, Matyash V, Parpura V, Kettenmann H, et al. Mitochondrial exchanger NCLX plays a major role in the intracellular Ca<sup>2+</sup> signaling, gliotransmission, and proliferation of astrocytes. *J Neurosci* 2013;33:7206–19. <https://doi.org/10.1523/JNEUROSCI.5721-12.2013>.
- Pereira OR, Ramos VM, Cabral-Costa JV, Kowaltowski AJ. Changes in mitochondrial morphology modulate LPS-induced loss of calcium homeostasis in BV-2 microglial cells. *J Bioenerg Biomembr* 2021;53:109–18. <https://doi.org/10.1007/s10863-021-09878-4>.
- Serna JDC, de Miranda Ramos V, Cabral-Costa JV, Vilas-Boas EA, Amaral AG, Ohya G, et al. Measuring mitochondrial Ca<sup>2+</sup> efflux in isolated mitochondria and permeabilized cells. *Bioenerg Comm* 2022. <https://doi.org/10.26124/BEC:2022-0007>.
- Vilas-Boas EA, Cabral-Costa JV, Ramos VM, da Silva CCC, Kowaltowski AJ. Goldilocks calcium and the mitochondrial respiratory chain: too much, too little, just right. *bioRxiv* 2022. <https://doi.org/10.1101/2022.04.12.488015>.

---

<sup>1</sup> Following the Vancouver system, in accordance with the *Diretrizes para apresentação de dissertações e teses da USP – Parte IV* (Funaro et al., 2016).



**ANNEX LIST**

**A.** Curriculum summary

**B.** Kowaltowski et al., 2019 (FASEB J., 33:13176–88)

**C.** Pereira et al., 2021 (J. Bioenerg. Biomembr., 53:109–18)

**D.** Vilas-Boas et al., 2022 (bioRxiv)

**E.** Serna et al., 2022 (Bioenerg. Comm., 2022:0007)

**F.** Serpentino et al., 2017 (Rev. Cult. Ext. USP, 17:23–40)

## **ANNEX A**

### **Curriculum summary**

# **CURRICULUM SUMMARY**

## **1. Personal information**

**Name:** João Victor Cabral Costa

**Birthplace:** Ipatinga, MG, Brazil

**Birthdate:** 15/03/1990

## **2. Education**

### **PhD - Biochemistry & Molecular Biology**

**Chemistry Institute, University of São Paulo, Brazil**

2017 — PRESENT (GPA 4.0/4.0)

### **MSc - Pharmacology**

**Institute of Biomedical Sciences, University of São Paulo, Brazil**

2015 — 2017 (GPA 4.0/4.0)

### **Exchange Biomedical Sciences Student**

**University of Minnesota, USA**

2012 — 2013 (GPA 3.92/4.0; DEAN'S LIST)

### **Pharmacy & Biochemistry**

**Faculty of Pharmaceutical Sciences, University of São Paulo, Brazil**

2008 — 2014 (GPA 8.5/10.0; 97.4<sup>TH</sup> PERCENTILE)

## **3. Experience**

### **PhD candidate**

**Energy Metabolism Laboratory**

**Chemistry Institute, University of São Paulo, Brazil**

JUNE 2017 — PRESENT

Supervised by Dr. Alicia J. Kowaltowski. Main project: Mitochondrial Ca<sup>2+</sup> handling in the central nervous system and energy metabolism regulation.

### **Visiting PhD candidate**

**Neuroenergetic and Metabolism Group**

**IBFG, University of Salamanca, Spain**

FEBRUARY 2020 — JANUARY 2021

Supervised by Dr. Juan Pedro Bolaños. Main project: NCLX in astrocytic function: metabolism and neuronal homeostasis.

### **Master's student**

**Molecular and Functional Neurobiology Laboratory**

**Institute of Biomedical Sciences, University of São Paulo, Brazil**

JANUARY 2015 — MAY 2017

Supervised by Dr. Elisa M. Kawamoto. Main project: Evaluation of the PTEN signaling effects over neurogenesis and cognition of mice under a physical exercise regimen.

### **Undergraduate researcher**

**Molecular Neuropharmacology Laboratory**

**Institute of Biomedical Sciences, University of São Paulo, Brazil**

DECEMBER 2013 — DECEMBER 2014

Supervised by Dr. Cristoforo Scavone & Dr. Elisa M. Kawamoto. Main project: Biochemical Effects of PTEN Signaling Pathway under an Intermittent Diet Regimen.

### **Summer intern**

**Laboratory of Neurosciences  
National Institute on Aging/NIH, USA**

JUNE 2013 — AUGUST 2013

Supervised by Dr. Mark P. Mattson, Dr. Simonetta Camandola & Dr. Mark A. Wilson. Main project: Effect of Food Sensing on Longevity and Respiration Rate: skn-1 as a sensory modulator of dietary restriction-induced effects.

### **Pharmacovigilance analyst**

**Pharmacovigilance Division  
Health Surveillance Center, State Health Secretariat of São Paulo, Brazil**

AUGUST 2010 — JULY 2011

Supervised by Dr. Eunice Kano & Adalton Ribeiro. Main project: Analysis of Adverse Drug Reaction Profiles of Immunobiological TNF-alpha inhibitors.

### **Summer intern**

**Laboratory of Innovative and Translational Technologies  
Harvard Medical School, USA**

JULY 2010 — JULY 2010

Supervised by Dr. Winston P. Kuo.

### **Undergraduate researcher**

**Energy Metabolism Laboratory  
Chemistry Institute, University of São Paulo, Brazil**

JANUARY 2009 — JULY 2010

Supervised by Dr. Alicia J. Kowaltowski. Main project: Impact of a hyperlipidic diet on mitochondrial physiology of mice hepatocytes.

## **4. Supervising and teaching experience**

### **Co-supervisions**

Julia Kuhl Teles Martini (undergraduate researcher)

JAN 2022 — AUG 2022

Oswaldo Pereira Rodrigues (undergraduate researcher)

APR 2018 — DEC 2020

Vinicius Watanabe Nakao (undergraduate researcher)

JAN 2016 — DEC 2017

### **Teaching experience**

#### **Graduate Teaching Assistant – Theory and Experimental classes**

**Chemistry Institute, University of São Paulo, Brazil**

AUG/2017 — DEC/2017

Basic Biochemistry – 90 h

#### **Graduate Teaching Assistant (voluntary) – Flipped classroom**

**Institute of Biomedical Sciences, University of São Paulo, Brazil**

FEB/2016 — MAR/2016

Pharmacology & Pathophysiology – 30 h

#### **Graduate Teaching Assistant – Theory and Experimental classes**

**Institute of Biomedical Sciences, University of São Paulo, Brazil**

AUG/2015 — DEC/2015

Pharmacology & Physiology – 90 h

#### **Undergraduate Teaching Assistant (voluntary) – Theory classes**

**Institute of Biomedical Sciences, University of São Paulo, Brazil**

FEB/2014 — JUN/2014

Pathophysiology, Pharmacology, Medicinal Chemistry, Social Toxicology – 90 h



## 5. Publications (\*1st author; # corresponding author)

13. **Mitochondrial sodium/calcium exchanger NCLX regulates glycolysis in astrocytes, impacting on cognitive performance**  
Cabral-Costa, J.V.\*,#; Vicente-Gutiérrez, C.; Agulla, J.; Lapresa, R.; Elrod, J.W.; Almeida, A.; Bolaños, JP#; Kowaltowski, A.J., bioRxiv, 2022. [Original work](#) (preprint).
12. **Mitochondrial Ca<sup>2+</sup> handling as a cell signaling hub: lessons from astrocytic function**  
Cabral-Costa, J.V.\*,#; Kowaltowski, A.J., MitoFit Preprints 2022.27, [Review](#) (preprint).
11. **Measuring mitochondrial Ca<sup>2+</sup> efflux in isolated mitochondria and permeabilized cells**  
Serna, J.D.C.; Ramos, V.M.; Cabral-Costa, J.V.; Vilas-Boas, E.A.; Amaral, G.A.; Ohya, G.; Caldeira da Silva, C.C.; Kowaltowski, A.J.#, 2022:0007, Bioenerg. Communic., 2022. [Original work](#).
10. **Goldilocks calcium and the mitochondrial respiratory chain: too much, too little, just right**  
Vilas-Boas, E.A.; Cabral-Costa, J.V.; Ramos, V.M.; Caldeira da Silva, C.C.; Kowaltowski, A.J.#, 2022.04.12.488015, bioRxiv, 2022. [Original work](#) (preprint).
9. **Changes in mitochondrial morphology modulate LPS-induced loss of calcium homeostasis in BV-2 microglial cells**  
Pereira Jr. O.R.; Ramos, V.M.; Cabral-Costa, J.V.#; Kowaltowski, A.J.#, 53:109-118, J. Bioenerg. Biomemb., 2021. [Original work](#).
8. **Neurological disorders and mitochondria**  
Cabral-Costa, J.V.\* and Kowaltowski, A.J., 71:100826, Mol. Aspects Med., 2020. [Review](#).
7. **Mitochondrial morphology regulates organellar Ca<sup>2+</sup> uptake and changes cellular Ca<sup>2+</sup> homeostasis**  
Kowaltowski, A.J.; Menezes-Filho, S.L.; Assali, E.A.; Gonçalves, I.G.; Cabral-Costa, J.V.; Abreu, P.; Miller, N.; Nolasco, P.; Laurindo, F.R.M.; Bruni-Cardoso, A.; Shirihai, O.S., 33(12):13176-13188, FASEB J., 2019. [Original work](#).
6. **Intermittent fasting uncovers and rescues cognitive phenotypes in PTEN neuronal haploinsufficient mice**  
Cabral-Costa, J.V.\*; Andreotti, D.Z.; Mello, N.P.; Scavone, C.; Camandola, S.; Kawamoto, E.M., 8:8595, Sci. Rep., 2018. [Original work](#).
5. **The conjunction of Extension, Teaching and Research: the experience of the Scientific Journey of Pharmacy and Biochemistry Students**  
Serpentino, A.H.; Cabral-Costa, J.V.; Souza, R.R.; Jorge, T.M.; Epiphany, S.; Giarolla, J.; Borelli, P., 17:23-40, Rev. Cult. Ext. USP, 2017. [portuguese] [Descriptive article](#).
4. **skn-1 is required for interneuron sensory integration and foraging behavior in Caenorhabditis elegans**  
Wilson, M.A.; Iser, W.B.; Son, T.G.; Logie, A.; Cabral-Costa, J.V.; Mattson, M.P.; Camandola, S., 12(5):e0176798, PLoS One, 2017. [Original work](#).
3. **The role of steroid hormones in the modulation of neuroinflammation by dietary interventions**  
Vasconcelos, A.R.\*; Cabral-Costa, J.V.\*; Mazucanti, C.H.\*; Scavone, C.; Kawamoto, E.M., 7:9, Front. Endocrinol., 2016. [Review](#).
2. **Longevity pathways (mTOR, SIRT, Insulin/IGF-1) as key modulatory targets on aging and neurodegeneration**  
Mazucanti, C.H.\*; Cabral-Costa, J.V.\*; Vasconcelos, A.R.; Andreotti, D.Z.; Scavone, C.; Kawamoto, E.M., 15(21):2116-38, Curr. Top. Med. Chem., 2015. [Review](#).
1. **Effects of a high fat diet on liver mitochondria: Increased ATP-sensitive K<sup>+</sup> channel activity and reactive oxygen species generation**  
Cardoso, A.R.; Cabral-Costa, J.V.; Kowaltowski, A.J., 42:245–253, J. Bioenerg. Biomemb., 2010. [Original work](#).

## 6. Grants & Awards

### Grants (individual/self-funded)

- (2019) FAPESP Research Internship Abroad Fellowship ([#2019/22178-2](#)).
- (2017) FAPESP Doctorate Fellowship ([#2017/14713-0](#)).
- (2014) FAPESP Masters Fellowship ([#2014/18689-8](#)).
- (2013) FAPESP Scientific Initiation Fellowship ([#2013/20594-2](#)).
- (2012) Brazilian Scientific Mobility Program, Ministry of Education, Brazil.
- (2010) Brazilian Education Through Work Scholarship, Ministry of Health, Brazil.
- (2009) PIBIC/CNPq Scholarship, Ministry of Science and Technology, Brazil.

### Awards – Scientific Events

- (2022) FEBS OpenBio Award – Best Poster of the Day  
Event: [IUBMB-FEBS-PABMB 2022 Biochemistry Global Summit](#)
- (2022) Young Scientists’ Forum – Best Oral Presentation  
Event: [Young Scientists’ Forum \(YSF\) 2022](#)
- (2022) Young Scientists’ Forum – Selected Participant  
Event: [YSF 2022 – IUBMB-FEBS-PABMB 2022 Biochemistry Global Summit](#)
- (2018) PABMB Event Participation Scholarship  
Event: [Mitochondria: bioenergetics, oxidative metabolism and signaling](#)
- (2016) Honorable Mention Award  
Brazilian Society of Pharmacology and Experimental Therapeutics (SBFTE)
- (2015) VII Science Quality Award "Prof. Dr. João Garcia Leme"  
Pharmacology Department, University of São Paulo
- (2015) Honorable Mention Award  
Brazilian Society of Pharmacology and Experimental Therapeutics (SBFTE)
- (2014) VI Science Quality Award "Prof. Dr. João Garcia Leme"  
Pharmacology Department, University of São Paulo
- (2011) Best Undergraduate Researcher Presentation Award  
XVI Pharmaceutical Sciences and Technology Meeting, University of São Paulo
- (2011) Honorable Mention & “Top 15 Presentations” Award  
18<sup>o</sup> International Symposium of Undergraduate Research, University of São Paulo

### Awards – Science Outreach

- (2018) Finalist, [FameLab Brasil 2018](#) [PT-BR]
- (2016) Finalist, [FameLab Brasil 2016](#) [PT-BR]

## 7. Congresses and seminars

- (2022) IUBMB-FEBS-PABMB Biochemistry Global Summit (Lisbon, Portugal)  
Poster presentation
- (2022) FEBS Young Scientists’ Forum (Vimeiro, Portugal)  
Oral presentation
- (2022) Redoxoma Annual Meeting (São Paulo, Brazil)  
Poster presentation

- (2022)** Biochemistry Department Seminars (University of São Paulo, São Paulo, Brazil)  
Invited speaker
- (2022)** Experimental Biology / ASBMB-ASP-ASIP-ASPET-AAA (Philadelphia, USA)  
Poster presentation
- (2022)** MITOchat Seminar (online)  
Oral presentation
- (2021)** Scientific Meeting – *Instituto Israelita de Ensino e Pesquisa Albert Einstein* (São Paulo, Brazil)  
Invited speaker
- (2019)** Symposium – *Fronteiras do Metabolismo* (São Paulo, Brazil)  
Poster presentation
- (2018)** XI Mitomeeting (Guapé, Brazil)  
Oral presentation
- (2016)** 2<sup>nd</sup> Congresso de Graduação da Universidade de São Paulo (Piracicaba, Brazil)  
Oral presentation
- (2016)** 48<sup>th</sup> Brazilian Congress of Pharmacology and Experimental Therapeutics (Foz do Iguaçu, Brazil)  
Poster presentation
- (2016)** NAPNA Meeting – *Núcleo de Apoio à Pesquisa em Neurociência Aplicada* (São Paulo, Brazil)  
Oral presentation
- (2015)** 47<sup>th</sup> Brazilian Congress of Pharmacology and Experimental Therapeutics (Foz do Iguaçu, Brazil)  
Poster presentation
- (2015)** VII Science Quality Award "Prof. Dr. João Garcia Leme" (São Paulo, Brazil)  
Oral and poster presentations
- (2015)** IBRO Congress (Rio de Janeiro, Brazil)  
Poster presentation
- (2014)** VI Science Quality Award "Prof. Dr. João Garcia Leme" (São Paulo, Brazil)  
Oral and poster presentations
- (2011)** XVI Pharmaceutical Sciences and Technology Meeting (São Paulo, Brazil)  
Oral and poster presentations
- (2011)** XXX Denman's Undergraduate Research Forum (Columbus, USA)  
Poster presentation
- (2010)** 18<sup>th</sup> International Symposium of Undergraduate Research (Ribeirão Preto, Brazil)  
Poster presentation
- (2009)** 17<sup>th</sup> International Symposium of Undergraduate Research (Ribeirão Preto, Brazil)  
Poster presentation

## 8. Extracurricular activities

### **2022 ASAPbio Fellow Program**

Volunteer fellow. Contributing on campaigns aimed to raise awareness and recognition of preprints; working towards increased visibility and recognition of preprint reviews and crowd reviews.

### **Presentations / Discussions on Science Dissemination**

(2021) ASAPbio - The impact of preprints for early career researchers

(2021) Science Outreach - From lasagnas to synapses: how metabolism rules our lives [PT-BR]

(2020) Science Outreach - Connecting Science [PT-BR]

(2020) Lecture - Communicating Science [PT-BR]

(2020) Lecture - The importance of science communication [PT-BR]

(2020) Lecture - Preprints: what they are and why do they matter? [PT-BR]

(2020) Evidence Based-Beer - Efficacy in times of COVID-19 [PT-BR]

(2019) Evidence Based-Beer - Preprints & Open Science

(2019) Pint of Science 2019

(2018) Pint of Science 2018

### **Nunca Vi 1 Cientista ("I Have Never Seen a Scientist")**

Multi-platform science outreach channel on Youtube, Instagram, Facebook, and Twitter [PT-BR]

**General public:** H1N1 & Coronavirus & Hidroxichloroquine; Coronavirus updates & Hand sanitizers; Does expired food make you sick?; Confirmation bias; Medicinal plants

**For children:** Why are there forest fires in Winter?; What is respect?; What are metals made of?; How do we know if a word is wrong in the dictionary?; Why do sloths move so slowly?

### **Volunteer work**

Scientific Journey of the Pharmaceutical Sciences Students

(May/2019 - present) – Scientific Consultant

(Feb/2011 - Jan/2012) – Main Coordinator

(Feb/2010 - Jan/2011) – Healthcare Campaign & Activities Coordinator

(May/2009 - Jan/2010) – Fieldwork voluntary

## **ANNEX B**

**Kowaltowski et al., 2019  
(FASEB J., 33:13176–88)**

# Mitochondrial morphology regulates organellar Ca<sup>2+</sup> uptake and changes cellular Ca<sup>2+</sup> homeostasis

Alicia J. Kowaltowski,<sup>\*1</sup> Sergio L. Menezes-Filho,<sup>\*</sup> Essam A. Assali,<sup>†</sup> Isabela G. Gonçalves,<sup>\*</sup> João Victor Cabral-Costa,<sup>\*</sup> Phablo Abreu,<sup>\*</sup> Nathanael Miller,<sup>†</sup> Patricia Nolasco,<sup>‡</sup> Francisco R. M. Laurindo,<sup>‡</sup> Alexandre Bruni-Cardoso,<sup>\*</sup> and Orian S. Shirihai<sup>†,2</sup>

<sup>\*</sup>Departamento de Bioquímica, Instituto de Química, Universidade de São Paulo, São Paulo, Brazil; <sup>†</sup>Department of Molecular and Medical Pharmacology and Department of Medicine, Division of Endocrinology, David Geffen School of Medicine, (UCLA), Los Angeles, California, USA; and <sup>‡</sup>Laboratório de Biologia Vascular, Biologia Cardiovascular Translacional (LIM-64), Instituto do Coração (InCor), Hospital das Clínicas, Faculdade de Medicina, Universidade de São Paulo, São Paulo, Brazil

**ABSTRACT:** Changes in mitochondrial size and shape have been implicated in several physiologic processes, but their role in mitochondrial Ca<sup>2+</sup> uptake regulation and overall cellular Ca<sup>2+</sup> homeostasis is largely unknown. Here we show that modulating mitochondrial dynamics toward increased fusion through expression of a dominant negative (DN) form of the fission protein [dynamin-related protein 1 (DRP1)] markedly increased both mitochondrial Ca<sup>2+</sup> retention capacity and Ca<sup>2+</sup> uptake rates in permeabilized C2C12 cells. Similar results were seen using the pharmacological fusion-promoting M1 molecule. Conversely, promoting a fission phenotype through the knockdown of the fusion protein mitofusin (MFN)-2 strongly reduced the mitochondrial Ca<sup>2+</sup> uptake speed and capacity in these cells. These changes were not dependent on modifications in mitochondrial calcium uniporter expression, inner membrane potentials, or the mitochondrial permeability transition. Implications of mitochondrial morphology modulation on cellular calcium homeostasis were measured in intact cells; mitochondrial fission promoted lower basal cellular calcium levels and lower endoplasmic reticulum (ER) calcium stores, as indicated by depletion with thapsigargin. Indeed, mitochondrial fission was associated with ER stress. Additionally, the calcium-replenishing process of store-operated calcium entry was impaired in MFN2 knockdown cells, whereas DRP1-DN-promoted fusion resulted in faster cytosolic Ca<sup>2+</sup> increase rates. Overall, our results show a novel role for mitochondrial morphology in the regulation of mitochondrial Ca<sup>2+</sup> uptake, which impacts cellular Ca<sup>2+</sup> homeostasis.—Kowaltowski, A. J., Menezes-Filho, S. L., Assali, E. A., Gonçalves, I. G., Cabral-Costa, J. V., Abreu, P., Miller, N., Nolasco, P., Laurindo, F. R. M., Bruni-Cardoso, A., Shirihai, O. Mitochondrial morphology regulates organellar Ca<sup>2+</sup> uptake and changes cellular Ca<sup>2+</sup> homeostasis. *FASEB J.* 33, 13176–13188 (2019). www.fasebj.org

**KEY WORDS:** mitochondria • calcium • ER stress • metabolism • bioenergetics

Recent advances in imaging techniques have allowed for detailed studies of mitochondrial morphology and their dynamic changes in live cells. Mitochondria not only vary in size and shape in different cell types but also rapidly

remodel their morphology in response to environmental changes like nutrient availability (1–5). Interestingly, changes in mitochondrial morphology occur not only in response to metabolic cues but also reciprocally regulate cellular metabolic responses (4). Dynamic changes in mitochondrial morphology additionally regulate organelle turnover, the maintenance of a healthy mitochondrial pool, and the interaction between mitochondria and other organelles such as the endoplasmic reticulum (ER) and lipid droplets (5–9).

The core proteins responsible for modulation of mitochondrial morphology include mitofusin (MFN)-1 and MFN2, outer membrane dynamin-related GTPases that form complexes between neighboring mitochondria and mediate outer membrane fusion. This process is followed by inner membrane fusion mediated by optic atrophy 1, a GTPase also involved in cristae remodeling (5). MFN2 also plays a key role in Ca<sup>2+</sup> signaling by mediating the interaction between mitochondria and the ER (10) and

**ABBREVIATIONS:** ΔΨ, inner mitochondrial membrane potential; BSA, bovine serum albumin; CsA, cyclosporin A; DN, dominant negative; DRP1, dynamin-related protein 1; ER, endoplasmic reticulum; FBS, fetal bovine serum; HEPES, 4-(2-hydroxyethyl)-1-piperazineethanesulfonic acid; KD, kinase dead; MCU, mitochondrial calcium uniporter; MFN, mitofusin; RR, ruthenium red; SOCE, store-operated calcium entry; TBST, Tris-buffered saline, 0.1% Tween 20

<sup>1</sup> Correspondence: Instituto de Química, Universidade de São Paulo, Av. Prof. Lineu Prestes, 748, São Paulo SP 05508-900, Brazil. E-mail: alicia@iq.usp.br

<sup>2</sup> Correspondence: Instituto de Química, Universidade de São Paulo, Av. Prof. Lineu Prestes, 748, São Paulo SP 05508-900, Brazil. E-mail: oshirihai@mednet.ucla.edu

doi: 10.1096/fj.201901136R

This article includes supplemental data. Please visit <http://www.fasebj.org> to obtain this information.

regulating mitophagy (11). Increased MFN-mediated mitochondrial fusion is often associated with enhanced bioenergetic efficiency (4, 12). Mitochondrial fission, on the other hand, is often associated with low bioenergetic efficiency and is controlled by the cytosolic dynamin-related protein 1 (DRP1), which assembles as oligomers around the fission site. GTP hydrolysis and DRP1 superstructure constriction then promote mitochondrial fragmentation (5). Interestingly, the location of mitochondrial outer membrane constriction is determined by ER-mitochondrial contact sites (13). Recent findings also suggest that inner mitochondrial membrane fission occurs at ER-mitochondrial contact sites in response to enhanced mitochondrial  $\text{Ca}^{2+}$  uptake from ER stores, independently of DRP1 (14, 15).

ER-mitochondrial interactions are important not only for the regulation of mitochondrial morphology but also for the regulation of intracellular  $\text{Ca}^{2+}$  signals (5, 16–18). Intracellular and intramitochondrial  $\text{Ca}^{2+}$ , on the other hand, are central metabolic regulators that affect the activity of both cytosolic and mitochondrial metabolic pathways (19–21). Although the close interaction between the ER and mitochondria is important for adequate signaling, recent studies have shown that ER-mitochondrial interactions increase excessively in high-fat diets, resulting in mitochondrial  $\text{Ca}^{2+}$  overload and dysfunction. Disrupting these interactions can increase animal health despite their diet, demonstrating the importance of mitochondrial  $\text{Ca}^{2+}$  in metabolic control (22, 23).

$\text{Ca}^{2+}$  uptake into the mitochondrial matrix occurs through a mitochondrial calcium uniporter (MCU) and is driven by the inner mitochondrial membrane potential ( $\Delta\Psi$ ), which attracts positively charged species (24). Mitochondria take up  $\text{Ca}^{2+}$  with very high capacity, allowing for the accumulation of large quantities of the ion, although with low affinity relative to the ER. Within mitochondria,  $\text{Ca}^{2+}$  ions act as regulators of important metabolic pathways, determining ATP synthesis rates (19–21). Excessive mitochondrial  $\text{Ca}^{2+}$  uptake, however, is disruptive for cell integrity under a number of pathologic conditions, including stroke, ischemic heart disease, and inflammatory liver conditions (23, 25–28). Under these conditions, dysfunction is associated with the mitochondrial permeability transition, a loss of inner mitochondrial membrane impermeability promoted by  $\text{Ca}^{2+}$  overload, oxidative imbalance, and protein misfolding (21, 29, 30).

We have recently found that mitochondria isolated from animals maintained on a chronic calorically restricted diet present increased  $\text{Ca}^{2+}$  accumulation capacity and resistance against mitochondrial permeability transition (31, 32), whereas acute unfed periods promote increased susceptibility to permeability transition and reduced  $\text{Ca}^{2+}$  accumulation capacity (33). This further supports the notion that dietary interventions may not only affect physiologic  $\text{Ca}^{2+}$  handling but also modulate damaging effects of supraphysiologic  $\text{Ca}^{2+}$  accumulation. Interestingly, caloric restriction and nutrient starvation also modulate mitochondrial morphology, thus stimulating mitochondrial fusion (34–36), whereas nutrient overload is often associated with mitochondrial fission (4, 37, 38).

Altogether, a wealth of evidence supports links between nutritional status, mitochondrial morphology and dynamics,  $\text{Ca}^{2+}$  signaling, and bioenergetic efficiency. However, a specific and central point that has not been studied is whether changes in mitochondrial morphology directly promote changes in mitochondrial  $\text{Ca}^{2+}$  uptake that impact intracellular  $\text{Ca}^{2+}$  signaling. Here we show that modifying mitochondrial morphology alters  $\text{Ca}^{2+}$  uptake rates and capacity, with larger mitochondria exhibiting faster and larger  $\text{Ca}^{2+}$  uptake. We also found that mitochondrial morphology regulates the cellular calcium-replenishing process of store-operated calcium entry (SOCE). Our results uncover a novel role for mitochondrial morphology in the control of mitochondrial  $\text{Ca}^{2+}$  uptake, which impacts cellular  $\text{Ca}^{2+}$  homeostasis.

## MATERIALS AND METHODS

### Cell cultures

C2C12 cells (passages 6–21) were cultured in high-glucose DMEM with 10% fetal bovine serum, 1 mM pyruvate, 100 U/ml penicillin, and 1000  $\mu\text{g}/\text{ml}$  streptomycin and were trypsinized every 2–3 d and typically split 1:7.

### Modulation of mitochondrial morphology

Mitochondrial fusion was promoted by infection with an adenovirus containing a dominant negative (DN) form of DRP1 (DRP1 DN; Welgen, Worcester, MA, USA) at a multiplicity of infection level of 200. Mitochondrial fission was promoted by MFN2 silencing using an adenovirus from Welgen at a multiplicity of infection of 20. Cells were treated when split, and the medium was changed after 24 h. Experiments were conducted 72 h after, when infection rates were maximized (12). Cell viability was assessed by Trypan blue exclusion (MilliporeSigma, Burlington, MA, USA), and >95% for all experiments conducted.

### Analysis of mitochondrial morphology

Cells were plated on glass-bottomed plates 72 h prior to imaging and loaded with Mitotracker Green (Thermo Fisher Scientific, Waltham, MA, USA) (200 nM) for 30 min followed by washout just prior to the experiment. A Zeiss LSM 880 confocal microscope in Airyscan mode was used for superresolution imaging, with a 488 nm Argon laser and Zeiss  $\times 63/1.4$  numerical aperture oil immersion objective (Carl Zeiss, Oberkochen, Germany). At least 10 images per experimental condition were collected. Cells were individualized as areas of interest using ImageJ (National Institutes of Health, Bethesda, MD, USA), and automated mitochondrial circularity and aspect ratios (the proportional relationship between width and height) were measured. Data are presented as symbols that represent average circularity and aspect ratio per cell. Mitochondrial fission is expected to increase circularity and decrease the aspect ratio. Representative images shown were adjusted in brightness and contrast for better visualization.

### Digitonin-permeabilized cells

Cells were trypsinized, washed, and suspended in 200  $\mu\text{l}$  of 140 mM NaCl, 3 mM KCl, 400  $\mu\text{M}$   $\text{KH}_2\text{PO}_4$ , 20 mM 4-(2-hydroxyethyl)-1-piperazineethanesulfonic acid (HEPES), 5 mM

NaHPO<sub>4</sub>, 5 mM glucose, and 1 mM MgCl<sub>2</sub>, pH 7 (NaOH). They were counted and kept in this medium at room temperature for, at most, 90 min while experiments were conducted, and then they were resuspended in permeabilized cell medium just prior to each trace. Ideal cell quantities and digitonin titers were determined by following plasma membrane permeabilization using safranin (39) and were found to be  $2.5 \cdot 10^6$ /ml cells in the presence of 0.0025% digitonin (added just prior to the trace). Under these conditions, cells were safranin-permeant (indicating plasma membrane permeabilization) and maintained inner membrane potentials for 40 min (indicating mitochondrial membrane integrity).

### Mitochondrial Ca<sup>2+</sup> uptake

Extramitochondrial Ca<sup>2+</sup> uptake was followed in digitonin-permeabilized cells using the fluorescent calcium probe Ca<sup>2+</sup> Green (Thermo Fisher Scientific) (100 nM; 31, 40) in medium containing 125 mM KCl, 2 mM KH<sub>2</sub>PO<sub>4</sub>, 10 mM HEPES, 1 mM MgCl<sub>2</sub>, 5 mM succinate, 5 mM malate, and 5 mM glutamate, with pH 7 (KOH). Fluorescence was measured with constant stirring, in a cuvette fluorimeter at 506 nm excitation and 532 nm emission. Where indicated in the figures, successive additions of 50 μM CaCl<sub>2</sub> were made until Ca<sup>2+</sup> accumulation capacity was exhausted, as indicated by lack of further uptake and release. A calibration curve was constructed using known CaCl<sub>2</sub> concentrations, and maximal calcium uptake capacity and initial uptake rates were calculated for each trace. Where indicated, 1 μM cyclosporin A (CsA), a mitochondrial permeability transition inhibitor, or 1 μM ruthenium red (RR), an MCU inhibitor, were present. Cells were treated either with 10 μM M1 or equivalent volumes of DMSO (control group) in the culture medium 16 h prior to membrane permeabilization and Ca<sup>2+</sup> uptake measurements.

### Western blotting

Approximately  $100 \cdot 10^3$  (in control and DRP1 DN groups) or  $125 \cdot 10^3$  [in MFN2 kinase dead (KD) group] cells were seeded on P100 plates and treated as previously described to modulate mitochondrial morphology. Cells were washed with PBS, quickly frozen in dry ice, and lysed in RIPA buffer containing protease and phosphatase inhibitors. This extract was centrifuged at 1000 g for 10 min at 4°C, and the supernatant was collected and stored at -20°C. Protein concentration was determined using the BCA Protein Assay Kit (Thermo Fisher Scientific, Waltham, MA, USA), and extracts were diluted in sample buffer at a final concentration of 1.25 μg/μl. Samples (20 μg) were resolved by SDS-PAGE in 10% polyacrylamide gels, transferred onto nitrocellulose membranes, and blocked by 5% bovine serum albumin (BSA) in Tris-buffered saline, 0.1% Tween 20 (TBST) buffer. Primary antibodies were incubated for 1 h at room temperature (anti-β-actin, ab8226; Abcam, Cambridge, MA, USA, 1:10,000 1% BSA in TBST) or overnight at 4°C (anti-MCU, 14997, 1:1000 1% BSA in TBST; Cell Signaling Technology, Danvers, MA, USA). Secondary antibodies were incubated for 2 h at room temperature [anti-rabbit, IRDye 680RD (926-68071) and anti-Mouse IRDye 800CW (925-32210), 1:20,000 1% BSA in TBST], and imaged with near-infrared detection by Odyssey (Li-Cor Biosciences, Lincoln, NE, USA). Signals were quantified by densitometry using Fiji/ImageJ. All bands were normalized to the respective β-actin sample values.

### Mitochondrial membrane potentials

Inner mitochondrial membrane potentials ( $\Delta\Psi$ ) were determined in permeabilized cells by following the fluorescence of 5 μM

safranin O at 485-nm excitation and 586-nm emission. For ideal digitonin permeabilization determination, the same medium as Ca<sup>2+</sup> uptake measurements was used, and the digitonin concentration that promoted permeabilization (seen as a low, stable fluorescence) in <5 min and sustained for at least 40 min, was used. For  $\Delta\Psi$  quantification, medium devoid of K<sup>+</sup> was prepared (all K<sup>+</sup> salts were substituted for Na<sup>+</sup>, except KCl, which was substituted by 250 mM sucrose). Fluorescence was related to known  $\Delta\Psi$ s by adding 50 nM valinomycin and known KCl concentrations, allowing  $\Delta\Psi$  to be calculated using the Nernst equation. A calibration curve was constructed relating  $\Delta\Psi$  and fluorescence and extrapolated for basal fluorescence measured in the absence of added KCl (39).

### Ca<sup>2+</sup> uptake in permeabilized cells with clamped $\Delta\Psi$

Cells were incubated in the same medium used for  $\Delta\Psi$  quantification, with 50 nM valinomycin plus 0.41 mM KCl, which was sufficient to reach the same  $\Delta\Psi$  as found in MFN2 KD cells. Ca<sup>2+</sup> uptake was measured as described. Controls were conducted without the addition of KCl, in the same media. Samples were paired for preparations from the same flask/passage.

### Cellular Ca<sup>2+</sup> imaging

Three days prior to the experiment, cells were plated in Greiner 627871 4-compartment glass-bottom cell culture dishes (Greiner Bio-One, Kremmsmünster, Austria) and mitochondrial morphology was modulated as described above. Fura-2 AM loading and imaging protocols were adapted from Arruda *et al.* (41), with modifications. On the experimental day, the culture medium was removed, and cells were washed twice with experimental buffer containing 10 mM HEPES, 150 mM NaCl, 4 mM KCl, 1 mM MgCl<sub>2</sub>, and 10 mM D-glucose (pH 7.4) and then were incubated with 10 μM Fura-2 AM, 0.1% pluronic acid, and 2 mM CaCl<sub>2</sub> in that same medium for 40 min at 37°C and 5% CO<sub>2</sub> in order to load the probe. After incubation, the medium was removed and cells were washed twice in the experimental buffer. Cells were then incubated in 1 ml experimental buffer and placed inside the chamber of a Leica DMi-8 microscope equipped with a Fura-2 filter (Leica Microsystems, Buffalo Grove, IL, USA) and a ×40 objective. Fura-2 cytosolic Ca<sup>2+</sup> imaging was conducted by alternatively illuminating the cells with wavelengths of 340 and 387 nm. Images were acquired every 5 s. Cytosolic Ca<sup>2+</sup> levels are shown in the figures as the 340/387 ratios for the Fura-2 channels, which are proportional to Ca<sup>2+</sup> concentrations. Intensities were calculated using Fiji/ImageJ extension by converting the videos obtained in each channel to grayscale and then plotting the mean gray values over time for each cell. Thirty seconds after the beginning of the experiment, 2 μM thapsigargin was added to the experimental medium in order to promote ER Ca<sup>2+</sup> release. At 630 s, 2 mM CaCl<sub>2</sub> was added in order to trigger store-operated Ca<sup>2+</sup> reentry. Experiments were repeated on 3 separate days, with 7–10 cells analyzed per day under each experimental condition. Cytosolic Ca<sup>2+</sup> (340/387 nm ratio) increase rates after the addition of 2 mM CaCl<sub>2</sub> were measured by adjusting a linear fit using Origin 8 Pro software (OriginLab, Northampton, MA, USA).

### ER stress marker evaluation by real-time PCR

On the third day after infection, total RNA from the cells was extracted and purified using Trizol reagent (Thermo Fisher



Scientific) and quality-checked using 260/230 and 260/280 nm scores in a NanoDrop Ppctrophotometer. Equivalent contents of RNA were reverse transcribed using a High-Capacity cDNA Reverse Transcription Kit (Thermo Fisher Scientific). Synthesized cDNA was stored at  $-20^{\circ}\text{C}$  prior to the real-time PCR assay. Data shown here are expressed as the ratio of the target gene to the hypoxanthine phosphoribosyl transferase (HPRT) reference/housekeeping gene, which was validated through deletion experiments (42). cDNA amplification was performed using Platinum SYBR Green quantitative PCR SuperMix UDG (Thermo Fisher Scientific) and evaluated by real-time PCR using Rotor Gene 3000 apparatus (Corbett Research, Mortlake, Australia). Quantitative RT-PCR primer sequences were obtained from the Harvard database PrimerBank (43), as listed in Supplemental Data, and had their efficiency (90% minimum) and concentration standardized. Fold changes were calculated by the  $2^{-\Delta\Delta C_t}$  method.

## Statistical analysis

Comparisons were made using Prism software (GraphPad, La Jolla, CA, USA), with Student's *t* tests for simple comparisons between 2 groups and ANOVA for multiple comparisons.

## RESULTS

To study the effects of mitochondrial morphology modulation on  $\text{Ca}^{2+}$  uptake by this organelle, we used C2C12 myoblast cells, which have a functional and dynamic mitochondrial network (44, 45), are amenable to automated mitochondrial morphologic quantification (46), and display robust intracellular  $\text{Ca}^{2+}$  signaling (47). **Figure 1**

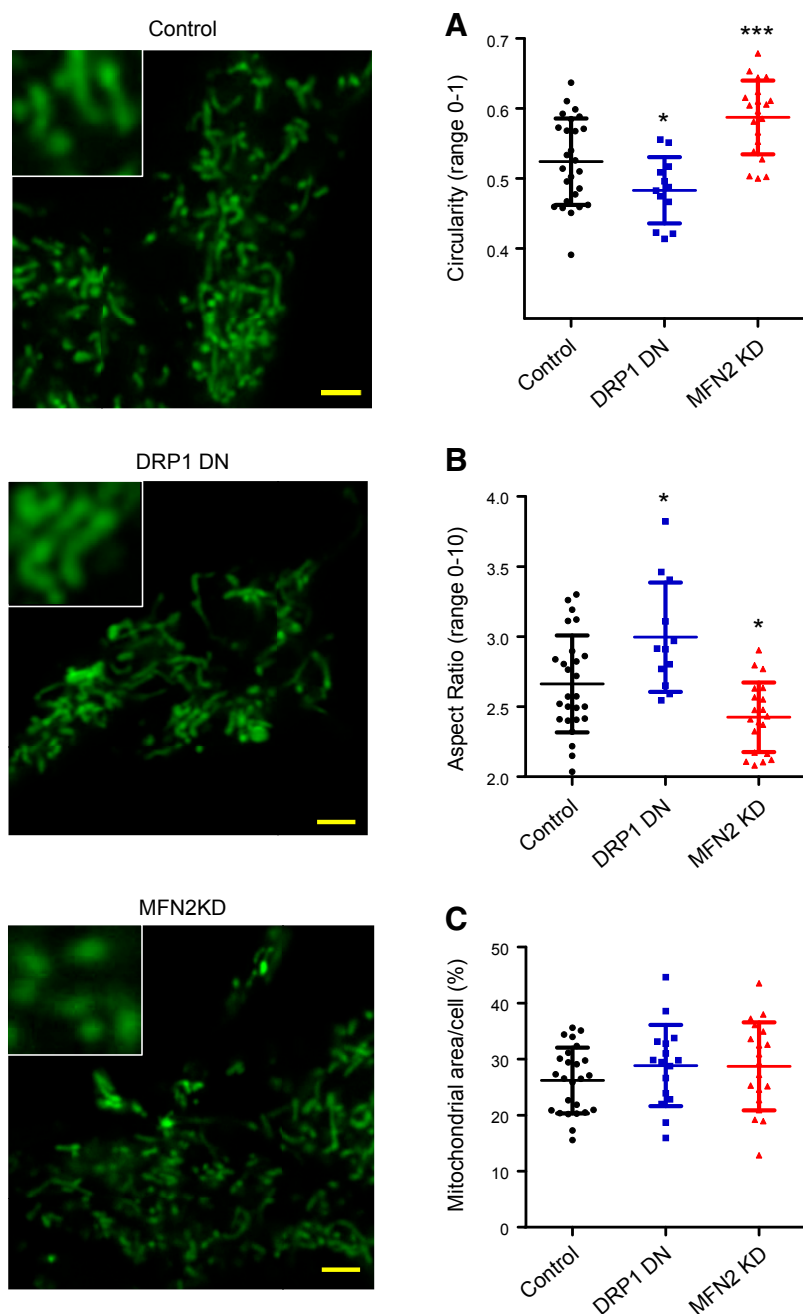


**Figure 1.** Mitochondrial morphology is modulated by DRP1 and MFN2. C2C12 mitochondria were marked with MitoTracker Green and imaged in intact cells as described in Materials and Methods (left panels, scale bars, 10  $\mu\text{m}$ ). The inserts show higher magnifications of selected areas. Mitochondrial circularity (A), aspect ratios (B), and cross-sectional area relative to the cellular area (C) were quantified from these images;  $n > 10$  cells per condition. \* $P < 0.05$ , \*\*\* $P < 0.001$  relative to control cells.

(leftmost panels) shows typical superresolution images of stained mitochondria in these cells, such as those used for automated morphologic analysis. We found that DRP1 DN cells, in which the fission machinery is inhibited, presented mitochondria with lower circularity (Fig. 1A) and higher aspect ratios (the proportional relationship between width and height, Fig. 1B) when compared with control cells. This indicates that DRP1 DN cells, as expected, had longer and less circular mitochondria as a consequence of the inhibition of fission. Conversely, MFN2 KD cells, in which fusion was partially impaired (mRNA levels were decreased on average by 40%), presented enhanced mitochondrial fragmentation, as indicated by higher circularity (Fig. 1A) and lower aspect ratios (Fig. 1B). Notably, the changes in morphology were expected for physiologic conditions (4). Neither genetic interference affected the area occupied by mitochondria (Fig. 1C), which indicates that no large-scale disruption of mitochondrial content occurred. Furthermore, cell viability was above 95% under all conditions, showing that we were able to successfully modulate mitochondrial morphology without compromising cell integrity.

Next, we determined if the changes in mitochondrial morphology modified  $\text{Ca}^{2+}$  uptake by these organelles using digitonin-permeabilized cell suspensions. Plasma membrane permeabilization under these conditions has been shown to keep mitochondrial and cell architecture, as well as the cytoskeleton, intact (48) while largely diluting cytosolic components, allowing for a direct assessment of organellar  $\text{Ca}^{2+}$  dynamics. Calcium levels were followed in permeabilized cells using the membrane-impermeable probe Calcium Green, which fluoresces in the presence of  $\text{Ca}^{2+}$  in the experimental buffer but does not enter membrane-bound organelles. **Figure 2A** shows a scheme of the experimental setup. Adding successive  $\text{Ca}^{2+}$  boluses (where indicated by the arrows) to a suspension of permeabilized cells results in a rapid increase in  $\text{Ca}^{2+}$  levels, followed by gradual decrease in  $\text{Ca}^{2+}$  detection due to the uptake of the ion by membrane-bound organelles. Uptake of the ion continues after each bolus addition until the maximal capacity is reached. Beyond this point, addition of  $\text{Ca}^{2+}$  to the extramitochondrial medium is not followed by its uptake by these organelles. Eventually, calcium overload leads to spontaneous  $\text{Ca}^{2+}$  release.

$\text{Ca}^{2+}$  removal from the medium is due to mitochondrial activity, as uptake by this organelle occurs with higher capacity than that by the ER. Indeed,  $\text{Ca}^{2+}$  uptake in control cells (Fig. 2B, black line) was completely prevented in the presence of the MCU inhibitor RR (Fig. 2B, pink line). Inhibition of the mitochondrial permeability transition with CsA (Fig. 2B, light blue line) resulted in a large increase in  $\text{Ca}^{2+}$  uptake capacity, further confirming that mitochondrial  $\text{Ca}^{2+}$  uptake was measured.

Two characteristics of mitochondrial  $\text{Ca}^{2+}$  uptake can be calculated from traces generated by this assay: calcium retention capacity, the maximal amount of  $\text{Ca}^{2+}$  taken up by mitochondria (see blue lines in Fig. 2A) before spontaneous release, and calcium uptake rates (see the dotted red line in Fig. 2A), the speed in which

the ion is removed from the medium after the first addition. We found that DRP1 DN cells, in which mitochondria become elongated, have higher calcium retention capacity (blue traces in Fig. 2C, and blue columns in Fig. 2D) and higher calcium uptake rates (Fig. 2E) when compared with control cells (black traces and columns, Fig. 2C–E). This enhanced accumulation was due to augmented mitochondrial  $\text{Ca}^{2+}$  uptake because the MCU inhibitor RR completely inhibited it (Fig. 2D, E). On the other hand, MFN2 KD cells, with fragmented mitochondria, present lower calcium uptake capacity (Fig. 2C, red trace, and Fig. 2D, red columns) and lower  $\text{Ca}^{2+}$  uptake rates (Fig. 2E, red columns). Overall, this shows that increased mitochondrial fusion enhances  $\text{Ca}^{2+}$  uptake speed and capacity, whereas mitochondrial fission decreases  $\text{Ca}^{2+}$  uptake. On the other hand, the affinity for  $\text{Ca}^{2+}$  in cells with different mitochondrial morphologies was equal, as evaluated by residual concentrations of the ion left in the medium after uptake stabilized.

The presence of CsA (Fig. 2D) enhanced calcium retention capacity in all cell types, although uptake with CsA was still larger in DRP1 DN mitochondria and lower in MFN2 KD. Interestingly, CsA had a particularly pronounced effect on the MFN2 KD mitochondrial  $\text{Ca}^{2+}$  uptake. We calculated the proportional effect of the mitochondrial permeability transition on  $\text{Ca}^{2+}$  uptake capacity and rates by comparing these values in the absence and presence of permeability transition inhibitor CsA. Our results indicate that proportional susceptibility to permeability transition is not changed in DRP1 DN cells, yet this process is facilitated by mitochondrial fission promoted by MFN2 knock-down: both mitochondrial  $\text{Ca}^{2+}$  uptake capacity (Fig. 2F) and rates (Fig. 2G) are proportionally lower in MFN2 KD cells when normalized to these measurements in the presence of CsA. Thus, MFN2 KD-promoted fragmentation increases mitochondrial permeability transition activity. However, despite the effects of permeability transition in MFN2 KD cells, the absolute differences in  $\text{Ca}^{2+}$  uptake capacity and rates promoted by changes in mitochondrial morphology persisted even in the presence of CsA (Fig. 2D, E). This shows that the permeability transition is not solely responsible for the changes in  $\text{Ca}^{2+}$  uptake observed with modified mitochondrial morphology but rather an additional factor governing  $\text{Ca}^{2+}$  homeostasis in this organelle.

Interestingly, we found that MCU protein quantities were equal in control, DRP1 DN, and MFN2 KD cells, as detected by Western blots (**Fig. 3**). Thus, modifications in uptake rates and capacity cannot be attributed to enhanced MCU expression. Regulation of the MCU activity also does not seem to be involved in the modulation of  $\text{Ca}^{2+}$  uptake by mitochondrial morphology because spermine, an MCU activator, did not enhance mitochondrial uptake in control or MFN2 KD cells (unpublished results).

In order to verify whether an independent and more acute morphology-modulating intervention could reproduce the effects seen by genetically manipulating mitochondria, we tested the effects of fusion-promoting

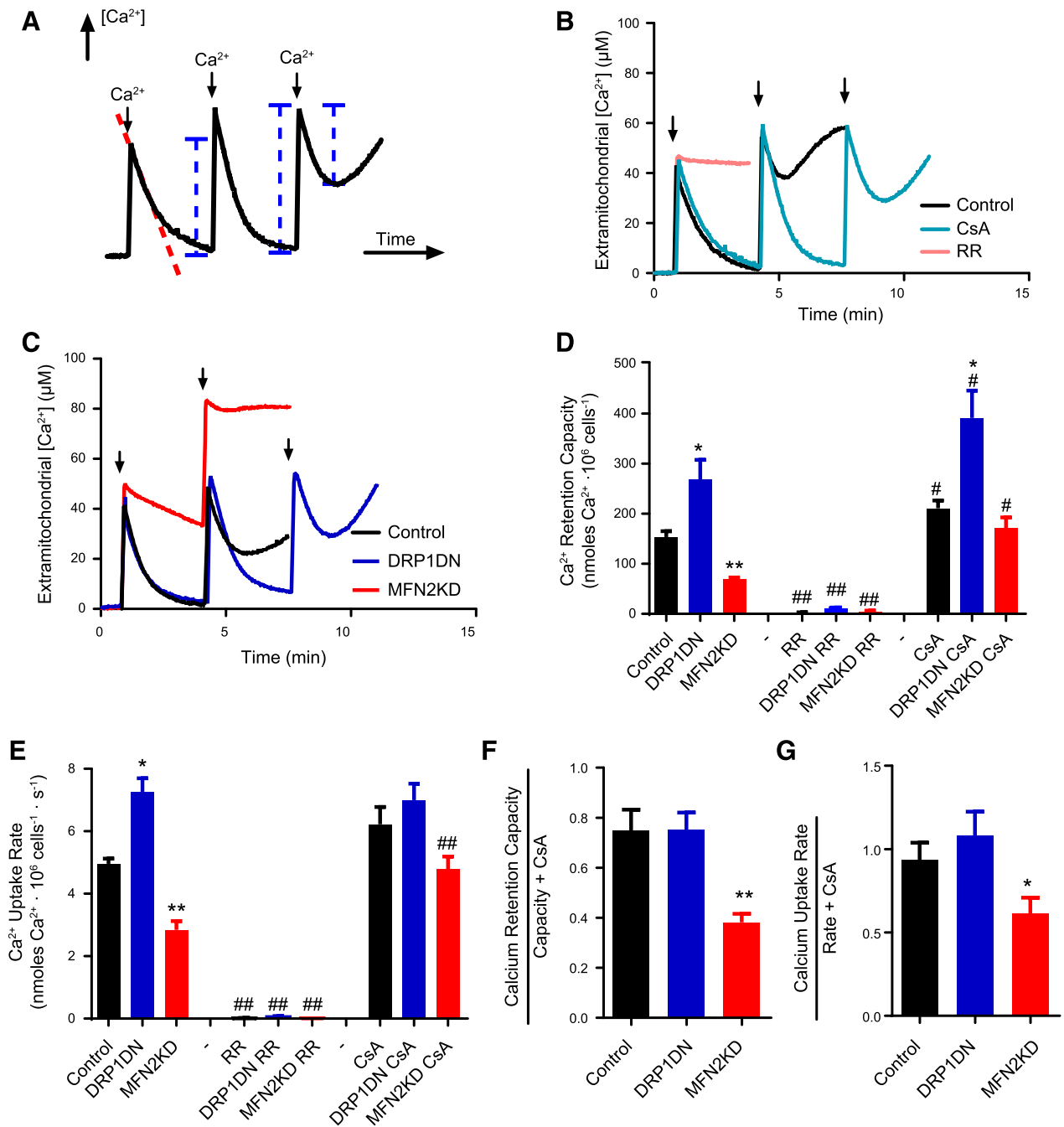


**Figure 2.** Ca<sup>2+</sup> uptake is modulated by mitochondrial morphology. Ca<sup>2+</sup> uptake was measured in permeabilized cells as described in Materials and Methods, in control (black lines/columns), DRP1 DN (dark blue lines/columns) and MFN2 KD (red lines/columns) (B–D) cells, as indicated. A) The measurement technique used: Ca<sup>2+</sup> uptake by mitochondria is followed by measuring extramitochondrial [Ca<sup>2+</sup>] concentrations over time, after the addition of successive boluses of the ion to the experimental medium where indicated by arrows. The dotted red line indicates data used to measure Ca<sup>2+</sup> uptake rates. Blue lines represent Ca<sup>2+</sup> quantities that, when added, reflect maximal retention capacity. B) Only control cells were used, and, where indicated, 1 μM CsA (light blue line) or 1 μM RR (pink line) were present. Arrows indicate bolus 50 μM Ca<sup>2+</sup> additions. C) Typical traces in control (black), DRP1 DN (blue), and MFN2 KD (red) cell types. Arrows indicate bolus 50 μM Ca<sup>2+</sup> additions. D) Quantification of Ca<sup>2+</sup> retention capacity in traces such as those shown in B and C. E) Quantification of Ca<sup>2+</sup> uptake rates over the first 20 s after the first Ca<sup>2+</sup> addition in traces such as those in B and C. F, and G) Basal calcium retention capacity relative to retention in the presence of CsA (F) and basal uptake rates relative to rates in the presence of CsA (G) were plotted; n ≥ 5 independent repetitions. \*P < 0.05, \*\*P < 0.01 relative to noninfected cells under the same conditions; #P < 0.05, ##P < 0.01, relative to the same cells in the absence of CsA or RR.

compounds. In preliminary experiments, mdivi-1, identified as a mitochondrial division inhibitor 1 in a chemical screen (49), promoted extensive cell death within 16 h,

possibly because of its effect as a complex I inhibitor (50). A second small molecule, mitochondrial fusion promoter M1, did not affect cell viability when tested and was used

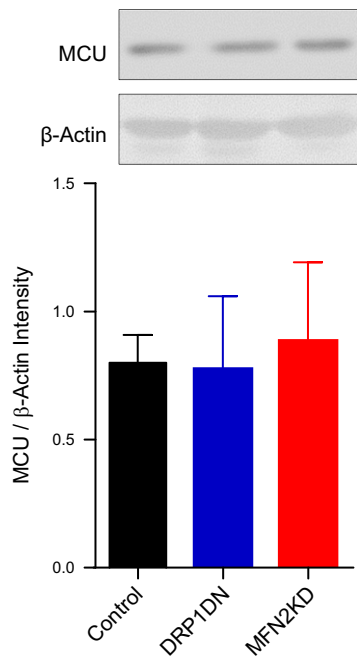


**Figure 3.** Mitochondrial morphology does not affect MCU expression. Protein expression in control (black), DRP1 DN (blue), and MFN2 KD (red) C2C12 cells was assessed by Western blotting as described in Materials and Methods. No significant differences were measured;  $n = 5$  independent samples.

to induce acute fusion in the cells (Fig. 4). M1 treatment robustly increased both calcium retention capacity (Fig. 4A) and uptake rates (Fig. 4B) in control cells, confirming through a pharmacological approach that mitochondrial fusion promotes an increase in  $\text{Ca}^{2+}$  uptake by this organelle.

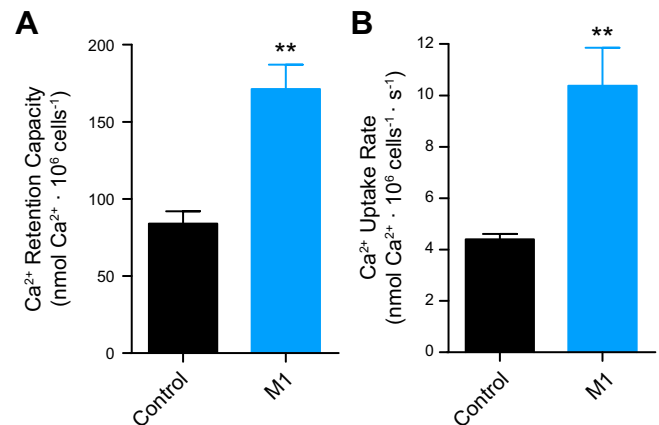
The fact that mitochondrial  $\text{Ca}^{2+}$  homeostasis could be modulated by 2 different methods to change mitochondrial morphology (genetically manipulating protein levels and use of a fusion-inducing small molecule), despite equal MCU expression, led us to seek a mechanistic explanation for the changes in  $\text{Ca}^{2+}$  uptake.  $\text{Ca}^{2+}$  extrusion from mitochondria mediated by the  $\text{Na}^+/\text{Ca}^{2+}$  exchanger (NCLX) could be excluded as a cause for these differences because sodium was not added to the medium in these experiments, rendering this pathway inactive (51). A possible reason could be a modification of the  $\Delta\Psi$ , the driving force for  $\text{Ca}^{2+}$  uptake. We thus measured  $\Delta\Psi$  using plasma membrane-impermeable safranin O fluorescence, which allows for quantitative  $\Delta\Psi$  determinations in isolated mitochondria or permeabilized cells [Fig. 5 (39, 52)].

Figure 5A shows typical safranin fluorescence traces over time after cell permeabilization with digitonin. The downward deflection of the curve over time is a result of  $\Delta\Psi$ -driven accumulation of the cationic probe in the mitochondrial matrix, which decreases its fluorescence (39, 52). Safranin accumulation in DRP1 DN cells (blue trace) was consistently higher than that in control cells (black trace), whereas MFN2 KD cells (red trace) accumulated less safranin. This result could be indicative of changes

in  $\Delta\Psi$  promoted by manipulating mitochondrial morphology. However, accumulation and fluorescence of  $\Delta\Psi$ -sensitive probes is also modified by mitochondrial size and shape (39, 53). To overcome this possible artifact and quantify changes in  $\Delta\Psi$ , we calibrated safranin fluorescence curves in  $\text{K}^+$ -free medium in the presence of the  $\text{K}^+$  ionophore valinomycin, by adding known quantities of extramitochondrial  $\text{K}^+$  into the medium and following fluorescence changes [Fig. 5B (52)]. Under these conditions,  $\Delta\Psi$  can be calculated for each added  $\text{K}^+$  concentration using the Nernst equation, and basal  $\Delta\Psi$  can be extrapolated, in millivolts, from the calibration curves (39, 52). Carbonyl cyanide 4-(trifluoromethoxy) phenylhydrazone, a proton ionophore, was added at the end of each trace to complete the dissipation of  $\Delta\Psi$ . By using  $\text{K}^+$  calibrations, we found that, despite differences in safranin accumulation and fluorescence, control and DRP1 DN mitochondria displayed the same  $\Delta\Psi$  (in the range of 180 mV, Fig. 5C), whereas MFN2 KD mitochondria had significantly lower  $\Delta\Psi$  (in the range of 155 mV, Fig. 5C). Despite this lower  $\Delta\Psi$ , MFN2 KD mitochondria were still capable of promoting oxidative phosphorylation, as demonstrated by measuring a decrease in  $\Delta\Psi$  upon the addition of 2 mM ADP (unpublished results).

These results highlight a highly important and often overlooked caveat of studies using mitochondrially accumulated probes under conditions in which morphology is modified: in the absence of calibration for each individual condition, changes in fluorescence may be misinterpreted as changes in the parameter the probe is measuring (39, 53), when they may only reflect variations in calibration.

Overall, our  $\Delta\Psi$  quantifications do not explain the increase in  $\text{Ca}^{2+}$  uptake capacity and rates in DRP1 DN mitochondria because  $\Delta\Psi$  was unchanged relative to the control cells. However, the decrease in  $\Delta\Psi$  observed in MFN2 KD mitochondria may be the cause for lower  $\text{Ca}^{2+}$



**Figure 4.** Mitochondrial fusion promoted by M1 increases  $\text{Ca}^{2+}$  uptake. Control cells were incubated in the presence or absence of 10  $\mu\text{M}$  M1, as described in Materials and Methods, and  $\text{Ca}^{2+}$  retention capacity (A) and uptake rates (B) were measured as described for Fig. 2;  $n = 4$  independent repetitions. \*\* $P < 0.01$  relative to DMSO-treated (control) cells.

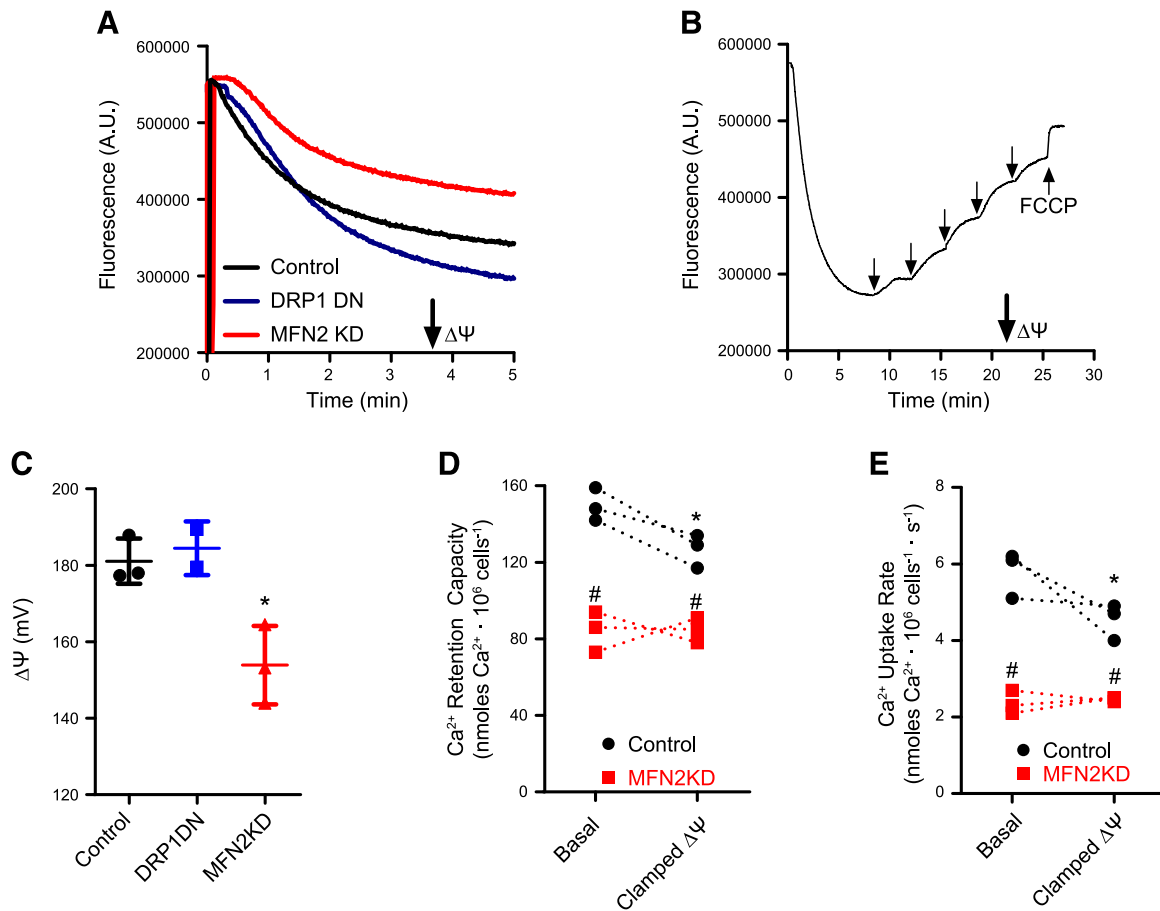


**Figure 5.** Mitochondrial morphology affects  $\Delta\Psi$  measurements.  $\Delta\Psi$  were measured using safranin O fluorescence as described in Materials and Methods. *A*) Typical safranin fluorescence traces in control (black), DRP1 DN (blue), and MFN2 KD (red) permeabilized cells. *B*) A typical  $\Delta\Psi$  calibration procedure in control cells, conducted as described in Materials and Methods. Arrows indicate where  $\text{K}^+$  and the uncoupler carbonyl cyanide 4-(trifluoromethoxy) phenylhydrazone (FCCP; 1  $\mu\text{M}$ ) were added. *C*) Presentation of calibrated  $\Delta\Psi$  determinations in control (black symbols), DRP1 DN (blue symbols) permeabilized cells;  $n = 5$ .  $*P < 0.05$  relative to control cells. *D*)  $\text{Ca}^{2+}$  uptake capacity was evaluated in control (black circles) and MFN2 KD (red squares) permeabilized cells under basal conditions or when  $\Delta\Psi$  was clamped to the average measured MFN2 KD  $\Delta\Psi$  (see Materials and Methods). *E*)  $\text{Ca}^{2+}$  uptake rates were evaluated in control (black circles) and MFN2 KD (red squares) permeabilized cells under basal conditions or when  $\Delta\Psi$  was clamped to the average measured MFN2 KD  $\Delta\Psi$ ;  $n = 3$  independent repetitions.  $*P < 0.05$  relative to basal  $\Delta\Psi$ ;  $\#P < 0.05$  relative to control cells under the same  $\Delta\Psi$  condition; traces connect paired experiments.

uptake capacity and rates as well as higher permeability transition susceptibility observed in Fig. 2. To assess this possibility, we designed an experiment in which the  $\Delta\Psi$  of control cell mitochondria was forcibly clamped at the same level as the  $\Delta\Psi$  of MFN2 KD mitochondria using added extramitochondrial  $\text{K}^+$  and valinomycin (see Materials and Methods). Calcium uptake was then quantified under these conditions, comparing the effects of clamping  $\Delta\Psi$  on  $\text{Ca}^{2+}$  retention capacity (Fig. 5D) and uptake rates (Fig. 5E). MFN2 KD cells presented equal calcium retention and uptake rates under basal and clamped  $\Delta\Psi$  conditions (red squares; connected traces show individual replicates under basal conditions paired with the same sample with clamped  $\Delta\Psi$ ). This result was expected because  $\Delta\Psi$  was clamped at the same level as basal  $\Delta\Psi$  in MFN2 KD cells. On the other hand, control cells (black circles) presented a decrease in retention capacity and uptake rates when the  $\Delta\Psi$  was clamped. However, mitochondrial  $\text{Ca}^{2+}$  uptake capacity and rates were still significantly higher in control

cells relative to MFN2 KD cells under clamped  $\Delta\Psi$  conditions, indicating that  $\Delta\Psi$  is not the only factor decreasing  $\text{Ca}^{2+}$  uptake in cells with impaired mitochondrial fusion. This result is in line with the finding that DRP1 DN mitochondria do not present changes in  $\Delta\Psi$  but rather take up more  $\text{Ca}^{2+}$  at faster rates. Furthermore, changes in  $\Delta\Psi$  would be expected to impact uptake rates but not necessarily retention capacity. Overall, our results conclusively demonstrate that changes in mitochondrial morphology and dynamics are sufficient to change  $\text{Ca}^{2+}$  homeostasis in this organelle.

Our next question was whether these modifications in mitochondrial  $\text{Ca}^{2+}$  homeostasis have an impact on cellular calcium handling. To investigate this, we evaluated cytosolic  $\text{Ca}^{2+}$  levels in intact cells in which mitochondrial morphology was modulated (Fig. 6). Figure 5A shows typical Fura-2 fluorescence ratio traces (which are directly proportional to intracellular calcium concentrations) of cells acutely incubated in the absence of extracellular

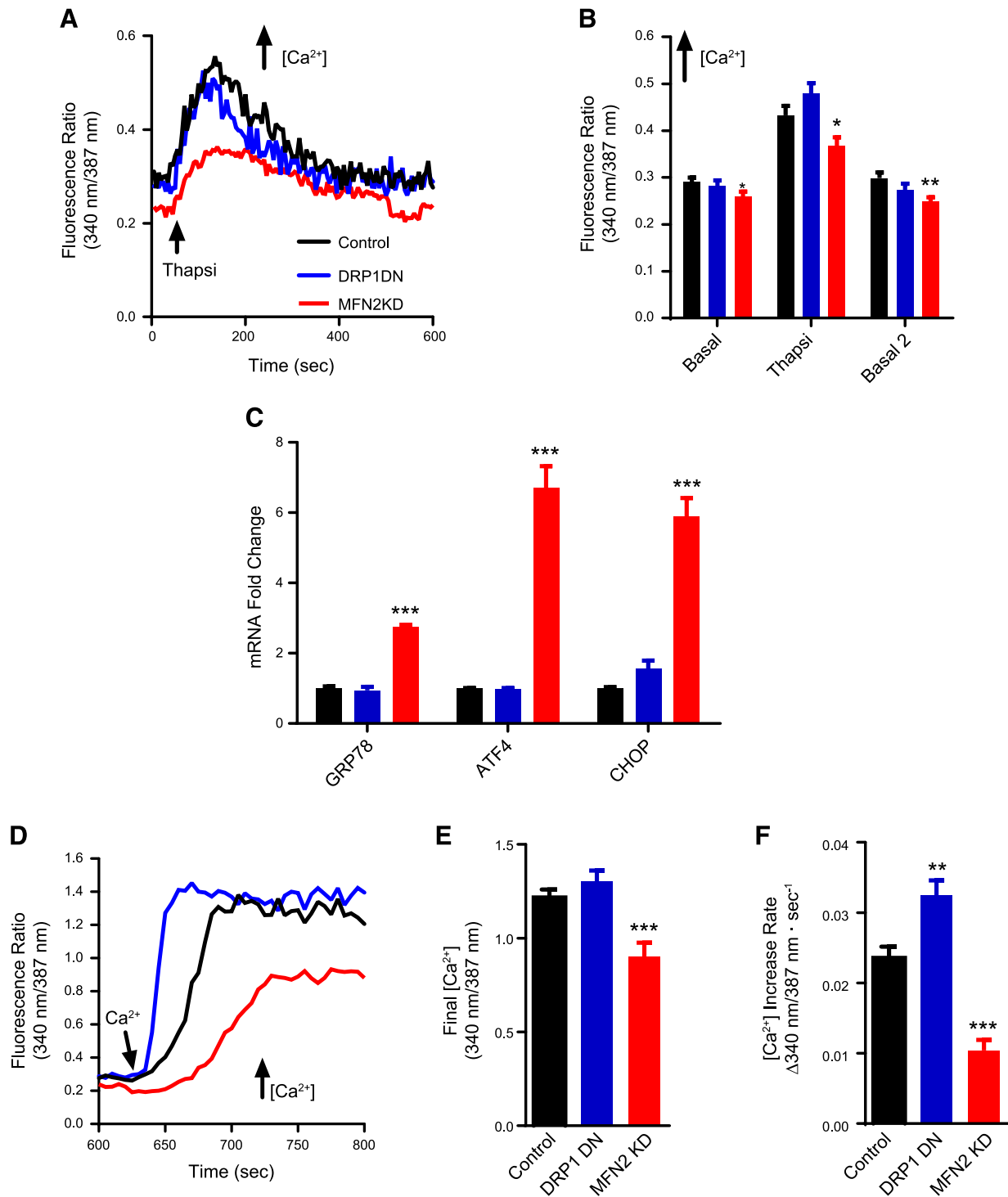


**Figure 6.** Mitochondrial morphology affects cellular Ca<sup>2+</sup> homeostasis and ER stress responses. *A*) Representative traces of Fura-2 ratios corresponding to cytosolic Ca<sup>2+</sup> concentrations in intact control (black), DRP1 DN (blue), and MFN2 KD (red) plated cells. Where indicated, 2 μM thapsigargin (Thapsi) was added. *B*) Quantifications of these traces, including basal initial ratios, peak Thapsi ratios, and basal 2 ratios, after Thapsi. *C*) mRNA levels of ER stress markers 78 kDa glucose-regulated protein (GRP78), activating transcription factor 4 (ATF4), and C/EBP homologous protein (CHOP) are expressed as the fold change relative to the housekeeping gene hypoxanthine phosphoribosyl transferase (HPRT). *D*) Representative traces of Fura-2 ratios after the addition of 2 mM extracellular Ca<sup>2+</sup>, to activate SOCE. Final SOCE fluorescence ratios are quantified in *E*. *F*) quantifies SOCE fluorescence increase rates; *n* = 23–27 cells/condition. \**P* < 0.05, \*\**P* < 0.01, \*\*\**P* < 0.001 compared with control cells.

calcium. We found that MFN2 KD cells had consistently lower basal calcium levels (typical traces in Fig. 6A are quantified in Fig. 6B), whereas levels in control and DRP1 DN cells were equal. Upon promoting calcium release

from the ER with thapsigargin (indicated by the arrow in Fig. 6A), MFN2 KD cells showed lower cytosolic Ca<sup>2+</sup> increments (Fig. 6B) relative to control and DRP1 DN cells, suggestive of lower ER Ca<sup>2+</sup> stores. After ER calcium



release, basal cytosolic  $\text{Ca}^{2+}$  levels were requantified and once again found to be lower in MFN2 KD cells (basal 2, Fig. 6B). Overall, these results show that MFN2 KD cells had lower cytosolic and ER  $\text{Ca}^{2+}$  concentrations.

Disruption of ER  $\text{Ca}^{2+}$  homeostasis is linked to ER stress responses (54), so we evaluated the expression levels of ER stress markers 78 kDa glucose-regulated protein [an ER chaperone also known as BiP (55)], activating transcription factor 4, and C/EBP homologous protein [transcription factors that induce protein synthesis in the unfolded protein response (56)] in our cells (Fig. 6C) as a second indication of a disruption in ER  $\text{Ca}^{2+}$  homeostasis. We found that the mRNA expression of all 3 proteins was strongly up-regulated in MFN2 KD cells compared with control or DRP1 DN cells, indicating that the low basal and ER  $\text{Ca}^{2+}$  levels in MFN2 KD cells were accompanied by ER stress.

Because ER calcium stores appeared depleted in MFN2 KD cells, we additionally evaluated SOCE, or the capacity to activate  $\text{Ca}^{2+}$  influx into the cell from the extracellular environment as a mechanism to compensate the emptying of intracellular  $\text{Ca}^{2+}$  stores (57). SOCE is known to be regulated by mitochondria through mechanisms that involve active mitochondrial  $\text{Ca}^{2+}$  uptake and release (58–60). We measured SOCE in our cells by re-adding extracellular  $\text{Ca}^{2+}$  to cells preincubated in  $\text{Ca}^{2+}$ -free medium and in which ER stores had been previously depleted by thapsigargin, as shown in Fig. 6A. This promoted a rapid re-entry of the ion into the cytosol, increasing Fura-2 fluorescence ratios (Fig. 6D). We found that uptake of SOCE into MFN2 KD cells was impaired, reaching lower maximal calcium when compared with control cells (Fig. 6E) and occurring at slower rates (Fig. 6F). This result is compatible with the depletion of ER  $\text{Ca}^{2+}$  stores we found previously. DRP1 DN cells, on the other hand, displayed maximal calcium replenishment similar to control cells (Fig. 6E) but at significantly faster rates (~30% faster, Fig. 6F). Taken together, these experiments demonstrate that regulating mitochondrial morphology has an expressive impact on different aspects of cellular physiologic  $\text{Ca}^{2+}$  handling.

## DISCUSSION

We demonstrate here that inducing moderate changes in the morphology of the mitochondrial network, promoting either fission or fusion (Fig. 1), alters mitochondrial  $\text{Ca}^{2+}$  uptake and retention properties as well as cellular  $\text{Ca}^{2+}$  homeostasis and ER stress. Specifically, promoting mitochondrial fission through MFN2 KD enhances mitochondrial permeability transition (Fig. 2), possibly because of its effects of decreasing  $\Delta\Psi$  (Fig. 5), a known inducer of this process [see Arruda *et al.* (21) for a comprehensive review]. MFN2 KD also significantly changes mitochondrial  $\text{Ca}^{2+}$  homeostasis; it decreases both  $\text{Ca}^{2+}$  uptake rates and  $\text{Ca}^{2+}$  retention capacity in mitochondria (Fig. 2). Additionally, MFN2 KD has effects on cellular ion homeostasis, as it lowers basal  $\text{Ca}^{2+}$  levels and ER  $\text{Ca}^{2+}$  stores, activates ER stress and hampers SOCE after intracellular  $\text{Ca}^{2+}$  store depletion (Fig. 6). Although these last effects, seen in intact

cells, may be related to MFN2's properties in mediating the interaction between mitochondria and the ER (5, 10, 61, 62), it is important to note that mitochondrial  $\text{Ca}^{2+}$  uptake assays conducted in permeabilized cells are independent of these interactions because  $\text{Ca}^{2+}$  is added directly to the extramitochondrial microenvironment and uptake by the ER is not quantitatively relevant (Fig. 2B, D, E).

The changes observed were independent of alterations in MCU expression (Fig. 3), a result compatible with the finding that changes in MCU expression occur in cells derived from MFN2 knockout animals, but were not found in acute MFN2 knockdown cells such as our model (61). Interestingly, the Scorrano group (10, 62) has found that MFN2 knockout cells have higher ER calcium stores and higher mitochondrial  $\text{Ca}^{2+}$  uptake, although this was not consistently observed in other studies (61). The reasons for these differences may be the use of distinct cell types, the levels of MFN2 depletion (which in our case were <50%), and the fact that their cells were derived from knockout animals, which were found to have changes in MCU (61). Finally, it should be noted that these prior studies measured intramitochondrial calcium concentrations (10, 61, 62) but not uptake rates or total uptake capacity in mitochondria. Because mitochondrial volumes change in MFN2 KD cells, uptake rate and capacity can change despite equal intramitochondrial  $\text{Ca}^{2+}$  concentrations. Indeed, we suggest that the changes in mitochondrial  $\text{Ca}^{2+}$  homeostasis observed here are related to changes in mitochondrial matrix volumes, as supported by experiments promoting mitochondrial fusion.

Mitochondrial fusion in DRP1 DN cells (Fig. 2) or M1-treated (fission-inhibited) cells (Fig. 4) significantly enhances both mitochondrial  $\text{Ca}^{2+}$  uptake capacity and rates in a manner independent of changes in  $\Delta\Psi$  (Fig. 5). Although mitochondrial permeability transition may be responsible for the increments in uptake rates in DRP1 DN cells relative to control cells (uptake rates are equal in these cells in the presence of CsA, Fig. 2E), it does not account for enhanced  $\text{Ca}^{2+}$  uptake capacity, which remains higher in more fused mitochondria even in the presence of a permeability transition inhibitor (Fig. 2D). Indeed, enhanced  $\text{Ca}^{2+}$  uptake is probably attributable to mitochondrial morphologic changes themselves because these modify organellar matrix capacity, which is where the ions accumulate. Demonstrating that mitochondrial fusion also impacts cellular  $\text{Ca}^{2+}$  physiology, DRP1 DN cells had similar basal  $\text{Ca}^{2+}$  levels and ER  $\text{Ca}^{2+}$  stores but displayed enhanced SOCE rates relative to control cells (Fig. 6D, F). Consistently, data published during the revision process of this manuscript (63) showed that a muscle-specific DRP1 knockout mouse displayed unchanged ER calcium stores but increased mitochondrial  $\text{Ca}^{2+}$  uptake, although in this model, DRP1 disruption was accompanied by increased MCU expression.

This finding complements prior work showing that mitochondrial function, and specifically  $\text{Ca}^{2+}$  uptake and release, is determinant in SOCE-mediated cellular  $\text{Ca}^{2+}$  store replenishing (58, 59). Importantly, it suggests that mitochondrial morphology may be an important physiologic regulator of SOCE, which was, to date, related to mitochondrial function through the use of nonphysiologic

stimuli, such as uncouplers or direct inhibition of  $\text{Ca}^{2+}$  uptake and release pathways in these organelles (58–60). Interestingly, there is also evidence that the location of mitochondria near plasma membrane  $\text{Ca}^{2+}$  entry sites can be important in SOCE (64), a result compatible with our findings because the regulation of mitochondrial morphology also impacts mitochondrial transport and positioning in the cell (65).

In a more global sense, our results demonstrate a tight link between mitochondrial morphology and cellular and mitochondrial  $\text{Ca}^{2+}$  homeostasis. These findings are supported by prior experiments that indirectly suggest an association between mitochondrial morphology and  $\text{Ca}^{2+}$  uptake into the organelle. For example, Szabadkai *et al.* (66) showed that DRP1-mediated mitochondrial fission disrupted mitochondrial networks and impacted on intra-organelle calcium wave propagation, indicating a role for mitochondrial plasticity in cell-wide mitochondrial  $\text{Ca}^{2+}$  dissemination. Additionally, Lewis *et al.* (67) recently found that MFF-mediated mitochondrial fission changed axonal  $\text{Ca}^{2+}$  homeostasis and impacted synaptic function due to changes in mitochondrial  $\text{Ca}^{2+}$  uptake, connecting this effect to mitochondrial mass in the axon. Both results can also be explained by a decrease in mitochondrial  $\text{Ca}^{2+}$  uptake rates and capacity secondary to mitochondrial fission, as seen in our present study. Our results are also in line with the work of Sebastián *et al.* (68), who found that MFN2 knockout mice presented elevated levels of ER stress markers, similar to our findings in MFN2 KD cells, although the authors did not connect these findings to  $\text{Ca}^{2+}$  changes.

Many central important biologic events involve simultaneous changes in mitochondrial morphology and in  $\text{Ca}^{2+}$  homeostasis, including immune activation (69, 70), differentiation (12, 71), insulin secretion (72, 73), and fatty acid metabolism (9, 74, 75), among others. It is tempting to speculate that at least part of the regulatory mechanisms in these processes involve changes in mitochondrial and cellular  $\text{Ca}^{2+}$  homeostasis promoted by the modulation of mitochondrial morphology we describe here. **[FJ]**

## ACKNOWLEDGMENTS

The authors acknowledge Edson Alves Gomes and Camille Caldeira da Silva (both from Universidade de São Paulo) for their outstanding technical support. This work was funded by Fundação de Amparo à Pesquisa do Estado de São Paulo (FAPESP) CEPID Grants 2014-10492-0 and 2013/07937-8, CAPES (Coordenação de Aperfeiçoamento de Pessoal de Nível Superior Finance Code 001), Conselho Nacional de Pesquisa e Desenvolvimento (CNPq), the U.S. National Institutes of Health (NIH)/National Institute of Diabetes and Digestive and Kidney Diseases (NIDDK) Grants R01DK099618-02 and R01DK56690, University of California, Los Angeles (UCLA) Department of Medicine Chair commitment and University of California, San Diego (UCSD)/UCLA Diabetes Research Center pilot grant, and NIH/NIDDK P30 DK063491. The funders had no role in study design, data collection and analysis, decision to publish, or preparation of the manuscript. P.N. is supported by São Paulo Research Foundation (FAPESP) Fellowship 2014/24511-7. S.L.M.-F. was a CAPES Ph.D. fellowship recipient. J.V.C.-C. is supported by

FAPESP Grant 2017/14713-0. P.A. is supported by FAPESP Grant 2016/18633-8. The authors declare no conflicts of interest.

## AUTHOR CONTRIBUTIONS

A. J. Kowaltowski designed the research, performed the research, contributed new reagents or analytic tools, analyzed data, and wrote the paper; S. L. Menezes-Filho designed the research, performed the research, contributed new reagents or analytic tools, and analyzed data; E. A. Assali performed the research; J. V. Cabral-Costa performed research and analyzed data; P. Abreu performed the research and analyzed data; I.G.G. performed research and analyzed data; N. Miller analyzed the data and contributed new analytic tools; P. Nolasco, F. R. M. Laurindo, and A. Bruni-Cardoso designed the research and contributed new reagents or analytic tools; and O. Shirihai designed the research, contributed new reagents or analytic tools, and wrote the manuscript.

## REFERENCES

1. Chan, D. C. (2006) Mitochondria: dynamic organelles in disease, aging, and development. *Cell* **125**, 1241–1252
2. Westermann, B. (2010) Mitochondrial fusion and fission in cell life and death. *Nat. Rev. Mol. Cell Biol.* **11**, 872–884
3. Liesa, M., Palacín, M., and Zorzano, A. (2009) Mitochondrial dynamics in mammalian health and disease. *Physiol. Rev.* **89**, 799–845
4. Liesa, M., and Shirihai, O. S. (2013) Mitochondrial dynamics in the regulation of nutrient utilization and energy expenditure. *Cell Metab.* **17**, 491–506
5. Pernas, L., and Scorrano, L. (2016) Mito-Morphosis: mitochondrial fusion, fission, and cristae remodeling as key mediators of cellular function. *Annu. Rev. Physiol.* **78**, 505–531
6. Klecker, T., Böckler, S., and Westermann, B. (2014) Making connections: interorganelle contacts orchestrate mitochondrial behavior. *Trends Cell Biol.* **24**, 537–545
7. Stotland, A., and Gottlieb, R. A. (2015) Mitochondrial quality control: easy come, easy go. *Biochim. Biophys. Acta* **1853**, 2802–2811
8. Valm, A. M., Cohen, S., Legant, W. R., Melunis, J., Hershberg, U., Wait, E., Cohen, A. R., Davidson, M. W., Betzig, E., and Lippincott-Schwartz, J. (2017) Applying systems-level spectral imaging and analysis to reveal the organelle interactome. *Nature* **546**, 162–167
9. Benador, I. Y., Veliova, M., Liesa, M., and Shirihai, O. S. (2019) Mitochondria bound to lipid droplets: where mitochondrial dynamics regulate lipid storage and utilization. *Cell Metab.* **29**, 827–835
10. De Brito, O. M., and Scorrano, L. (2008) Mitofusin 2 tethers endoplasmic reticulum to mitochondria. *Nature* **456**, 605–610; erratum: 513, 266
11. Chen, Y., and Dorn, G. W. II (2013) PINK1-phosphorylated mitofusin 2 is a Parkin receptor for culling damaged mitochondria. *Science* **340**, 471–475
12. Forni, M. F., Peloggia, J., Trudeau, K., Shirihai, O., and Kowaltowski, A. J. (2016) Murine mesenchymal stem cell commitment to differentiation is regulated by mitochondrial dynamics. *Stem Cells* **34**, 743–755
13. Friedman, J. R., Lackner, L. L., West, M., DiBenedetto, J. R., Nunnari, J., and Voeltz, G. K. (2011) ER tubules mark sites of mitochondrial division. *Science* **334**, 358–362
14. Chakrabarti, R., Ji, W. K., Stan, R. V., de Juan Sanz, J., Ryan, T. A., and Higgs, H. N. (2018) INF2-mediated actin polymerization at the ER stimulates mitochondrial calcium uptake, inner membrane constriction, and division. *J. Cell Biol.* **217**, 251–268
15. Rizzuto, R., Pinton, P., Carrington, W., Fay, F. S., Fogarty, K. E., Lifshitz, L. M., Tuft, R. A., and Pozzan, T. (1998) Close contacts with the endoplasmic reticulum as determinants of mitochondrial  $\text{Ca}^{2+}$  responses. *Science* **280**, 1763–1766
16. Csordás, G., Renken, C., Várnai, P., Walter, L., Weaver, D., Buttle, K. F., Balla, T., Mannella, C. A., and Hajnóczky, G. (2006) Structural



- and functional features and significance of the physical linkage between ER and mitochondria. *J. Cell Biol.* **174**, 915–921
17. Jackson, J. G., and Robinson, M. B. (2015) Reciprocal regulation of mitochondrial dynamics and calcium signaling in astrocyte processes. *J. Neurosci.* **35**, 15199–15213
  18. Wu, H., Carvalho, P., and Voeltz, G. K. (2018) Here, there, and everywhere: the importance of ER membrane contact sites. *Science* **361**, eaan5835
  19. Clapham, D. E. (2007) Calcium signaling. *Cell* **131**, 1047–1058
  20. Gunter, T. E., and Sheu, S. S. (2009) Characteristics and possible functions of mitochondrial  $\text{Ca}^{2+}$  transport mechanisms. *Biochim. Biophys. Acta* **1787**, 1291–1308
  21. Vercesi, A. E., Castilho, R. F., Kowaltowski, A. J., de Oliveira, H. C. F., de Souza-Pinto, N. C., Figueira, T. R., and Busanello, E. N. B. (2018) Mitochondrial calcium transport and the redox nature of the calcium-induced membrane permeability transition. *Free Radic. Biol. Med.* **129**, 1–24
  22. Arruda, A. P., Pers, B. M., Parlakgöl, G., Güney, E., Inouye, K., and Hotamisligil, G. S. (2014) Chronic enrichment of hepatic endoplasmic reticulum-mitochondria contact leads to mitochondrial dysfunction in obesity. *Nat. Med.* **20**, 1427–1435
  23. Arruda, A. P., and Hotamisligil, G. S. (2015) Calcium homeostasis and organelle function in the pathogenesis of obesity and diabetes. *Cell Metab.* **22**, 381–397
  24. Baughman, J. M., Perocchi, F., Girgis, H. S., Plovanich, M., Belcher-Timme, C. A., Sancak, Y., Bao, X. R., Strittmatter, L., Goldberger, O., Bogorad, R. L., Kotliansky, V., and Mootha, V. K. (2011) Integrative genomics identifies MCU as an essential component of the mitochondrial calcium uniporter. *Nature* **476**, 341–345
  25. Duchen, M. R. (2000) Mitochondria and calcium: from cell signalling to cell death. *J. Physiol.* **529**, 57–68
  26. Brookes, P. S., Yoon, Y., Robotham, J. L., Anders, M. W., and Sheu, S. S. (2004) Calcium, ATP, and ROS: a mitochondrial love-hate triangle. *Am. J. Physiol. Cell Physiol.* **287**, C817–C833
  27. Murphy, E., and Steenbergen, C. (2008) Mechanisms underlying acute protection from cardiac ischemia-reperfusion injury. *Physiol. Rev.* **88**, 581–609
  28. Nicholls, D. G. (2009) Mitochondrial calcium function and dysfunction in the central nervous system. *Biochim. Biophys. Acta* **1787**, 1416–1424
  29. Figueira, T. R., Barros, M. H., Camargo, A. A., Castilho, R. F., Ferreira, J. C., Kowaltowski, A. J., Sluse, F. E., Souza-Pinto, N. C., and Vercesi, A. E. (2013) Mitochondria as a source of reactive oxygen and nitrogen species: from molecular mechanisms to human health. *Antioxid. Redox Signal.* **18**, 2029–2074
  30. Biasutto, L., Azzolini, M., Szabò, I., and Zoratti, M. (2016) The mitochondrial permeability transition pore in AD 2016: an update. *Biochim. Biophys. Acta* **1863**, 2515–2530
  31. Amigo, I., Menezes-Filho, S. L., Luévano-Martínez, L. A., Chausse, B., and Kowaltowski, A. J. (2017) Caloric restriction increases brain mitochondrial calcium retention capacity and protects against excitotoxicity. *Aging Cell* **16**, 73–81
  32. Menezes-Filho, S. L., Amigo, I., Prado, F. M., Ferreira, N. C., Koike, M. K., Pinto, I. F. D., Miyamoto, S., Montero, E. F. S., Medeiros, M. H. G., and Kowaltowski, A. J. (2017) Caloric restriction protects livers from ischemia/reperfusion damage by preventing  $\text{Ca}^{2+}$ -induced mitochondrial permeability transition. *Free Radic. Biol. Med.* **110**, 219–227
  33. Menezes-Filho, S. L., Amigo, I., Luévano-Martínez, L. A., and Kowaltowski, A. J. (2019) Fasting promotes functional changes in liver mitochondria. *Biochim. Biophys. Acta Bioenerg.* **1860**, 129–135
  34. Rambold, A. S., Cohen, S., and Lippincott-Schwartz, J. (2015) Fatty acid trafficking in starved cells: regulation by lipid droplet lipolysis, autophagy, and mitochondrial fusion dynamics. *Dev. Cell* **32**, 678–692
  35. Khraiwesh, H., López-Domínguez, J. A., Fernández del Río, L., Gutiérrez-Casado, E., López-Lluch, G., Navas, P., de Cabo, R., Ramsey, J. J., Burón, M. I., Villalba, J. M., and González-Reyes, J. A. (2014) Mitochondrial ultrastructure and markers of dynamics in hepatocytes from aged, calorie restricted mice fed with different dietary fats. *Exp. Gerontol.* **56**, 77–88
  36. Cerqueira, F. M., Chausse, B., Baranovski, B. M., Liesa, M., Lewis, E. C., Shirihai, O. S., and Kowaltowski, A. J. (2016) Diluted serum from calorie-restricted animals promotes mitochondrial  $\beta$ -cell adaptations and protect against glucolipotoxicity. *FEBS J.* **283**, 822–833
  37. Molina, A. J., Wikstrom, J. D., Stiles, L., Las, G., Mohamed, H., Elorza, A., Walzer, G., Twig, G., Katz, S., Corkey, B. E., and Shirihai, O. S. (2009) Mitochondrial networking protects beta-cells from nutrient-induced apoptosis. *Diabetes* **58**, 2303–2315
  38. Alsabeeh, N., Chausse, B., Kakimoto, P. A., Kowaltowski, A. J., and Shirihai, O. (2018) Cell culture models of fatty acid overload: problems and solutions. *Biochim. Biophys. Acta Mol. Cell Biol. Lipids* **1863**, 143–151
  39. Kowaltowski, A. J., Cosso, R. G., Campos, C. B., and Fiskum, G. (2002) Effect of Bcl-2 overexpression on mitochondrial structure and function. *J. Biol. Chem.* **277**, 42802–42807
  40. Bambrick, L. L., Chandrasekaran, K., Mehrabian, Z., Wright, C., Krueger, B. K., and Fiskum, G. (2006) Cyclosporin A increases mitochondrial calcium uptake capacity in cortical astrocytes but not cerebellar granule neurons. *J. Bioenerg. Biomembr.* **38**, 43–47
  41. Arruda, A. P., Pers, B. M., Parlakgöl, G., Güney, E., Goh, T., Cagampan, E., Lee, G. Y., Goncalves, R. L., and Hotamisligil, G. S. (2017) Defective STIM-mediated store operated  $\text{Ca}^{2+}$  entry in hepatocytes leads to metabolic dysfunction in obesity. *eLife* **6**, e29968
  42. Nicot, N., Hausman, J. F., Hoffmann, L., and Evers, D. (2005) Housekeeping gene selection for real-time RT-PCR normalization in potato during biotic and abiotic stress. *J. Exp. Bot.* **56**, 2907–2914
  43. Wang, D., Wang, J., Bonamy, G. M., Meeusen, S., Brusch, R. G., Turk, C., Yang, P., and Schultz, P. G. (2012) A small molecule promotes mitochondrial fusion in mammalian cells. *Angew. Chem. Int. Ed. Engl.* **51**, 9302–9305
  44. Wikstrom, J. D., Sereda, S. B., Stiles, L., Elorza, A., Allister, E. M., Neilson, A., Ferrick, D. A., Wheeler, M. B., and Shirihai, O. S. (2012) A novel high-throughput assay for islet respiration reveals uncoupling of rodent and human islets. *PLoS One* **7**, e33023; erratum: 8
  45. Sin, J., Andres, A. M., Taylor, D. J., Weston, T., Hiraumi, Y., Stotland, A., Kim, B. J., Huang, C., Doran, K. S., and Gottlieb, R. A. (2016) Mitophagy is required for mitochondrial biogenesis and myogenic differentiation of C2C12 myoblasts. *Autophagy* **12**, 369–380
  46. Valente, A. J., Maddalena, L. A., Robb, E. L., Moradi, F., and Stuart, J. A. (2017) A simple ImageJ macro tool for analyzing mitochondrial network morphology in mammalian cell culture. *Acta Histochem.* **119**, 315–326
  47. Gutierrez-Martín, Y., Martín-Romero, F. J., and Henao, F. (2005) Store-operated calcium entry in differentiated C2C12 skeletal muscle cells. *Biochim. Biophys. Acta* **1711**, 33–40
  48. Fiskum, G., Craig, S. W., Decker, G. L., and Lehninger, A. L. (1980) The cytoskeleton of digitonin-treated rat hepatocytes. *Proc. Natl. Acad. Sci. USA* **77**, 3430–3434
  49. Cassidy-Stone, A., Chipuk, J. E., Ingerman, E., Song, C., Yoo, C., Kuwana, T., Kurth, M. J., Shaw, J. T., Hinshaw, J. E., Green, D. R., and Nunnari, J. (2008) Chemical inhibition of the mitochondrial division dynamin reveals its role in Bax/Bak-dependent mitochondrial outer membrane permeabilization. *Dev. Cell* **14**, 193–204
  50. Bordt, E. A., Clerc, P., Roelofs, B. A., Saladino, A. J., Tretter, L., Adam-Vizi, V., Cherek, E., Khalil, A., Yadava, N., Ge, S. X., Francis, T. C., Kennedy, N. W., Picton, L. K., Kumar, T., Uppuluri, S., Miller, A. M., Itoh, K., Karbowski, M., Sesaki, H., Hill, R. B., and Polster, B. M. (2017) The putative Drp1 inhibitor mdv1-1 is a reversible mitochondrial complex I inhibitor that modulates reactive oxygen species. *Dev. Cell* **40**, 583–594.e6
  51. Palty, R., and Sekler, I. (2012) The mitochondrial  $\text{Na}^{+}/\text{Ca}^{2+}$  exchanger. *Cell Calcium* **52**, 9–15
  52. Akerman, K. E., and Wikström, M. K. (1976) Safranin as a probe of the mitochondrial membrane potential. *FEBS Lett.* **68**, 191–197
  53. Kowaltowski, A. J. (2019) Strategies to detect mitochondrial oxidants. *Redox Biol.* **21**, 101065
  54. Krebs, J., Agellon, L. B., and Michalak, M. (2015)  $\text{Ca}^{2+}$  homeostasis and endoplasmic reticulum (ER) stress: an integrated view of calcium signaling. *Biochem. Biophys. Res. Commun.* **460**, 114–121
  55. Lee, A. S. (2005) The ER chaperone and signaling regulator GRP78/BiP as a monitor of endoplasmic reticulum stress. *Methods* **35**, 373–381
  56. Han, J., Back, S. H., Hur, J., Lin, Y. H., Gildersleeve, R., Shan, J., Yuan, C. L., Krokowski, D., Wang, S., Hatzoglou, M., Kilberg, M. S., Sartor, M. A., and Kaufman, R. J. (2013) ER-stress-induced transcriptional regulation increases protein synthesis leading to cell death. *Nat. Cell Biol.* **15**, 481–490
  57. Parekh, A. B., and Putney, J. W., Jr. (2005) Store-operated calcium channels. *Physiol. Rev.* **85**, 757–810
  58. Malli, R., and Graier, W. F. (2017) The role of mitochondria in the activation/maintenance of SOCE: the contribution of mitochondrial  $\text{Ca}^{2+}$  uptake, mitochondrial motility, and location to store-operated  $\text{Ca}^{2+}$  entry. *Adv. Exp. Med. Biol.* **993**, 297–319

59. Spät, A., and Szanda, G. (2017) The role of mitochondria in the activation/maintenance of SOCE: store-operated  $\text{Ca}^{2+}$  entry and mitochondria. *Adv. Exp. Med. Biol.* **993**, 257–275
60. Ben-Kasus Nissim, T., Zhang, X., Elazar, A., Roy, S., Stolwijk, J. A., Zhou, Y., Motiani, R. K., Gueguinou, M., Hempel, N., Hershinkel, M., Gill, D. L., Trebak, M., and Sekler, I. (2017) Mitochondria control store-operated  $\text{Ca}^{2+}$  entry through  $\text{Na}^+$  and redox signals. *EMBO J.* **36**, 797–815
61. Filadi, R., Greotti, E., Turacchio, G., Luini, A., Pozzan, T., and Pizzo, P. (2015) Mitofusin 2 ablation increases endoplasmic reticulum-mitochondria coupling. *Proc. Natl. Acad. Sci. USA* **112**, E2174–E2181
62. Naon, D., Zaninello, M., Giacomello, M., Varanita, T., Grespi, F., Lakshminarayanan, S., Serafini, A., Semenzato, M., Herkenne, S., Hernández-Alvarez, M. I., Zorzano, A., De Stefani, D., Dorn II, G. W., and Scorrano, L. (2016) Critical reappraisal confirms that mitofusin 2 is an endoplasmic reticulum-mitochondria tether. *Proc. Natl. Acad. Sci. USA* **113**, 11249–11254
63. Favaro, G., Romanello, V., Varanita, T., Andrea Desbats, M., Morbidoni, V., Tezze, C., Albiero, M., Canato, M., Gherardi, G., De Stefani, D., Mammucari, C., Blaauw, B., Boncompagni, S., Protasi, F., Reggiani, C., Scorrano, L., Salviati, L., and Sandri, M. (2019) DRP1-mediated mitochondrial shape controls calcium homeostasis and muscle mass. *Nat. Commun.* **10**, 2576
64. Fonteriz, R., Matesanz-Isabel, J., Arias-Del-Val, J., Alvarez-Illera, P., Montero, M., and Alvarez, J. (2016) Modulation of calcium entry by mitochondria. *Adv. Exp. Med. Biol.* **898**, 405–421
65. Anestî, V., and Scorrano, L. (2006) The relationship between mitochondrial shape and function and the cytoskeleton. *Biochim. Biophys. Acta* **1757**, 692–699
66. Szabadkai, G., Simoni, A. M., Chami, M., Wieckowski, M. R., Youle, R. J., and Rizzuto, R. (2004) Drp-1-dependent division of the mitochondrial network blocks intraorganellar  $\text{Ca}^{2+}$  waves and protects against  $\text{Ca}^{2+}$ -mediated apoptosis. *Mol. Cell* **16**, 59–68
67. Lewis, T. L., Jr., Kwon, S. K., Lee, A., Shaw, R., and Polleux, F. (2018) MFF-dependent mitochondrial fission regulates presynaptic release and axon branching by limiting axonal mitochondria size. *Nat. Commun.* **9**, 5008
68. Sebastián, D., Hernández-Alvarez, M. I., Segalés, J., Sorianello, E., Muñoz, J. P., Sala, D., Waget, A., Liesa, M., Paz, J. C., Gopalacharyulu, P., Orešič, M., Pich, S., Burcelin, R., Palacín, M., and Zorzano, A. (2012) Mitofusin 2 (Mfn2) links mitochondrial and endoplasmic reticulum function with insulin signaling and is essential for normal glucose homeostasis. *Proc. Natl. Acad. Sci. USA* **109**, 5523–5528
69. Vig, M., and Kinet, J. P. (2009) Calcium signaling in immune cells. *Nat. Immunol.* **10**, 21–27; erratum: 223
70. Baïxauli, F., Martín-Cófreces, N. B., Morlino, G., Carrasco, Y. R., Calabia-Linares, C., Veiga, E., Serrador, J. M., and Sánchez-Madrid, F. (2011) The mitochondrial fission factor dynamin-related protein 1 modulates T-cell receptor signalling at the immune synapse. *EMBO J.* **30**, 1238–1250
71. Tonelli, F. M., Santos, A. K., Gomes, D. A., da Silva, S. L., Gomes, K. N., Ladeira, L. O., and Resende, R. R. (2012) Stem cells and calcium signaling. *Adv. Exp. Med. Biol.* **740**, 891–916
72. Flatt, P. R., Boquist, L., and Hellman, B. (1980) Calcium and pancreatic beta-cell function. The mechanism of insulin secretion studied with the aid of lanthanum. *Biochem. J.* **190**, 361–372
73. Stiles, L., and Shirihai, O. S. (2012) Mitochondrial dynamics and morphology in beta-cells. *Best Pract. Res. Clin. Endocrinol. Metab.* **26**, 725–738
74. Otto, D. A., and Ontko, J. A. (1978) Activation of mitochondrial fatty acid oxidation by calcium. Conversion to the energized state. *J. Biol. Chem.* **253**, 789–799
75. Rambold, A. S., Kostecky, B., Elia, N., and Lippincott-Schwartz, J. (2011) Tubular network formation protects mitochondria from autophagosomal degradation during nutrient starvation. *Proc. Natl. Acad. Sci. USA* **108**, 10190–10195

Received for publication May 3, 2019.  
Accepted for publication July 16, 2019.

## **ANNEX C**

**Pereira et al., 2021**

**(J. Bioenerg. Biomembr., 53:109–18)**



# Changes in mitochondrial morphology modulate LPS-induced loss of calcium homeostasis in BV-2 microglial cells

O. R. Pereira Jr<sup>1</sup> · V. M. Ramos<sup>1</sup> · J. V. Cabral-Costa<sup>1</sup> · A. J. Kowaltowski<sup>1</sup>

Received: 9 September 2020 / Accepted: 5 February 2021 / Published online: 14 February 2021  
© The Author(s), under exclusive licence to Springer Science+Business Media, LLC part of Springer Nature 2021

## Abstract

Microglial activation involves both fragmentation of the mitochondrial network and changes in cellular Ca<sup>2+</sup> homeostasis, but possible modifications in mitochondrial calcium uptake have never been described in this context. Here we report that activated microglial BV-2 cells have impaired mitochondrial calcium uptake, including lower calcium retention capacity and calcium uptake rates. These changes were not dependent on altered expression of the mitochondrial calcium uniporter. Respiratory capacity and the inner membrane potential, key determinants of mitochondrial calcium uptake, are both decreased in activated microglial BV-2 cells. Modified mitochondrial calcium uptake correlates with impaired cellular calcium signaling, including reduced ER calcium stores, and decreased replenishment by store operated calcium entry (SOCE). Induction of mitochondrial fragmentation through Mfn2 knockdown in control cells mimicked this effect, while inhibiting LPS-induced mitochondrial fragmentation by a dominant negative form of Drp1 prevented it. Overall, our results show that mitochondrial fragmentation induced by LPS promotes altered Ca<sup>2+</sup> homeostasis in microglial cells, a new aspect of microglial activation that could be a key feature in the inflammatory role of these cells.

**Keywords** Calcium handling · Mitochondrial morphology · Metabolism · Inflammation

## Introduction

Central nervous system (CNS) physiology relies on an interchange between different cell types maintaining and regulating the function of neuronal and glial cells. Because of the endothelial blood-brain barrier and blood-cerebrospinal fluid barrier, which separate brain cells from the constantly changing conditions of blood stream (Engelhardt and Sorokin 2009), immune cells have restricted access to the CNS. Immune responses, such as cell corpse phagocytosis and infection control, are therefore performed by microglia, immune cells that reside in

the brain (Hanisch and Kettenmann 2007; Salter and Stevens 2017). Microglia monitor molecular signals related to damage or infection (Hines et al. 2009), and respond by reprogramming their gene expression and inducing extensive changes in their phenotype, a process called microglial activation (Dheen et al. 2007; Allen and Barres 2009; Salter and Stevens 2017). This activation includes an increase in nitric oxide production (Park et al. 2013), metabolic reprogramming (Chausse et al. 2019), changes in cellular calcium handling systems (Hoffmann et al. 2003; Heo et al. 2015), and fragmentation of the mitochondrial network (Park et al. 2013, 2016).

Mitochondria are dynamic organelles, and can undergo fusion and fission, generating either larger more tubular or smaller and rounded mitochondria, respectively. These processes are regulated, and many biological phenomena involve changes in the proportion of each type of morphology (Pernas and Scorrano 2016). Additionally, many biological responses, including metabolic shifts and immune activation, can be modulated by changing mitochondrial morphology (Forni et al. 2016; Gao et al. 2017; Wang et al. 2017; Nair et al. 2019), demonstrating that organellar plasticity is involved in cell signaling.

Recently, genetic manipulation of mitochondrial dynamics was shown to have direct consequences on mitochondrial

✉ J. V. Cabral-Costa  
joao.victor.costa@usp.br

✉ A. J. Kowaltowski  
alicia@iq.usp.br

O. R. Pereira, Jr  
osvaldo.pereira@usp.br

V. M. Ramos  
ramosvm@usp.br

<sup>1</sup> Departamento de Bioquímica, Instituto de Química, Universidade de São Paulo, Av. Prof. Lineu Prestes, 748, São Paulo, SP 05508-000, Brazil

calcium uptake (Kowaltowski et al. 2019). The entry of calcium ions into the mitochondrial matrix through a complex formed by the pore-forming mitochondrial calcium uniporter (MCU) protein, driven by the mitochondrial inner membrane potential ( $\Delta\psi_m$ ) (Baughman et al. 2011; De Stefani et al. 2011), is an organellar function of utmost importance, involved in the regulation of cytosolic calcium as well as endoplasmic reticulum (ER) calcium homeostasis (Rizzuto et al. 2012). Indeed, as observed in C2C12 myoblast cells, down-regulation of mitofusin-2 (Mfn2), a key protein in the process of mitochondrial fusion, promotes mitochondrial fragmentation and impairment in mitochondrial calcium uptake. Mfn2 knockdown also impaired ER calcium replenishment from extracellular stores by store operated calcium entry (SOCE) (Kowaltowski et al. 2019). Conversely, increasing mitochondrial fusion promoted enhanced SOCE rates (Kowaltowski et al. 2019), demonstrating that mitochondrial morphology is determinant in cellular calcium homeostasis.

Although mitochondrial morphology has been correlated to mitochondrial calcium uptake and microglial activation is known to promote mitochondrial fragmentation, the implications of mitochondrial calcium handling on microglial activation are still not understood. Here, we show that mitochondrial calcium uptake is impaired in activated microglia, impacting on cellular calcium homeostasis and calcium signaling in these cells, in a manner influenced by mitochondrial morphology.

## Material and methods

### Cell cultures, LPS treatment and viral infection

BV-2 cells (ICLC Cat# ATL03001, RRID:CVCL\_0182) were cultivated in DMEM (25 mM glucose, 1 mM pyruvate and 2 mM glutamine; 12800, Thermo Fisher Scientific, USA) supplemented with 10% fetal bovine serum, 100 U/ml penicillin and 1000 mg/ml streptomycin, and kept in 37 °C incubators with 5% CO<sub>2</sub>. Cells were plated on poly-L-Lys-covered P100 plates and, 24 h after seeding, media was changed for DMEM without FBS for lipopolysaccharide (LPS) treatment. Cells were incubated for 24 h in FBS-free media containing freshly diluted LPS (100 ng/mL).

### Viral transduction

Mitochondrial morphology was manipulated either by promoting fusion, using an adenovirus to stimulate expression of a dominant negative (DN) form of Drp1 (DRP1DN; Welgen, Worcester, USA), or promoting fission, using a knockdown (KD) of Mfn2 (Mfn2KD; Welgen, Worcester, USA). As in Kowaltowski et al. (2019), multiplicity of infection (MOI) levels were 200 (Drp1DN) and 20 (Mfn2KD).

Cells were split 72 h prior to experiments and incubated with the adenovirus for 24 h. Media were then replaced by complete DMEM for 24 h, then replaced by FBS-free DMEM. At this time point, cells were submitted to LPS treatment.

### Nitrite measurements

NO<sup>•</sup> production was estimated by assessing nitrite secreted into the culture media through the Griess reaction (Guevara et al. 1998). 50 μL of reagent A (100 μM sulfanilamide, 5% H<sub>3</sub>PO<sub>4</sub>) were added to 50 μL of culture media from each sample and incubated for 5–10 min at room temperature, protected from light. 50 μL of 350 μM N-1-naphthylethylenediamine dihydrochloride were added, and the incubation was repeated. Absorbance was measured at 535 nm. Nitrite standard curves were used for data calibration.

### Cell permeabilization with digitonin

In order to titrate digitonin concentrations to optimize permeabilization, cells were suspended in a respiration buffer (HEPES 20 mM, KCl 125 mM, K<sub>2</sub>HPO<sub>4</sub> 2 mM, MgCl<sub>2</sub> 1 mM, EGTA 1 mM, pH = 7.2, adjusted with KOH) in the absence of substrates for mitochondrial respiration. The suspension was added to a high-resolution oxygraph (O2k, Oroboros Instruments Corp, Austria), and oxygen consumption was measured. Rotenone (1 μM), ADP (2 mM), and succinate (5 mM), an electron transport chain substrate that is impermeable to the plasma membrane, were added, followed by incremental digitonin additions, until concentrations sufficient to permeabilize the plasma membrane were achieved, promoting entrance of succinate into mitochondria, and thus increasing oxygen consumption. Using this setup, the minimal concentration of digitonin found to promote maximal respiration, 3.75 μg/mL, was determined as the optimized titer for 1 × 10<sup>6</sup> cells (Fiskum et al. 2000). This condition was used for all experiments with permeabilized cells.

### Mitochondrial membrane potentials ( $\Delta\psi_m$ ), calcium uptake and respiration

$\Delta\psi_m$  was estimated through the fluorescence of safranin O (Akerman and Wikström 1976; Kowaltowski et al. 2002). 1 × 10<sup>6</sup> cells were suspended in 2 mL experimental buffer (75 mM D-manitol, 25 mM sucrose, 5 mM KH<sub>2</sub>PO<sub>3</sub>, 20 mM Tris-HCl, 1 μM MgCl<sub>2</sub>, 100 mM KCl, 0.1% BSA, pH 7.2 adjusted with KOH) in the presence of 5 μM safranin O and permeabilized with digitonin. Fluorescence was measured in a F4500 Hitachi Fluorimeter at  $\lambda_{ex}$  = 485 nm and  $\lambda_{em}$  = 586 nm. To assess mitochondrial calcium uptake, cells were suspended and permeabilized with digitonin in experimental buffer containing 0.1 μM Calcium Green 5 N (Thermo Fisher Scientific, USA), a membrane-impermeable and fluorescent calcium

dye. Fluorescence was assessed at  $\lambda_{\text{ex}} = 506$  nm and  $\lambda_{\text{em}} = 532$  nm. 5  $\mu\text{M}$   $\text{CaCl}_2$  were added every 200 s to induce mitochondrial calcium uptake. Additions were stopped when the fluorescence decreases were no longer observed, indicating exhaustion of uptake capacity. Mitochondrial respiration was assessed in a high-resolution oxygraph chamber (O2k, Oroboros Instruments Corp, Austria). Cells were suspended in respiration buffer (20 mM HEPES, 125 mM KCl, 2 mM  $\text{K}_2\text{HPO}_4$ , 1 mM  $\text{MgCl}_2$ , 5 mM succinate, 5 mM malate, 5 mM pyruvate, 1 mM EGTA, pH 7.2 KOH) to a final concentration of  $2 \times 10^6 \times \text{mL}^{-1}$ , and permeabilized with digitonin. State 3 and 4 were induced by 3 mM ADP and 4  $\mu\text{g}/\text{mL}$  oligomycin, respectively. Respiratory control ratios (RCR) were calculated as state 3/state 4. All assays were performed at 37 °C with continuous stirring.

## Western blotting

Proteins were extracted with RIPA buffer (Thermo Fisher Scientific, USA) and concentrations were estimated using a BCA Protein Assay Kit (Thermo Fisher Scientific, USA). Lysates were diluted in Laemmli buffer to a final concentration of 0.9  $\mu\text{g}/\mu\text{L}$ , resolved by SDS-PAGE, transferred to nitrocellulose membranes, blocked, and incubated with primary anti-MCU (1:1000 1% BSA in TBST; 14,997, Cell Signaling Technology, USA) and anti- $\beta$ -actin (1:10,000 1% BSA in TBST; ab8226; Abcam, USA) antibodies, followed by secondary IRDye anti-mouse (925–32210) and anti-Rabbit (926–68071) antibodies. Images were obtained by near infrared detection in an Odyssey apparatus (Li-Cor Biosciences, Lincoln, NE, USA). Signals were quantified by densitometry using Fiji/ImageJ (Schindelin et al. 2012; Schneider et al. 2012).  $\beta$ -actin was used as loading control for normalization.

## Intracellular calcium detection

Cells were trypsinized, washed and resuspended in PBS with 2 mM EGTA and 0.5% fatty acid-free BSA containing 1  $\mu\text{M}$  of the ratiometric fluorescent dye Fura-2-AM for 30 min at room temperature. After incubation,  $5 \times 10^5$  cells were washed and resuspended in 2 mL of  $\text{Ca}^{2+}$ -free PBS. Fluorescence was assessed in a F4500 Hitachi Fluorimeter at  $\lambda_{\text{ex}} = 340$  and 380 nm and  $\lambda_{\text{em}} = 510$  nm. The basal signal was measured for 250 s, followed by addition of 5  $\mu\text{M}$  thapsigargin to exhaust ER calcium stores. After 250 s, SOCE was induced by adding 2 mM extracellular  $\text{CaCl}_2$ . Maximal and minimal fluorescence ratios were determined for each trace, by disrupting cell membranes with 1% Triton X-100 and chelating calcium with 2.5 mM EGTA, respectively. Fluorescence was converted to calcium concentrations employing the Grynkiewicz equation (Grynkiewicz et al. 1985), considering  $\text{Kd}_{\text{Fura-2}} = 225$  nM at 37 °C.

## Mitochondrial network staining and imaging

Cells were trypsinized and plated over poly-L-lysine-coated coverslips and placed on 24 well plates ( $10^4$  cells/well) 24 h before LPS treatment. After LPS treatment, 50 nM of MitoTracker Deep Red (Thermo Fisher Scientific, USA) was added to each well and incubated for 30 min at 37 °C. Media were then removed and cells were incubated for 15 min at 37 °C in 4% formaldehyde. After, cells were washed 3 times with PBS and coverslips were mounted onto glass slides using Prolong Gold mounting medium (Thermo Fisher Scientific, USA). Slides were allowed to dry overnight before imaging acquisition. Images were acquired using the Axio Imager Z2 confocal microscope from Zeiss. Presented images were processed using the Fiji software and represent a projection of 5–7 Z-axis slices using the Zproject Maximum Intensity (MAX) tool.

## Statistical analysis

All data were analyzed using GraphPad Prism 7.0 (GraphPad Software, USA) and are represented as averages  $\pm$  standard deviation. Statistical analyses were conducted through Student's t test (paired by experiment) or repeated measures two-way ANOVA (paired by experiment and sample) followed by Holm-Šidak's post-hoc test, as indicated in the figure legends. Outliers were identified through the ROUT method.

## Results

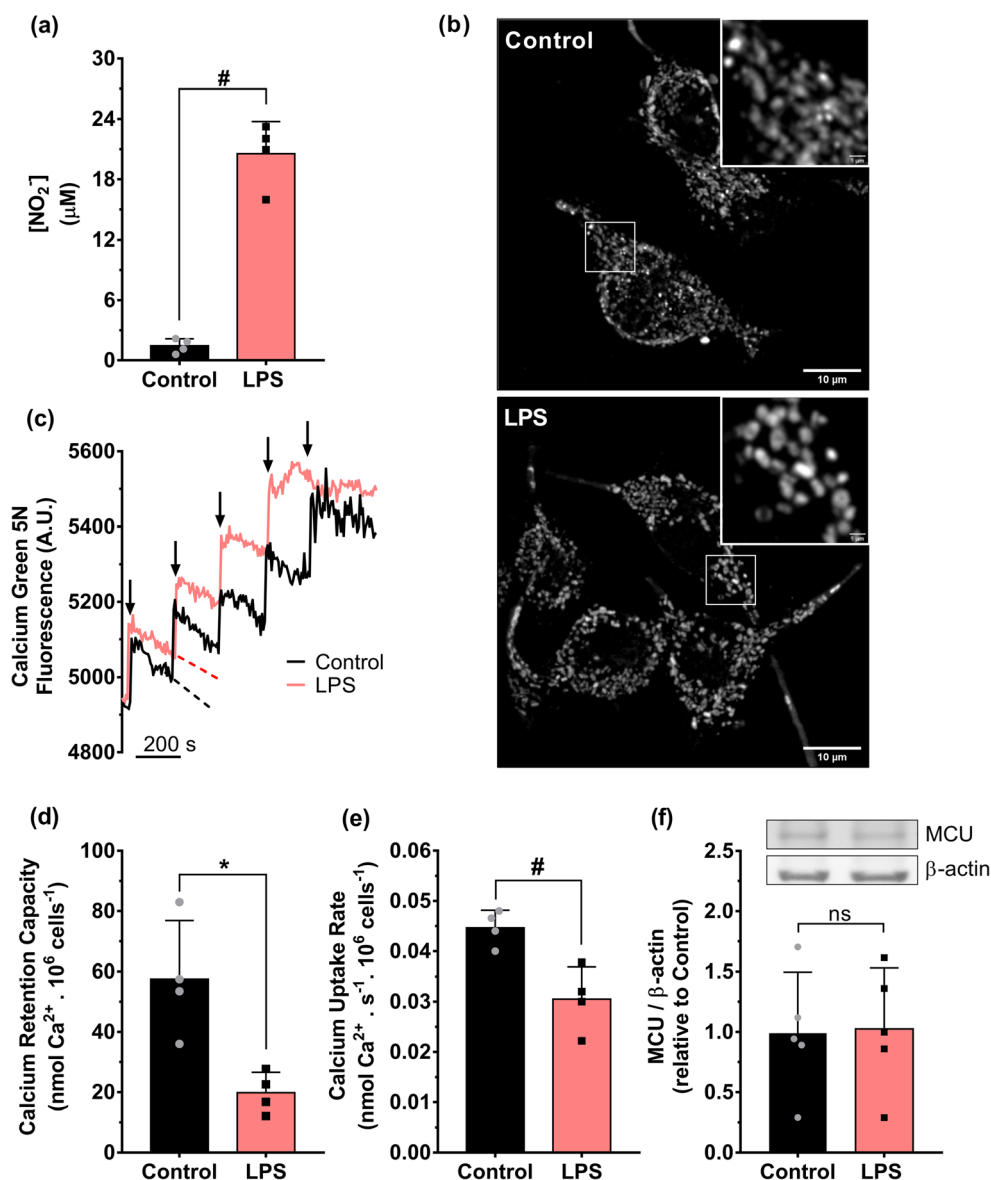
### Mitochondrial calcium uptake is decreased upon LPS activation

Our group has previously found that mitochondrial morphology can modulate organellar  $\text{Ca}^{2+}$  uptake in C2C12 myoblasts (Kowaltowski et al. 2019). In order to investigate if microglial activation, which promotes mitochondrial fragmentation (Park et al. 2013), can also modulate mitochondrial calcium uptake, we submitted microglial BV-2 cells to a classical cellular activation protocol, using LPS as an inducer of inflammatory response (Chausse et al. 2019). Microglial activation was confirmed by estimating nitric oxide production through the detection of nitrite in the culture media (Fig. 1a). LPS robustly increased this production, as expected. LPS-treated cells also showed a more punctiform mitochondrial network (Fig. 1b; Suppl. Fig. 1), consistent with an increase in mitochondrial fragmentation, in agreement with previous findings (Park et al. 2013, 2016).

Cells were then suspended and the plasma membrane was permeabilized by a titrated amount of digitonin (see materials and methods), which maintains mitochondrial integrity and cellular architecture, while allowing for the assessment of mitochondrial calcium handling (Fiskum et al. 1980). Under these conditions, extramitochondrial  $\text{Ca}^{2+}$  levels were



**Fig. 1** LPS activation of BV-2 cells induces mitochondrial network fragmentation and decreases mitochondrial calcium uptake. (a) Nitric oxide production was indirectly assessed by measuring nitrite concentrations in the culture media 24 h after incubation.  $n = 4$ , paired Student's *t* test, #  $p < 0.01$ . (b) Representative images of the mitochondrial network stained with MitoTracker; inserts show higher magnifications of indicated areas. (c–e) Mitochondrial calcium uptake was assessed in suspended and permeabilized BV-2 cells, activated by LPS for 24 h (red line), in the presence of the fluorescent probe calcium green 5 N. Successive additions of  $5 \mu\text{M Ca}^{2+}$  (c, as indicated by the arrows) were made while mitochondrial  $\text{Ca}^{2+}$  uptake, indicated by the downward curve inflection, was followed over time, until maximum uptake. LPS-activated BV-2 cells (red bars) showed decreased calcium retention capacity (panel d) and calcium uptake rates (panel e). \* $p \leq 0.05$ , Student's *t* test,  $n = 4$  independent experiments. (f) Western blots indicated no significant differences in MCU protein levels between the two groups. Student's *t* test,  $n = 5$  independent experiments



monitored using Calcium Green 5 N, a cell impermeant probe that fluoresces when bound to  $\text{Ca}^{2+}$ . Additions of  $5 \mu\text{M CaCl}_2$  were made at 200 s intervals, as indicated by arrows in Fig. 1c, inducing an immediate increase in fluorescence. This was followed by a signal decrease, attributable to mitochondrial calcium uptake (Kowaltowski et al. 2019). From this experiment, two parameters were quantified: calcium retention capacity, or the maximum amount of  $\text{Ca}^{2+}$  taken up by mitochondria (Fig. 1d), and calcium uptake rates, the velocity in which  $\text{Ca}^{2+}$  is removed from the experimental buffer after the first  $\text{Ca}^{2+}$  addition (Fig. 1e). We found that LPS-activated cells displayed a significant decrease in both parameters, showing that BV-2 activation has an impact on mitochondrial calcium uptake. This effect was not associated with differences in MCU expression, which was similar between control and LPS cells (Fig. 1f; Suppl. Fig. 2).

### Mitochondrial respiration and inner membrane potentials ( $\Delta\psi_m$ ) are impaired in LPS-activated BV-2 cells

Considering the lower efficiency in  $\text{Ca}^{2+}$  uptake by activated BV-2 mitochondria, we reasoned that respiratory function in these cells could also be impaired. Indeed, mitochondrial  $\text{Ca}^{2+}$  uptake occurs down the inner membrane potential ( $\Delta\psi_m$ ), which is generated by proton pumping by the electron transport chain (Baughman et al. 2011). We evaluated oxygen consumption in permeabilized cells using high-resolution Oroboros oxygraphy; typical traces of oxygen concentration changes over time are shown in Fig. 2a. LPS-activated cells displayed significantly decreased ADP-stimulated (state 3) respiratory rates, while oligomycin-insensitive (state 4) respiration was unaffected (quantified in Fig. 2b). Consequently, the

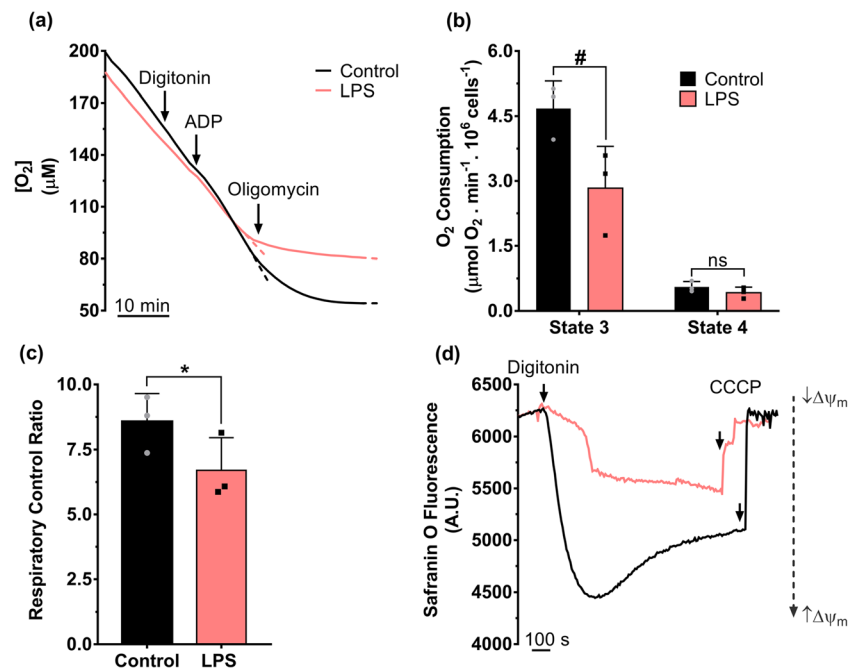


**Fig. 2** LPS-activation decreases state 3 mitochondrial respiration, coupling and membrane potentials. (a) Representative oxygen concentration traces of permeabilized BV-2 cells suspended in a high resolution oxygraph chamber with media containing malate, pyruvate, and succinate as substrates. Digitonin, ADP and oligomycin were added where indicated. (b) Quantification of ADP-stimulated (state 3) and oligomycin-

insensitive (state 4) respiration. (c) Respiratory control ratios, calculated as the ratio between states 3 and 4. (d) Mitochondrial membrane potentials ( $\Delta\psi_m$ ) were assessed through safranin O fluorescence in suspended and permeabilized cells.  $\Delta\psi_m$  is inversely correlated with the fluorescent signal. Student's t test,  $n = 3$  independent experiments,  $*p \leq 0.05$ ,  $^{\#}p \leq 0.01$ , ns = not significant

ratio between states 3 and 4, defined as the respiratory control ratio, was significantly decreased in LPS-activated cells, indicating impaired coupling between respiration and ATP synthesis (Fig. 2c). Additionally,  $\Delta\psi_m$  was remarkably reduced in LPS-activated cells, as estimated by a decrease in the uptake of the fluorescent  $\Delta\psi_m$ -sensitive probe safranin O (Fig. 2d).

### LPS treatment leads to changes in ER Ca<sup>2+</sup> signaling and SOCE in BV-2 cells

Mitochondrial calcium uptake is crucial for cellular calcium homeostasis (Rizzuto et al. 2012). Disruptions in mitochondrial calcium homeostasis can impact ER Ca<sup>2+</sup> stores (Rizzuto et al. 1998, 2012) and their replenishment by SOCE (Ben-Kasus Nissim et al. 2017; Kowaltowski et al. 2019). We thus investigated whether LPS activation could promote changes in calcium signaling in intact cells by incubating with a cell-permeant calcium probe, Fura-2-AM. Intracellular Ca<sup>2+</sup> was assessed under basal conditions, followed by induction of ER Ca<sup>2+</sup> release by thapsigargin (Lytton et al. 1991), and intracellular and ER Ca<sup>2+</sup> replenishment by extracellular Ca<sup>2+</sup> through SOCE, induced by the addition of extracellular Ca<sup>2+</sup> (Fig. 3a shows a typical trace). We observed that, although basal Ca<sup>2+</sup> levels were similar, both thapsigargin-stimulated and SOCE Ca<sup>2+</sup> levels were significantly decreased in LPS-treated cells (Fig. 3b).

### BV-2 cellular Ca<sup>2+</sup> homeostasis is modulated by mitochondrial morphology

Since mitochondrial morphology was shown to regulate organellar Ca<sup>2+</sup> uptake (Kowaltowski et al. 2019) and mitochondria-ER Ca<sup>2+</sup> exchange in C2C12 cells (Szabadkai et al. 2004), manipulating mitochondrial morphology could be sufficient to prevent the SOCE impairment induced by LPS activation in BV2 cells. We used adenovirus-based genetic interference to generate cells with reduced levels of Mfn2 (through knockdown, Mfn2KD) or Drp1 (through expression of a dominant-negative form, Drp1DN), thus promoting either predominance of fragmented or tubular shapes within the mitochondrial network, respectively (Fig. 4; Suppl. Fig. 3; Fomi et al. 2016; Kowaltowski et al. 2019).

Intracellular calcium was assessed both in control and Mfn2KD or Drp1DN cells, testing whether mitochondrial fragmentation was sufficient to promote the phenotype of LPS-activated cells (Fig. 5a). As previously described (Fig. 3b), both thapsigargin-stimulated (Fig. 5b) and SOCE (Fig. 5c) Ca<sup>2+</sup> levels were significantly decreased by LPS activation of control cells. Induction of mitochondrial fragmentation by Mfn2 KD effectively mimicked the effect of LPS treatment. On the other hand, Drp1DN completely prevented the LPS-induced effect (Fig. 5b,c), strongly indicating that the



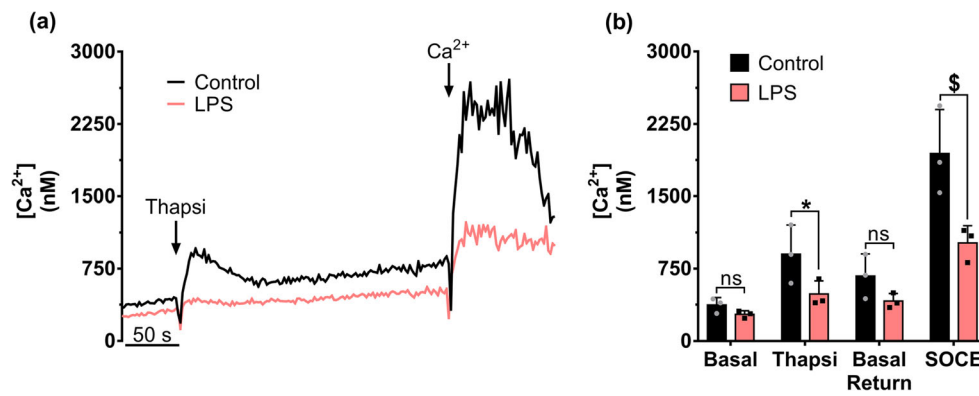


**Fig. 3** LPS activation depletes ER calcium and impairs SOCE. (a) Representative traces of cytosolic  $[Ca^{2+}]_i$  determination, ER  $Ca^{2+}$  release promoted by 5  $\mu$ M thapsigargin and SOCE induction by external 2 mM  $Ca^{2+}$  addition, assessed by Fura-2-AM fluorescence. (b) Quantification of

$[Ca^{2+}]_i$  under each condition. \* $p \leq 0.05$ ,  $^{\$}p \leq 0.001$ , repeated measures two-way ANOVA followed by Holm-Šidak's post-hoc test,  $n = 3$  independent experiments

impairment of  $Ca^{2+}$  handling occurs secondarily to mitochondrial fragmentation. Overall, these results show that mitochondrial morphology modulates cellular calcium homeostasis changes promoted by LPS in BV-2 cells, demonstrating that mitochondrial fragmentation is a critical point of control for changes in calcium handling during microglial activation.

## Discussion

Prior work has extensively demonstrated that LPS induces mitochondrial fragmentation both in murine primary microglia and BV-2 cells. This LPS-induced change in mitochondrial morphology is accompanied by a metabolic shift, with decreased oxidative phosphorylation and increased glycolysis

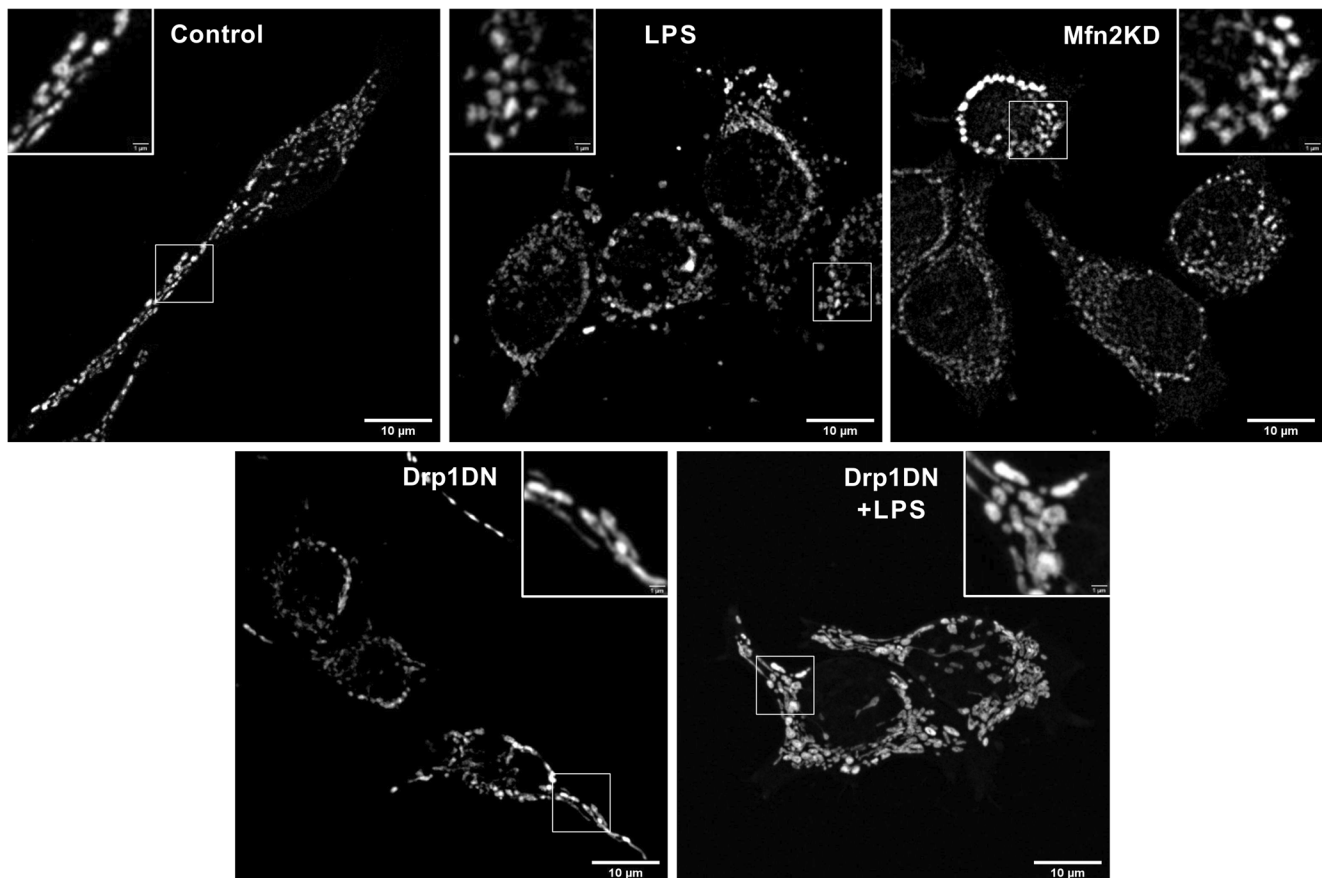
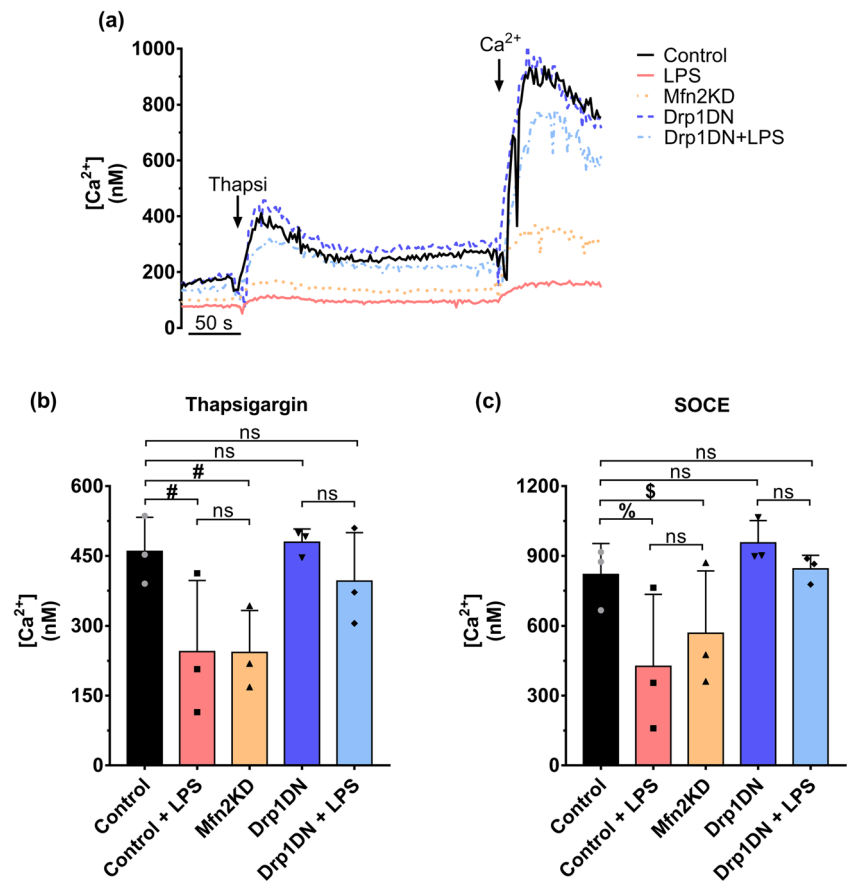


**Fig. 4** Modulation of mitochondrial morphology by Mfn2KD and Drp1DN. Representative images of the mitochondrial network stained with MitoTracker Deep Red in cells infected with adenoviral constructs

to modulate mitochondrial fusion (mitofusin-2 knockdown, Mfn2KD) and fission (Drp1 dominant negative, DN) proteins. Inserts show higher magnifications of indicated areas

**Fig. 5** Mitochondrial fragmentation promotes LPS-induced ER Ca<sup>2+</sup> depletion and SOCE impairment. (a) Representative traces of cytosolic [Ca<sup>2+</sup>]<sub>i</sub> determination, ER Ca<sup>2+</sup> release promoted by 5 μM thapsigargin and SOCE induction by external 2 mM Ca<sup>2+</sup> addition, assessed by Fura-2-AM fluorescence. Cells were infected with adenoviral constructs to modulate mitochondrial fusion (mitofusin-2 knockdown, Mfn2KD) and fission (Drp1 dominant negative, DN) proteins. Quantification of [Ca<sup>2+</sup>]<sub>i</sub> at the thapsigargin-induced peak (b) and after SOCE (c). \**p* ≤ 0.05, #*p* ≤ 0.01, \$*p* ≤ 0.001, %*p* < 0.0001 repeated measures two-way ANOVA followed by Holm-Sidak’s post-hoc test (analysis included basal and basal return conditions, suppressed here for clarity), n = 3 independent experiments



(Orihuela et al. 2016; Chausse et al. 2019). The shift towards glycolytic metabolism is not induced by ATP demand, since occurs prior to the loss of mitochondrial ATP production (Chausse et al. 2019). Therefore, metabolic reprogramming induced by LPS treatment may be mainly related to the production of inflammatory intermediates required for immune response (O’Neill and Pearce 2016).

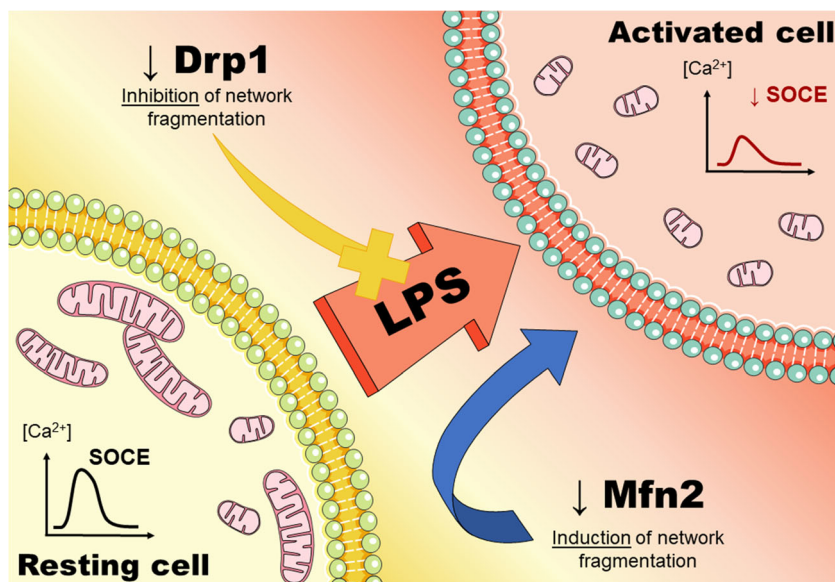
Interestingly, inhibition of mitochondrial fragmentation prevents microglial activation (Park et al. 2013, 2016; Katoh et al. 2017; Wang et al. 2017; Mo et al. 2019). Park et al. (2016) proposed that fragmentation may occur through Ca<sup>2+</sup>-dependent activation of Drp1 by calcineurin. Indeed, LPS-mediated microglial activation has also been extensively linked to changes in intracellular Ca<sup>2+</sup> homeostasis (Mustaly-Kalimi et al. 2018). While modifications in intracellular Ca<sup>2+</sup> levels can change mitochondrial morphology, we investigated here if the reverse was also true: if changes mitochondrial size and shape promoted by LPS could have an impact on Ca<sup>2+</sup> levels. This possibility was based on the fact that mitochondrial morphology was recently shown to have an impact on Ca<sup>2+</sup> uptake by mitochondria and cellular Ca<sup>2+</sup> homeostasis in non-inflammatory cells (Kowaltowski et al. 2019). We hypothesized that, by inducing mitochondrial fission in microglial cells, LPS

could also promote changes in Ca<sup>2+</sup> homeostasis. Indeed, we demonstrate here that mitochondrial dynamics play a critical role in calcium handling in BV-2 microglial cells.

We found that LPS promotes a significant decrease in both mitochondrial Ca<sup>2+</sup> uptake capacity and uptake rates (Fig. 1), associated with lower mitochondrial coupling, as indicated by decreased respiratory control ratios and inner membrane potentials ( $\Delta\Psi$ , Fig. 2). Interestingly, the changes in mitochondrial Ca<sup>2+</sup> homeostasis are not related to the expression of the MCU, but rather to the lack of  $\Delta\Psi$  as a driving force (Fig. 2) as well as LPS-driven mitochondrial fragmentation (Figs. 4, 5), as smaller mitochondria have been shown to have decreased Ca<sup>2+</sup> uptake (Kowaltowski et al. 2019).

Concomitantly to changes in mitochondrial ion homeostasis, we find that LPS depletes ER Ca<sup>2+</sup> stores and hampers SOCE-mediated intracellular Ca<sup>2+</sup> replenishing (Fig. 3). Our results are compatible with previous data in primary microglia showing that LPS impairs SOCE and reduces ER Ca<sup>2+</sup> stores (Heo et al. 2015). This suggests that Ca<sup>2+</sup>-dependent signals, including cytoskeleton remodeling, alterations in cellular motility and cytokine secretion could display significantly altered responses in LPS-activated cells (Boddeke et al. 1999b;

**Fig. 6** Working model. LPS-activated microglia present changes in mitochondrial and cellular  $\text{Ca}^{2+}$  homeostasis, including hampered store-operated calcium entry (SOCE), due to LPS-induced mitochondrial fragmentation



Möller 2002; Suzuki et al. 2006). Many of these responses are already known to be modified by LPS activation (De Simone et al. 2010; Boddeke et al. 1999a), supporting the idea that changes in mitochondrial  $\text{Ca}^{2+}$  handling are an important mechanistic hub controlling microglial function.

Interestingly, we also found that inhibition of LPS-induced mitochondrial fragmentation in Drp1DN cells prevented both the depletion of ER  $\text{Ca}^{2+}$  stores and inhibition of SOCE (Figs. 4, 5). This suggests that mitochondrial fragmentation induced by LPS is a cause of LPS-induced  $\text{Ca}^{2+}$  homeostasis disruption. In line with this idea, knockdown of the fusion protein Mfn2, which promotes fission, leads to similar effects to those observed with LPS (Figs. 4, 5). Park et al. (2016) proposed that microglial mitochondrial fragmentation is also linked to mitochondrial oxidant production. Furthermore, the disruption of inner mitochondrial membrane integrity promoted by calcium ions and mitochondrial permeability transition is mediated by oxidants generated in mitochondria (Castilho et al. 1995; Kowaltowski et al. 2009; Vercesi et al. 2018). Higher susceptibility to mitochondrial permeability transition is strongly associated with increased vulnerability to cell death (Menezes-Filho et al. 2017; Amigo et al. 2017), and Xie et al. (2017) showed that inhibition of mitochondrial calcium uptake through MCU was effective in preventing amyloid- $\beta$ -induced apoptosis in both primary microglia and BV-2 cells, in an oxidant-dependent manner. Once again, these results support the idea that the responses of LPS-activated microglia are dependent on an interplay between changes in mitochondrial morphology, ion transport, and cellular  $\text{Ca}^{2+}$  homeostasis (Fig. 6).

Overall, our results show that changes in mitochondrial morphology result in altered calcium handling in microglia. This is a novel aspect of cell signaling observed during microglial activation, which may be central toward the role of these cells in inflammation.

**Supplementary Information** The online version contains supplementary material available at <https://doi.org/10.1007/s10863-021-09878-4>.

**Acknowledgments** The authors acknowledge Sirlei Mendes de Oliveira and Camille Caldeira da Silva (Universidade de São Paulo) for their outstanding technical support. The graphical abstract was created from adapted figures and templates available at Servier Medical Art by Servier (<https://smart.servier.com>) under a Creative Commons Attribution 3.0 Unported License.

**Authors' contributions** O.R.P.Jr., J.V.C.-C., and A.J.K designed the experiments; O.R.P.Jr., V.M.R., and J.V.C.-C. acquired and analyzed the data; O.R.P.Jr., J.V.C.-C., and A.J.K wrote the manuscript. All authors revised and approved the manuscript.

**Funding** This work was funded by grants #2020/06970–5 and #2013/07937–8 from the *Fundação de Amparo à Pesquisa do Estado de São Paulo* (FAPESP), *Centro de Pesquisa, Inovação e Difusão de Processos Redox em Biomedicina* (CEPID Redoxoma), *Conselho Nacional de Desenvolvimento Científico e Tecnológico* (CNPq) and *Coordenação de Aperfeiçoamento de Pessoal de Nível Superior* (CAPES). O.R.P.Jr. is supported by FAPESP grant #2018/21487–9. V.M.R. is supported by FAPESP grant #2019/18402–4. J.V.C.-C. is supported by FAPESP grants #2017/14713–0 and #2019/22178–2.

## Declarations

**Conflicts of interest/competing interests** The authors declare no conflicts of interest.

**Availability of data and material (data transparency)** Raw data are fully available upon request.

## References

- Amigo I, Menezes-Filho SL, Luévano-Martínez LA, Chausse B, Kowaltowski AJ (2017) Caloric restriction increases brain mitochondrial calcium retention capacity and protects against excitotoxicity. *Aging Cell* 16:73–81. <https://doi.org/10.1111/ace.12527>
- Akerman KE, Wikström MK (1976) Safranin as a probe of the mitochondrial membrane potential. *FEBS Lett* 68:191–197. [https://doi.org/10.1016/0014-5793\(76\)80434-6](https://doi.org/10.1016/0014-5793(76)80434-6)
- Allen NJ, Barres BA (2009) Glia - more than just brain glue. *Nature* 457:675–677. <https://doi.org/10.1038/457675a>
- Baughman JM, Perocchi F, Girgis HS, Plovanich M, Belcher-Timme CA, Sancak Y, Bao XR, Strittmatter L, Goldberger O, Bogorad RL, Kotliansky V, Mootha VK (2011) Integrative genomics identifies MCU as an essential component of the mitochondrial calcium uniporter. *Nature* 476:341–345. <https://doi.org/10.1038/nature10234>
- Ben-Kasus Nissim T, Zhang X, Elazar A, Roy S, Stolwijk JA, Zhou Y, Motiani RK, Gueguinou M, Hempel N, Hershfinkel M, Gill DL, Trebak M, Sekler I (2017) Mitochondria control store-operated  $Ca^{2+}$  entry through  $Na^{+}$  and redox signals. *EMBO J*. 36:797–815. <https://doi.org/10.15252/embj.201592481>
- Boddeke EW, Meigel I, Frentzel S, Biber K, Renn LQ, Gebicke-Härter P (1999a) Functional expression of the fractalkine (CX3C) receptor and its regulation by lipopolysaccharide in rat microglia. *Eur J Pharmacol* 374:309–313. [https://doi.org/10.1016/S0014-2999\(99\)00307-6](https://doi.org/10.1016/S0014-2999(99)00307-6)
- Boddeke EW, Meigel I, Frentzel S, Gourmal NG, Harrison JK, Buttini M, Spleiss O, Gebicke-Härter P (1999b) Cultured rat microglia express functional  $\beta$ -chemokine receptors. *J Neuroimmunol* 98:176–184. [https://doi.org/10.1016/S0165-5728\(99\)00096-X](https://doi.org/10.1016/S0165-5728(99)00096-X)
- Castilho RF, Kowaltowski AJ, Meinicke AR, Bechara EJ, Vercesi AE (1995) Permeabilization of the inner mitochondrial membrane by  $Ca^{2+}$  ions is stimulated by t-butyl hydroperoxide and mediated by reactive oxygen species generated by mitochondria. *Free Radic Biol Med* 18:479–486. [https://doi.org/10.1016/0891-5849\(94\)00166-h](https://doi.org/10.1016/0891-5849(94)00166-h)
- Chausse B, Kakimoto PA, Caldeira-da-Silva CC, Chaves-Filho AB, Yoshinaga MY, da Silva RP, Miyamoto S, Kowaltowski AJ (2019) Distinct metabolic patterns during microglial remodeling by oleate and palmitate. *Biosci Rep* 39:BSR20190072. <https://doi.org/10.1042/BSR20190072>
- De Simone R, Niture CE, De Nuccio C, Ajmone-Cat MA, Visentin S, Minghetti L (2010) TGF- $\beta$  and LPS modulate ADP-induced migration of microglial cells through P2Y1 and P2Y12 receptor expression. *J Neurochem* 115:450–459. <https://doi.org/10.1111/j.1471-4159.2010.06937.x>
- De Stefani D, Raffaello A, Teardo E, Szabò I, Rizzuto R (2011) A 40 kDa protein of the inner membrane is the mitochondrial calcium uniporter. *Nature* 476:336–340. <https://doi.org/10.1038/nature10230>
- Dheen ST, Kaur C, Ling EA (2007) Microglial activation and its implications in the brain diseases. *Curr Med Chem* 14:1189–1197. <https://doi.org/10.2174/092986707780597961>
- Engelhardt B, Sorokin L (2009) The blood-brain and the blood-cerebrospinal fluid barriers: function and dysfunction. *Semin Immunopathol* 31:497–511. <https://doi.org/10.1007/s00281-009-0177-0>
- Fiskum G, Craig SW, Decker GL, Lehninger AL (1980) The cytoskeleton of digitonin-treated rat hepatocytes. *Proc Natl Acad Sci U S A* 77:3430–3434. <https://doi.org/10.1073/pnas.77.6.3430>
- Fiskum G, Kowaltowski AJ, Andreyev AY, Kushnareva YE, Starkov AA (2000) Apoptosis-related activities measured with isolated mitochondria and digitonin-permeabilized cells. *Methods Enzymol* 322:222–234. [https://doi.org/10.1016/S0076-6879\(00\)22023-5](https://doi.org/10.1016/S0076-6879(00)22023-5)
- Forni MF, Pelliggia J, Trudeau K, Shirihai O, Kowaltowski AJ (2016) Murine mesenchymal stem cell commitment to differentiation is regulated by mitochondrial dynamics. *Stem Cells* 34:743–755. <https://doi.org/10.1002/stem.2248>
- Gao Z, Li Y, Wang F, Huang T, Fan K, Zhang Y, Zhong J, Cao Q, Chao T, Jia J, Yang S, Zhang L, Xiao Y, Zhou JY, Feng XH, Jin J (2017) Mitochondrial dynamics controls anti-tumour innate immunity by regulating CHIP-IRF1 axis stability. *Nat Commun* 8:1805. <https://doi.org/10.1038/s41467-017-01919-0>
- Gryniewicz G, Poenie M, Tsien RY (1985) A new generation of  $Ca^{2+}$  indicators with greatly improved fluorescence properties. *J Biol Chem* 260:3440–3450
- Guevara I, Iwanek J, Dembińska-Kieć A, Pankiewicz J, Wanat A, Anna P, Gołabek I, Bartuś S, Malczewska-Malec M, Szczudlik A (1998) Determination of nitrite/nitrate in human biological material by the simple Griess reaction. *Clin Chim Acta* 274:177–188. [https://doi.org/10.1016/S0009-8981\(98\)00060-6](https://doi.org/10.1016/S0009-8981(98)00060-6)
- Hanisch UK, Kettenmann H (2007) Microglia: active sensor and versatile effector cells in the normal and pathologic brain. *Nat Neurosci* 10:1387–1394. <https://doi.org/10.1038/nn1997>
- Heo DK, Lim HM, Nam JH, Lee MG, Kim JY (2015) Regulation of phagocytosis and cytokine secretion by store-operated calcium entry in primary isolated murine microglia. *Cell Signal* 27:177–186. <https://doi.org/10.1016/j.cellsig.2014.11.003>
- Hines DJ, Hines RM, Mulligan SJ, Macvicar BA (2009) Microglia processes block the spread of damage in the brain and require functional chloride channels. *Glia*. 57:1610–1618. <https://doi.org/10.1002/glia.20874>
- Hoffmann A, Kann O, Ohlemeyer C, Hanisch UK, Kettenmann H (2003) Elevation of basal intracellular calcium as a central element in the activation of brain macrophages (microglia): suppression of receptor-evoked calcium signaling and control of release function. *J Neurosci* 23:4410–4419. <https://doi.org/10.1523/JNEUROSCI.23-11-04410.2003>
- Katoh M, Wu B, Nguyen HB, Thai TQ, Yamasaki R, Lu H, Rietsch AM, Zorlu MM, Shinozaki Y, Saitoh Y, Saitoh S, Sakoh T, Ikenaka K, Koizumi S, Ransohoff RM, Ohno N (2017) Polymorphic regulation of mitochondrial fission and fusion modifies phenotypes of microglia in neuroinflammation. *Sci Rep* 7:4942. <https://doi.org/10.1038/s41598-017-05232-0>
- Kowaltowski AJ, Cosso RG, Campos CB, Fiskum G (2002) Effect of Bcl-2 overexpression on mitochondrial structure and function. *J Biol Chem* 277:42802–42807. <https://doi.org/10.1074/jbc.M207765200>
- Kowaltowski AJ, de Souza-Pinto NC, Castilho RF, Vercesi AE (2009) Mitochondria and reactive oxygen species. *Free Radic Biol Med* 47:333–343. <https://doi.org/10.1016/j.freeradbiomed.2009.05.004>
- Kowaltowski AJ, Menezes-Filho SL, Assali EA, Gonçalves IG, Cabral-Costa JV, Abreu P, Miller N, Nolasco P, Laurindo FRM, Brunica Cardoso A, Shirihai OS (2019) Mitochondrial morphology regulates organellar  $Ca^{2+}$  uptake and changes cellular  $Ca^{2+}$  homeostasis. *FASEB J* 33:13176–13188. <https://doi.org/10.1096/fj.201901136R>
- Lytton J, Westlin M, Hanley MR (1991) Thapsigargin inhibits the sarcoplasmic or endoplasmic reticulum ca-ATPase family of calcium pumps. *J Biol Chem* 266:17067–17071
- Menezes-Filho SL, Amigo I, Prado FM, Ferreira NC, Koike MK, Pinto IFD, Miyamoto S, Montero EFS, Medeiros MHG, Kowaltowski AJ (2017) Caloric restriction protects livers from ischemia/reperfusion damage by preventing  $Ca^{2+}$ -induced mitochondrial permeability transition. *Free Radic Biol Med* 110:219–227. <https://doi.org/10.1016/j.freeradbiomed.2017.06.013>
- Mo Y, Deng S, Zhang L, Huang Y, Li W, Peng Q, Liu Z, Ai Y (2019) SS-31 reduces inflammation and oxidative stress through the inhibition of Fis1 expression in lipopolysaccharide-stimulated microglia. *Biochem Biophys Res Commun* 520:171–178. <https://doi.org/10.1016/j.bbrc.2019.09.077>



- Möller T (2002) Calcium signaling in microglial cells. *Glia* 40:184–194. <https://doi.org/10.1002/glia.10152>
- Mustaly-Kalimi S, Littlefield AM, Stutzmann GE (2018) Calcium signaling deficits in glia and autophagic pathways contributing to neurodegenerative disease. *Antioxid Redox Signal* 29:1158–1175. <https://doi.org/10.1089/ars.2017.7266>
- Nair S, Sobotka KS, Joshi P, Gressens P, Fleiss B, Thornton C, Mallard C, Hagberg H (2019) Lipopolysaccharide-induced alteration of mitochondrial morphology induces a metabolic shift in microglia modulating the inflammatory response in vitro and in vivo. *Glia* 67:1047–1061. <https://doi.org/10.1002/glia.23587>
- O'Neill LAJ, Pearce EJ (2016) Immunometabolism governs dendritic cell and macrophage function. *J Exp Med* 213:15–23. <https://doi.org/10.1084/jem.20151570>
- Orihuela R, McPherson CA, Harry GJ (2016) Microglial M1/M2 polarization and metabolic states. *Br J Pharmacol* 173:649–665. <https://doi.org/10.1111/bph.13139>
- Park J, Choi H, Kim B, Chae U, Lee DG, Lee SR, Lee S, Lee HS, Lee DS (2016) Peroxiredoxin 5 (Prx5) decreases LPS-induced microglial activation through regulation of Ca<sup>2+</sup>/calcineurin-Drp1-dependent mitochondrial fission. *Free Radic Biol Med* 99:392–404. <https://doi.org/10.1016/j.freeradbiomed.2016.08.030>
- Park J, Choi H, Min JS, Park SJ, Kim JH, Park HJ, Kim B, Chae JI, Yim M, Lee DS (2013) Mitochondrial dynamics modulate the expression of pro-inflammatory mediators in microglial cells. *J Neurochem* 127:221–232. <https://doi.org/10.1111/jnc.12361>
- Pernas L, Scorrano L (2016) Mito-morphosis: mitochondrial fusion, fission, and cristae remodeling as key mediators of cellular function. *Annu Rev Physiol* 78:505–531. <https://doi.org/10.1146/annurev-physiol-021115-105011>
- Rizzuto R, De Stefani D, Raffaello A, Mammucari C (2012) Mitochondria as sensors and regulators of calcium signalling. *Nat Rev Mol Cell Biol* 13:566–578. <https://doi.org/10.1038/nrm3412>
- Rizzuto R, Pinton P, Carrington W, Fay FS, Fogarty KE, Lifshitz LM, Tuft RA, Pozzan T (1998) Close contacts with the endoplasmic reticulum as determinants of mitochondrial Ca<sup>2+</sup> responses. *Science* 280:1763–1766. <https://doi.org/10.1126/science.280.5370.1763>
- Salter MW, Stevens B (2017) Microglia emerge as central players in brain disease. *Nat Med* 23:1018–1027. <https://doi.org/10.1038/nm.4397>
- Schindelin J, Arganda-Carreras I, Frise E, Kaynig V, Longair M, Pietzsch T, Preibisch S, Rueden C, Saalfeld S, Schmid B, Tinevez JY, White DJ, Hartenstein V, Eliceiri K, Tomancak P, Cardona A (2012) Fiji: an open-source platform for biological-image analysis. *Nat Methods* 9:676–682. <https://doi.org/10.1038/nmeth.2019>
- Schneider CA, Rasband WS, Eliceiri KW (2012) NIH image to ImageJ: 25 years of image analysis. *Nat Methods* 9:671–675. <https://doi.org/10.1038/nmeth.2089>
- Suzuki T, Hide I, Matsubara A, Hama C, Harada K, Miyano K, Andrá M, Matsubayashi H, Sakai N, Kohsaka S, Inoue K, Nakata Y (2006) Microglial  $\alpha 7$  nicotinic acetylcholine receptors drive a phospholipase C/IP3 pathway and modulate the cell activation toward a neuroprotective role. *J Neurosci Res* 83:1461–1470. <https://doi.org/10.1002/jnr.20850>
- Szabadkai G, Simoni AM, Chami M, Wieckowski MR, Youle RJ, Rizzuto R (2004) Drp-1-dependent division of the mitochondrial network blocks intraorganellar Ca<sup>2+</sup> waves and protects against Ca<sup>2+</sup>-mediated apoptosis. *Mol Cell* 16:59–68. <https://doi.org/10.1016/j.molcel.2004.09.026>
- Vercesi AE, Castilho RF, Kowaltowski AJ, de Oliveira HCF, de Souza-Pinto NC, Figueira TR, Busanello ENB (2018) Mitochondrial calcium transport and the redox nature of the calcium-induced membrane permeability transition. *Free Radic Biol Med* 129:1–24. <https://doi.org/10.1016/j.freeradbiomed.2018.08.034>
- Wang Y, Subramanian M, Yurdagul A Jr, Barbosa-Lorenzi VC, Cai B, de Juan-Sanz J, Ryan TA, Nomura M, Maxfield FR, Tabas I (2017) Mitochondrial fission promotes the continued clearance of apoptotic cells by macrophages. *Cell* 171:331–345. <https://doi.org/10.1016/j.cell.2017.08.041>
- Xie N, Wu C, Wang C, Cheng X, Zhang L, Zhang H, Lian Y (2017) Inhibition of the mitochondrial calcium uniporter inhibits A $\beta$ -induced apoptosis by reducing reactive oxygen species-mediated endoplasmic reticulum stress in cultured microglia. *Brain Res* 1676:100–106. <https://doi.org/10.1016/j.brainres.2017.08.035>

**Publisher's note** Springer Nature remains neutral with regard to jurisdictional claims in published maps and institutional affiliations.

## **ANNEX D**

**Vilas-Boas et al., 2022**

**(bioRxiv)**

# **Goldilocks calcium and the mitochondrial respiratory chain: too much, too little, just right**

Eloisa A. Vilas-Boas\*, João Victor Cabral-Costa, Vitor M. Ramos, Camille C.C. da Silva,  
Alicia J. Kowaltowski\*.

Departamento de Bioquímica, Instituto de Química, Universidade de São Paulo, São Paulo, SP, Brazil.

\*To whom correspondence should be addressed:

Tel.: +55 11 30912922

Email: elovilasboas@usp.br, alicia@iq.usp.br

**Running title:** Calcium and mitochondrial respiratory regulation.

**Keywords:** calcium transport, mitochondria, electron transfer chain, oxidative phosphorylation.

## Abstract

Calcium ( $\text{Ca}^{2+}$ ) is a key regulator in diverse intracellular signaling pathways, and has long been implicated in metabolic control and mitochondrial function. Mitochondria can actively take up large amounts of  $\text{Ca}^{2+}$ , thereby acting as important intracellular  $\text{Ca}^{2+}$  buffers and affecting cytosolic  $\text{Ca}^{2+}$  transients. Excessive mitochondrial matrix  $\text{Ca}^{2+}$  is known to be deleterious due to opening of the mitochondrial permeability transition pore (mPTP) and consequent membrane potential dissipation, leading to mitochondrial swelling, rupture and cell death. But moderate  $\text{Ca}^{2+}$  within the organelle can directly or indirectly activate mitochondrial matrix enzymes, possibly impacting on ATP production. However, *in vitro* studies involving the regulation of mitochondrial enzymes by  $\text{Ca}^{2+}$  may not uncover its full effects on oxidative phosphorylation. Here, we aimed to determine if extra or intramitochondrial  $\text{Ca}^{2+}$  modulate oxidative phosphorylation in mouse liver mitochondria and intact hepatocytes. We found that isolated mitochondria present increased respiratory control ratios (a measure of oxidative phosphorylation efficiency) when incubated with low and medium  $\text{Ca}^{2+}$  concentrations in the presence of complex I-linked substrates pyruvate plus malate and  $\alpha$ -ketoglutarate, respectively, but not complex II-linked succinate. In intact hepatocytes, both low and high cytosolic  $\text{Ca}^{2+}$  led to decreased respiratory rates, while ideal rates were present under physiological conditions. High  $\text{Ca}^{2+}$  decreased mitochondrial respiration in cells in a substrate-dependent manner, mediated by mPTP. Overall, our results uncover a Goldilocks effect of  $\text{Ca}^{2+}$  on liver mitochondria, with specific “just right” concentrations that activate oxidative phosphorylation.



## 1. Introduction

Calcium ( $\text{Ca}^{2+}$ ) is an important second messenger and participates in a myriad of cellular functions. Mitochondria are one of the central intracellular regulators of  $\text{Ca}^{2+}$  homeostasis (1), as they can actively take up the ion down their electrochemical potential (2,3). While the affinity for  $\text{Ca}^{2+}$  uptake is lower than for the endoplasmic reticulum (ER), mitochondria can absorb very large amounts of the ion from the cytosol (4-6). Mitochondria can also release  $\text{Ca}^{2+}$ , and are thus recognized as important rheostats for cytosolic  $\text{Ca}^{2+}$  dynamics and signaling. Furthermore, mitochondria also participate in crosstalk signals between intracellular compartments, such as with the ER, through microdomains formed between both organelles in which ions have distinct concentrations and their exchange mediates inter-organelle communication (7).

$\text{Ca}^{2+}$  uptake across the inner mitochondrial membrane into the mitochondrial matrix occurs through the mitochondrial  $\text{Ca}^{2+}$  uniporter complex (MCU) (8-10). The membrane potential generated by the electron transport chain (ETC), with a negative matrix charge, provides the electrochemical force necessary for positively charged ions, such as  $\text{Ca}^{2+}$ , to enter.  $\text{Ca}^{2+}$  efflux from the mitochondrial matrix occurs through the  $\text{Na}^+/\text{Ca}^{2+}$  exchanger (NCLX) (11), located in the inner mitochondrial membrane (IMM), and by a  $\text{Ca}^{2+}/\text{H}^+$  exchanger, which may have been recently identified (12,13).

Mitochondrial  $\text{Ca}^{2+}$  transients are believed to provide a link between cytosolic  $\text{Ca}^{2+}$  signaling and the control of cellular energy demand by regulating ATP production. Pyruvate dehydrogenase, isocitrate dehydrogenase, and  $\alpha$ -ketoglutarate dehydrogenase within the mitochondrial matrix have increased activities in the presence of  $\text{Ca}^{2+}$ , as uncovered through *in vitro* studies (14-17). For these activities to translate into enhanced oxidative phosphorylation *in vivo*, two conditions need to be met: first, the change in enzymatic activity promoted by  $\text{Ca}^{2+}$  needs to be sufficient to overcome rate-limiting steps in oxidative phosphorylation and, second,  $\text{Ca}^{2+}$  concentrations need to be below those that hamper mitochondrial function. Mitochondrial  $\text{Ca}^{2+}$  overload leads to swelling of the organelle and opening of the mitochondrial permeability transition pore (mPTP), often culminating in loss of function and cell death (18-20). This process has been implicated in various diseases (21,22).

In theory, and when present at lower concentrations than those that lead to mPTP opening,  $\text{Ca}^{2+}$  should activate mitochondrial electron transport and ATP production, but direct studies so far are limited to uncovering the modulation of isolated enzyme activity, and only show increases in substrate affinity, not maximal velocity. The effects of

changes in the affinity of these enzymes on overall mitochondrial metabolic pathway flux have not been determined. We explore this gap here, to determine if extra or intramitochondrial  $\text{Ca}^{2+}$  modulates oxidative phosphorylation supported by different substrates in isolated mitochondria, focusing on the liver, since a rich metabolic regulation by  $\text{Ca}^{2+}$  occurs in this tissue. We also explore how mitochondrial  $\text{Ca}^{2+}$  transport influences oxidative phosphorylation in intact hepatocytes. Our results demonstrate that  $\text{Ca}^{2+}$  concentrations greatly impact mitochondrial respiration, with a Goldilocks-type effect, in which both too much and too little  $\text{Ca}^{2+}$  limit oxidative phosphorylation, but the “just right” concentration promotes significant activation.

## 2. Results

### *2.1. Ca<sup>2+</sup> increases liver oxidative phosphorylation efficiency in a substrate- and concentration-dependent manner*

To gain insight into the effects of extramitochondrial Ca<sup>2+</sup> addition on mitochondrial respiration, we used isolated mouse liver mitochondria in the presence of different substrates and measured oxygen consumption over time using an Oroboros high-resolution oxygraph. Ca<sup>2+</sup> was added at different concentrations, followed by additions of ADP (to induce oxidative phosphorylation, state 3), oligomycin (to inhibit ATP synthase and measure respiration dependent on the proton leak, state 4) and CCCP (to induce maximum electron transport). We determined residual Ca<sup>2+</sup> concentrations present after mitochondrial isolation daily, and then calculated the amount of Ca<sup>2+</sup> added so it was equal between biological replicates, classifying conditions as no added Ca<sup>2+</sup>, low ( $2.4 \pm 0.6 \mu\text{M}$ ), medium ( $22.0 \pm 2.4 \mu\text{M}$ ) and high ( $52.9 \pm 2.5 \mu\text{M}$ ) added Ca<sup>2+</sup> concentrations.

Complex I substrates such as pyruvate and malate were chosen initially to study the effects of Ca<sup>2+</sup> on electron transport and oxidative phosphorylation, due to the known enhancement of pyruvate dehydrogenase (PDH) affinity in response to Ca<sup>2+</sup> signaling (14-17). Ca<sup>2+</sup> uptake traces with low and medium Ca<sup>2+</sup> concentrations are shown in Fig. 1A. The downward deflection in the curve within 2-3 min indicates a decrease in extramitochondrial Ca<sup>2+</sup> measured with the fluorophore Ca<sup>2+</sup> Green due to uptake by mitochondria (Fig. 1A). High Ca<sup>2+</sup> led to mitochondrial dysfunction with these substrates (Fig. S1A) and was thus not included in further experiments; O<sub>2</sub> consumption traces were measured using only low and medium Ca<sup>2+</sup> additions, and are shown as oxygen consumption rates (OCR) in Figs. 1B-D, and quantified results in panels E-H.

We found that the presence of low Ca<sup>2+</sup> concentrations strongly increased state 3 respiration, when oxidative phosphorylation is active (Fig. 1E). State 4 respiration, which occurs in the absence of ATP synthase and is limited by the inner membrane impermeability to protons, was stimulated by both low and medium Ca<sup>2+</sup> concentrations when supported by pyruvate and malate (Fig. 1F). The respiratory control ratio (RCR, Fig. 1G) is the ratio between state 3 and state 4 oxygen consumption, and is used as a proxy for oxidative phosphorylation efficiency, as it shows the relative stimulation of oxygen consumption by the production of mitochondrial ATP (23). We found that the RCR was increased at low but not medium Ca<sup>2+</sup> concentrations (Fig. 1G). This shows that oxidative phosphorylation supported by pyruvate and malate has a tight relationship with

mitochondrial  $\text{Ca}^{2+}$ , and is more effective within a very specific range of added extramitochondrial  $\text{Ca}^{2+}$ .

We investigated next if the increase in oxidative phosphorylation efficiency observed was dependent on mitochondrial  $\text{Ca}^{2+}$  uptake or cycling, using pharmacological inhibitors of the MCU (Ruthenium red, RuRed), which prevents  $\text{Ca}^{2+}$  uptake, and of the NCLX (CGP-37157, CGP), which prevents  $\text{Ca}^{2+}$  extrusion from mitochondria (Fig. 1H). Both RuRed and CGP reversed the increase in RCR promoted by low  $\text{Ca}^{2+}$  concentrations; this indicates that  $\text{Ca}^{2+}$  must enter the mitochondrial matrix to exert this effect, as RuRed prevents this uptake. The effect of CGP could also indicate that increased RCRs are dependent on  $\text{Ca}^{2+}$  cycling, as it inhibits  $\text{Ca}^{2+}$  extrusion from mitochondria through  $\text{Ca}^{2+}$  exchange with  $\text{Na}^+$  (11). Alternatively, CGP treatment of mitochondria, by promoting more  $\text{Ca}^{2+}$  retention in the matrix, could induce mPTP opening and thus decrease RCRs.

To further investigate the role of  $\text{Ca}^{2+}$  on oxidative phosphorylation, we performed similar experiments using  $\alpha$ -ketoglutarate (Fig. 2), another substrate metabolized by a dehydrogenase in which affinity is modulated by  $\text{Ca}^{2+}$  *in vitro* (14-17). Once again, only low and medium, but not high (Fig. S1B),  $\text{Ca}^{2+}$  concentrations could be taken up and retained by mitochondria respiring on  $\alpha$ -ketoglutarate (Fig. 2A). Using  $\alpha$ -ketoglutarate as substrate, medium  $\text{Ca}^{2+}$  concentrations ( $22.0 \pm 2.4 \mu\text{M Ca}^{2+}$ ) increased states 3, 4, and RCR (Fig. 2B-G). Low  $\text{Ca}^{2+}$  concentrations did not present a significant effect when  $\alpha$ -ketoglutarate was used as the substrate. The beneficial effect of  $\text{Ca}^{2+}$  on mitochondrial oxidative phosphorylation supported by  $\alpha$ -ketoglutarate was partially attenuated by inhibition of  $\text{Ca}^{2+}$  release by NCLX and totally prevented by inhibition of  $\text{Ca}^{2+}$  entry with RuRed (Fig. 2H), demonstrating again the need for  $\text{Ca}^{2+}$  entry into the matrix for the stimulatory effect. These results show that the specific “sweet spot” for enhanced electron transport capacity in mitochondria induced by  $\text{Ca}^{2+}$  varies with the substrate used.

To further investigate substrate-specific effects of  $\text{Ca}^{2+}$ , we performed similar experiments using the complex II substrate succinate in the presence of complex I inhibition with rotenone, to ensure no effect of contaminating or downstream NADH-reducing substrates. With succinate, mitochondria were able to retain a wider range of  $\text{Ca}^{2+}$  loads (Fig. 3A), so low, medium, and high concentrations were tested for their respiratory effects. Interestingly, using succinate, none of these  $\text{Ca}^{2+}$  concentrations used led to a significant increase in state 3 or RCR (Fig. 3F,H). A small increase in state 4, in which respiration is not linked to oxidative phosphorylation, was observed with the

medium  $\text{Ca}^{2+}$  concentration (Fig. 3G), suggesting enhanced proton leak, possibly due to  $\text{Ca}^{2+}$  cycling or mPTP induction in a subpopulation of the mitochondrial suspension.

Taken together, results using isolated mouse liver mitochondria and various substrates show that a low increase in mitochondrial  $\text{Ca}^{2+}$  enhances oxidative phosphorylation capacity and efficiency. This positive effect depends on the substrate used and, when present, requires  $\text{Ca}^{2+}$  entry into the mitochondrial matrix.

## ***2.2. Both low and high cytosolic $\text{Ca}^{2+}$ impair mitochondrial respiration in cultured hepatocytes***

We investigated next how mitochondrial and cytosolic  $\text{Ca}^{2+}$  modulate electron transport and oxidative phosphorylation in intact hepatocytes (Fig. 4). Since primary isolated hepatocytes undergo major metabolic alterations during and after isolation (24), defeating the purpose of using a freshly isolated cell, we used AML12 cells, a non-tumoral hepatocyte cell line (25), and thus a more physiological liver cell model. OCRs were measured in plated cells using a Seahorse Extracellular Flux system (26).

To measure the respiratory effects of physiological  $\text{Ca}^{2+}$  concentrations, we removed increasing amounts of this ion from the cytosol by incubating AML12 cells in complete medium with a cytosolic  $\text{Ca}^{2+}$  chelator, BAPTA-AM, at different concentrations (Fig. 4 A-C). BAPTA-AM reduced maximal OCR respiration in a dose-dependent manner (Fig. 4C), but no changes were observed in basal respiration (Fig. 4B), which in intact cells corresponds to the respiration necessary to maintain normal levels of oxidative phosphorylation for typical cell function, in addition to the proton leak and non-mitochondrial oxygen consumption (inhibited in each trace by the addition of rotenone plus antimycin A, R/AA). Thus, decreasing physiological cytosolic  $\text{Ca}^{2+}$  levels hampers maximal electron transfer capacity in hepatocytes, but not sufficiently to decrease ATP-linked respiration under normal (basal) conditions of cell function.

In order to increase physiological intracellular  $\text{Ca}^{2+}$  levels and study the effects on mitochondrial oxidative phosphorylation, we used a sarco-/endoplasmic reticulum  $\text{Ca}^{2+}$  ATPase (SERCA) pump inhibitor, thapsigargin (TG), which releases the ion from endoplasmic reticulum (ER) stores. As the ER and mitochondria are closely connected in microdomains called mitochondria-associated ER membranes, this is expected to impact on mitochondrial  $\text{Ca}^{2+}$  homeostasis. Interestingly, AML12 cells exposed to different concentrations of TG displayed a decrease in basal and maximal respiration (Fig. 4D-F). Taken together, the results in Fig. 4 show that physiological intracellular  $\text{Ca}^{2+}$

homeostasis is maintained close to the Goldilocks “sweet spot” for oxidative phosphorylation activity, with both increases and decreases in this concentration hampering ideal electron transport function.

### ***2.3. Ca<sup>2+</sup>-induced impairment of mitochondrial respiration in hepatocytes is substrate-dependent***

We next speculated if the Ca<sup>2+</sup> effects on respiration in intact cells could also be substrate-dependent. We used three inhibitors that affect the oxidation of primary substrates that fuel mitochondria: glucose/pyruvate (UK5099), glutamine (BPTES), and long-chain fatty acids (etomoxir). We found that the decrease in basal and maximal respiration was prevented with glucose/pyruvate metabolism inhibition by UK5099 (Fig. 5A,B), showing that the modulation of respiration by Ca<sup>2+</sup> in intact hepatocytes is dependent on pyruvate oxidation, corroborating data observed in the isolated liver mitochondria (Fig. 1).

### ***2.4. Inhibition of mitochondrial Ca<sup>2+</sup> entry impairs mitochondrial respiration in cultured hepatocytes***

We then questioned if the effects of Ca<sup>2+</sup> on OCRs in intact cells required Ca<sup>2+</sup> entry into the matrix, as we found in isolated mitochondria. Inhibition of the MCU or NCLX was promoted in AML12 cells both pharmacologically with RuRed or CGP and by silencing with specific siRNAs. We found that an acute inhibition of the transporters (1 h in the presence of these drugs) did not influence basal respiration (Fig. 6A,B), but MCU inhibition with RuRed led to a tendency toward decreased maximal respiration (Fig. 6A,C). Cells in which NCLX was inhibited by CGP had similar profiles to untreated control cells (Fig. 6A-C).

We then checked how prolonged inhibition of those channels impacted respiration by silencing MCU or NCLX with siRNAs (Fig. S2). Interestingly, we found that overall cytosolic Ca<sup>2+</sup> levels were similar in these cells, despite the lack of these major mitochondrial Ca<sup>2+</sup> regulatory pathways (Fig. S3), both under basal conditions and after ER Ca<sup>2+</sup> depletion due to TG addition. Chronic inhibition of both channels led to a modest tendency toward a decrease in basal respiration (Fig. 6D,E), while MCU knockdown led to a significant decrease in maximal respiration (Fig. 6D,F). This shows that both short and long-term MCU inhibition impact on mitochondrial activity in intact hepatic cells.

## ***2.5. Ca<sup>2+</sup>-induced impairment of mitochondrial respiration in hepatocytes occurs secondarily to mPTP opening***

Having uncovered the effects of mitochondrial Ca<sup>2+</sup> cycling on cellular respiration under physiological conditions, we sought to dissect the reasons for decreased basal respiration induced by Ca<sup>2+</sup> release from the ER promoted by TG (Fig. 7). Acute MCU inhibition with RuRed (Fig. 7A-D), as well as chronic MCU inhibition with MCU knockdown (Fig. 7E-H) protects mitochondrial respiration against TG-induced decreases, indicating that Ca<sup>2+</sup> from the ER released by TG is taken up by mitochondria and affects electron transport. In line with this, cytosolic Ca<sup>2+</sup> chelation with BAPTA-AM also protected from TG-induced decrease of mitochondrial respiration (Fig. 8). Ca<sup>2+</sup> overload in mitochondria is known to promote the opening of mPTP (18-20), which can decrease OCRs by limiting mitochondrial cytochrome c content and affecting substrate import into the organelle. Thus, we incubated cells with TG in the presence of the mPTP inhibitor cyclosporin A (CsA), which efficiently prevented TG effects (Fig. 8), showing the involvement of mPTP in TG-induced OCR decrease.



### 3. Discussion

Mitochondria are well recognized as a major hub for calcium ( $\text{Ca}^{2+}$ ) handling and energy metabolism (1), however, the precise relationship between these two processes under physiologically relevant conditions in the liver was, surprisingly, not studied to date. Instead, small amounts of  $\text{Ca}^{2+}$  have been shown to increase the affinity of some matrix dehydrogenases, and thus assumed to possibly positively impact on ATP production. This assumption is a tricky one, since  $\text{Ca}^{2+}$  acts in different ways in mitochondria depending on concentration. Indeed, matrix  $\text{Ca}^{2+}$  overload is the focus of many studies, and has been shown to promote impairment of mitochondrial function and cell death (27) in a myriad of pathological conditions.

We designed two types of experiments aimed at understanding the effects of  $\text{Ca}^{2+}$  ions on oxidative phosphorylation in a more global manner, both focused on liver metabolism, as the effects of  $\text{Ca}^{2+}$  ions on this organ's rich metabolic activities have, surprisingly, not been dissected to date with respect to mitochondrial electron transport and ATP synthase activity. The first approach involved isolated mitochondria (Figs. 1-3), in which precise concentrations of extramitochondrial  $\text{Ca}^{2+}$  can be added, and the oxidation of different substrates can be examined while still preserving intact oxidative phosphorylation pathways, thus allowing to establish the impact of  $\text{Ca}^{2+}$  ions on overall metabolic fluxes.

Our results show that isolated liver mitochondria present enhanced oxidative phosphorylation efficiency promoted by  $\text{Ca}^{2+}$ , in a manner dependent on the substrate used and  $\text{Ca}^{2+}$  concentrations. Increased respiratory control ratios (RCRs) were achieved with low extramitochondrial  $\text{Ca}^{2+}$  ( $2.4 \pm 0.6 \mu\text{M}$ ) additions in the presence of the complex I substrates pyruvate plus malate (Fig. 1), and with medium  $\text{Ca}^{2+}$  ( $22.0 \pm 2.4 \mu\text{M}$ ) in the presence of  $\alpha$ -ketoglutarate (Fig. 2). Interestingly, previous reports show that pyruvate dehydrogenase (PDH) and  $\alpha$ -ketoglutarate dehydrogenase ( $\alpha$ -KGDH) are directly or indirectly activated by  $\text{Ca}^{2+}$  within the same concentration range (0.1 to 10  $\mu\text{M}$ ) in rat mitochondria from heart (30,31), skeletal muscle (32), adipose tissue (33) and liver (34). However, our results suggest that more  $\text{Ca}^{2+}$  is required to change  $\alpha$ -KGDH- versus PDH-supported respiration in mouse liver mitochondria (Figs. 1,2). This confirms that results showing changes in affinities of isolated enzymes cannot be used as predictors on metabolic fluxes in intact organelles; indeed, measured changes in affinity cannot predict metabolic fluxes without considering the concentrations of the substrates/intermediates,



as enzymes activated by  $\text{Ca}^{2+}$  may already be at their  $V_{\text{max}}$  in the microenvironment of the mitochondrial matrix.

On the other hand, when complex II substrate succinate was used, extramitochondrial  $\text{Ca}^{2+}$  did not modulate mitochondrial efficiency (Fig. 3). In line with this, recent results (28) show that isolated heart and kidney mitochondria exposed to pyruvate plus malate or  $\alpha$ -ketoglutarate plus malate have increased RCRs when in the presence of small increases in  $\text{Ca}^{2+}$  concentrations (in the nanomolar range), but had decreased RCRs when  $\text{Ca}^{2+}$  was further augmented. In contrast,  $\text{Ca}^{2+}$  addition to isolated brain mitochondria energized by pyruvate plus malate leads to reduced RCRs, in a concentration-dependent manner, with no effect on PDH activity (29). These results, overall, show that positive effects of  $\text{Ca}^{2+}$  on respiration are highly tissue-dependent, and, when present, occur within a tight range of concentrations.

A major concern regarding  $\text{Ca}^{2+}$  effects presented in the literature is a possible lack of homogeneity in  $\text{Ca}^{2+}$  concentrations used not only between different studies, but also in replicates within each study. Different  $\text{Ca}^{2+}$  amounts can be present in distinct isolated mitochondrial preparations, as these carry with them varying quantities of chelators from the isolation buffer. In order to minimize possible confounding results, we found it crucial to determine the amount of  $\text{Ca}^{2+}$  present after isolation daily and adjust  $\text{Ca}^{2+}$  added, so it was equal between biological replicates. This may have been a seminal feature which allowed us to uncover activating  $\text{Ca}^{2+}$  effects, as these were often subtle and concentration-specific. We also exclusively tested on respiration  $\text{Ca}^{2+}$  concentrations in which we observed no mitochondrial permeability transition pore (mPTP) opening, as indicated by the fact that mitochondrial preparations were able to uptake and retain the ion. Interestingly, the concentrations necessary to induce mPTP are different with distinct substrates, and larger for succinate (Fig. 3) than NADH-linked substrates (Fig. S1), thus allowing us to test more  $\text{Ca}^{2+}$  concentrations on respiration supported by succinate (with negative results).

But while isolated mitochondrial studies allow the dissection of precise effects of substrates and specific ion concentrations, they do not represent the metabolic state of oxidative phosphorylation in intact cells. Thus, our second approach was to modulate mitochondrial  $\text{Ca}^{2+}$  levels in the non-tumor AML12 hepatocyte cell line (25). In intact cells, overall  $\text{Ca}^{2+}$  concentrations are in the 100-150 nM range (Fig. S3), which is much lower than concentrations that activate oxidative phosphorylation in isolated mitochondria, but does not reflect differences in local ion concentrations, such as those

in the  $\text{Ca}^{2+}$ -rich mitochondrial-endoplasmic reticulum (ER) contact sites, where  $\text{Ca}^{2+}$  concentration may be up to 10 times higher than in the bulk cytosol (30-32).

We found that the  $\text{Ca}^{2+}$  concentrations in mitochondria *in situ* are both necessary and sufficient to enhance electron transport capacity through various different approaches. First, chelation of intracellular  $\text{Ca}^{2+}$  with BAPTA-AM decreased maximal OCR (Fig. 4C), without affecting mitochondrial membrane integrity, as indicated by the lack of change in oligomycin-insensitive respiration (Fig. 4A). Second, inhibition of mitochondrial  $\text{Ca}^{2+}$  uptake with ruthenium red (RuRed) or by silencing the mitochondrial  $\text{Ca}^{2+}$  uniporter (MCU) (Fig. 6) also decreased maximal electron transport capacity in intact cells, indicating that ideal respiratory chain function requires both the presence of physiological levels of cytosolic  $\text{Ca}^{2+}$  and its uptake by mitochondria. Our results are compatible with data showing that genetic manipulation of MCU and consequent impairment of mitochondrial  $\text{Ca}^{2+}$  uptake disrupts oxidative phosphorylation and lowers cellular ATP in HeLa cells (39). Similarly, mitochondria from a liver-specific MCU knockout mouse model also had inhibition of mitochondrial  $\text{Ca}^{2+}$  uptake and reduced oxidative phosphorylation (40).

Conversely, we increased cytosolic levels to ~200 nM by adding thapsigargin (TG) to induce ER  $\text{Ca}^{2+}$  depletion (Fig. S3, Fig. 4). TG is a well-known sarco-/endoplasmic reticulum  $\text{Ca}^{2+}$  ATPase (SERCA) pump inhibitor. SERCA is localized at mitochondrial-associated ER membrane microdomains where the ER and mitochondria are in close proximity, allowing for communication between both organelles and  $\text{Ca}^{2+}$  exchange (33,34). We also increased mitochondrial  $\text{Ca}^{2+}$  by inhibiting the NCLX extrusion pathway with CGP or silencing. Both strategies to increase  $\text{Ca}^{2+}$  in intact cells lead to lower maximal respiratory rates (Figs. 4 and 6), indicating that physiological  $\text{Ca}^{2+}$  levels in mitochondria are at the ideal level to maximize electron transport, with both decreases and increases leading to lower efficiency in this process. These results are in line with the finding that constitutive IP3R-mediated ER  $\text{Ca}^{2+}$  release to mitochondria is essential for efficient mitochondrial respiration and maintenance of normal cell bioenergetics (35). On the other hand, cells expressing a truncated variant of SERCA-1 with increased ER-mitochondria contact sites and increased  $\text{Ca}^{2+}$  transfer from the ER to mitochondria show signs of mitochondrial dysfunction due to  $\text{Ca}^{2+}$  overload (36).

Maximal OCR limitation observed under these conditions of  $\text{Ca}^{2+}$  overload in intact cells is due to uptake of the ion into the mitochondrial matrix, as it is inhibited by BAPTA-AM, MCU silencing or pharmacological inhibition (Figs. 7 and 8). Excess

mitochondrial  $\text{Ca}^{2+}$  is known to lead to mPTP opening and consequent dissipation of the mitochondrial membrane potential, mitochondrial swelling and rupture, culminating in cell death (18-20). Since the decrease in OCR observed under our conditions of mitochondrial  $\text{Ca}^{2+}$  overload was prevented by mPTP inhibitor cyclosporin A (CsA, Fig. 8), it is attributable to this form of mitochondrial inner membrane permeabilization.

While it may seem instinctively obvious that physiological resting mitochondrial  $\text{Ca}^{2+}$  levels would be at ideal quantities to activate maximum electron transport achievable, but not generate mitochondrial damage, it should be noted that not all intracellular signaling situations operate physiologically at maximum capacity. Perhaps the best example in this context is mitochondrial electron transfer itself, which is typically lower under basal conditions than maximum capacity uncovered when in the presence of uncoupler (see Figs. 4-8). Indeed, the difference between basal OCR and maximal achievable electron transport, known as reserve capacity, is thought to be important in resistance toward stress; a manner to allow fast increments in ATP synthesis when necessary (37). On the other hand, our results in hepatocytes show clearly that physiological  $\text{Ca}^{2+}$  levels in mitochondria are specifically those that maintain the highest maximal OCR without promoting mPTP. Overall, we demonstrate that hepatocytes maintain cellular and mitochondrial  $\text{Ca}^{2+}$  concentrations in strictly controlled ranges, maximizing electron transport capacity by promoting the Goldilocks  $\text{Ca}^{2+}$  “sweet spot” for oxidative phosphorylation activity: neither too much, nor too little, but just right.

## **4. Experimental procedures**

### **4.1. Reagents**

Culture medium (DMEM/F-12), fetal bovine serum (FBS), insulin-transferrin-selenium (ITS), Ca<sup>2+</sup> Green 5N and Pierce BCA protein assay kit were from Thermo Fischer Scientific (Waltham, MA, USA); thapsigargin, BAPTA-AM, CGP37157, ruthenium red, UK5099, BPTES, etomoxir and RIPA buffer were from Sigma-Aldrich (St. Louis, MO, USA); lipofectamine RNAiMAX, Trizol reagent and Fura-2 AM were from Invitrogen (Waltham, MA, USA); Bradford was from Bio-Rad Laboratories (Hercules, CA, USA); siRNAs against MCU (ID s103465), NCLX (ID s100747) or negative control (#4390844) were from Ambion Inc. (Austin, TX, USA); anti-MCU (#14997S) was from Cell Signaling (Danvers, MA, USA); anti- $\beta$ -actin (#ab8226) was from Abcam (Cambridge, UK); fluorescent secondary antibodies (goat anti-mouse #926-68070 and goat anti-rabbit #926-68071) were from Licor (Lincoln, NE, USA).

### **4.2. Animals**

C57BL/6NTac male mice were bred and housed in the animal facility of the Faculty of Pharmaceutical Sciences and Chemistry Institute of the University of São Paulo, devoid of murine pathogens. Animals were maintained in collective cages (max 4/cage) at controlled temperatures (23°C) in a 12–12 h light/dark cycle with free access to food/water. We used 10–12-week-old mice. All procedures were conducted in accordance with the Ethical Principles of Animal Manipulation of the local animal ethics committee, under protocol CEUA-IQ/USP 196/2021.

### **4.3. Isolation of liver mitochondria**

After deep anesthesia (4% isoflurane) followed by cervical dislocation, the abdomen was dissected and the liver was removed. Mitochondria were isolated by differential centrifugation. All steps were carried out at 4°C, over ice. Briefly, the liver was chopped into small pieces, suspended in isolation buffer (250 mM sucrose, 10 mM HEPES, 1 mM EGTA, 1 mM EDTA, 1 mg/ml BSA, pH 7.2) and manually homogenized using a Potter-Elvehjem tissue grinder. To remove blood from the mixture, it was centrifuged twice (800 g, 4°C, 4 min) and the pellet was discharged. The supernatant was further centrifuged at 9,000 g, 4°C for 10 min. The pellet was resuspended in resuspension buffer (300 mM sucrose, 10 mM HEPES and 2 mM EGTA, pH 7.2) and centrifuged again (9,000 g, 4°C,

10 min). The pellet was resuspended in 125  $\mu$ L of resuspension buffer and total protein was quantified using the Bradford method.

#### **4.4. Oxygen consumption by isolated liver mitochondria**

Oxygen consumption was measured using a high-resolution Oxygraph-2k (O2k) respirometer (Oroboros Instruments, Innsbruck, Austria). Mitochondria (600  $\mu$ g protein for pyruvate/malate and  $\alpha$ -ketoglutarate; 200  $\mu$ g protein for succinate/rotenone) were incubated in 2 mL of experimental buffer (125 mM sucrose, 65 mM KCl, 10 mM HEPES, 2 mM  $MgCl_2$ , 2 mM  $KH_2PO_4$  and 0.1 mg/ml BSA) containing 100  $\mu$ M EGTA and different substrates (1 mM pyruvate + 1 mM malate, 1 mM  $\alpha$ -ketoglutarate or 1 mM succinate + 1  $\mu$ M rotenone) and/or inhibitors (10  $\mu$ M ruthenium red or 10  $\mu$ M CGP37157) at 37°C with continuous stirring (700 rpm). After basal respiration was measured,  $CaCl_2$  was injected at different concentrations, as indicated. After reaching a steady state (as indicated by  $Ca^{2+}$  uptake measurements), state 3 respiration was measured by adding 1 mM ADP, followed by addition of 1  $\mu$ M oligomycin (State 4), and 0.5  $\mu$ M CCCP (state 3u). Respiratory control ratios (RCR) were calculated as State 3/State 4.

#### **4.5. Calcium ( $Ca^{2+}$ ) uptake assays**

$Ca^{2+}$  measurement assays were performed simultaneously to oxygen consumption measurements, in order to determine the approximate free extramitochondrial  $Ca^{2+}$  concentration and to monitor  $Ca^{2+}$  levels over time, as done in (38), as well as to monitor mPTP opening. Mitochondria (600  $\mu$ g protein for pyruvate/malate and  $\alpha$ -ketoglutarate; 200  $\mu$ g protein for succinate/rotenone) were incubated in 2 mL of the same experimental buffer used in the oxygen consumption assay, containing 0.1  $\mu$ M Calcium Green 5N, 100  $\mu$ M EGTA and different substrates and inhibitors, as indicated. Calcium Green fluorescence was measured at  $\lambda_{ex} = 506$  nm and  $\lambda_{em} = 532$  nm, using a F4500 and a F2500 Hitachi Fluorimeters at 37°C with continuous stirring. After a 100 s baseline interval, a  $CaCl_2$  solution was added to achieve the target  $Ca^{2+}$  concentrations (low, medium and high, as indicated), and fluorescence was monitored for 20 min. Each trace was followed by three 10  $\mu$ M  $Ca^{2+}$ , three 1 mM  $Ca^{2+}$ , and three 3 mM EGTA additions, to allow the estimation of the Calcium Green 5N experimental  $K_d$ , and maximal ( $F_{max}$ ) and minimal ( $F_{min}$ ) fluorescence, respectively. Absolute fluorescence values ( $F$ ) were calibrated into  $[Ca^{2+}]$  through the formula  $[Ca^{2+}] = K_d \cdot (F - F_{min}) / (F_{max} - F)$ .

#### **4.6. AML-12 cell cultures**

The hepatocyte AML-12 cell line was maintained in DMEM/F-12 medium supplemented with 10% (v/v) FBS, a mixture of insulin, transferrin, and selenium (ITS; Collaborative Research), 1% antibiotics (100 U/ml penicillin, 0.1 mg/ml streptomycin), pH 7.4, at 37°C in a humidified atmosphere of 5% CO<sub>2</sub>.

#### **4.7. Small interfering RNA (siRNA) transfection**

AML-12 cells were transfected with siRNAs against MCU, NCLX or scramble RNA as a negative control (Ambion Inc.), using Lipofectamine RNAiMAX and a reverse transfection protocol. Briefly, lipofectamine and siRNAs were diluted in Opti-MEM medium and were added to the cell suspension at a final concentration of 20 nM. Cells were kept overnight at 37°C in DMEM/F-12 containing ITS, without antibiotics. After transfection, the medium was replaced by complete medium. 48 h after transfection, cells were seeded for experiments and let for additional 24 h.

#### **4.8. RT-qPCR**

After transfections with siRNAs, AML-12 cells were collected with Trizol™ Reagent and RNA was isolated following the manufacturer's instructions. Total RNA was quantified using a NanoDrop® spectrophotometer and cDNA synthesis was performed using the High-Capacity cDNA Reverse Transcription Kit. qPCR reactions were performed using the Platinum® SYBR® Green qPCR SuperMix-UDG along with specific primers for *Mcu* (FW 5'-ACTCACCAGATGGCGTTCG-3'; RV 5'-CATGGCTTAGGAGGTCTCTCTT-3'), *Nclx* (FW 5'-TGTCACCTTCCTGGCCTTTG-3'; RV 5'-CACCCCTGCACCAAACAGA-3'), *Hmbs* (FW 5'-CAGCTACAGAGA AAGTTCCCC-3'; RV 5'-AGGACGATGGCACTGAATTC-3') and *B2m* (FW 5'-CTGGTCTTTCTATATCCTGGCTC-3'; RV 5'-TGCTTGATCACATGTCTCGATC-3') genes. Amplification data was analyzed by the 2<sup>(-ΔΔCt)</sup> method using the mean of *Hmbs* and *B2m* Ct values as housekeeping. The housekeeping choice was based on the stability value of the gene or combination of genes calculated by the NormFinder Software (39).

#### **4.9. Western blot**

In order to validate MCU silencing, we performed a western blot analysis of MCU levels in transfected AML-12 cells. Briefly, cells were lysed in RIPA buffer containing protease and phosphatase inhibitor cocktails, and total protein levels were quantified using Pierce

BCA Protein Assay kit. Lysates were prepared in sample buffer (2% SDS, 10% Glycerol, 0.062 M Tris pH 6.8, 0.002% Bromophenol Blue, 5% 2-mercaptoethanol), loaded onto SDS-PAGE gels and electrotransferred to PVDF membranes. Membranes were blocked with 5% BSA in TTBS (20 mM Tris pH 7.5, 150 mM NaCl and 0.1% Tween 20) for 1 hour at room temperature before overnight incubation with MCU (1:1,000) and  $\beta$ -actin (1:5,000) primary antibodies at 4°C. Fluorescent secondary antibodies (1:15,000) were incubated for 1 hour at room temperature prior to fluorescence detection using a ChemiDoc™ Imaging System (Bio-Rad). Quantification of band densitometry was performed using the FIJI ImageJ software.

#### **4.10. Cytosolic $Ca^{2+}$ measurements**

After MCU or NCLX silencing, AML-12 cells were seeded at  $1.5 \times 10^6$  cells in 4 mL complete medium in 60 mm cell culture dishes. After 24 h, cells were loaded with 5  $\mu$ M Fura-2 AM for 1 h at 37°C. After the loading period, cells were trypsinized and suspended in Krebs-Henseleit buffer without  $CaCl_2$  (115 mM NaCl, 24 mM  $NaHCO_3$ , 5 mM KCl, 1 mM  $MgSO_4$ , 1.2 mM  $KH_2PO_4$ ).  $1 \times 10^6$  cells (final volume: 2 mL) were checked for basal cytosolic  $Ca^{2+}$  levels and after ER  $Ca^{2+}$  depletion with thapsigargin using a F4500 Hitachi Fluorimeter at 37°C with continuous stirring. Fluorescence was measured at excitation 340/380 nm and emission 505 nm. Each trace was followed by 4% Triton X-100 (50  $\mu$ L) and 60 mM EGTA (150  $\mu$ L) additions, to allow the estimation of maximal ( $R_{max}$ ) and minimal ( $R_{min}$ ) fluorescence ratio, respectively. Intracellular  $Ca^{2+}$  concentrations,  $[Ca^{2+}]_i$ , were calculated as described in (40) through the formula  $[Ca^{2+}]_i$  (nM) =  $K_d \times [(R - R_{min}) / (R_{max} - R)] \times S_{fb}$ , where the  $K_d$  for  $Ca^{2+}$  binding to Fura-2 at 37°C = 225 nM and  $S_{fb}$  is the ratio of baseline fluorescence at 380 nm.

#### **4.11. Oxygen consumption in intact AML-12 cells**

Cells were seeded at 30,000 cells per well in 100  $\mu$ L DMEM/F-12 medium (with 10% FBS, 1% P/S, ITS) on Agilent Seahorse XF24 cell culture microplates and allowed to adhere overnight. Oxygen consumption was measured using a Seahorse Extracellular Flux Analyzer (Agilent Technologies, Santa Clara, CA, EUA). For that, cells were washed thrice with 500  $\mu$ L DMEM/F-12 containing 1% P/S and 5 mM HEPES. Media did not contain bicarbonate nor FBS. Cells were kept for 1 h in a humidified incubator at 37°C without  $CO_2$ , in the absence or presence of different additions (BAPTA-AM, 10  $\mu$ M ruthenium red, 10  $\mu$ M CGP37157), as indicated. After incubation, plates were placed in



the equipment and oxygen consumption rates (OCR) were measured under basal conditions, followed by different injections: a) thapsigargin (TG, final concentration: 2  $\mu\text{M}$ ) or same volume of DMSO in control wells; b) oligomycin (final concentration: 1  $\mu\text{M}$ ); c) CCCP (final concentration: 5  $\mu\text{M}$ ); d) antimycin and rotenone (R/AA, final concentration: 1  $\mu\text{M}$  each). Cell-free wells were incubated with same medium for background correction, calculated by subtracting changes observed from the experiments in the presence of cells. OCR values obtained were normalized per amount of total protein in each well. For that, at the end of each experiment, the medium was removed, cells were PBS-washed, lysed with RIPA buffer, and total protein was quantified using the BCA Pierce protocol.

#### ***4.12. Substrate oxidation test***

Different substrate oxidation effects on respiration were evaluated using inhibitors for three primary substrates that fuel mitochondria: glucose/pyruvate (12  $\mu\text{M}$  UK5099), glutamine (8  $\mu\text{M}$  BPTES) and long-chain fatty acids (14  $\mu\text{M}$  Etomoxir). Oxygen consumption was measured in AML-12 cells in suspension using a high-resolution O2k respirometer (Oroboros Instruments).  $1 \times 10^6$  cells were incubated in 2 mL of the same medium used in Seahorse experiments in the absence or presence of 2  $\mu\text{M}$  thapsigargin and/or inhibitors, at 37°C with continuous stirring (400 rpm). After basal respiration, 1  $\mu\text{M}$  oligomycin was injected, followed by 5  $\mu\text{M}$  CCCP, to calculate maximal respiration.

#### ***4.13. Statistical analysis***

Statistical analysis was carried out using GraphPad Prism 8 Software for at least three independent experiments (biological replicates). Student's t test was used to compare differences between treated and untreated conditions and One-way ANOVA followed by Sidak was used to compare multiple conditions, with confidence levels set to  $p < 0.05$ . Data shown in scatter graphs are individual biological replicates, averages and standard deviations.



## Figure legends

**Figure 1. Ca<sup>2+</sup> uptake increases liver mitochondrial oxidative phosphorylation supported by pyruvate and malate.** Isolated mouse liver mitochondria (600 µg) were incubated with 1 mM pyruvate + 1 mM malate. **A)** Representative Ca<sup>2+</sup> uptake curves measured using Ca<sup>2+</sup> Green N to measure extramitochondrial Ca<sup>2+</sup>, in the presence of low Ca<sup>2+</sup> (2.4 ± 0.6 µM, black line) and medium Ca<sup>2+</sup> (22.0 ± 2.4 µM, blue line) concentrations. **B-D)** Representative O<sub>2</sub> consumption rate (OCR) traces using a high-resolution Oxygraph-2k (O2k) respirometer in response to no Ca<sup>2+</sup> (**B**), low Ca<sup>2+</sup> (**C**) and medium Ca<sup>2+</sup> (**D**) additions, followed by injection of 1 mM ADP, 1 µM oligomycin and 0.5 µM CCCP. **E)** State 3, after ADP injection. **F)** State 4, after oligomycin injection. **G)** Respiratory control ratios (RCR, state 3 / state 4). **H)** RCR in the presence of low Ca<sup>2+</sup> and 10 µM CGP37157 (CGP) or 10 µM ruthenium red (RuRed). N = 4 independent experiments. \*p<0.05 versus control using One-way ANOVA followed by Sidak.

**Figure 2. Ca<sup>2+</sup> uptake increases liver mitochondrial oxidative phosphorylation supported by α-ketoglutarate.** Isolated mouse liver mitochondria (600 µg) were energized with 1 mM α-ketoglutarate. **A)** Representative Ca<sup>2+</sup> uptake curves in the presence of low Ca<sup>2+</sup> (2.4 ± 0.6 µM, black line) and medium Ca<sup>2+</sup> (22.0 ± 2.4 µM, blue lines). **B-D)** Representative OCR traces with zero Ca<sup>2+</sup> (**B**), low Ca<sup>2+</sup> (**C**) and medium Ca<sup>2+</sup> (**D**), followed by injection of 1 mM ADP, 1 µM oligomycin and 0.5 µM CCCP. **E)** State 3, after ADP injection. **F)** State 4, after oligomycin injection. Respiratory control ratio (RCR, state 3 / state 4). **H)** RCR in the presence of medium Ca<sup>2+</sup> and CGP or RuRed. N = 4 independent experiments. \*p<0.05 and \*\*p<0.01 versus control using One-way ANOVA followed by Sidak.

**Figure 3. Ca<sup>2+</sup> uptake does not increase liver mitochondrial oxidative phosphorylation supported by succinate.** Isolated mouse liver mitochondria (200 µg) were energized with 1 mM succinate in the presence of 1 µM rotenone. **A)** Representative Ca<sup>2+</sup> uptake curves in the presence of low Ca<sup>2+</sup> (2.4 ± 0.6 µM, black line), medium Ca<sup>2+</sup> (22.0 ± 2.4 µM, blue line) and high Ca<sup>2+</sup> (52.9 ± 2.5 µM, purple line). **B-E)** Representative OCR traces in response to no Ca<sup>2+</sup> (**B**), low Ca<sup>2+</sup> (**C**), medium Ca<sup>2+</sup> (**D**), and high Ca<sup>2+</sup> (**E**), followed by injection of 1 mM ADP, 1 µM oligomycin and 0.5 µM CCCP. **F)** State 3, after ADP injection. **G)** State 4, after oligomycin injection. **H)** Respiratory control

ratios (RCR, state 3 / state 4). N = 4 independent experiments. \* $p < 0.01$  versus control using One-way ANOVA followed by Sidak.

**Figure 4. Depletion of intracellular  $\text{Ca}^{2+}$  stores in hepatocytes limits maximal mitochondrial respiration.** **A-C)** AML12 cells were pre-incubated for 1 h in the absence (control) or presence of a cytosolic  $\text{Ca}^{2+}$  chelator, BAPTA-AM, at different concentrations (5 - 20  $\mu\text{M}$ , as shown), and OCRs was measured using a Seahorse Extracellular Flux Analyzer. **C-E)** OCRs was measured under basal conditions, followed by the injection of DMSO (diluent) or thapsigargin (TG, 0.2, 0.5 or 2  $\mu\text{M}$  as indicated). Oligomycin (oligo, 1  $\mu\text{M}$ ), CCCP (5  $\mu\text{M}$ ) and rotenone + antimycin (R/AA, 1  $\mu\text{M}$  each) were added to all traces as indicated. Results are expressed as representative traces (**A**, **D**) or means  $\pm$  SEM (B, C, E, F) of 5 independent biological experiments. \* $p < 0.05$  and \*\*\* $p < 0.001$  versus control using One-way ANOVA followed by Sidak.

**Figure 5. Intracellular  $\text{Ca}^{2+}$  modulates mainly mitochondrial pyruvate oxidation.** AML12 cells were incubated in the absence (CT) or presence of 2  $\mu\text{M}$  thapsigargin (TG) and inhibitors (12  $\mu\text{M}$  UK5099, 8  $\mu\text{M}$  BPTES or 14  $\mu\text{M}$  Etomoxir). OCRs were measured under basal conditions, followed by injection of oligomycin (oligo, 1  $\mu\text{M}$ ) and CCCP (5  $\mu\text{M}$ ), to induce maximal respiration. **A)** Quantification of basal respiration. **B)** Quantification of maximal respiration. Results are expressed as means  $\pm$  SEM of 4 independent experiments. \* $p < 0.05$  versus respective untreated control using Student's t-test.

**Figure 6. Mitochondrial  $\text{Ca}^{2+}$  uptake increases maximal, but not basal, respiration in intact hepatocytes.** **A-C)** Cells were incubated for 1 h in the absence (control) or presence of 10  $\mu\text{M}$  of RuRed or CGP. **D-F)** AML12 with siRNAs against MCU (siMCU) or NCLX (siNCLX) or a negative control (siCT). **A,D)** OCRs were measured using a Seahorse Extracellular Flux Analyzer; oligomycin (oligo, 1  $\mu\text{M}$ ), CCCP (5  $\mu\text{M}$ ), and rotenone + antimycin (R/AA, 1  $\mu\text{M}$  each) were added where indicated. **B,E)** Quantification of basal respiration. **C,F)** Quantification of maximal respiration. Results are expressed as means  $\pm$  SEM of 3–4 independent experiments. \* $p < 0.05$  versus control using Student's t-test.

**Figure 7. High intracellular Ca<sup>2+</sup> limits maximal respiration in a manner dependent on mitochondrial Ca<sup>2+</sup> uptake. A-D)** Cells were incubated for 1 h in the absence (CT) or presence of 10 μM of RuRed or CGP. **E-H)** Cells treated with specific siRNAs against the MCU (siMCU) or NCLX (siNCLX) or a negative control (siCT). OCRs were measured in a Seahorse Extracellular Flux Analyzer under basal conditions, followed by injection of DMSO (diluent) or 2 μM thapsigargin (TG), oligomycin (oligo, 1 μM), CCCP (5 μM) and rotenone + antimycin (R/AA, 1 μM each). **C, D)** Quantifications of basal and **(G,H)** maximal respiration. Results are expressed as mean ± SEM of 3–4 independent experiments. \*p<0.05 and \*\*\*p<0.001 versus respective control using Student's t-test.

**Figure 8. Respiratory inhibition promoted by excess Ca<sup>2+</sup> is due to mPTP. A-C)** OCRs were under basal conditions followed by injection of i) DMSO (diluent) or 2 μM thapsigargin (TG) or 10 μM cyclosporin A (CsA) or TG + CsA, ii) oligomycin (oligo, 1 μM), iii) CCCP (5 μM) and iv) rotenone + antimycin (R/AA, 1 μM each). **B)** Cells were pre-incubated for 1 h in the absence or presence of a cytosolic Ca<sup>2+</sup> chelator, 10 μM BAPTA-AM (BAPTA), before OCR measurements. **D)** Quantification of basal respiration. **E)** Quantification of maximal respiration. Results are expressed as mean ± SEM of 4 independent experiments. \*p<0.05 and \*\*p<0.01 versus respective control using Student's t-test.

**Figure S1. High Ca<sup>2+</sup> concentration leads to mPTP opening in liver mitochondria in the presence of pyruvate plus malate or α-ketoglutarate. A,B)** Representative Ca<sup>2+</sup> uptake curves measured using Ca<sup>2+</sup> Green N, in the presence of high Ca<sup>2+</sup> concentrations. Isolated mouse liver mitochondria (600 μg) were incubated with 1 mM pyruvate plus 1 mM malate (pyr + mal, **A**) or 1 mM α-ketoglutarate (α-KG, **B**). Calcium uptake by mitochondria leads to a decrease in fluorescence over the first few minutes, which was not maintained over time, indicating lack of mitochondrial ability to maintain high Ca<sup>2+</sup> uptake over the experimental time period.

**Figure S2. MCU and NCLX silencing. A)** NCLX mRNA levels after 48, 72 and 96 h of transfection with specific siRNA against NCLX (siNCLX) or a negative control (siCT). **B)** MCU mRNA levels after 48 and 72 h of transfection with specific siRNA against MCU (siMCU) or a negative control (siCT). **C)** Representative western blots of MCU and β-actin (internal control) after 72 h of transfection with specific siRNA against

MCU (siMCU) or a negative control (siCT). **D)** Densitometric analysis of the Western blots. \* $p < 0.05$  and \*\*\* $p < 0.0001$  versus respective control using Student's t-test.

**Figure S3. Cytosolic Ca<sup>2+</sup> levels in siMCU or siNCLX cells are preserved.** **A)** Typical cytosolic Ca<sup>2+</sup> measurements performed using Fura-2. **B)** Quantification under basal conditions. **C)** Quantification of the peak after the addition of thapsigargin.

### **Data availability**

All data are contained within the manuscript and supporting information.

### **Acknowledgements**

This work was supported mainly by the *Fundação de Amparo à Pesquisa do Estado de São Paulo* (FAPESP) under grant numbers 13/07937-8, 17/14713-0, 19/18402-4, and 21/02481-2, as well as the *Conselho Nacional de Desenvolvimento Científico e Tecnológico* (CNPq) and *Coordenação de Aperfeiçoamento de Pessoal de Nível Superior* (CAPES) line 001. We acknowledge Silvânia M. P. Neves and her animal facility crew for exceptional expert animal care.

### **Conflict of interest**

The authors declare that they have no conflicts of interest.

### **Author contributions**

E.A.V.-B. and A.J.K. are responsible for concept and design; E.A.V.-B., J.V.C.-C., V.M.R. and C.C.C.S. performed experiments; E.A.V.-B., J.V.C.-C. and A.J.K. interpreted the data and discussed the results; E.A.V.-B. and A.J.K. prepared figures and drafted the manuscript; all authors revised and approved final version of manuscript.

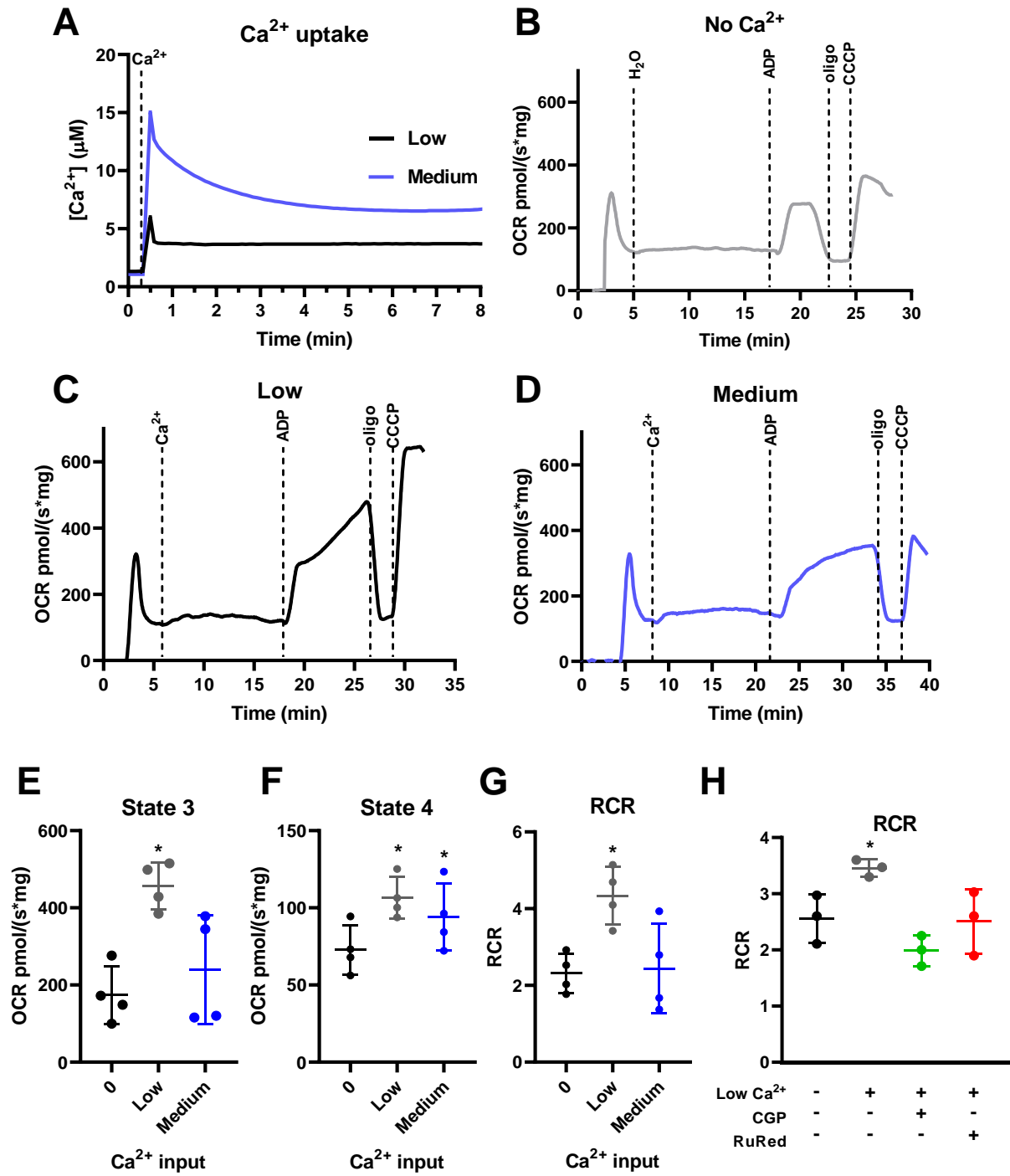
## REFERENCES

1. Giorgi, C., Marchi, S., and Pinton, P. (2018) The machineries, regulation and cellular functions of mitochondrial calcium. *Nat Rev Mol Cell Biol* **19**, 713-730
2. Deluca, H. F., and Engstrom, G. W. (1961) Calcium uptake by rat kidney mitochondria. *Proc Natl Acad Sci U S A* **47**, 1744-1750
3. Vasington, F. D., and Murphy, J. V. (1962) Ca ion uptake by rat kidney mitochondria and its dependence on respiration and phosphorylation. *J Biol Chem* **237**, 2670-2677
4. Budd, S. L., and Nicholls, D. G. (1996) A reevaluation of the role of mitochondria in neuronal Ca<sup>2+</sup> homeostasis. *J Neurochem* **66**, 403-411
5. Hartmann, J., and Verkhratsky, A. (1998) Relations between intracellular Ca<sup>2+</sup> stores and store-operated Ca<sup>2+</sup> entry in primary cultured human glioblastoma cells. *J Physiol* **513 ( Pt 2)**, 411-424
6. Williams, G. S., Boyman, L., Chikando, A. C., Khairallah, R. J., and Lederer, W. J. (2013) Mitochondrial calcium uptake. *Proc Natl Acad Sci U S A* **110**, 10479-10486
7. Naon, D., and Scorrano, L. (2014) At the right distance: ER-mitochondria juxtaposition in cell life and death. *Biochim Biophys Acta* **1843**, 2184-2194
8. Kirichok, Y., Krapivinsky, G., and Clapham, D. E. (2004) The mitochondrial calcium uniporter is a highly selective ion channel. *Nature* **427**, 360-364
9. Baughman, J. M., Perocchi, F., Girgis, H. S., Plovanich, M., Belcher-Timme, C. A., Sancak, Y., Bao, X. R., Strittmatter, L., Goldberger, O., Bogorad, R. L., Koteliansky, V., and Mootha, V. K. (2011) Integrative genomics identifies MCU as an essential component of the mitochondrial calcium uniporter. *Nature* **476**, 341-345
10. De Stefani, D., Raffaello, A., Teardo, E., Szabò, I., and Rizzuto, R. (2011) A forty-kilodalton protein of the inner membrane is the mitochondrial calcium uniporter. *Nature* **476**, 336-340
11. Palty, R., Silverman, W. F., Hershinkel, M., Caporale, T., Sensi, S. L., Parnis, J., Nolte, C., Fishman, D., Shoshan-Barmatz, V., Herrmann, S., Khananshvil, D., and Sekler, I. (2010) NCLX is an essential component of mitochondrial Na<sup>+</sup>/Ca<sup>2+</sup> exchange. *Proc Natl Acad Sci U S A* **107**, 436-441
12. [preprint] Austin, S., Mekis, R., Mohammed, S. E. M., Scalise, M., Pfeiffer, C., Galluccio, M., Borovec, T., Parapatics, K., Vitko, D., Dinhopl, N., Bennett, K. L., Indiveri, C., and Nowikovsky, K. (2021) MICS1 is the Ca<sup>2+</sup>/H<sup>+</sup> antiporter 1 of mammalian mitochondria. BioRxiv. 10.1101/2021.11.11.468204v1
13. [preprint] Patron, M., Tarasenko, D., Nolte, H., Ghosh, M., Ohba, Y., Lasarzewski, Y., Ahmadi, Z. A., Cabrera-Orefice, A., Eyiyama, A., Kellermann, T., Rugarli, E. I., Brandt, U., Meinecke, M., and Langer, T. (2021) Regulation of mitochondrial proteostasis by the proton gradient. BioRxiv. 10.1101/2021.12.12.470907

14. Denton, R. M., and McCormack, J. G. (1985)  $\text{Ca}^{2+}$  transport by mammalian mitochondria and its role in hormone action. *Am J Physiol* **249**, E543-554
15. Hansford, R. G. (1985) Relation between mitochondrial calcium transport and control of energy metabolism. *Rev Physiol Biochem Pharmacol* **102**, 1-72
16. Rossi, A., Pizzo, P., and Filadi, R. (2019) Calcium, mitochondria and cell metabolism: A functional triangle in bioenergetics. *Biochim Biophys Acta Mol Cell Res* **1866**, 1068-1078
17. Denton, R. M. (2009) Regulation of mitochondrial dehydrogenases by calcium ions. *Biochim Biophys Acta* **1787**, 1309-1316
18. Haworth, R. A., and Hunter, D. R. (1979) The  $\text{Ca}^{2+}$ -induced membrane transition in mitochondria. II. Nature of the  $\text{Ca}^{2+}$  trigger site. *Arch Biochem Biophys* **195**, 460-467
19. Jia, K., and Du, H. (2021) Mitochondrial permeability transition: a pore intertwines brain aging and alzheimer's disease. *Cells* **10** (3), 649
20. Modesti, L., Danese, A., Angela Maria Vitto, V., Ramaccini, D., Aguiari, G., Gafà, R., Lanza, G., Giorgi, C., and Pinton, P. (2021) Mitochondrial  $\text{Ca}^{2+}$  signaling in health, disease and therapy. *Cells* **10** (6), 1317
21. Bravo-Sagua, R., Parra, V., López-Crisosto, C., Díaz, P., Quest, A. F., and Lavandero, S. (2017) Calcium transport and signaling in mitochondria. *Compr Physiol* **7**, 623-634
22. Filadi, R., and Greotti, E. (2021) The yin and yang of mitochondrial  $\text{Ca}^{2+}$  signaling in cell physiology and pathology. *Cell Calcium* **93**, 102321
23. Brand, M. D., and Nicholls, D. G. (2011) Assessing mitochondrial dysfunction in cells. *Biochem J* **435**, 297-312
24. Cassim, S., Raymond, V. A., Lapierre, P., and Bilodeau, M. (2017) From in vivo to in vitro: major metabolic alterations take place in hepatocytes during and following isolation. *PLoS One* **12**, e0190366
25. Wu, J. C., Merlino, G., and Fausto, N. (1994) Establishment and characterization of differentiated, nontransformed hepatocyte cell lines derived from mice transgenic for transforming growth factor alpha. *Proc Natl Acad Sci U S A* **91**, 674-678
26. Ferrick, D. A., Neilson, A., and Beeson, C. (2008) Advances in measuring cellular bioenergetics using extracellular flux. *Drug Discov Today* **13**, 268-274
27. Duchen, M. R., Verkhatsky, A., and Muallem, S. (2008) Mitochondria and calcium in health and disease. *Cell Calcium* **44**, 1-5
28. Zhang, X., Tomar, N., Kandel, S. M., Audi, S. H., Cowley, A. W., and Dash, R. K. (2021) Substrate- and calcium-dependent differential regulation of mitochondrial oxidative phosphorylation and energy production in the heart and kidney. *Cells* **11** (1), 131
29. Pandya, J. D., Nukala, V. N., and Sullivan, P. G. (2013) Concentration dependent effect of calcium on brain mitochondrial bioenergetics and oxidative stress parameters. *Front Neuroenergetics* **5**, 10

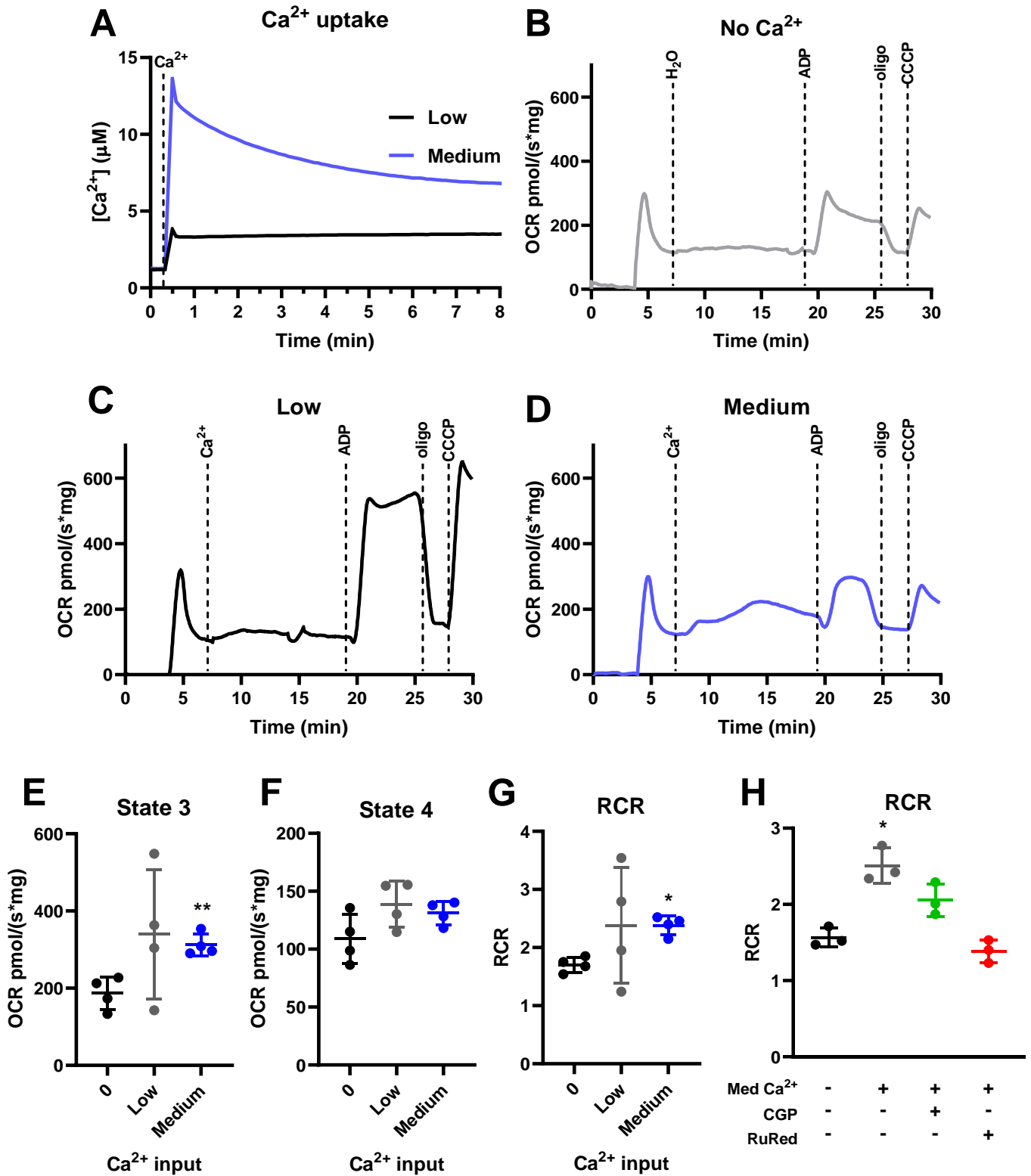


30. Tubbs, E., and Rieusset, J. (2017) Metabolic signaling functions of ER-mitochondria contact sites: role in metabolic diseases. *J Mol Endocrinol* **58**, R87-R106
31. Rizzuto, R., and Pozzan, T. (2006) Microdomains of intracellular  $Ca^{2+}$ : molecular determinants and functional consequences. *Physiol Rev* **86**, 369-408
32. Cremer, T., Neefjes, J., and Berlin, I. (2020) The journey of  $Ca^{2+}$  through the cell – pulsing through the network of ER membrane contact sites. *J Cell Sci* **133**
33. Lee, S., and Min, K. T. (2018) The interface between ER and mitochondria: molecular compositions and functions. *Mol Cells* **41**, 1000-1007
34. Csordás, G., Weaver, D., and Hajnóczky, G. (2018) Endoplasmic reticulum-mitochondrial contactology: structure and signaling functions. *Trends Cell Biol* **28**, 523-540
35. Cárdenas, C., Miller, R. A., Smith, I., Bui, T., Molgó, J., Müller, M., Vais, H., Cheung, K. H., Yang, J., Parker, I., Thompson, C. B., Birnbaum, M. J., Hallows, K. R., and Foskett, J. K. (2010) Essential regulation of cell bioenergetics by constitutive InsP3 receptor  $Ca^{2+}$  transfer to mitochondria. *Cell* **142**, 270-283
36. Chami, M., Oulès, B., Szabadkai, G., Tacine, R., Rizzuto, R., and Paterlini-Bréchet, P. (2008) Role of SERCA1 truncated isoform in the proapoptotic calcium transfer from ER to mitochondria during ER stress. *Mol Cell* **32**, 641-651
37. Hill, B. G., Benavides, G. A., Lancaster, J. R., Ballinger, S., Dell'Italia, L., Jianhua, Z., and Darley-Usmar, V. M. (2012) Integration of cellular bioenergetics with mitochondrial quality control and autophagy. *Biol Chem* **393**, 1485-1512
38. Kowaltowski, A. J., Menezes-Filho, S. L., Assali, E. A., Gonçalves, I. G., Cabral-Costa, J. V., Abreu, P., Miller, N., Nolasco, P., Laurindo, F. R. M., Bruni-Cardoso, A., and Shirihai, O. S. (2019) Mitochondrial morphology regulates organellar  $Ca^{2+}$  uptake and changes cellular  $Ca^{2+}$  homeostasis. *FASEB J* **33**, 13176-13188
39. Andersen, C. L., Jensen, J. L., and Ørntoft, T. F. (2004) Normalization of real-time quantitative reverse transcription-PCR data: a model-based variance estimation approach to identify genes suited for normalization, applied to bladder and colon cancer data sets. *Cancer Res* **64**, 5245-5250
40. Patel, A., Hirst, R. A., Harrison, C., Hirota, K., and Lambert, D. G. (2013) Measurement of  $[Ca^{2+}]_i$  in whole cell suspensions using Fura-2. *Methods Mol Biol* **937**, 37-47

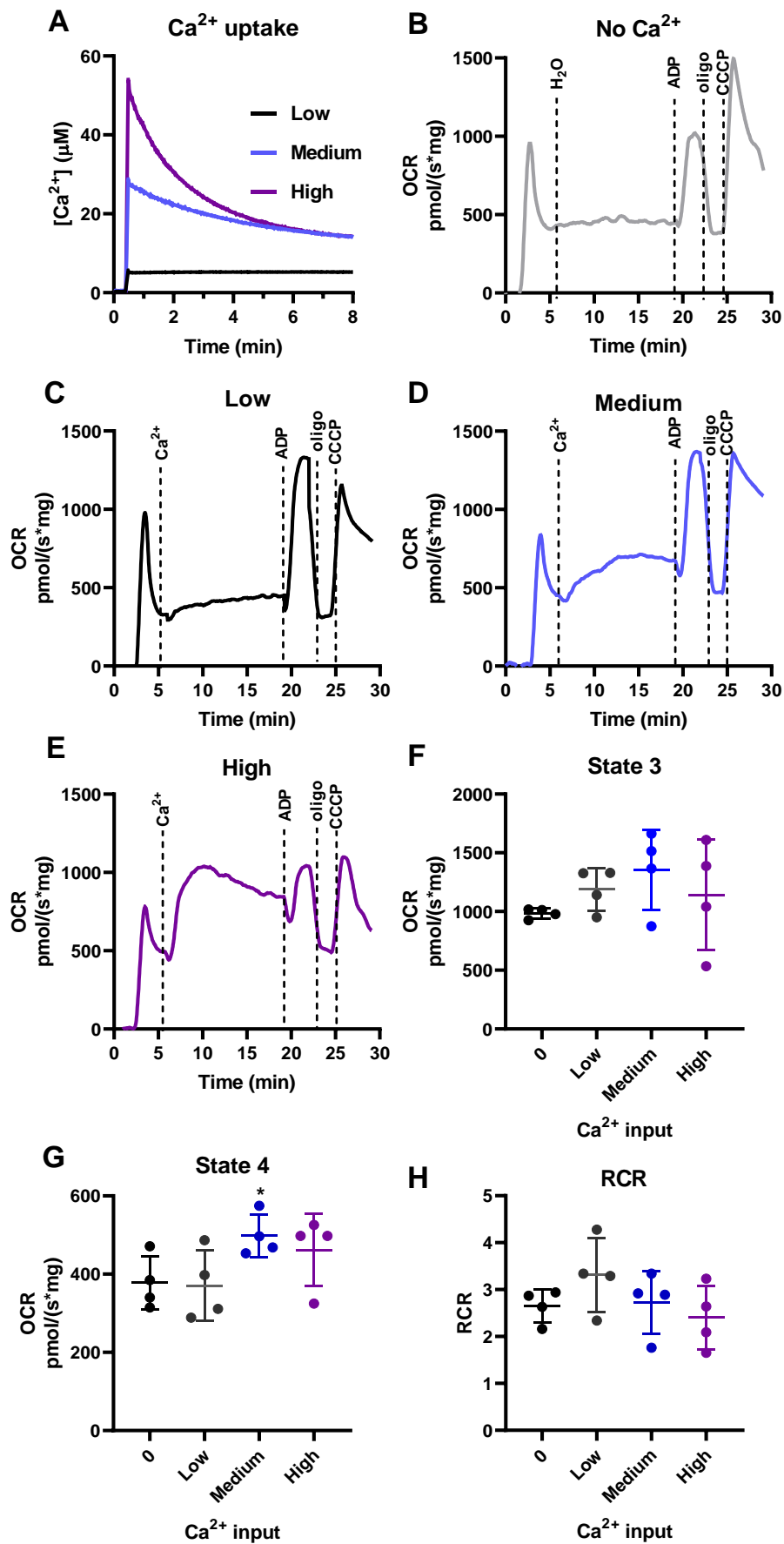


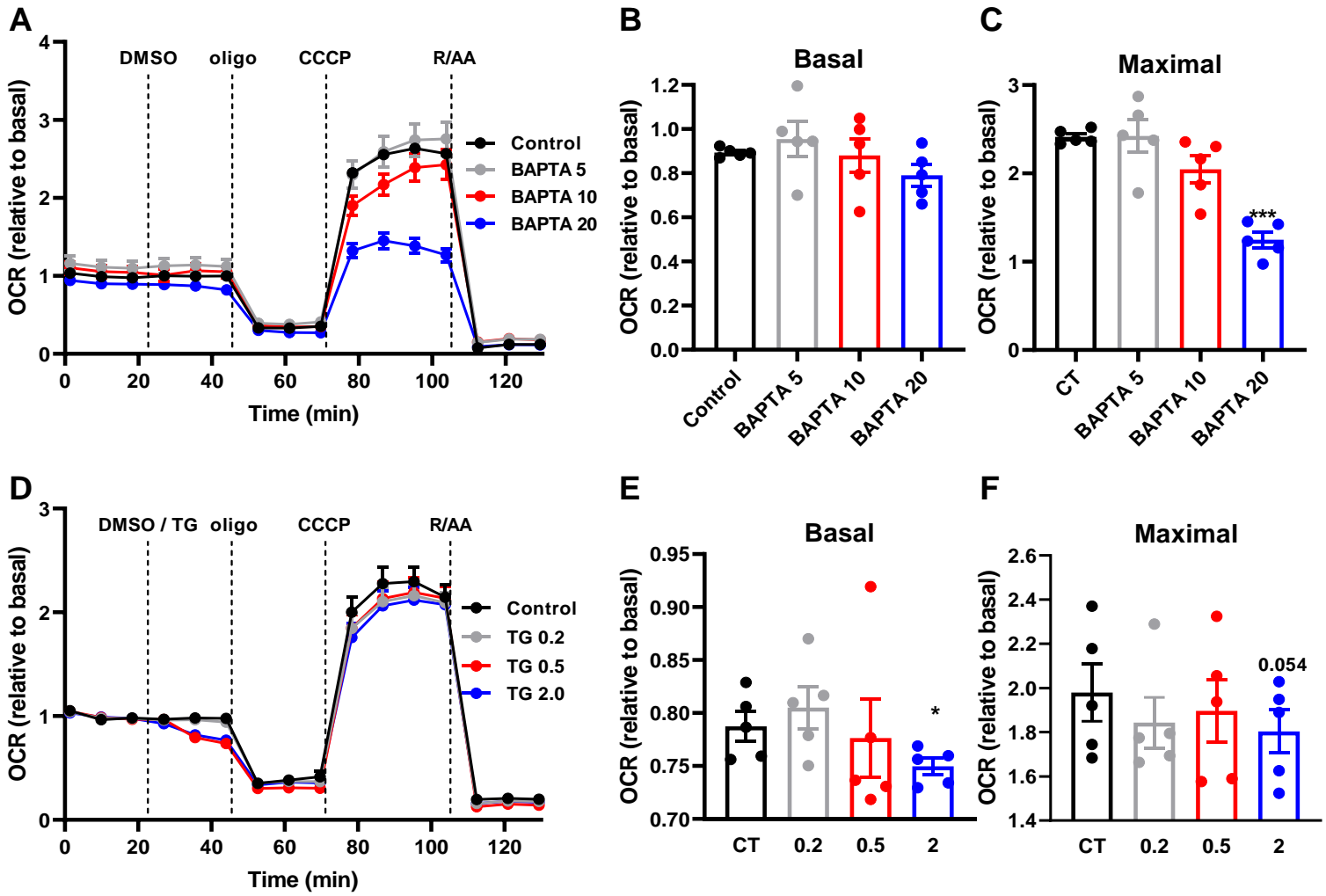
Vilas-Boas et al., 2022, Fig. 1



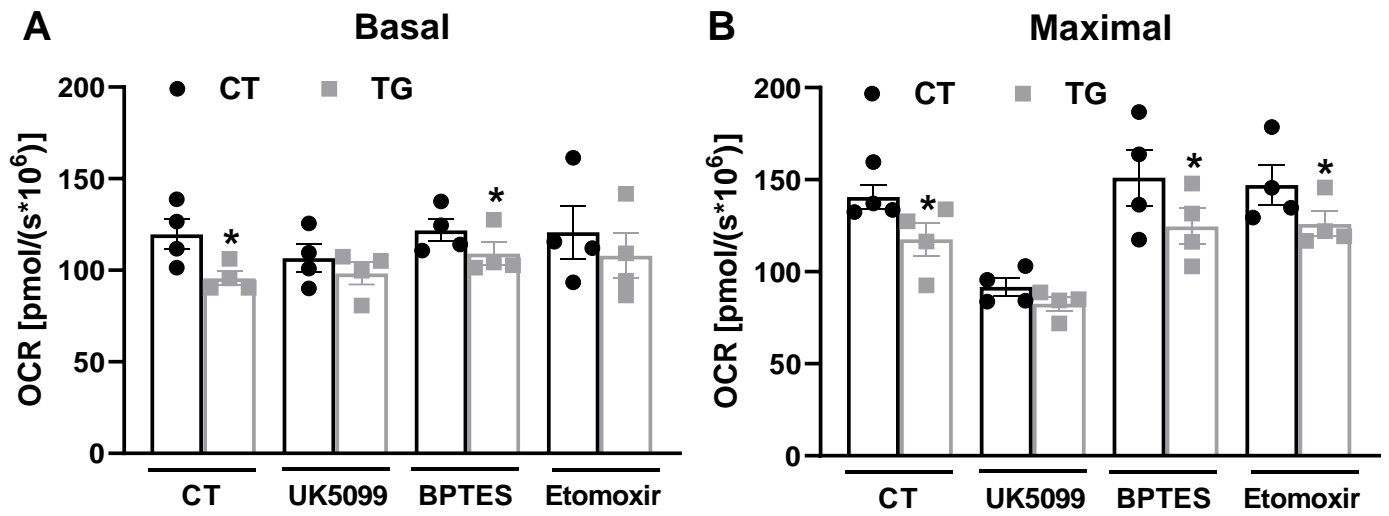


Vilas-Boas et al., 2022, Fig. 2

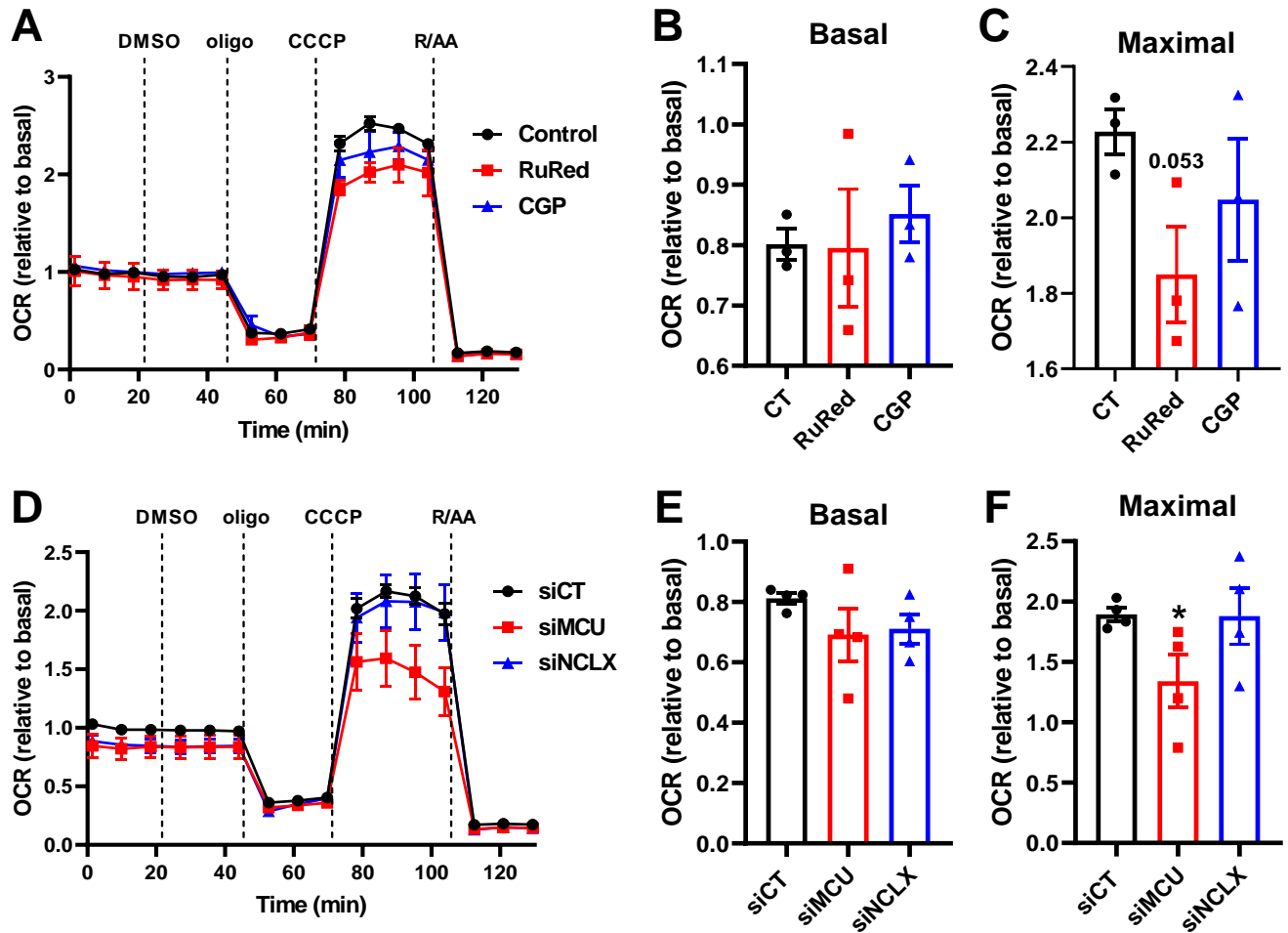




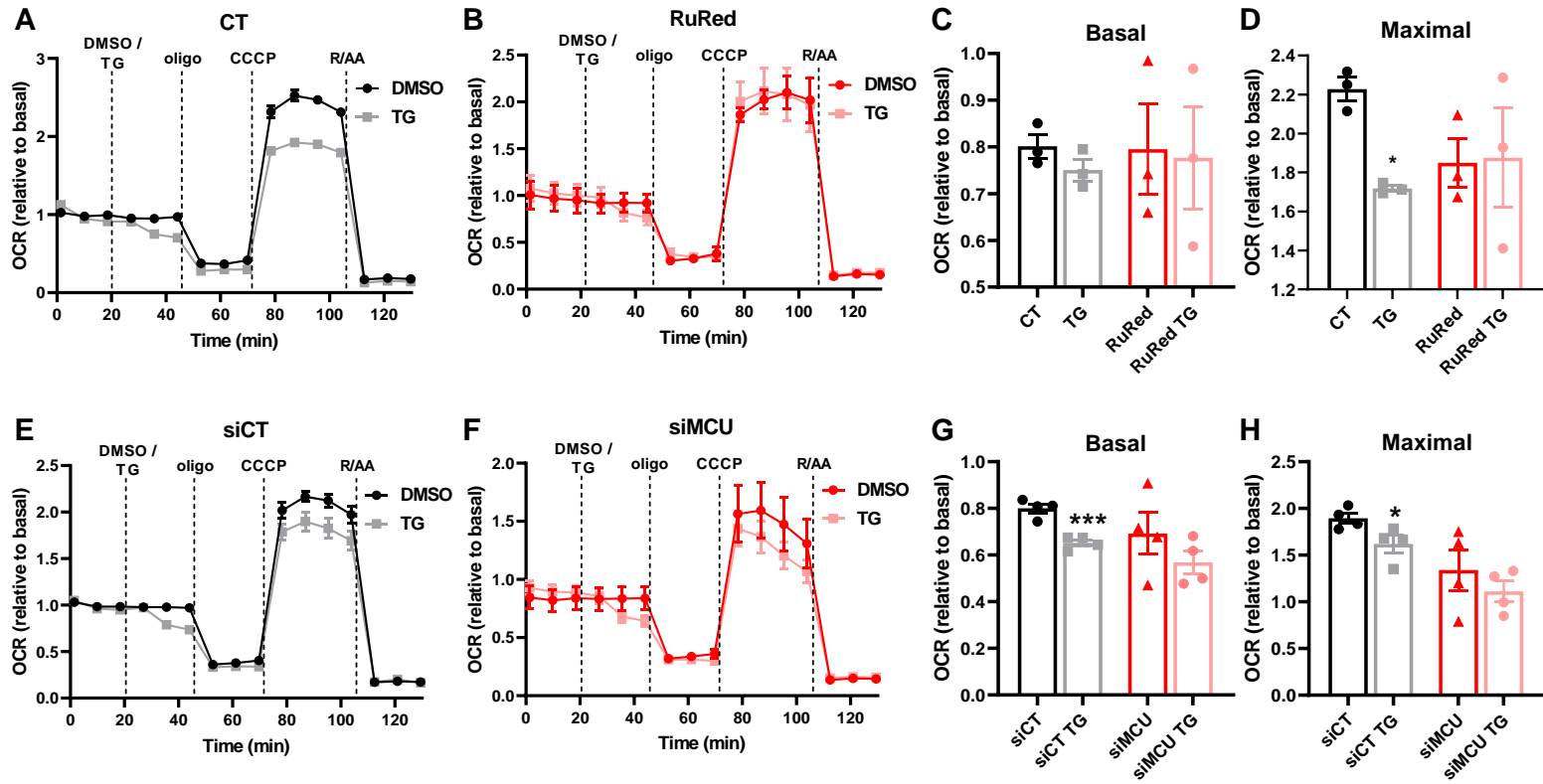
Vilas-Boas et al., 2022, Fig. 4



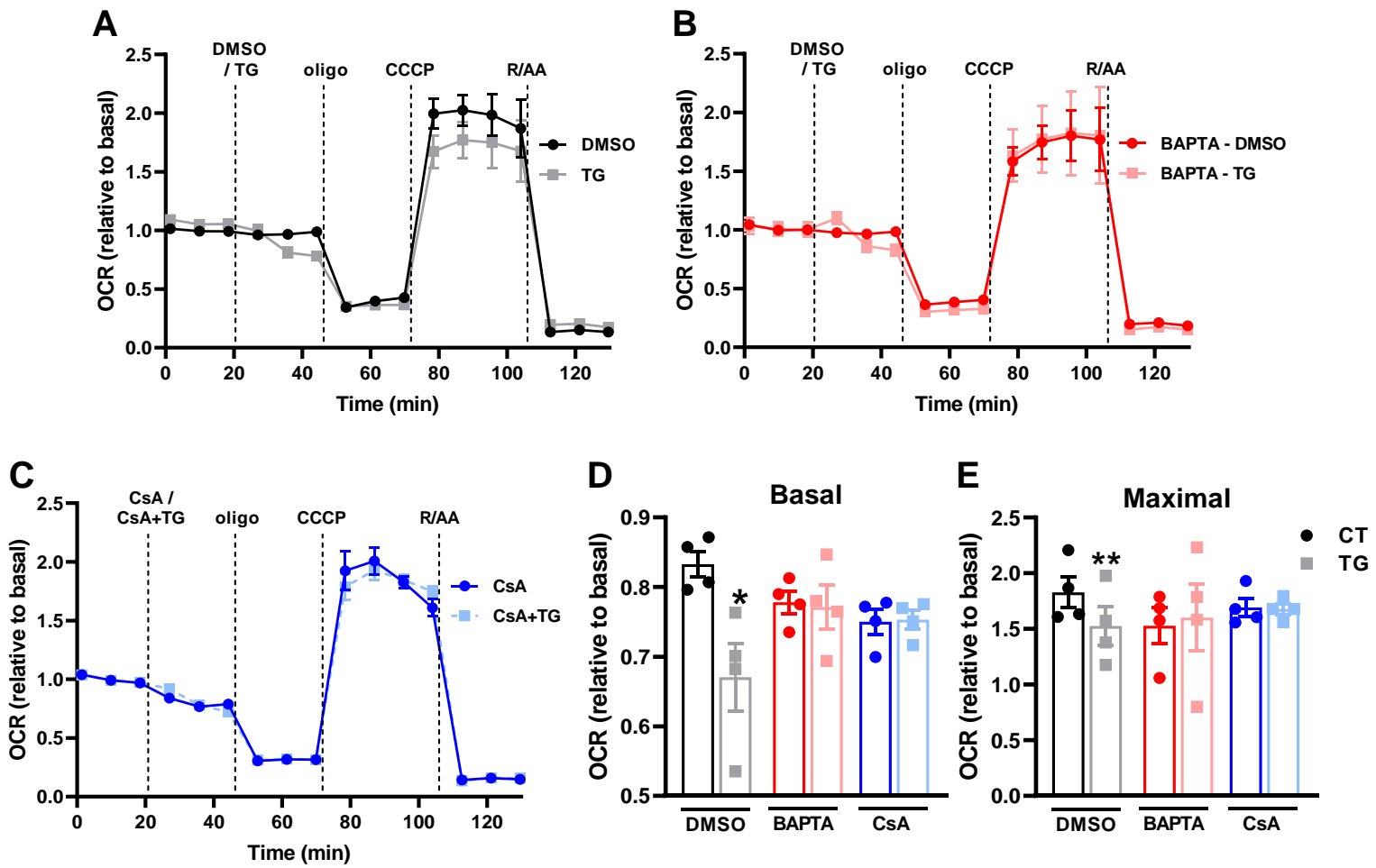
Vilas-Boas et al., 2022, Fig. 5



Vilas-Boas et al., 2022, Fig. 6

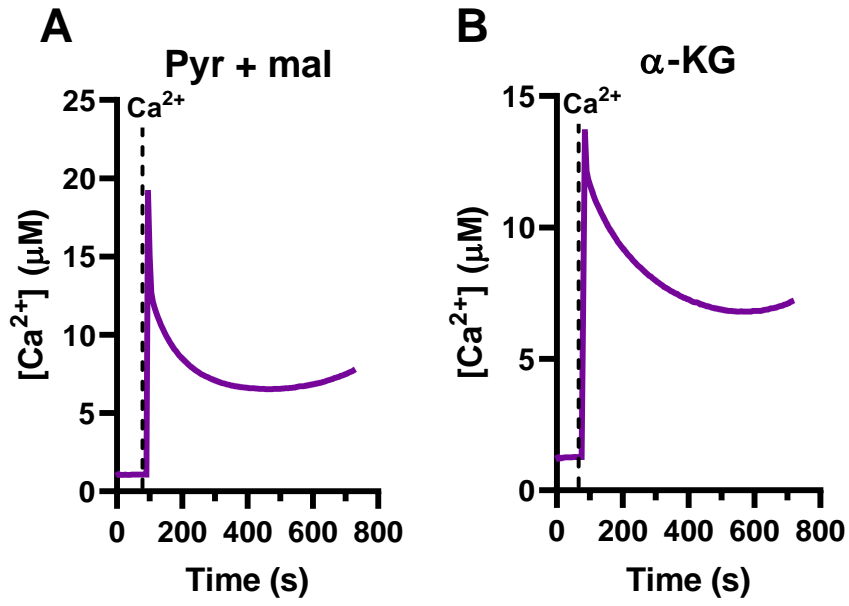


Vilas-Boas et al., 2022, Fig. 7

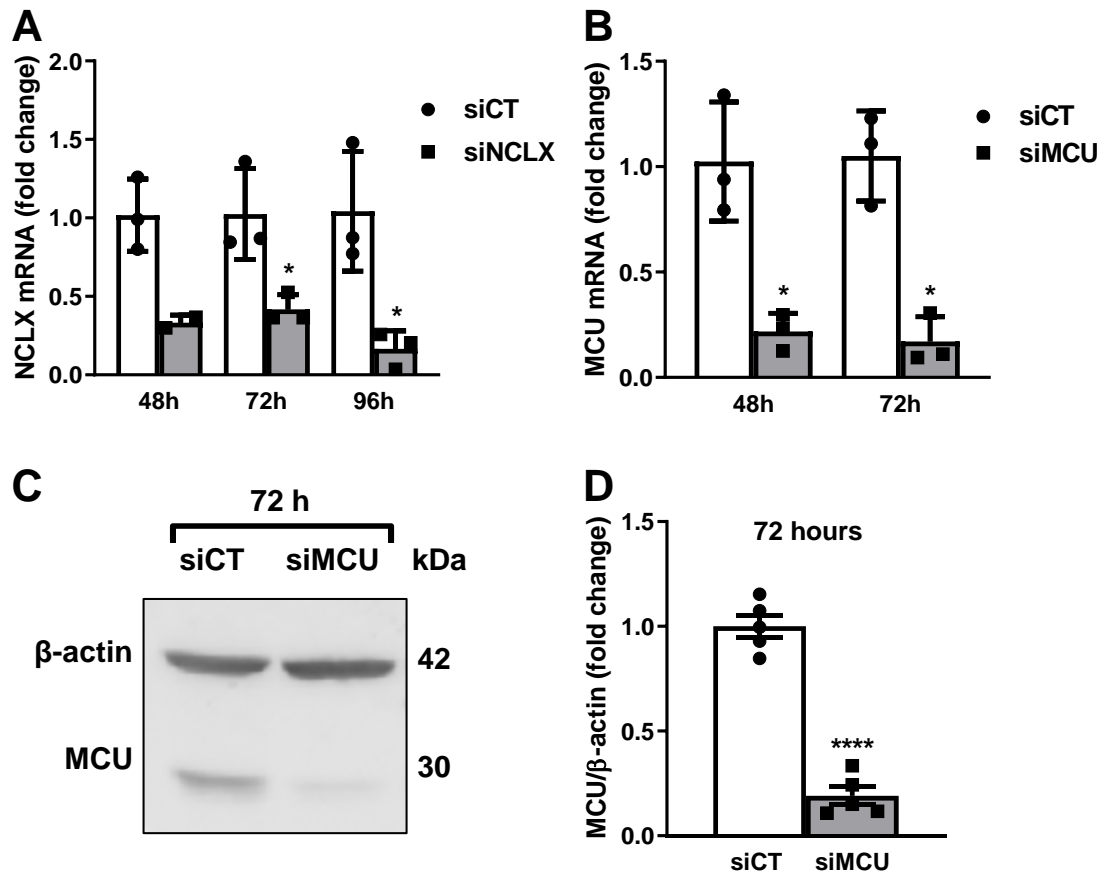


Vilas-Boas et al., 2022, Fig. 8

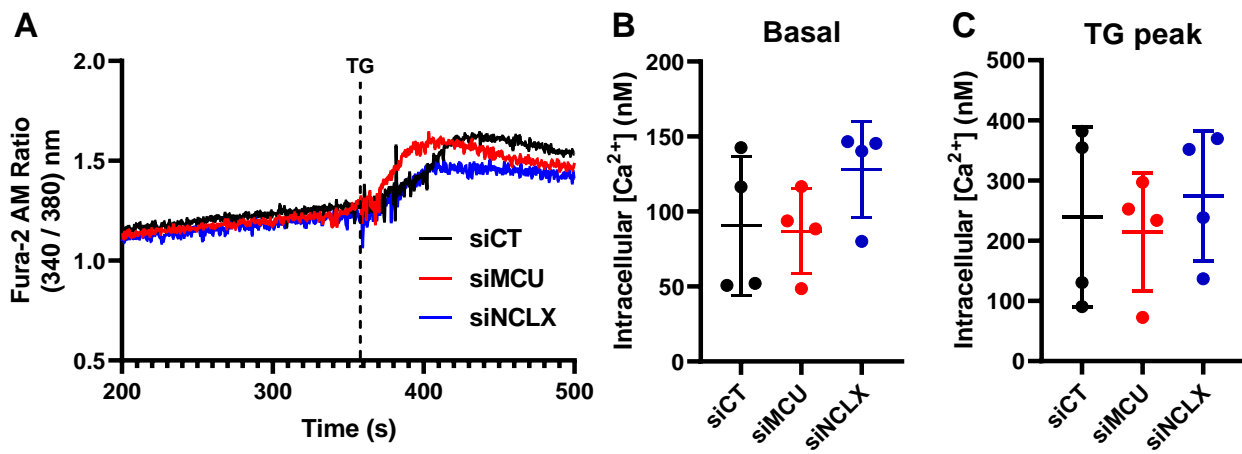




Vilas-Boas et al., 2022, Supplementary Fig. 1



Vilas-Boas et al., 2022, Supplementary Fig. 2



Vilas-Boas et al., 2022, Supplementary Fig. 3

## **ANNEX E**

**Serna et al., 2022**

**(Bioenerg. Comm., 2022:0007)**

**Technical communication**

**Cite**

Serna JDC, Ramos VM, Cabral-Costa JV, Vilas-Boas EA, Amaral AG, Ohya G, Caldeira da Silva CC, Kowaltowski AJ (2022) Measuring mitochondrial Ca<sup>2+</sup> efflux in isolated mitochondria and permeabilized cells. <https://doi.org/10.26124/bec:2022-0007>

**Author contributions**

Data collection and analysis was performed by JDCS, JVCC, VMR, EAVB, AGA, GO, and CCCS. All authors wrote the manuscript. VMR contributed all artwork. JDCS and AJK conceived and designed the framework of the manuscript.

**Conflicts of interest**

The authors declare they have no conflict of interest.

**Academic editor**

Christos Chinopoulos

**Reviewers**

Cristiane Cecatto  
 Nicolas Place

**Copyeditors**

Luiza Cardoso  
 Erich Gnaiger  
 Lisa Tindle-Solomon

Received 2022-05-13

Reviewed 2022-06-28

Resubmitted 2022-07-06

Accepted 2022-07-06

Published 2022-07-28

**Editorial and peer review record:**

<https://doi.org/10.26124/bec:2022-0007>

**Data availability**









The raw data used for this manuscript are available upon reasonable request to the corresponding author.

**Preprint**

MitoFit Preprints 2022.7

<https://doi.org/10.26124/mitofit:2022-0021>

# Measuring mitochondrial Ca<sup>2+</sup> efflux in isolated mitochondria and permeabilized cells

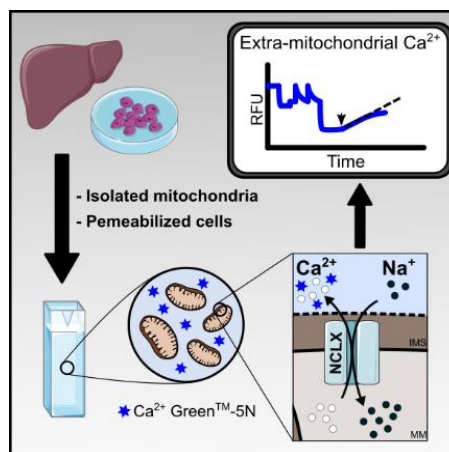
 Julian DC Serna<sup>1</sup>,  Vitor de Miranda Ramos<sup>1</sup>,  João Victor Cabral-Costa<sup>1</sup>,  Eloisa A Vilas-Boas<sup>1</sup>,  Andressa G Amaral<sup>2</sup>,  Georgia Ohya<sup>1</sup>,  Camille C Caldeira da Silva<sup>1</sup>,  Alicia J Kowaltowski<sup>1,\*</sup>

<sup>1</sup> Departamento de Bioquímica, Instituto de Química, Universidade de São Paulo, 05508-900, Brazil

<sup>2</sup> Departamento de Fisiologia, Instituto de Ciências Biomédicas, Universidade de São Paulo, 05509-900, Brazil

\* Corresponding author: [alicia@iq.usp.br](mailto:alicia@iq.usp.br)

**Abstract**



Mitochondrial Ca<sup>2+</sup> efflux is essential for mitochondrial and cell Ca<sup>2+</sup> homeostasis. Mitochondrial inner membrane Ca<sup>2+</sup>/H<sup>+</sup> and Na<sup>+</sup>/Li<sup>+</sup>/Ca<sup>2+</sup> (NCLX) exchangers are known today to be plastic transporters, with important roles in physiological responses and pathological states.

Until now, however, no consensus protocols were available to measure mitochondrial Ca<sup>2+</sup> efflux, and we find that some published protocols may induce mitochondrial permeability transition, underestimating the effects of these exchangers. In this work, we describe a method to measure Na<sup>+</sup>-sensitive and insensitive mitochondrial Ca<sup>2+</sup> efflux activity in isolated mitochondria and permeabilized cells using the Ca<sup>2+</sup> Green indicator and a fluorimeter. A checklist is provided to avoid artifacts as well as pinpoint adaptations necessary in specific experimental models.

**Keywords** – mitochondria; Ca<sup>2+</sup> efflux; NCLX; mtPTP; liver

## 1. Introduction

Mitochondria are metabolic and signaling hubs, essential players in the life and death of eukaryotic cells (Spinelli, Haigis 2018; Giacomello et al 2020). Their ability to take up, store, and release calcium ( $\text{Ca}^{2+}$ ) in a regulated manner helps shape spatiotemporal features of  $\text{Ca}^{2+}$  signaling events (Rizzuto et al 2012). Small and transient increases in  $\text{Ca}^{2+}$  within mitochondria physiologically regulate both oxidative phosphorylation and the production of oxidants but can also mediate organellar damage when in excessive amounts (Rossi et al 2019; Vercesi et al 2018; Vilas-Boas et al 2022). Mitochondrial  $\text{Ca}^{2+}$  uptake and release take place through independent pathways, and both activities are supported by protonmotive force (Giorgi et al 2018).

The MCU complex (MCUc) is the most active pathway for  $\text{Ca}^{2+}$  uptake (Figure 1) (Feno et al 2021). Conversely, three main pathways have been described for  $\text{Ca}^{2+}$  efflux (Giorgi et al 2018): (1) a  $\text{Ca}^{2+}/\text{H}^+$  exchanger, the protein nature of which still lacks in consensus; (2) the sodium ( $\text{Na}^+$ ) / lithium ( $\text{Li}^+$ ) /  $\text{Ca}^{2+}$  exchanger (NCLX) that mediates  $\text{Na}^+$ -dependent  $\text{Ca}^{2+}$  release (Palty et al 2010); and (3) the mitochondrial permeability transition pore (mtPTP), which is a high conductance pathway that unselectively releases small molecules, including  $\text{Ca}^{2+}$ . mtPT is commonly induced by mitochondrial  $\text{Ca}^{2+}$  overload and oxidative imbalance (Figure 1) (Vercesi et al 2018).

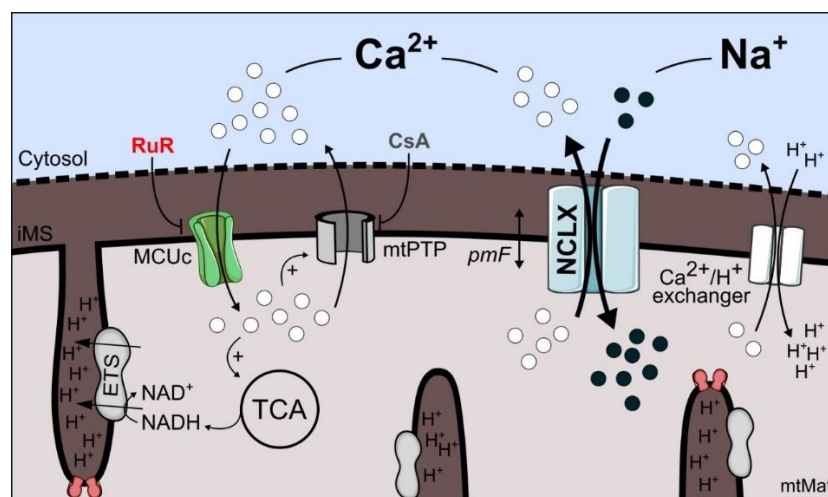


**Figure 1. Mitochondrial inner membrane  $\text{Ca}^{2+}$  transport pathways.**  $\text{Ca}^{2+}$  entry into the mitochondrial matrix (mtMat) from the intermembrane space (iMS) is mediated by the MCU complex (MCUc), a ruthenium red (RuR)-sensitive pathway.  $\text{Ca}^{2+}$  stimulates tricarboxylic acid cycle (TCA) dehydrogenases and inner mitochondrial membrane substrate transport.  $\text{Ca}^{2+}$  overload stimulates the formation of a high conductance pathway for  $\text{Ca}^{2+}$  efflux: the cyclosporin A (CsA)-inhibited mitochondrial permeability transition pore (mtPTP).  $\text{Ca}^{2+}/\text{H}^+$  and  $\text{Na}^+/\text{Li}^+/\text{Ca}^{2+}$  (NCLX) exchangers avoid matrix  $\text{Ca}^{2+}$  overload under physiological conditions. Both pathways depend on the proton electrochemical potential difference ( $pmF$ ) generated by the electron transfer system (ETS).

$\text{Na}^+$ -dependent mitochondrial  $\text{Ca}^{2+}$  efflux through NCLX has emerged as an important regulator of different cellular processes and may be a promising therapeutic target for diseases such as cancer (Pathak et al 2020) and Alzheimer's (Jadiya et al 2019).

Thus, reliable protocols to test modulators of NCLX activity, as well as to investigate changes in its function, are needed. A comprehensive protocol would distinguish different efflux pathways and can be used for *in vivo* and *in vitro* studies.

Here, we briefly discuss the current pros and cons of available approaches to measure mitochondrial  $\text{Ca}^{2+}$  efflux and provide a step-by-step protocol to assess  $\text{Ca}^{2+}$  efflux rates in isolated mitochondria or permeabilized cells, focusing mainly on the activity of NCLX. We also discuss important experimental precautions that are essential to achieve reliable measurements.

### 1.1. Mitochondrial $\text{Ca}^{2+}$ transport measurements in living cells

In experiments using living cells,  $\text{Ca}^{2+}$  concentrations ( $[\text{Ca}^{2+}]$ ) are commonly assessed through imaging methods using either genetically encoded (Cameleons, Pericams, Aequorins, etc) or exogenous  $\text{Ca}^{2+}$  probes (such as acetoxymethyl esters of Fura 2 or  $\text{Ca}^{2+}$  Green<sup>TM</sup>-5N), some of which can uncover  $\text{Ca}^{2+}$  signaling events at the subcellular level (Whitaker 2010; Gryniewicz et al 1985; Minta et al 1989; Rudolf et al 2003). The free  $[\text{Ca}^{2+}]$  in each cell compartment is the result of the balance between  $\text{Ca}^{2+}$  uptake, efflux, binding to chelators, and the formation of precipitates (Williams et al 2013).

Mitochondrial  $\text{Ca}^{2+}$  transport (uptake and efflux) is often studied by measuring cytoplasmic and matrix  $[\text{Ca}^{2+}]$  during a signaling event. Although this approach does measure mitochondrial  $\text{Ca}^{2+}$  transport in a more physiological state, the complexity of the system does not always allow for accurate determinations of sources and mechanisms in which changes occur. Modulation of endoplasmic reticulum (ER)  $\text{Ca}^{2+}$  stores or the activity of plasma membrane  $\text{Ca}^{2+}$  transporters may alter cytoplasmic signals independently of mitochondrial ionic transport. Indeed,  $\text{Ca}^{2+}$  levels in the mitochondrial matrix are determined by several factors that involve mitochondrial  $\text{Ca}^{2+}$  uptake and extrusion properties, the proximity with the ER or plasma membrane, their ability to buffer or precipitate  $\text{Ca}^{2+}$ , and the matrix volume, among other factors (de Brito, Scorrano 2008; Nita et al 2012; Kuo et al 2019; Kowaltowski et al 2019). Notably, the formation of  $\text{Ca}^{2+}$  precipitates in the matrix makes it difficult to obtain true measurements of  $\text{Ca}^{2+}$  flux using these techniques, as it underestimates total uptake into the organelle. Other limitations in whole cell measurements involve difficulties with the use of pharmacological inhibitors, which often have off-target effects.

### 1.2. Assessment of mitochondrial $\text{Ca}^{2+}$ transport in isolated mitochondrial preparations

A more reductionist approach to study  $\text{Ca}^{2+}$  transport using isolated mitochondrial samples solves several of the pitfalls mentioned above, although it does not, of course, uncover conditions *in situ*. On the other hand, the mitochondrial microenvironment can be tightly controlled with isolated preparations, including the availability/concentration of substrates, inhibitors, and ions ( $\text{Na}^+$ ,  $\text{Ca}^{2+}$ , and  $\text{Li}^+$ ). Modulators such as ruthenium red (RuR – an MCU inhibitor) or CGP-37157 (CGP – an NCLX inhibitor) can dissect the effects of uptake and efflux pathways (Cox et al 1993).

Mitochondrial isolation from organs, tissues, or cell cultures relies on differential centrifugation and/or the use of density gradients (Gnaiger et al 2020; Gnaiger 2020). Mitochondrial isolation from cell cultures can be laborious and require large amounts of cells; in these models, permeabilized cell protocols are a more suitable option, as

discussed below. Isolation of mitochondria from organs is easier and in general gives good yields. While the reductionist approach using isolated mitochondria facilitates specific measurements and decreases artifacts, the physiological relevance of this approach is limited, and several caveats should be noted (Gnaiger et al 2020; Gnaiger 2020; Schmidt et al 2021), including that the mitochondrial population is biased, as swollen mitochondria may be lost during isolation, and the composition of the media does not truly reflect the cytoplasm. Several cytoplasmic components, such as proteins and metabolites, are essential regulators of mitochondrial function. In isolated brain mitochondria, for example, the absence of adenine nucleotides deeply impairs their ability to take up and store Ca<sup>2+</sup>. In these cases, it is important to add ADP/ATP to the buffer (Kristian et al 2002; Amigo et al 2017). Finally, morphology and interactions with other cell components, such as membranes and cytoskeleton, are expectedly lost in isolated mitochondrial preparations.

Because of Ca<sup>2+</sup> precipitation in the matrix, which leads to underestimation of total uptake when using intramitochondrial probes, extracellular Ca<sup>2+</sup> probes can be more accurate choices to measure mitochondrial Ca<sup>2+</sup> fluxes. Mitochondrial Ca<sup>2+</sup> uptake assays to determine entry rates as well as uptake capacity are more frequently performed than efflux assays (examples can be seen in Amigo et al 2017; Serna et al 2020; Serna et al 2022). While quite straightforward, authors should note that the fluorescence of extramitochondrial probes can be influenced by media composition, making calibration under different conditions essential (Rudolf et al 2003).

Mitochondrial efflux assays are less commonly performed and have the added difficulty that distinguishing between the different pathways (Ca<sup>2+</sup>/H<sup>+</sup>, NCLX, or mtPTP) may be tricky. The main problems with measurements of Ca<sup>2+</sup>/H<sup>+</sup> and NCLX activity are related to the masking effect of mtPT induction. As mitochondria must be loaded with Ca<sup>2+</sup> to measure extrusion, permeability transition is often induced in at least a subset of the mitochondrial population, as we will show below. Since Ca<sup>2+</sup> efflux through the exchangers is supported by protonmotive force, mtPT hampers the detection of the activity of both exchangers (Haworth et al 1980; Boyman et al 2013; Giorgi et al 2018).

### **1.3. Assessment of mitochondrial Ca<sup>2+</sup> transport in permeabilized cells**

Permeabilized cell models represent a midway option between living cell studies and isolated mitochondrial approaches (Fiskum et al 1980; Schmidt et al 2021). While they preserve cell architecture and the relationship between some organelles, they allow for direct control and access to the mitochondrial microenvironment, including precise Ca<sup>2+</sup> uptake and release measurements using extramitochondrial Ca<sup>2+</sup> sensors. Permeabilization is promoted by using substances such as digitonin,  $\alpha$ -tomatin, or saponin to disrupt the integrity of the plasma membrane, preserving mitochondrial membranes, as well as mitochondrial morphology, interactions with other cell components, and function. This is achieved by titration of these detergents, and using the fact that mitochondria are poor in cholesterol (Fiskum et al 1980; Fiskum et al 2000; Vercesi et al 1991; Kuznetsov et al 2008; Saks et al 1998). Plasma membrane permeabilization establishes a continuity between the cytoplasm and the extracellular medium, allowing for experiments that modulate mitochondrial function directly, and avoiding any limitation imposed by the plasma membrane for substrate, inhibitor, or ion availability. Additional ion transport activities exerted by non-mitochondrial membranes



such as the ER are also excluded by permeabilization or using specific inhibitors as controls.

## 2. Mitochondrial Ca<sup>2+</sup> efflux – isolated mitochondria

Isolated mitochondria may be obtained using many different protocols, and choices depend largely on the experimental model being studied. Here, we isolated mitochondria from the livers of 3 to 4-month-old male mice (C57BL/6NTac) and 6-month-old Sprague Dawley male rats (NTac: SD), as described previously (Tahara et al 2009, with modifications) and detailed below.

### 2.1. Liver mitochondrial isolation

Animal procedures were conducted in accordance with guidelines from the Ethical Committee for Animal Research (CEUA-IQ/USP 196/2021 and 109/2018). Animals were anaesthetized, euthanized, and had their livers immediately dissected. Mitochondria were isolated as follows:

1. Transfer the dissected liver (~1.5 g) to a beaker containing approximately 50 mL of ice-cold phosphate buffered saline (PBS) (Table 2). Keep all subsequent materials and solutions over ice.
2. Thoroughly mince the tissue into small fragments, using sharp scissors. Alternatively, a polytron grinder may be used to obtain a more homogeneous suspension and smaller organ fragments.
3. Wash repeatedly with PBS to remove excess contaminating blood.
4. Remove the PBS and add ice-cold isolation buffer to suspend the tissue fragments up to 2.5 % (m/V) (Table 3). For a whole mouse liver (or one quarter of a rat liver), this corresponds to ~60 mL.
5. Using an electric Potter-Elvehjem tissue grinder, homogenize the tissue (approximately five to six strokes, or until the tissue is clearly dissociated). Operate the Teflon pestle at 1 800 rpm.
6. Centrifugation #1 (remove cellular debris and blood): centrifuge at 900 *g*, 4 °C, for 4 min.
7. Transfer the supernatant to a new tube, discarding the pellet.
8. Centrifugation #2: re-centrifuge the supernatant at 900 *g*, 4 °C, for 4 min; discard the pellet.
9. Centrifugation #3 (pellet mitochondria): centrifuge the supernatant at 9000 *g*, 4 °C, for 5 min.
10. Discard the supernatant and resuspend the pellet in 60 mL of ice-cold isolation buffer (Table 3).
11. Centrifugation #4 (wash the pellet): centrifuge the suspension at 9000 *g*, 4 °C, for 5 min. Resuspend in 60 mL of ice-cold resuspension buffer (Table 4).
12. Centrifugation #5 (remove BSA from samples): centrifuge the resuspension at 9000 *g*, 4 °C, for 10 min.
13. For a whole mouse liver, resuspend the pellet in 300 µL ice-cold resuspension buffer (Table 4).
14. Maintain isolated mitochondria over ice to avoid degradation.
15. Measure protein concentrations using the Bradford method.

**Note:** Experiments were typically conducted with freshly isolated mitochondria soon after isolation and can be typically performed up to until 4 hours later, depending on sample run-down.

## 2.2. Defining ideal substrates by measuring Ca<sup>2+</sup> retention capacity (CRC)

Before proceeding with the mitochondrial Ca<sup>2+</sup> efflux assessment *per se*, it is of interest to determine the optimal conditions for the given experimental model. The ability to take up and store Ca<sup>2+</sup> varies greatly depending on the organ or cells from which the mitochondria originated. Ions, proteins, and organic molecules in the experimental medium modulate the maximal amount of Ca<sup>2+</sup> that can be taken up by mitochondria before overt mitochondrial mtPT induction. This upper limit of Ca<sup>2+</sup> uptake ability is known as Ca<sup>2+</sup> retention capacity (CRC). Mg<sup>2+</sup> and adenine nucleotides (ATP, ADP, and AMP) may increase CRCs, while lipids and oxidants typically decrease CRCs (reviewed by Bonora et al 2022). In brain mitochondria, for example, adenine nucleotides are required in the medium to observe significant mitochondrial Ca<sup>2+</sup> uptake (Amigo et al 2017). Our experimental medium also contains phosphate (P<sub>i</sub>). Even though P<sub>i</sub> can limit free Ca<sup>2+</sup> concentration in the matrix, as Ca<sup>2+</sup> precipitates are formed in its presence, we add it, as it is physiologically relevant and used in most experimental paradigms. The chosen energizing substrate(s) also deeply influence CRCs. In rat or mouse kidney mitochondria, for example, lower CRCs are observed when pyruvate and malate (which energize mitochondria mainly through Complex I) are employed as substrates, relative to succinate plus rotenone (which fuels electron transport mainly through Complex II) (Serna et al 2022).

Defining the optimal substrates involves measuring mitochondrial CRC under each condition. Ca<sup>2+</sup> uptake assays are performed as shown in [Figure 2](#) and described below.

### 2.2.1. Prepare the cuvette

1. Use a cuvette fluorimeter (we employed an F4500 Hitachi fluorimeter) with stirring and temperature control. Select an appropriate cuvette. For standardized 2 mL cuvettes, add 2 mM pyruvate plus 2 mM malate (or 2 mM succinate plus 1 μM rotenone), 15 μM EGTA, and 75 nM Calcium Green<sup>TM</sup>-5N in 2 mL experimental buffer ([Table 5](#)).  
**Note:** the pH of substrates and EGTA needs to be adjusted to 7.2 using KOH when preparing the stock solutions.
2. Place the cuvette in the fluorimeter, with constant stirring, at 37 °C.
3. Wait a couple of minutes until the buffer temperature and composition are homogeneous.
4. Start measuring fluorescence at λ<sub>ex</sub> = 506 nm and λ<sub>em</sub> = 532 nm. Fluorimeter slits (or lamp voltage) should be adjusted to avoid saturation of the system.

### 2.2.2. Ca<sup>2+</sup> loading traces to determine Ca<sup>2+</sup> retention capacities

1. Add 0.5-1 mg of mitochondrial protein and wait for around 100 s for equilibration.
2. Perform sequential additions of 10 μM CaCl<sub>2</sub>, waiting approximately 300 s between them or until the Ca<sup>2+</sup> bolus is completely taken up by mitochondria. Usually, because of the EGTA present, a few CaCl<sub>2</sub> additions need to be made at the beginning of each trace before Ca<sup>2+</sup> uptake is observed (marked by a

- decrease in the Calcium Green<sup>TM</sup>-5N fluorescence; true Ca<sup>2+</sup> uptake exhibits an exponential-like decay shape, Figure 2).
- Proceed with additions until a widespread mtPT in the mitochondrial population is reached, indicated by the increase in fluorescence in the absence of added Ca<sup>2+</sup> boluses, or until fluorescence stabilizes after Ca<sup>2+</sup> additions, with no further measurable mitochondrial uptake.

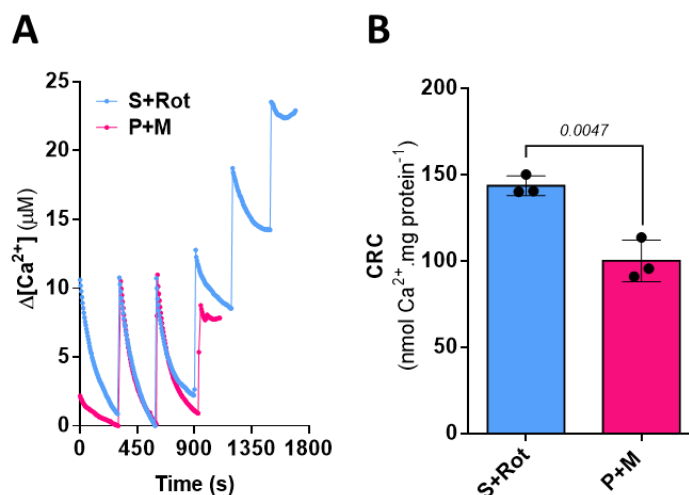


**Figure 2. Ca<sup>2+</sup> retention capacities in isolated mouse liver mitochondria: effect of different substrates.** 500  $\mu g$  liver mitochondria were incubated in 2 mL experimental buffer using either succinate plus rotenone (S+Rot) or pyruvate plus malate (P&M) as substrates. Extramitochondrial  $[Ca^{2+}]$  were recorded over time using Calcium Green<sup>TM</sup>-5N. **(A)** Typical Ca<sup>2+</sup> uptake trace. Each peak in the trace results from the sequential addition of 10  $\mu M$   $CaCl_2$  boluses in the media. The subsequent decrease in extramitochondrial  $[Ca^{2+}]$  results from Ca<sup>2+</sup> uptake into the matrix. When the ability to take up and store Ca<sup>2+</sup> is surpassed,  $[Ca^{2+}]$  in the media no longer decreases. **(B)** Quantified Ca<sup>2+</sup> retention capacities (CRC), or the total amount of Ca<sup>2+</sup> taken up per mg mitochondrial protein over the full loading trace, obtained from traces such as panel A. CRCs are higher when succinate (plus rotenone) is employed as the substrate. Distinct biological repetitions are indicated by individual data dots in panel B. Data were compared using an unpaired t-test and are presented as means  $\pm$  SD.

### 2.3. Measuring mitochondrial Ca<sup>2+</sup> efflux

Given the results seen in Figure 2, we chose succinate plus rotenone as the optimal energizing condition to measure Ca<sup>2+</sup> efflux rates in mouse liver mitochondria. We can now proceed to conduct Ca<sup>2+</sup> efflux measurements.

#### 2.3.1. Choosing Ca<sup>2+</sup> loads for efflux measurements: avoiding mtPTP opening

For obvious reasons, mitochondria must be loaded with Ca<sup>2+</sup> to measure efflux rates, and different Ca<sup>2+</sup> loads may generate different efflux rates. mtPTP opening, which is bolstered by higher Ca<sup>2+</sup> loads, will interfere with exchanger activity measurements, as it eliminates or decreases protonmotive force. It should, thus, be avoided when measuring Ca<sup>2+</sup>/H<sup>+</sup> exchanger and NCLX activities. Widespread mtPT induction is easily identifiable when measuring Ca<sup>2+</sup> fluxes, as it leads to overt Ca<sup>2+</sup> release, but we find it can often be overlooked when affecting a subset of the mitochondrial population, as exemplified by the

results in Figure 3: Mitochondria were loaded with three different amounts of  $\text{Ca}^{2+}$ , and subsequent extrusion rates were measured in the absence or presence of mtPTP inhibitor cyclosporin A (CsA). We find that CsA-insensitive  $\text{Ca}^{2+}$  efflux ( $\text{Ca}^{2+}/\text{H}^+$  efflux, in this instance, since  $\text{Na}^+$  was not added) is similar under all conditions tested. However, total efflux rates increase with increasing  $\text{Ca}^{2+}$  loads due to a CsA-sensitive activity, which indicates that the mtPTP was responsible. These results demonstrate that using higher  $\text{Ca}^{2+}$  loads promotes mtPTP opening even when the CRC has not been exceeded. Indeed, electron microscopy data support the heterogeneity of mtPTP induction (Beatrice et al 1982).

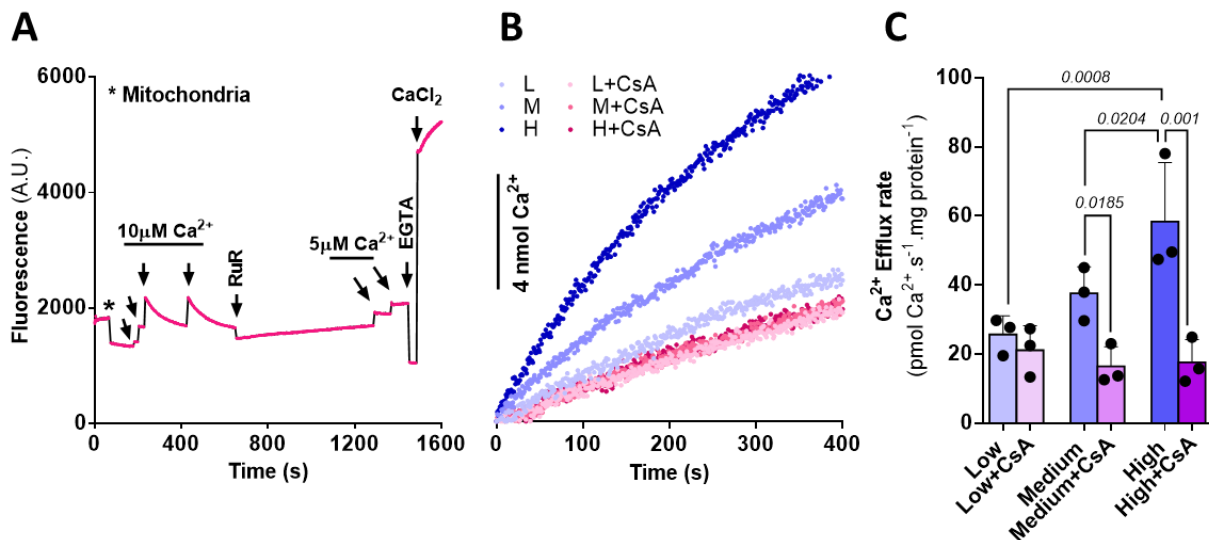


**Figure 3. Permeability transition in mitochondrial subpopulations affects  $\text{Ca}^{2+}$  efflux measurements.** 500  $\mu\text{g}$  liver mitochondria were incubated in 2 mL experimental buffer with 2 mM succinate plus 1  $\mu\text{M}$  rotenone. Extramitochondrial  $\text{Ca}^{2+}$  concentrations were recorded using Calcium Green<sup>TM</sup>-5N. **(A)** Representative plot for the full  $\text{Ca}^{2+}$  efflux assay, following Calcium Green fluorescence over time. Mitochondria were added (\*) and allowed to equilibrate. The first two 10  $\mu\text{M}$   $\text{CaCl}_2$  additions did not result in ion uptake as the chelator EGTA was present (discussed above). The gradual decrease in fluorescence observed after the third and fourth  $\text{CaCl}_2$  additions is due to mitochondrial  $\text{Ca}^{2+}$  uptake. After the 40 nmol  $\text{Ca}^{2+}$  load, ruthenium red (RuR) was added, resulting in a small immediate fluorescence quenching. The slow increase in fluorescence that follows is due to mitochondrial  $\text{Ca}^{2+}$  efflux. After several minutes recording this efflux, two sequential additions of 5  $\mu\text{M}$   $\text{CaCl}_2$  were performed for calibration purposes. Along with this, minimal and maximal fluorescence values were determined by the addition of 1.5 mM EGTA and 10 mM  $\text{CaCl}_2$ , respectively. **(B)** Representative  $\text{Ca}^{2+}$  efflux traces. Initially, mitochondria were loaded either with low (L - 20 nmol), medium (M - 40 nmol) or high (H - 60 nmol) amounts of  $\text{Ca}^{2+}$ , in the presence or absence of 5  $\mu\text{M}$  cyclosporin A (CsA). To measure mitochondrial  $\text{Ca}^{2+}$  efflux, ruthenium red (RuR) was added, and extrusion was followed over time. **(C)** Initial  $\text{Ca}^{2+}$  efflux rates were determined as the slope of the linear portion of the efflux trace just after RuR addition. Distinct biological repetitions are indicated by individual data dots in panel C. Data were compared using repeated measures one-way ANOVA with Tukey's multiple comparisons test and are presented as means  $\pm$  SD.

### 2.3.2. Measuring mtPT- and Na<sup>+</sup>-independent mitochondrial Ca<sup>2+</sup> efflux

We established that the CsA-sensitive efflux rate under our conditions was not significant when 40 nmol Ca<sup>2+</sup>/mg mitochondrial protein were employed as a calcium load, and used this condition to study exchanger-dependent Ca<sup>2+</sup> efflux, as follows:

1. Add 0.5-1 mg of mitochondria to a fluorimeter cuvette and media containing Calcium Green<sup>TM</sup>-5N, as described in uptake experiments, above. Wait around 100 s for equilibration.  
**Note:** experimental modulators of mitochondrial activity, such as CsA, CGP, or ATP, should be added before mitochondria. If a low enough Ca<sup>2+</sup> load to avoid mtPTP opening cannot be achieved, CsA may be used in all traces.
2. Add 40 nmol CaCl<sub>2</sub>/mg mitochondrial protein and wait for fluorescence to stabilize after Ca<sup>2+</sup> is taken up.  
**Note:** sequential additions may be needed to overcome EGTA chelation. Assessing the activity of Ca<sup>2+</sup> exchangers requires Ca<sup>2+</sup> load optimization to avoid mtPTP opening (see critical point [above](#)).
3. Add 0.5-2.5 μM RuR (or another MCU inhibitor) to inhibit mitochondrial Ca<sup>2+</sup> uptake.  
**Note:** final RuR concentrations should be titrated for each mitochondrial amount employed. Wingrove and Gunter (1986) observed inhibition of Na<sup>+</sup>-stimulated Ca<sup>2+</sup> efflux in liver mitochondria with RuR above 10 nmol/mg protein. In liver, kidney, and heart mitochondria, we find 0.5-2.5 μM RuR works well.
4. Record Ca<sup>2+</sup> efflux during at least 400 s. We will refer to the Na<sup>+</sup>-independent mitochondrial Ca<sup>2+</sup> efflux (or non-stimulated Ca<sup>2+</sup> efflux) as basal efflux from here onward.

### 2.3.3. Measuring Na<sup>+</sup>-dependent mitochondrial Ca<sup>2+</sup> efflux

The protocol to assess Na<sup>+</sup>(or Li<sup>+</sup>)-stimulated Ca<sup>2+</sup> efflux is essentially the same as that to measure basal Ca<sup>2+</sup> efflux, but with added Na<sup>+</sup>:

1. Repeat steps 1-3 [above](#).
2. After Ca<sup>2+</sup> loading and inhibition of the MCU with RuR, allow the system to equilibrate for 100-200 s.
3. Add 20 mM NaCl (or LiCl) to induce a Na<sup>+</sup>(Li<sup>+</sup>)-dependent Ca<sup>2+</sup> efflux. Record fluorescence changes for at least 400 s.  
**Note:** Ca<sup>2+</sup> efflux rates must be calculated and compared using the same initial and final time points: matrix Ca<sup>2+</sup> concentrations decrease over time, and efflux rates do too.
4. To estimate NCLX-dependent efflux, subtract the basal efflux rate from the with Na<sup>+</sup> stimulation.

[Figure 4](#) shows an example in which Ca<sup>2+</sup> efflux rates were measured in isolated mouse liver mitochondria. We observed significant and similar Na<sup>+</sup> and Li<sup>+</sup> stimulation of Ca<sup>2+</sup> efflux under these conditions, indicating the presence of NCLX activity corresponding to more than half of the total extrusion activity in these mitochondria. Our results contrast with those of others, who were unable to observe Na<sup>+</sup>-stimulated efflux in liver mitochondria (Rysted et al 2021), possibly due to mtPTP induction, given a high Ca<sup>2+</sup> load was employed. Indeed, Haworth et al (1980) reported similar Na<sup>+</sup>-stimulated efflux values to those we obtained, and Wingrove and Gunter (1986) also observed Na<sup>+</sup>-stimulated efflux in liver mitochondria.



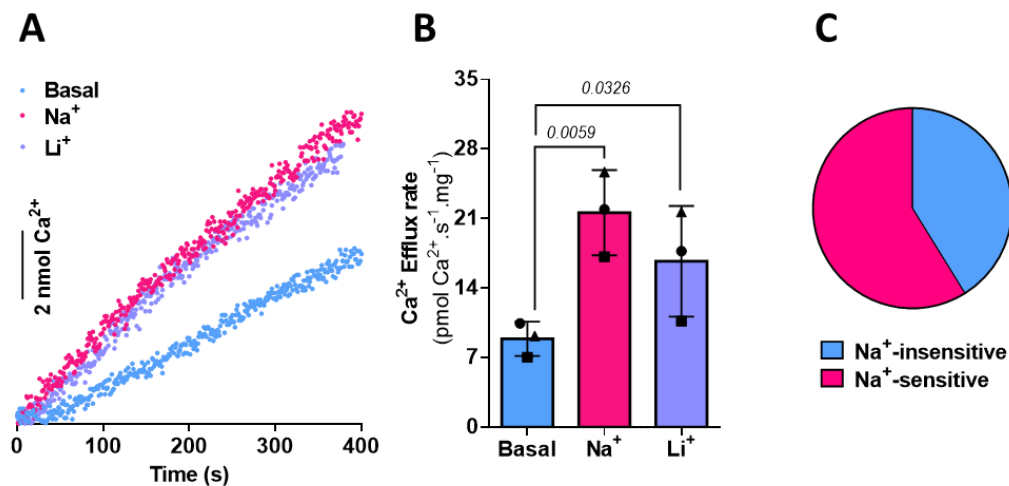


**Figure 4. Ca<sup>2+</sup> efflux in mouse liver mitochondria.** 1 mg liver mitochondria was incubated in 2 mL experimental buffer with 2 mM succinate plus 1  $\mu$ M rotenone. Extramitochondrial Ca<sup>2+</sup> was recorded using Calcium Green<sup>TM</sup>-5N. (A) Typical Ca<sup>2+</sup> extrusion traces. Mitochondria were loaded with 40 nmol Ca<sup>2+</sup>, as shown in Figure 3, and then treated with 1.25  $\mu$ M RuR. Ca<sup>2+</sup> efflux was measured under basal conditions (non-stimulated) or stimulated with 20 mM Na<sup>+</sup> or Li<sup>+</sup>, as indicated. (B) Ca<sup>2+</sup> efflux rates were determined from the slope just after Na<sup>+</sup> or Li<sup>+</sup> additions. (C) Relative contribution of Na<sup>+</sup>-sensitive and Na<sup>+</sup>-insensitive Ca<sup>2+</sup> efflux pathways. Data were compared using repeated measures one-way ANOVA with Tukey's multiple comparisons test and are presented as means  $\pm$  SD. Distinct biological repetitions are indicated by individual data dots in panel B.

We also measured mitochondrial Ca<sup>2+</sup> efflux rates in rat liver mitochondria, Figure 5. We observed similar Na<sup>+</sup>-dependent and independent effluxes to those measured by us in mouse liver mitochondria. To further characterize if this Na<sup>+</sup>-dependent efflux activity is due to NCLX, we measured efflux rates in the presence of Li<sup>+</sup>, K<sup>+</sup>, and Na<sup>+</sup> plus CGP-37157. Li<sup>+</sup> stimulates Ca<sup>2+</sup> efflux, but to a lesser extent than Na<sup>+</sup>. K<sup>+</sup> did not enhance Ca<sup>2+</sup> efflux, as expected (Haworth et al 1980). CGP-37157, a widely recognized NCLX selective inhibitor (Cox et al 1993), completely abolished Na<sup>+</sup>-stimulated Ca<sup>2+</sup> efflux. Overall, our results support the existence of NCLX in mouse and rat livers.

#### 2.3.4. Calibration: transforming Calcium Green fluorescence to [Ca<sup>2+</sup>]

Fluorescence changes of the Calcium Green<sup>TM</sup>-5N probe should be transformed into [Ca<sup>2+</sup>] by calibrating. We find that the addition of some mitochondrial modulators and ions alters probe response to changes in [Ca<sup>2+</sup>], so calibrations should be conducted separately for each experimental condition, as follows (see a sample trace in Figure 3A):

1. At the end of each experimental trace, make at least two consecutive additions of 5  $\mu$ M CaCl<sub>2</sub> to the experimental media while recording Calcium Green fluorescence.
2. Add 1.5 mM EGTA (or more, if necessary) to achieve minimal Calcium Green fluorescence ( $F_{\min}$ ).
3. Add 10 mM CaCl<sub>2</sub> (or more, if necessary) to reach maximal Calcium Green fluorescence ( $F_{\max}$ ).

4.  $K_d$  calculation: The  $K_d$  is empirically determined as the value in which the change in fluorescence ( $\Delta F$ ) before and after  $\text{Ca}^{2+}$  additions fits the  $5 \mu\text{M}$   $\text{Ca}^{2+}$  increase. This process is made by iteration, as follows:
  - Convert all fluorescence values to  $[\text{Ca}^{2+}]$  according to the equation  $[\text{Ca}^{2+}] = K_d \cdot (F - F_{\min}) / (F_{\max} - F)$  by using a pre-determined  $K_d$  value (e.g.  $50 \mu\text{M}$ ).
  - Calculate the  $\Delta[\text{Ca}^{2+}]$  from before and after the  $5 \mu\text{M}$   $\text{CaCl}_2$  additions.
  - Decrease or increase the  $K_d$  value in the formula until the  $\Delta[\text{Ca}^{2+}]$  value is equal to  $5 \mu\text{M}$  (iteration).
5. Calculate calcium concentrations for the experimental traces using the  $K_d$  value obtained and the formula:  $[\text{Ca}^{2+}] = K_d \cdot (F - F_{\min}) / (F_{\max} - F)$ .

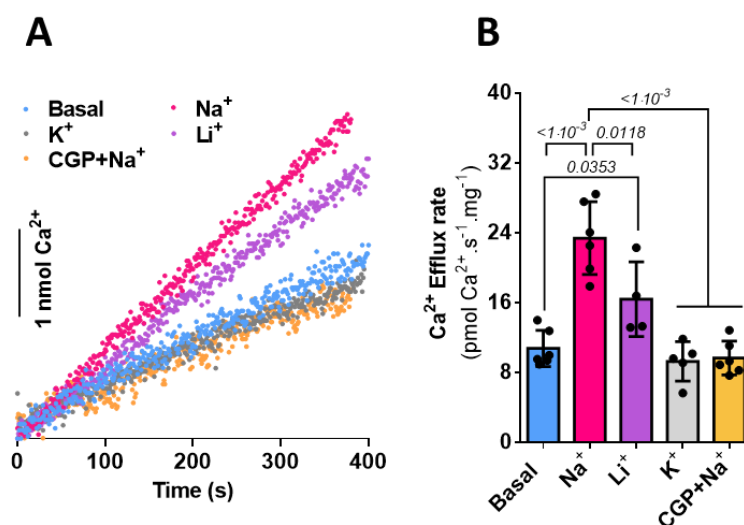


**Figure 5.  $\text{Ca}^{2+}$  efflux in rat liver mitochondria.**  $500 \mu\text{g}$  liver mitochondria were incubated in 2 mL experimental buffer with 2 mM pyruvate plus 2 mM glutamate. Extramitochondrial  $\text{Ca}^{2+}$  was recorded using Calcium Green<sup>TM</sup>-5N. (A) Typical  $\text{Ca}^{2+}$  extrusion traces. Mitochondria were loaded with 20 nmol  $\text{Ca}^{2+}$ , as shown in Figure 3, and then treated with  $1.25 \mu\text{M}$  RuR.  $\text{Ca}^{2+}$  efflux was measured under basal conditions (non-stimulated) or stimulated with 20 mM  $\text{Na}^+$ , 20 mM  $\text{K}^+$ , 20 mM  $\text{Li}^+$ , or 20 mM  $\text{Na}^+$  in the presence of  $5 \mu\text{M}$  CGP-37157, as indicated. (B)  $\text{Ca}^{2+}$  efflux rates were determined from the slope just after  $\text{Na}^+$ ,  $\text{Li}^+$ , or  $\text{K}^+$  additions. Distinct biological repetitions are indicated by individual data dots in panel B. Data were compared using one-way ANOVA with Tukey's multiple comparisons test; data are presented as means  $\pm$  SD.

### 3. Mitochondrial $\text{Ca}^{2+}$ efflux – permeabilized cells

Permeabilized cells allow for assessments using protocols similar to those used for isolated mitochondria, once optimal permeabilization conditions are established. We demonstrate here using human hepatoma PLC/PRF/5 cells.

#### 3.1. Digitonin titration for optimal permeabilization

We employed digitonin to selectively permeabilize cell membranes without disturbing mitochondrial integrity. Optimal digitonin concentrations were determined using an O2k high-resolution oxygraph (Oroboros Instruments, Austria). The titration assay relies on the low permeability of the plasmalemma to succinate, a restraint removed when the membrane is permeabilized, resulting in increased mitochondrial oxygen

consumption rates in the presence of rotenone. ADP is commonly added to increase respiration and titration sensitivity. A detailed digitonin titration protocol is:

### 3.1.1. Prepare the cell suspension

1. Plate cells to obtain  $> 1 \cdot 10^6$  cells at the desired confluence (e.g., a 100 mm culture dish per trace).
2. Wash cells with warm PBS.
3. Add 2 mL of trypsin-EDTA solution and incubate at 37 °C for 3-5 min (depending on cell type).
4. Inhibit trypsin with 4 mL culture media.
5. Collect cells and centrifuge at 200 *g* for 5 min.
6. Wash cells: resuspend in 4 mL experimental buffer supplemented with 1 mM EGTA.
7. Mix gently with a widened (cut) 1000  $\mu$ L pipette tip to disaggregate any cell clumps.
8. Centrifuge the cell suspension at 200 *g* for 5 min.
9. Resuspend cells in 500  $\mu$ L experimental buffer with 1 mM EGTA. Dilute the cell suspension (if required) and count viable cells.  
**Note:** when cells have a strong tendency to form clumps, dilute the cells with PBS supplemented with EGTA and EDTA before counting.

### 3.1.2. Titrating digitonin concentrations

1. Add 2 mM succinate, 1  $\mu$ M rotenone, and 1 mM ADP to experimental buffer in an O2k-chamber.
2. Add the cell suspension for a final cell concentration of  $0.5 \cdot 10^6 \text{ x mL}^{-1}$  in 2 mL experimental buffer (supplemented 1 mM EGTA).
3. Make sequential 0.5 % digitonin additions (aim for incremental additions of 0.5–1  $\mu$ L) and observe oxygen consumption increases. When digitonin amounts are excessive, oxygen consumption rates will gradually decrease (Figure 6).  
**Note:** allow time for oxygen flux stabilization. Initial digitonin additions are more time-demanding (usually between 2–6 min).
4. Optimal digitonin concentrations will be those that induce highest mitochondrial respiration.

### 3.1.3. Mitochondrial outer membrane integrity assay

To validate cell permeabilization quality, a control for mitochondrial outer membrane integrity can be performed. Excessive amounts of digitonin lead to outer membrane permeabilization and subsequent cytochrome *c* release. Under these conditions, oxygen consumption rates are lower. The assay can be conducted as follows:

1. Add 2 mM succinate and 1  $\mu$ M rotenone to experimental buffer in an O2k-chamber, plus the chosen digitonin concentration.
2. Add the cell suspension at a final cell concentration of  $0.5 \cdot 10^6 \text{ x mL}^{-1}$ .
3. Measure oxygen consumption in *P*: add 1 mM ADP.
4. Measure oxygen consumption in *P* + cytochrome *c*: add 10  $\mu$ M cytochrome *c*.
5. Measure oxygen consumption in *L* (LEAK respiration): add 1  $\mu$ M oligomycin.
6. Measure *Rox* (residual oxygen consumption): add 1  $\mu$ M antimycin A.



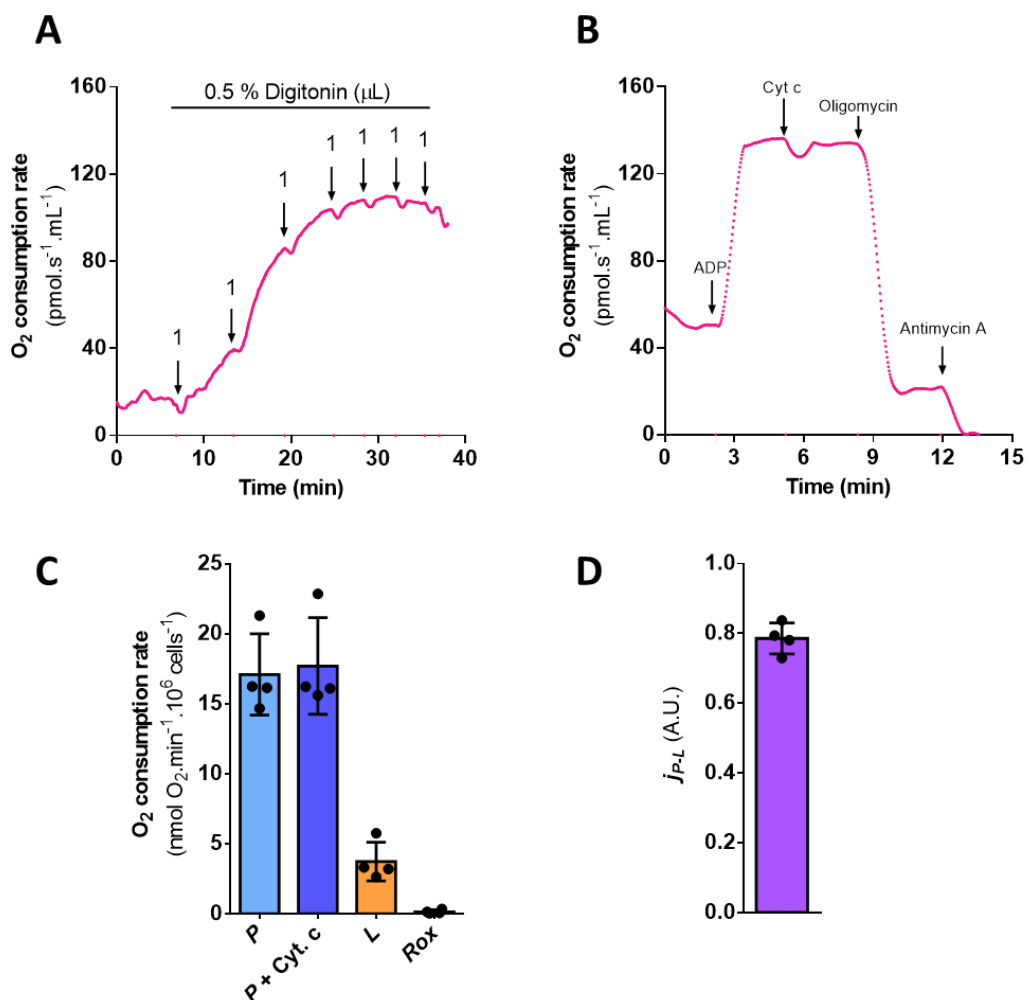


**Figure 6. Optimization of cell permeabilization by digitonin.**  $1\cdot 10^6$  PLC/PRF/5 cells were incubated in 2 mL experimental buffer the presence of 2 mM succinate and  $1\ \mu\text{M}$  rotenone. Oxygen consumption rates were measured with an Oroboros O2k. **(A)** Titration: sequential additions of  $1\ \mu\text{L}$  of 0.5% digitonin were made until respiratory inhibition was observed; 1 mM ADP was present from the beginning. **(B)** Representative trace for outer mitochondrial membrane integrity assessment using cytochrome *c* (cyt *c*) and  $6.25\cdot 10^{-3}$  % digitonin. 1 mM ADP,  $10\ \mu\text{M}$  cytochrome *c*,  $1\ \mu\text{M}$  oligomycin, and  $1\ \mu\text{M}$  antimycin A were added where indicated. **(C)** Quantifications for traces such as in Panel B; OXPHOS capacity (*P*), LEAK respiration (*L*) and Residual oxygen consumption (*Rox*). **(D)** *P-L* control efficiency ( $j_{P-L}$ ) was determined as  $1-(L/P)$ . Distinct biological repetitions are indicated by individual data dots in panels C and D.

Exogenous cytochrome *c* addition in the media recovers normal electron transfer activity if the outer membrane is ruptured. If cells have been properly permeabilized, no differences should be detected between respiratory rates in *P* (OXPHOS capacity: saturating ADP and  $P_i$ ) and *P* plus cytochrome *c*. As shown in Figure 6, the chosen digitonin concentration does not induce outer mitochondrial membrane disruption.

### 3.2. Define ideal substrates by measuring CRC

Follow the experiments described in Section 2.2 to determine ideal substrates to use with your cell type.

### 3.3. Measuring mitochondrial Ca<sup>2+</sup> efflux and assessing NCLX activity

Mitochondrial Ca<sup>2+</sup> efflux assessment in permeabilized suspended cells follows similar protocols to those described for isolated mitochondria:

#### 3.3.1. Prepare the cuvette

1. Add the chosen substrates and 20–40 μM EGTA in experimental buffer (Table 5) plus 75 nM Calcium Green<sup>TM</sup>-5N and the optimal digitonin concentration, as defined above.

**Note:** modulators of mitochondrial function, such as CsA, ATP, or CGP, should be added before the cells.

**Note:** EGTA concentrations are titrated in preliminary experiments, as follows: first, permeabilize cells in experimental medium supplemented with a small amount of EGTA, i.e. 10 μM EGTA. If Ca<sup>2+</sup> uptake is observed (marked by an exponential decay shaped decrease in fluorescence), increase EGTA concentrations until uptake is no longer present. Repeat the experiment with the concentration determined previously and verify if mitochondrial Ca<sup>2+</sup> uptake is not observed since the beginning of the trace.

2. Place the cuvette in the fluorimeter, with constant stirring, at 37 °C.
3. Wait a couple of minutes until the buffer temperature and composition is homogeneous.
4. Start measuring fluorescence at  $\lambda_{\text{ex}} = 506 \text{ nm}$  and  $\lambda_{\text{em}} = 532 \text{ nm}$ . Fluorimeter slits (or lamp voltage) should be adjusted to avoid saturation of the system.

#### 3.3.2. Ca<sup>2+</sup> loading

1. Add 1·10<sup>6</sup> cells and wait around 100 s for equilibration.
2. Add 10 μM (or 5 μM) CaCl<sub>2</sub> until cells have been loaded with 20–30 nmol Ca<sup>2+</sup>/1·10<sup>6</sup> cells. Usually, a few CaCl<sub>2</sub> additions are necessary before Ca<sup>2+</sup> uptake is observed.

**Note:** As discussed previously for isolated mitochondrial preparations, low Ca<sup>2+</sup> loads are necessary to avoid mtPTP opening.

3. Add 1.25 μM RuR to inhibit mitochondrial Ca<sup>2+</sup> uptake.

#### 3.3.3. Mitochondrial Ca<sup>2+</sup> efflux

- 3.1 Record Ca<sup>2+</sup> efflux during at least 700 s to determine basal efflux rates (non-stimulated Ca<sup>2+</sup> efflux).
- 3.2 Add 20 mM NaCl or LiCl to induce a Na<sup>+</sup>(Li<sup>+</sup>)-dependent Ca<sup>2+</sup> efflux, as shown in Figure 7. NCLX activity can be tested measuring Na<sup>+</sup>-dependent Ca<sup>2+</sup> efflux in the presence of 5 μM CGP-37157.

**Note:** Ca<sup>2+</sup> efflux rates must be calculated at equal time points, as discussed for isolated mitochondria, so parallel control experiments with/without Na<sup>+</sup> or Li<sup>+</sup> should be conducted.

- 3.3 Calibrate traces as described above.

#### 3.3.4. Calibration: transforming Ca<sup>2+</sup>-Green fluorescence into [Ca<sup>2+</sup>]

Fluorescence traces should be transformed into [Ca<sup>2+</sup>] measurements, as described in Section 2.3. Experimental and calibration steps can be combined in the same trace, as shown in Figure 3A.

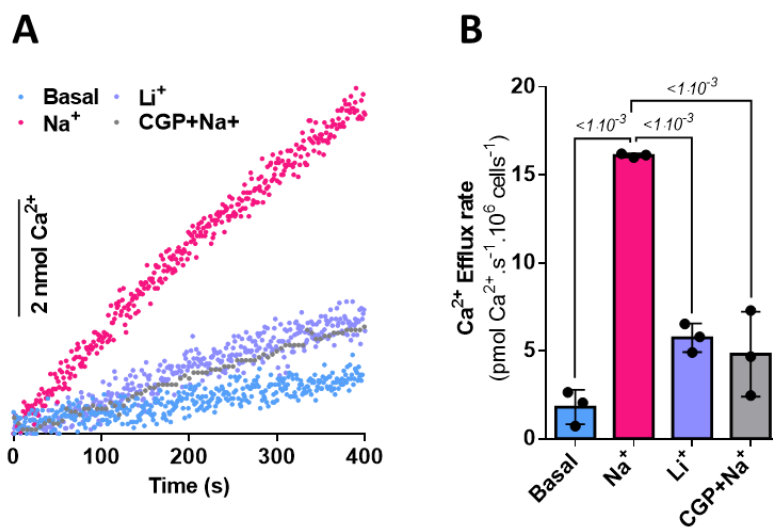


**Figure 7. Mitochondrial  $\text{Ca}^{2+}$  efflux in permeabilized PLC cells.**  $1 \cdot 10^6$  PLC/PRF/5 cells were incubated in 2 mL buffer in the presence of 2 mM succinate, 1  $\mu\text{M}$  rotenone, and  $6.25 \cdot 10^{-3}$  % digitonin.  $\text{Ca}^{2+}$  efflux was recorded following Calcium Green<sup>TM</sup>-5N fluorescence at 37 °C. (A) Representative  $\text{Ca}^{2+}$  efflux trace. Mitochondria were loaded with 20 nmol  $\text{Ca}^{2+}$

and then treated with 1.25  $\mu\text{M}$  RuR.  $\text{Ca}^{2+}$  efflux was measured under either basal conditions or stimulated with 20 mM  $\text{Na}^+$ ,  $\text{Li}^+$ , or 20 mM  $\text{Na}^+$  in the presence of 5  $\mu\text{M}$  CGP-37157. (B)  $\text{Ca}^{2+}$  efflux rates were quantified from the slope of the linear portion of the efflux trace just after  $\text{Na}^+$  or  $\text{Li}^+$  additions (or 200 s after RuR addition in the basal condition group). Distinct biological repetitions are indicated by individual data dots in panel B. Data were compared using repeated measures one-way ANOVA with Tukey's multiple comparisons test and are presented as means  $\pm$  SD.

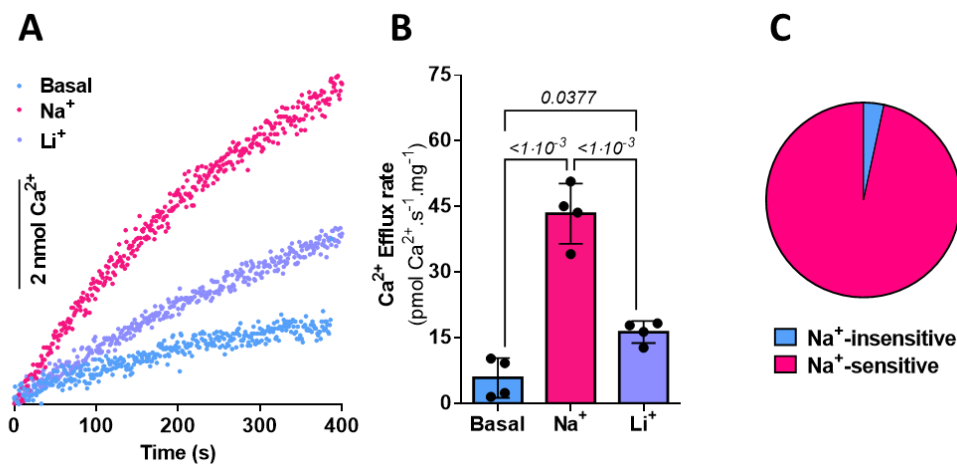


**Figure 8.  $\text{Ca}^{2+}$  efflux in rat heart mitochondria.** 500  $\mu\text{g}$  of heart mitochondria were incubated in 2 mL experimental buffer in the presence of 2 mM succinate plus 1  $\mu\text{M}$  rotenone. Extramitochondrial  $\text{Ca}^{2+}$  concentrations were recorded over time using Calcium Green<sup>TM</sup>-5N. (A) Typical  $\text{Ca}^{2+}$  release traces. Mitochondria were loaded with 20 nmol  $\text{Ca}^{2+}$  and then treated with 1.25  $\mu\text{M}$  RuR.  $\text{Ca}^{2+}$  efflux was measured under basal conditions or stimulated with 20 mM  $\text{Na}^+$  or  $\text{Li}^+$ . (B)  $\text{Ca}^{2+}$  efflux rates were determined as the slope of the linear portion of the efflux trace just after  $\text{Na}^+$  or  $\text{Li}^+$  addition (or 200 s after RuR addition in the basal condition group). (C) Relative contribution of  $\text{Na}^+$ -sensitive and  $\text{Na}^+$ -insensitive  $\text{Ca}^{2+}$  efflux pathways. Distinct biological repetitions are indicated by individual data dots in panel B. Data were compared using repeated measures one-way ANOVA with Tukey's multiple comparisons test and are presented as means  $\pm$  SD.

## 4. Protocol Validation and Reproducibility

To demonstrate the robustness of our protocols, we validated their applicability in two additional models: rat heart mitochondria and the INS-1E insulinoma cell line.

### 4.1. Isolated heart mitochondria

Rat heart mitochondria were isolated using a protocol that includes both subsarcolemmal and intermyofibrillar mitochondria (Gostimskaya, Galkim 2010; Serna et al 2020). We then measured  $\text{Ca}^{2+}$  efflux rates as described above for liver mitochondria; results are presented in Figure 8. We find that the protocol is also appropriate for  $\text{Ca}^{2+}$  efflux measurements in heart mitochondria, and also confirm data from previous work (Rysted et al 2021) demonstrating that the  $\text{Na}^{+}$ -sensitive pathway is predominant in heart, but that it is less stimulated by  $\text{Li}^{+}$ .

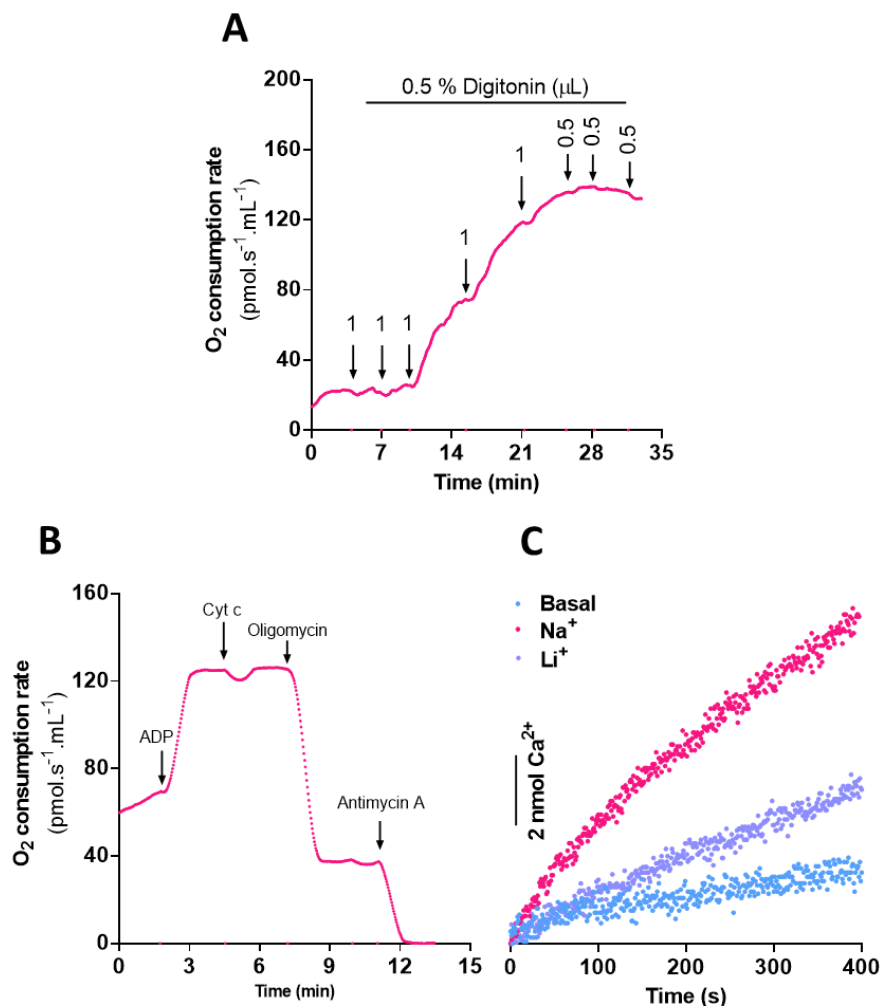


**Figure 9. Digitonin titration and  $\text{Ca}^{2+}$  efflux measurements in permeabilized INS-1E cells.**  $2.5 \cdot 10^6$  INS-1E cells were incubated in 2 mL experimental buffer the presence of 2 mM succinate plus 1  $\mu\text{M}$  rotenone. Oxygen consumption rates were measured with an O2k. (A) Titration: 1 mM ADP was added and sequential additions of 0.5 or 1  $\mu\text{L}$  of 0.5 % digitonin were made where indicated. (B) Representative trace for outer mitochondrial membrane integrity assessment using cytochrome *c* (cyt *c*). Mitochondrial activity was modulated by the sequential addition of

1 mM ADP, 10  $\mu\text{M}$  cyt *c*, 1  $\mu\text{M}$  oligomycin, and 5  $\mu\text{M}$  antimycin A. (C) Representative  $\text{Ca}^{2+}$  efflux trace. Mitochondria were loaded with 20 nmol  $\text{Ca}^{2+}$  and then treated with 1.25  $\mu\text{M}$  RuR.  $\text{Ca}^{2+}$  efflux was measured under basal conditions (non-stimulated) or stimulated with 20 mM  $\text{Na}^{+}$  or  $\text{Li}^{+}$ .

## 4.2. Digitonin-permeabilized INS-1E cells

INS-1E cells were trypsinized, collected, and counted as we described for PLC/PRF/5 cells. Digitonin was titrated and outer mitochondrial integrity controls were performed (Figure 9 A,B).  $\text{Ca}^{2+}$  efflux was assessed as in Section 3.3 (Figure 9C). As described for PLC cells,  $\text{Na}^+$  and  $\text{Li}^+$  are able to stimulate  $\text{Ca}^{2+}$  efflux, demonstrating that the described protocol is adaptable to other cell types.

## 5. Troubleshooting

**Table 1. Troubleshooting**

Problem	Possible reason	Solution
High basal ( $\text{Na}^+$ -independent) $\text{Ca}^{2+}$ efflux rates, or low $\text{Na}^+$ -sensitive $\text{Ca}^{2+}$ efflux rates.	Mitochondrial permeability transition is being induced.	Decrease mitochondrial $\text{Ca}^{2+}$ load or add cyclosporin A.
$\text{Ca}^{2+}$ uptake/efflux trace is noisy	Mitochondrial clumps are present in isolated mitochondrial samples.	Gently disaggregate mitochondrial pellets using a brush with soft bristles.
	Cells are not properly dissociated, forming clumps. Cell culture trypsinization is insufficient.	Optimize trypsinization protocol for each cell type.
	Dead cells release DNA, promoting clump formation.	Decrease trypsinization time (or trypsin amount).
Cytochrome <i>c</i> stimulates <i>P</i> oxygen consumption rates	Mitochondrial outer membrane permeabilization and cytochrome <i>c</i> release leading to electron transfer impairment.	Decrease digitonin concentrations in the experimental medium.
Abundant cell clumps when counting	Cell-cell interactions are preserved after sample preparation; these interactions are induced by $\text{Ca}^{2+}$ and $\text{Mg}^{2+}$ .	Dilute cell stocks in PBS supplemented with EDTA before counting.

## 6. Conclusion

We describe a method to measure  $\text{Ca}^{2+}$  efflux in isolated mitochondria and permeabilized cells, as indicated in the workflow in Figure 10. Our approach allows us to dissect between  $\text{Na}^+$ -sensitive and insensitive  $\text{Ca}^{2+}$  efflux. We demonstrate that a vital point in obtaining consistent and reliable  $\text{Ca}^{2+}$  extrusion activity measurements through mitochondrial exchangers is to avoid mtPTP opening by either using low  $\text{Ca}^{2+}$  loads or adding cyclosporin A to all traces. In the absence of this step, at least part of the activity of NCLX and  $\text{Ca}^{2+}/\text{H}^+$  exchange may be masked by mtPTP-promoted permeabilization. Using this method, we were able to demonstrate NCLX activity in isolated mouse and rat liver mitochondria, as well as permeabilized liver hepatoma PLC/PRF/5 cells. Additionally, we validated our method in isolated rat heart mitochondria, as well as the insulinoma INS-1E cell line.

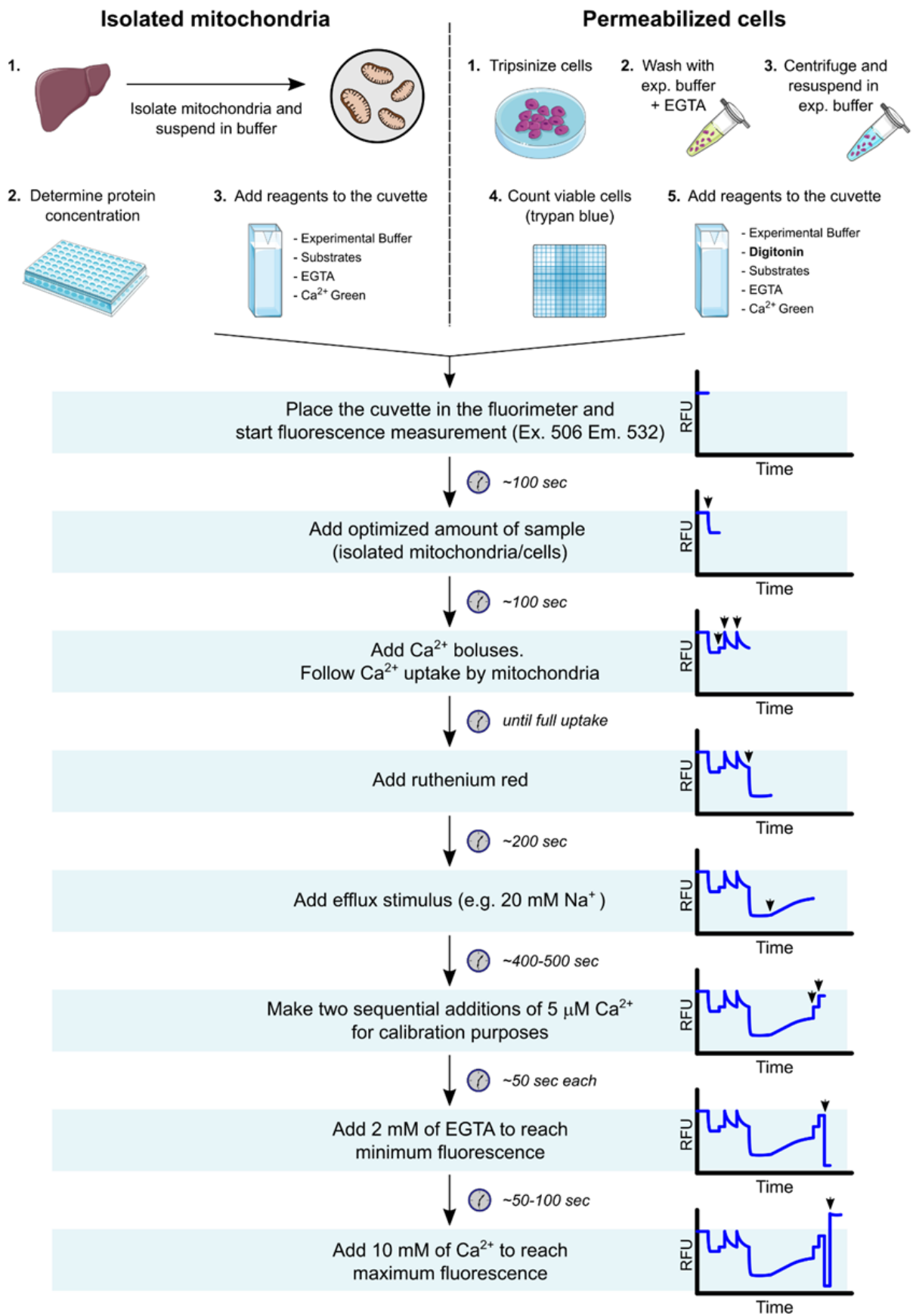


**Figure 10. Schematic workflow for mitochondrial  $\text{Ca}^{2+}$  efflux measurements.**



## 7. Media composition tables

**Table 2. Phosphate buffered saline (pH = 7.4, adjusted with NaOH)**

Reagent	Final concentration	Amount
NaCl	1.37 M	80.01 g
KCl	27 mM	2.01 g
Na <sub>2</sub> HPO <sub>4</sub>	100 mM	14.2 g
KH <sub>2</sub> PO <sub>4</sub>	18 mM	2.45 g
EDTA	10 mM	3.8 g
milliQ H <sub>2</sub> O	-	adjust to 1 L

**Table 3. Liver isolation buffer (pH = 7.2, adjusted with KOH)**

Reagent	Final concentration	Amount
Sucrose	250 mM	85.57 g
Hepes	10 mM	2.38 g
EGTA	1 mM	380 mg
EDTA	1 mM	380 mg
BSA (fatty-acid free)	1 mg/mL	1 g
milliQ H <sub>2</sub> O	-	adjust to 1 L

Note: To avoid formation of bubbles or clumps when diluting BSA, add the powder over the solution and leave still for a while. Adjust pH only with KOH and HCl. Store at 4 °C for up to a month.

**Table 4. Resuspension buffer (pH = 7.2, adjusted with KOH)**

Reagent	Final concentration	Amount
Sucrose	300 mM	20.54 g
Hepes	10 mM	476 mg
EGTA	2 mM	152 mg
milliQ H <sub>2</sub> O	-	adjust to 200 mL

Store at 4 °C for up to a month.

**Table 5. Experimental buffer (pH = 7.2, adjusted with KOH)**

Reagent	Final concentration	Amount
Sucrose	125 mM	21.39 g
KCl	65 mM	2.42 g
Hepes	10 mM	1.19 g
MgCl <sub>2</sub>	2 mM	95 mg
KH <sub>2</sub> PO <sub>4</sub>	2 mM	136 mg
BSA (fatty acid-free)	0.1 mg/mL	50 mg
milliQ H <sub>2</sub> O	-	adjust to 500 mL

To avoid formation of bubbles or clumps when diluting BSA, add the powder over the solution and leave it without stirring for a while. Store at 4 °C for up to a month. Adjust pH only with KOH and HCl.

### Abbreviations

<i>pmF</i>	protonmotive force	ETS	electron transfer system
<i>Rox</i>	residual oxygen consumption	mtPTP	mitochondrial permeability transition pore
BSA	bovine serum albumin	NCLX	Na <sup>+</sup> /Li <sup>+</sup> /Ca <sup>2+</sup> exchanger
CGP	CGP-37157	<i>j<sub>P-L</sub></i>	<i>P-L</i> control efficiency
CRC	calcium retention capacity	RuR	Ruthenium Red
CsA	Cyclosporin A	<i>P</i>	OXPHOS capacity
Cyt c	cytochrome <i>c</i>	<i>L</i>	LEAK respiration

## Acknowledgements

The authors would like to acknowledge remarkable technical support by Sirlei Mendes de Oliveira, and excellent animal care lead by Sylvania Neves and Flavia Ong in the IQ-FCF/USP animal facility. This work was funded by grant #2020/06970–5 from the *Fundação de Amparo à Pesquisa do Estado de São Paulo* (FAPESP), *Centro de Pesquisa, Inovação e Difusão de Processos Redox em Biomedicina* (CEPID Redoxoma, FAPESP grant #2013/07937–8), *Conselho Nacional de Desenvolvimento Científico e Tecnológico* (CNPq), and *Coordenação de Aperfeiçoamento de Pessoal de Nível Superior* (CAPES) line 001. Authors were supported by FAPESP fellowships #2017/14713-0 (JVCC), #2019/05226-3 (JDSC), #2019/18402-4 (VMR), #2021/02481-2 (EAVB), and #2021/13933-1 (GO). Parts of the figures were drawn by using pictures from Servier Medical Art. Servier Medical Art by Servier is licensed under a Creative Commons Attribution 3.0 Unported License (<https://creativecommons.org/licenses/by/3.0/>).

## References

- Amigo I, Menezes-Filho SL, Luévano-Martínez LA, Chausse B, Kowaltowski AJ (2017) Caloric restriction increases brain mitochondrial calcium retention capacity and protects against excitotoxicity. <https://doi.org/10.1111/accel.12527>
- Beatrice MC, Stiers DL, Pfeiffer DR (1982) Increased permeability of mitochondria during Ca<sup>2+</sup> release induced by t-butyl hydroperoxide or oxalacetate. The effect of ruthenium red. [https://doi.org/10.1016/S0021-9258\(18\)34551-4](https://doi.org/10.1016/S0021-9258(18)34551-4)
- Bonora M, Giorgi C, Pinton P (2022) Molecular mechanisms and consequences of mitochondrial permeability transition. <https://doi.org/10.1038/s41580-021-00433-y>
- Boyman L, Williams GSB, Khananshvil D, Sekler I, Lederer WJ (2013) NCLX: The mitochondrial sodium calcium exchanger. <https://doi.org/10.1016/j.yjmcc.2013.03.012>
- Cox DA, Conforti L, Sperelakis N, Matlib MA (1993) Selectivity of inhibition of Na<sup>+</sup>-Ca<sup>2+</sup> exchange of heart mitochondria by benzothiazepine CGP-37157. <https://doi.org/10.1097/00005344-199304000-00013>
- de Brito OM, Scorrano L (2008) Mitofusin 2 tethers endoplasmic reticulum to mitochondria. <https://doi.org/10.1038/nature07534>
- Feno S, Rizzuto R, Raffaello A, Vecellio Reane D (2021) The molecular complexity of the mitochondrial calcium uniporter. <https://doi.org/10.1016/j.ceca.2020.102322>
- Fiskum G, Craig SW, Decker GL, Lehninger AL (1980) The cytoskeleton of digitonin-treated rat hepatocytes. <https://doi.org/10.1073/pnas.77.6.3430>
- Fiskum G, Kowaltowski AJ, Andreyev AY, Kushnareva YE, Starkov AA (2000) Apoptosis-related activities measured with isolated mitochondria and digitonin-permeabilized cells. [https://doi.org/10.1016/S0076-6879\(00\)22023-5](https://doi.org/10.1016/S0076-6879(00)22023-5)
- Giacomello M, Pyakurel A, Glytsou C, Scorrano L (2020) The cell biology of mitochondrial membrane dynamics. <https://doi.org/10.1038/s41580-020-0210-7>
- Giorgi C, Marchi S, Pinton P (2018) The machineries, regulation and cellular functions of mitochondrial calcium. <https://doi.org/10.1038/s41580-018-0052-8>
- Gnaiger E - MitoEAGLE Task Group (2020) Mitochondrial physiology. <https://doi.org/10.26124/bec:2020-0001.v1>
- Gnaiger E (2020) Mitochondrial pathways and respiratory control. An introduction to OXPHOS analysis. <https://doi.org/10.26124/bec:2020-0002>
- Gostimskaya I, Galkin A (2010) Preparation of highly coupled rat heart mitochondria. <https://doi.org/10.3791/2202>
- Grynkiewicz G, Poenie M, Tsien RY (1985) A new generation of Ca<sup>2+</sup> indicators with greatly improved fluorescence properties. [https://doi.org/10.1016/S0021-9258\(19\)83641-4](https://doi.org/10.1016/S0021-9258(19)83641-4)



- Haworth RA, Hunter DR, Berkoff HA (1980) Na<sup>+</sup> releases Ca<sup>2+</sup> from liver, kidney and lung mitochondria. [https://doi.org/10.1016/0014-5793\(80\)80076-7](https://doi.org/10.1016/0014-5793(80)80076-7)
- Jadiya P, Kolmetzky DW, Tomar D, Di Meco A, Lombardi AA, Lambert JP, Luongo TS, Ludtmann MH, Praticò D, Elrod JW (2019) Impaired mitochondrial calcium efflux contributes to disease progression in models of Alzheimer's disease. <https://doi.org/10.1038/s41467-019-11813-6>
- Kowaltowski AJ, Menezes-Filho SL, Assali EA, Gonçalves IG, Cabral-Costa JV, Abreu P, Miller N, Nolasco P, Laurindo FRM, Bruni-Cardoso A, Shirihai OS (2019) Mitochondrial morphology regulates organellar Ca<sup>2+</sup> uptake and changes cellular Ca<sup>2+</sup> homeostasis. <https://doi.org/10.1096/fj.201901136R>
- Kristián T, Weatherby TM, Bates TE, Fiskum G (2002) Heterogeneity of the calcium-induced permeability transition in isolated non-synaptic brain mitochondria. <https://doi.org/10.1046/j.1471-4159.2002.01238.x>
- Kuo IY, Brill AL, Lemos FO, Jiang JY, Falcone JL, Kimmerling EP, Cai Y, Dong K, Kaplan DL, Wallace DP, Hofer AM, Ehrlich BE (2019) Polycystin 2 regulates mitochondrial Ca<sup>2+</sup> signaling, bioenergetics, and dynamics through mitofusin 2. <https://doi.org/10.1126/scisignal.aat7397>
- Kuznetsov AV, Veksler V, Gellerich FN, Saks V, Margreiter R, Kunz WS (2008) Analysis of mitochondrial function in situ in permeabilized muscle fibers, tissues and cells. <https://doi.org/10.1038/nprot.2008.61>
- Minta A, Kao JPY, Tsien RY (1989) Fluorescent indicators for cytosolic calcium based on rhodamine and fluorescein chromophores. [https://doi.org/10.1016/S0021-9258\(18\)83165-9](https://doi.org/10.1016/S0021-9258(18)83165-9)
- Nita II, Hershfinkel M, Fishman D, Ozeri E, Rutter GA, Sensi SL, Khananshvilid D, Lewis EC, Sekler I (2012) The mitochondrial Na<sup>+</sup>/Ca<sup>2+</sup> exchanger upregulates glucose dependent Ca<sup>2+</sup> signalling linked to insulin secretion. <https://doi.org/10.1371/journal.pone.0046649>
- Palty R, Silverman WF, Hershfinkel M, Caporale T, Sensi SL, Parnis J, Nolte C, Fishman D, Shoshan-Barmatz V, Herrmann S, Khananshvilid D, Sekler I (2010) NCLX is an essential component of mitochondrial Na<sup>+</sup>/Ca<sup>2+</sup> exchange. <https://doi.org/10.1073/pnas.0908099107>
- Pathak T, Gueguinou M, Walter V, Delierneux C, Johnson MT, Zhang X, Xin P, Yeast RE, Emrich SM, Yochum GS, Sekler I, Koltun WA, Gill DL, Hempel N, Trebak M (2020) Dichotomous role of the human mitochondrial Na<sup>+</sup>/Ca<sup>2+</sup>/Li<sup>+</sup> exchanger NCLX in colorectal cancer growth and metastasis. <https://doi.org/10.7554/eLife.59686>
- Rizzuto R, De Stefani D, Raffaello A, Mammucari C (2012) Mitochondria as sensors and regulators of calcium signalling. <https://doi.org/10.1038/nrm3412>
- Rossi A, Pizzo P, Filadi R (2019) Calcium, mitochondria and cell metabolism: A functional triangle in bioenergetics. <https://doi.org/10.1016/j.bbamcr.2018.10.016>
- Rudolf R, Mongillo M, Rizzuto R, Pozzan T (2003) Looking forward to seeing calcium. <https://doi.org/10.1038/nrm1153>
- Rysted JE, Lin Z, Walters GC, Rauckhorst AJ, Noterman M, Liu G, Taylor EB, Strack S, Usachev YM (2021) Distinct properties of Ca<sup>2+</sup> efflux from brain, heart and liver mitochondria: The effects of Na<sup>+</sup>, Li<sup>+</sup> and the mitochondrial Na<sup>+</sup>/Ca<sup>2+</sup> exchange inhibitor CGP37157. <https://doi.org/10.1016/j.ceca.2021.102382>
- Saks VA, Veksler VI, Kuznetsov AV, Kay L, Sikk P, Tiivel T, Tranqui L, Olivares J, Winkler K, Wiedemann F, Kunz WS (1998) Permeabilized cell and skinned fiber techniques in studies of mitochondrial function in vivo. <https://doi.org/10.1023/A:1006834912257>
- Schmidt CA, Kelsey H, Fisher-Wellman, Darrell Neuffer P (2021) From OCR and ECAR to energy: Perspectives on the design and interpretation of bioenergetics studies. <https://doi.org/10.1016/j.jbc.2021.101140>
- Serna JDC, Amaral AG, Caldeira da Silva CC, Munhoz AC, Vilas-Boas EA, Menezes-Filho SL, Kowaltowski AJ (2022) Regulation of kidney mitochondrial function by caloric restriction. <https://doi.org/10.1152/ajprenal.00461.2021>
- Serna JDC, Caldeira da Silva CC, Kowaltowski AJ (2020) Functional changes induced by caloric restriction in cardiac and skeletal muscle mitochondria. <https://doi.org/10.1007/s10863-020-09838-4>
- Spinelli JB, Haigis MC (2018) The multifaceted contributions of mitochondria to cellular metabolism. <https://doi.org/10.1038/s41556-018-0124-1>

- Tahara EB, Navarete FD, Kowaltowski AJ (2009) Tissue-, substrate-, and site-specific characteristics of mitochondrial reactive oxygen species generation. <https://doi.org/10.1016/j.freeradbiomed.2009.02.008>
- Vercesi AE, Bernardes CF, Hoffmann ME, Gadelha FR, Docampo R (1991) Digitonin permeabilization does not affect mitochondrial function and allows the determination of the mitochondrial membrane potential of *Trypanosoma cruzi* in situ. [https://www.jbc.org/article/S0021-9258\(18\)98703-X/pdf](https://www.jbc.org/article/S0021-9258(18)98703-X/pdf)
- Vercesi AE, Castilho RF, Kowaltowski AJ, de Oliveira HCF, de Souza-Pinto NC, Figueira TR, Busanello ENB (2018) Mitochondrial calcium transport and the redox nature of the calcium-induced membrane permeability transition. <https://doi.org/10.1016/j.freeradbiomed.2018.08.034>
- Vilas-Boas EA, Cabral-Costa JV, Ramos VM, da Silva CCC, Kowaltowski AJ (2022) Goldilocks calcium and the mitochondrial respiratory chain: too much, too little, just right. <https://doi.org/10.1101/2022.04.12.488015>
- Whitaker, M (2010) Genetically encoded probes for measurement of intracellular calcium. <https://doi.org/10.1016/B978-0-12-374841-6.00006-2>
- Williams GSB, Boyman L, Chikando AC, Khairallah RJ, Lederer WJ (2013) Mitochondrial calcium uptake. <https://doi.org/10.1073/pnas.1300410110>
- Wingrove DE, Gunter TE (1986) Kinetics of mitochondrial calcium transport. I. Characteristics of the sodium-independent calcium efflux mechanism of liver mitochondria. [https://www.jbc.org/article/S0021-9258\(18\)66846-2/pdf](https://www.jbc.org/article/S0021-9258(18)66846-2/pdf)

**Copyright** © 2022 The authors. This Open Access peer-reviewed communication is distributed under the terms of the Creative Commons Attribution License, which permits unrestricted use, distribution, and reproduction in any medium, provided the original authors and source are credited. © remains with the authors, who have granted BEC an Open Access publication license in perpetuity.



## **ANNEX F**

**Serpentino et al., 2017**  
**(Rev. Cult. Ext. USP, 17:23–40)**

# Interação entre Extensão, Ensino e Pesquisa: Experiência da Jornada Científica dos Acadêmicos de Farmácia e Bioquímica

## The Conjunction of Extension, Teaching and Research: the Experience of the Scientific Journey of Pharmacy and Biochemistry Students

### RESUMO

A Jornada Científica dos Acadêmicos de Farmácia-Bioquímica (JCAFB), da Faculdade de Ciências Farmacêuticas da Universidade de São Paulo (FCF/USP), é um projeto voluntário, autogerido e de extensão universitária. Criado em 1965, conta com a participação de professores, residentes farmacêuticos e estudantes. Inicialmente, teve a finalidade de investigar a presença de caramujos da espécie *Biomphalaria*, hospedeiro intermediário do *Schistosoma mansoni*, transmissor da esquistossomose, em Peruíbe-SP. Atualmente, caracteriza-se pela prestação de serviços voluntários de assistência farmacêutica em cidades com deficiências nas áreas de saúde e saneamento básico, visando melhorar as condições de vida da população, procurando soluções locais. Em um ciclo de 4 anos, durante os meses de janeiro, uma equipe de cerca de 50 estudantes realiza atividades educativas sobre saúde e meio ambiente, exames laboratoriais, análises físico-química e microbiológica da água, levantamento do perfil socioeconômico, orientações domiciliares sobre uso de medicamentos, capacitação dos agentes comunitários de saúde e promoção de saúde de animais domésticos. O projeto já envolveu mais de 1500 alunos da FCF/USP, além de residentes (farmacêuticos e veterinários), pós-graduandos e graduandos de outras unidades da Universidade. Preservando a indissociabilidade entre a pesquisa, ensino e extensão universitária, a Jornada visa proporcionar aprendizado científico, humanitário e social aos participantes.

**Palavras-chave:** Extensão Universitária. Educação. Saúde. Farmácia-bioquímica.

### ABSTRACT

The *Jornada Científica dos Acadêmicos de Farmácia e Bioquímica* (Scientific Journey of Pharmacy and Biochemistry Students, JCAFB), a project from the Faculty of Pharmaceutical Sciences of University of São Paulo (FCF/USP), is a volunteering, self-managed, extension project. Founded in 1965, it relies on the support of professors,

**ALICE HERMÍNIA  
SERPENTINO**

Universidade de São Paulo.  
Hospital Universitário, São  
Paulo/SP, Brasil.

**JOÃO VICTOR  
CABRAL-COSTA**

Universidade de São Paulo.  
Instituto de Química, São  
Paulo/SP, Brasil.

**RODOLFO RIBEIRO  
DE SOUZA, TAMARA  
RAMOS JORGE, SABRINA  
EPIPHANIO, JEANINE  
GIAROLLA, PRIMAVERA  
BORELLI**

Universidade de São Paulo.  
Faculdade de Ciências  
Farmacêuticas, São Paulo/SP,  
Brasil.

pharmaceutical residents, and undergraduate students. Initially, the goal was to investigate the presence of *Biomphalaria* snails, an intermediate host of the schistosomiasis transmitter, in Peruíbe-SP. Currently, the project is characterized as a volunteer pharmaceutical assistance service, acting in cities with healthcare and sanitation deficiencies, improving life quality through local solutions. In a 4-year cycle, a team of 50 undergraduate students performs educational activities on environment and healthcare topics, laboratorial tests, water quality analysis, socioeconomic data collection, lectures to community health agents, domiciliary orientations about rational use of medicines and health promotion of domestic animals. More than 1,500 students from FCF/USP have already participated, besides many pharmaceutical and medical veterinary residents, and undergraduate students from other institutions within the University of São Paulo. By preserving the principle of inseparability between university research, teaching, and extension, JCAFB aims to provide an opportunity for scientific, humanitarian and social learning to its participants.

**Keywords:** University Extension; Education; Healthcare; Pharmacy-biochemistry.

## INTRODUÇÃO

### Histórico

**A Jornada Científica dos Acadêmicos de Farmácia-Bioquímica (JCAFB), da Faculdade de Ciências Farmacêuticas da Universidade de São Paulo (FCF/USP), é um projeto de Educação para a Saúde, multi e interdisciplinar, caracterizado pela prestação de serviços voluntários de assistência farmacêutica às comunidades com baixos índices de desenvolvimento. As atividades da Jornada são realizadas em comunidades carentes, geralmente fora do município de São Paulo, proporcionando aos alunos o conhecimento de outras realidades culturais, sociais e econômicas, devido ao estreito contato com a população local.**

Criada em 1965, por iniciativa do Prof. Dr. Mario Demar Perez, docente de parasitologia da então Faculdade de Farmácia-Bioquímica da USP, a JCAFB iniciou suas atividades em 1966, no município de Peruíbe, SP (Figura 1). Durante 21 dias, a equipe de alunos, sob orientação do Prof. Perez, fez o levantamento parasitológico da população. A existência de esquistossomose foi confirmada, bem como a de outras verminoses, as quais foram encontradas em índices elevados [1]. A Jornada passou, ainda, pelas cidades paulistas de Itanhaém e Mongaguá, para estudar a possibilidade de disseminação da esquistossomose ao longo do litoral paulista. Posteriormente, Lavrinhas-SP, Bragança Paulista-SP e os postos indígenas Araribá, Icatu e Vanuíre também receberam o projeto. Devido aos resultados destas expedições, o projeto foi reconhecido por sua contribuição ao levantamento da Carta Planorbídica do Estado de São Paulo [2], realizado na década de 70 durante a Campanha de Combate à Esquistossomose (CACEsq). A Secretaria de Estado da Saúde promoveu esta expedição, a qual registrou os locais e as espécies dos caramujos responsáveis pelos focos da doença [3]. No período de 1974 a 1976, a Jornada Científica foi realizada no município

de Campo Florido-MG. Contudo, o projeto foi interrompido ainda na década de 70, devido ao surgimento do Projeto Rondon (no qual a USP teve participação importante e contínua, especialmente no Campus Avançado de Marabá).

Figura 1: "I Jornada Científica do Centro Acadêmico de Farmácia e Bioquímica", Peruíbe, SP, 1965. Fotografias por Antônio Altair Magalhães de Oliveira.



Em 2002, o planejamento da JCAFB foi retomado, por iniciativa com ampliação dos projetos desenvolvidos e o reinício das atividades foi em São Miguel Arcaño-SP (2003). A partir deste momento, a JCAFB passou a executar três atividades principais, intimamente ligadas: (1) a realização de exames laboratoriais e orientações acerca dos resultados; (2) coleta de dados socioeconômicos, bem como orientações sobre hábitos de higiene e uso de medicamentos; e (3) a realização de atividades educativas e recreativas para a população local. Assim, nos anos seguintes, a JCAFB seguiu para os estados de Minas Gerais e São Paulo, passando por 5 municípios até hoje: Olhos d'Água-MG (2004-2007); Córrego Fundo-MG (2008-2011); Canitar-SP (2012); Santa Cruz da Esperança-SP (2013-2016) e, atualmente, em Fernão-SP (2017).



## O projeto nos dias de hoje

Para as crianças participantes do projeto são realizados exames coproparasitológicos, pesquisa de *Enterobius vermicularis* e dosagem de hemoglobina (para detecção de anemia), cuja as faixas etárias são previamente definidas. Aos idosos, acrescentam-se a realização do exame de urina tipo I, bem como as determinações de glicemia, colesterol e avaliação da pressão arterial, exames estes que também são oferecidos a toda população do município em campanhas abertas. Com os resultados obtidos, associados às avaliações do uso de plantas medicinais, medicamentos, análise físico-química e microbiológica da água e perfil socioeconômico da população, são planejadas intervenções efetivas, realizadas tanto pela equipe do projeto, quanto por gestores e lideranças locais. Por fim, também são realizadas oficinas para capacitação de agentes comunitários de saúde (ACSs) e programações diversas com a finalidade de despertar a curiosidade acerca de assuntos relacionados à saúde, tais como teatro, exposições interativas e atividades específicas para as diversas faixas etárias (crianças, adolescentes, adultos, idosos).

Desde 2002, a JCAFB é organizada, coordenada e realizada por alunos da FCF/USP sob orientação da Profa. Dra. Primavera Borelli. Atualmente, a JCAFB também conta com a coordenação das Profas. Dras. Jeanine Giarolla e Sabrina Epiphânio. A execução do projeto no município tem duração média de 20 dias em janeiro, e permanece em cada cidade por um período de 3 a 5 anos. Todos os alunos do curso de graduação de Farmácia e Bioquímica da FCF/USP podem se candidatar. Após 8 meses de treinamentos e capacitação, cerca de 39 estudantes são selecionados para atuação na cidade, por meio de avaliações teórico-práticas. Além disso, a JCAFB conta, atualmente, com projetos transdisciplinares, com parcerias com o Programa de Residência em Farmácia Clínica e Atenção Farmacêutica da FCF/USP e HU/USP, com a Jornada Universitária da Saúde (JUS/USP) e com a Faculdade de Medicina Veterinária e Zootecnia (FMVZ/USP).

## OBJETIVO

O objetivo do projeto é promover a saúde e a educação, buscando soluções locais para os problemas detectados nas comunidades atendidas, bem como contribuir para a formação de multiplicadores de conhecimentos adquiridos. Por ser um projeto de extensão universitária, seu formato atual permite a interação entre a pesquisa e o ensino, oferecendo aos alunos participantes uma oportunidade única de vivenciar a essência do tripé universitário (Ensino, Pesquisa, Extensão).



## MATERIAIS E MÉTODOS

### Organização e equipe

A JCAFB é vinculada ao Centro Acadêmico de Farmácia e Bioquímica, sendo administrada e organizada na forma de autogestão. Foi retomada em 2002 por iniciativa do então estudante da FCF/USP, André Masson e da profa. Primavera Borelli. Sua estrutura de coordenação, bem como as atividades, tem evoluído a cada ano. Atualmente, a organização é composta por duas coordenações: uma Coordenação Executiva e uma Coordenação de Base, hierarquicamente iguais, porém com atribuições distintas. A Coordenação Executiva é constituída por 9 estudantes (não necessariamente membros da diretoria do Centro Acadêmico), sendo: um coordenador de Comunicação, dois coordenadores do Laboratório de Análises Clínicas, dois coordenadores das Campanhas de Saúde e Atividades abertas à população, dois coordenadores das atividades de Campo (visitas às casas participantes do projeto) e dois Coordenadores Gerais. A Coordenação Executiva é renovada anualmente, com base na análise de desempenho dos jornadeiros, realizada pela gestão anterior e em sugestões dos responsáveis. A supervisão docente e técnica são realizadas pelas Profas. Dras. Sabrina Epiphany, Jeanine Giarolla e Primavera Borelli, docentes da FCF/USP, e pela farmacêutica do Hospital Universitário da Universidade de São Paulo (HU/USP), Alice Hermínia Serpentino.

Na Coordenação Executiva, docentes e farmacêuticos responsáveis têm como responsabilidade a organização do trabalho realizado *in loco* nos meses de janeiro. Logo em fevereiro, após o encerramento das atividades de cada ano, o planejamento e o preparo do projeto para o ano seguinte são iniciados. Entre os preparativos estão submissão da proposta ao Comitê de Ética em Pesquisa da FCF/USP, obtenção de recursos financeiros (via Pró-Reitoria de Cultura e Extensão Universitária da USP, empresas e institutos apoiadores), levantamento de dados e análise de resultados anteriores, estruturação de treinamentos e de atividades a serem desenvolvidas na cidade escolhida, logística de atuação, realização de prova para seleção dos candidatos, entre diversas outras atividades responsáveis por executar e gerir o projeto como um todo.

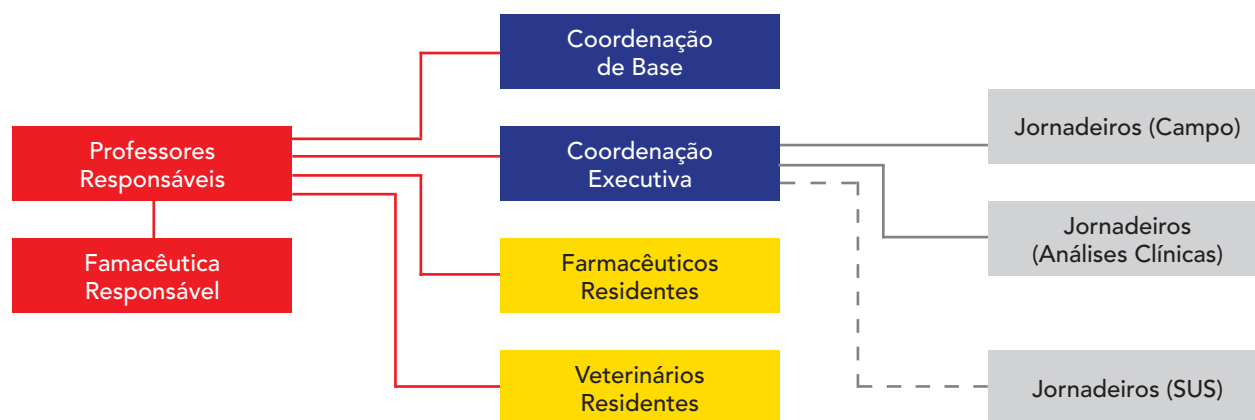
A Coordenação de Base, por sua vez, é composta majoritariamente por graduandos e graduados, que participaram da JCAFB como jornadeiros ou coordenadores em edições anteriores. Esta coordenação tem como princípio dar suporte à execução da JCAFB, auxiliando a Coordenação Executiva no planejamento das ações, buscando novos patrocínios e parcerias, além de fomentar a discussão e organização de novas funções que permitirão a expansão da estrutura do projeto.

Já os estudantes selecionados para compor a equipe como jornadeiros são responsáveis pela execução: (1) do Trabalho de Campo (28 estudantes), que consiste na realização de visitas domiciliares para a aplicação dos questionários socioeconômicos, coleta das amostras de fezes e urina, orientação quanto ao uso racional de medicamentos e entrega dos laudos dos exames laboratoriais, acompanhada de orientação sobre os seus resultados; (2) das Análises Laboratoriais (11 estudantes), que envolvem o recebimento, a preparação e a execução dos ensaios com as amostras

biológicas (fezes e sangue). Os exames de urina tipo I são realizados pelos 2 coordenadores do Laboratório, sendo, quando necessário, auxiliados pelo Coordenador de Comunicação; (3) da capacitação dos ACSs (supervisionada pela Coordenação Executiva), envolvendo discussões e orientações sobre tópicos de acordo com a demanda indicada pelos próprios agentes e pelos gestores locais; (4) da realização de exames e orientações nas campanhas de detecção de diabetes, hipercolesterolemia e hipertensão arterial, bem como do planejamento e realização de atividades abertas à toda a população (todos os estudantes).

Fruto de iniciativas recentes de pluralização do conhecimento, a JCAFB conta hoje com projetos inter e transdisciplinares, envolvendo farmacêuticos residentes do HU/USP, médicos veterinários residentes da FMVZ/USP e coordenadores da JUS/USP, graduandos de cursos variados da área da saúde. Esta estrutura encontra-se esquematizada na figura 2. Os pós-graduandos, com sua experiência clínica e em saúde pública, também contribuem com a JCAFB, trabalhando diretamente em projetos junto às secretarias e prefeitura do município, além de contribuírem para o enriquecimento da formação dos jornadeiros e das atividades de orientação à população.

**Figura 2** – Organograma geral da equipe da JCAFB.



### Treinamentos e processo seletivo da equipe

Para a definição dos participantes da Jornada há um processo seletivo que leva em conta a presença dos graduandos nos treinamentos e a aprovação em avaliações dissertativa e prática, que abordam os temas desenvolvidos nos treinamentos oferecidos ao longo de um semestre, aos alunos inscritos. No momento da inscrição, os alunos escolhem a área em que pretendem atuar: trabalho de Campo ou de Análises Clínicas. Na prova final teórica e discursiva são analisados os conceitos, o conhecimento e a clareza na abordagem dos temas de atuação. Esta avaliação é corrigida por 3 membros da coordenação do projeto, para minimizar discrepâncias em métodos de correção. As

questões que apresentam notas com mais de 2,0 pontos de diferença são revistas e discutidas pelos três avaliadores e, então, é obtida a média aritmética dos valores, a qual é ponderada pela frequência do aluno aos treinamentos. As provas são anônimas aos corretores, sendo identificadas por intermédio de códigos revelados apenas ao final do processo de correção, a fim de se garantir a imparcialidade durante este processo. Já a prova prática é realizada apenas pelos alunos inscritos em Análises Clínicas, na qual amostras de fezes contendo diferentes ovos e/ou cistos de parasitas intestinais são distribuídas aos participantes para identificação das estruturas. Portanto, a composição da nota do candidato de Análises Clínicas conta com a prova prática, que é corrigida pelos respectivos coordenadores.

Os treinamentos teóricos, obrigatórios para todos os alunos interessados, abordam temas relacionados às atividades do projeto (como, por exemplo, doenças crônicas não transmissíveis, parasitoses) e são ministrados pelos coordenadores e por palestrantes convidados. Na área de atenção farmacêutica, importante segmento deste projeto, os estudantes recebem treinamento sobre a promoção do uso racional de medicamentos, ministrado por farmacêuticos residentes do Programa de Residência em Farmácia Clínica e Atenção Farmacêutica do HU/USP. Também recebem treinamentos sobre acolhimento e humanização em saúde, ministrados por enfermeiros e psicólogos. O objetivo é proporcionar o embasamento teórico dos alunos, uma vez que não há restrições quanto ao período do curso de graduação para se candidatar ao processo. Paralelamente são ministrados, aos alunos inscritos para Análises Clínicas, treinamentos práticos orientados pelos coordenadores de análises clínicas e pela farmacêutica responsável, Alice Hermínia Serpentino, com o objetivo de capacitá-los à realização dos exames protoparasitológicos. Para tal, vale ressaltar que os coordenadores da área de Análises Clínicas participam de um treinamento intenso para o aperfeiçoamento das técnicas de reconhecimento microscópico de estruturas de parasitas intestinais em laboratório capacitado, anteriormente aos treinamentos oferecidos aos alunos candidatos. Além disso, juntamente com o coordenador de Comunicação, recebem treinamento prévio no Laboratório Clínico HU/USP para habilitá-los à realização de exame de urina tipo I.

Desta forma, dos cerca de 150 inscritos e capacitados a cada ano, 39 estudantes são selecionados. Após a seleção, inicia-se uma nova etapa de treinamentos teóricos e práticos. Os treinamentos teóricos, nessa fase, são direcionados para a elaboração de atividades educativas e orientação para aplicação correta dos questionários utilizados em campo e durante as campanhas de saúde, padronizando a coleta de dados. Já os treinamentos práticos, objetivam o aperfeiçoamento dos que irão trabalhar no laboratório (realizando exames de fezes, urina e dosagem de hemoglobina) e na habilitação de todos os jornaleiros para a realização dos procedimentos realizados durante as campanhas (dosagem de glicemia, colesterol, aferição da pressão arterial e coleta de sangue, por punção digital, para dosagem de hemoglobina).

## Seleção da cidade

A seleção da cidade a ser atendida é de responsabilidade da Coordenação Executiva e da equipe de docentes e farmacêuticos responsáveis, envolvendo três fases:

1. Selecionam-se as cidades que apresentam baixo Índice de Desenvolvimento Humano (IDH) (abaixo de 0,7) e cuja população seja menor que 5.000 habitantes, de modo que o projeto possa abranger praticamente toda a população dentro do período atividades, de 3 a 5 anos;
2. Analisam-se as cidades pré-selecionadas, baseando-se em indicadores disponibilizados pelo Instituto Brasileiro de Geografia e Estatística (IBGE) – área da cidade, número de crianças de 1 a 4 e de 5 a 9 anos de idade e número de escolas e creches – e pelo Departamento de Informática do SUS (DATASUS) – proporção de moradores por tipo de abastecimento de água e de instalação sanitária, e número de unidades de saúde. Obtém-se, assim, uma relação de cidades com o perfil alvo, nas quais as atividades do projeto apresentam maior potencial de execução e sucesso;
3. As secretarias de saúde das cidades pré-selecionadas são contatadas e é realizada uma visita ao local. São agendadas reuniões com as autoridades locais acerca da viabilidade financeira e estrutural do projeto, bem como para avaliar o interesse dos gestores para que, por fim, o município possa ser selecionado.
4. Em contrapartida à execução do projeto, a prefeitura do município compromete-se a fornecer espaço para alojamento e alimentação aos integrantes da JCAFB, além do transporte para zonas rurais do município. É importante, entretanto, ressaltar que a JCAFB não possui vínculos políticos ou ideológicos com a gestão municipal, sendo este um ponto fundamental do acordo para seleção da cidade.

## Logística

Após a confirmação do interesse e aceite das contrapartidas pelos gestores do município, a Coordenação Executiva agenda uma segunda visita, realizada com 6 meses de antecedência das atividades locais da JCAFB. Neste momento, coletam-se os dados cadastrais da população a ser atendida e realiza-se um mapeamento detalhado da cidade – detalhes das ruas, bairros, distritos e pontos de interesse, contribuindo para uma otimização das atividades do projeto. Estas visitas ao município são custeadas pela FCF/USP, com o apoio da FIPFARMA (Fundação Instituto Pesquisa Farmacêutica).

No período definido para realização da Jornada, o transporte dos viajantes para a localidade é feito por um ônibus disponibilizado pela FCF/USP. Já o transporte dentro da área do município é fornecido pelos gestores locais. Os estudantes são alojados em uma escola municipal previamente disponibilizada pela prefeitura, que também oferece alimentação completa. O alojamento é adaptado para o melhor aproveitamento do espaço: as salas de aula são temporariamente convertidas nos diversos ambientes requeridos: (1) Laboratório de Análises Clínicas, adaptado para realização completa e independente dos exames clínicos do projeto (Figura 3); (2) Secretaria, onde são realizadas as reuniões de coordenação e a organização dos documentos e laudos; (3) Almoxarifado, para alocação dos materiais de consumo; (4) Quartos, para alojamento dos viajantes, professores e

farmacêuticos; (5) Central de tecnologia da informação, para a organização do sistema de gestão e para conversão e armazenamento digital dos dados coletados.



Figura 3: Estrutura do laboratório de Análises Clínicas. Preparação de amostras (esquerda) e análise de lâminas (direita). Fotografia por Thiago André e Silvio Augusto Jr.



### Seleção e cadastramento da população

O perfil da população atendida pode apresentar pequenas alterações entre cada ciclo da JCAFB, de acordo com as principais necessidades do município, as quais são detectadas em demandas levantadas pelos gestores e pelos formadores de opinião consultados. Contudo, de uma forma geral, o atendimento do projeto baseia-se em dois grupos principais: crianças (de 3 a 9 anos de idade) e idosos. Realiza-se o levantamento das crianças do município com base no cadastro das escolas públicas locais. Já os idosos são cadastrados considerando os dados obtidos pelas equipes de saúde da família.

A estrutura da JCAFB permite a realização de exames de forma a atender uma proporção significativa das populações-alvo. Porém, na impossibilidade da cobertura total de um dado grupo – devido à dificuldade de acesso a certos bairros ou por somarem um número de pessoas além da capacidade de atendimento do projeto – os pacientes são selecionados de forma randomizada, mantendo-se as proporções de distribuição populacional pelas áreas do município. Para isto, faz-se uso de um sistema informatizado de cadastro. Nesta ferramenta de gestão, cedida pela CLVsol, todos os participantes do projeto são cadastrados e todas as informações (dados socioeconômicos, respostas dos

questionários e resultados de exames) são armazenadas de forma segura, consistente e rastreável, garantindo a confidencialidade das mesmas.

## RESULTADOS E DISCUSSÃO

### Levantamento do perfil socioeconômico e da prevalência de parasitoses

As parasitoses intestinais resultam em inúmeras consequências, como deficiências orgânicas, aumento da suscetibilidade a infecções bacterianas secundárias e de quadros críticos de anemia. Como consequências, podemos citar o comprometimento da qualidade de vida, e queda do rendimento laboral e escolar [4]. O saneamento básico também contribui de forma relevante para o controle da disseminação de doenças infecciosas [5]. Contudo, há também uma relação com a situação socioeconômica que, seja por hábitos culturais e/ou falta de informação, influencia na qualidade da educação sanitária da população, constituindo um ponto crítico para o controle efetivo dessas condições [6]. O projeto atende crianças de diferentes faixas etárias como um dos grupos prioritários de atendimento por estarem mais sujeitas às parasitoses intestinais, uma vez que estas estão mais expostas a fatores de risco e não apresentam imunidade completamente desenvolvida [7, 8].

O trabalho de campo é realizado por duplas de alunos de graduação da FCF/USP, previamente treinadas. Os pacientes selecionados recebem, previamente, uma correspondência explicativa do projeto e sobre as visitas domiciliares. Na visita de apresentação, as atividades propostas são explicadas detalhadamente, incluindo a apresentação do termo de consentimento ao responsável, autorizando a coleta de dados e realização dos exames de fezes e *swab* anal nas crianças (para pesquisa de *Enterobius vermicularis*). Por meio da aplicação do questionário socioeconômico, levantam-se os hábitos da população em relação à água de consumo, alimentação, higiene, saúde e renda familiar, dentre outros aspectos. Ao final da visita, são distribuídos os coletores universais para a coleta de fezes.

A equipe de Análises Clínicas analisa as amostras de fezes com o objetivo de verificar a presença de ovos e/ou cistos de parasitas intestinais, por meio de duas técnicas: método de Hoffmann (sedimentação espontânea) e método de Ritchie [9]. Em caso de detecção parasitária, frascos coletores são disponibilizados para os demais familiares. Ainda, faz-se uso da análise do *swab* anal, método mais eficaz para a detecção de ovos de *Enterobius vermicularis*, causador da oxiúriase, por vezes não detectados pelo exame de fezes devido a particularidades do ciclo de vida do parasita. Ao todo, são realizados cerca de 800 exames parasitológicos por ciclo do projeto.

Após as análises, a equipe de campo realiza nova visita domiciliar (figura 4) e entrega os laudos, orientando sobre as causas e consequências da contaminação pelos parasitas detectados, com ênfase em profilaxia. Para fins didáticos, utilizam-se fotos e esquemas dos ciclos de vida dos agentes infectantes. Em caso de resultado positivo, recomenda-se sempre consulta médica e acompanhamento pelos ACSs, enfatizando a importância em se buscar uma farmacoterapia adequada, além da tomada de ações preventivas.





Figura 4: Orientações domiciliares no trabalho de campo. Fotografias por Thiago André.

### Levantamento do perfil socioeconômico e da prevalência de anemia

As anemias são consideradas um problema de saúde pública mundial. Apesar das inúmeras causas de anemia, a desnutrição e o baixo nível socioeconômico são os fatores de risco mais relevantes, sendo a anemia por deficiência de ferro a mais prevalente. Outras importantes causas incluem deficiência de vitamina B12 e folato, doenças parasitárias (malária e enteroparasitoses). Vale destacar que a anemia aumenta o risco de outras comorbidades, principalmente em mulheres grávidas e crianças [10, 11].

As amostras de sangue são submetidas à análise por método automatizado pelo aparelho Horiba ABX-Micros 60 para detecção de níveis de hemoglobina e, consequentemente, identificação de pacientes com anemias. São aplicados questionários para avaliação de quadro sugestivo da doença, bem como suas possíveis causas, o que contribui para uma orientação mais eficaz. A cada ciclo do projeto, realizam-se mais de 750 dosagens de hemoglobina nas crianças e idosos cadastrados.

### Atenção à saúde do idoso

Estudos internacionais e nacionais voltados para a incapacidade funcional dos idosos ressaltam diversos aspectos críticos, envolvendo fatores como autonomia, independência, cognição, suporte financeiro e social. Neste sentido, diversas legislações brasileiras vigentes [12,13] visam incentivar a autossuficiência e a integração dos idosos na sociedade, e promover melhoria de sua qualidade de vida. Dessa maneira, a JCAFB oferece ações específicas voltadas para os idosos, visando não somente melhoria da saúde desta população, mas também sua integração [11].

A equipe de campo é responsável pelas visitas às casas dos idosos cadastrados no projeto, cuja estrutura é semelhante à descrita anteriormente (vide “*Levantamento do perfil socioeconômico e da prevalência de parasitoses*”). Os frascos coletores universais são entregues aos indivíduos que aceitaram realizar os exames de urina e coproparasitológicos. As duplas de jornalheiros responsáveis por cada residência encaminham as amostras coletadas para a equipe de Análises Clínicas, a qual avalia as amostras e emite os resultados. A cada ciclo do projeto, são realizados cerca de 400 exames de urina, cujos laudos embasam uma orientação mais direcionada às necessidades dos idosos.



## Uso racional de medicamentos

O trabalho de campo compreende, também, a promoção do uso racional de medicamentos. Os estudantes, durante as visitas domiciliares, enfatizam a importância do esclarecimento referente ao preparo caseiro e uso de plantas medicinais, muitas vezes para o tratamento de doenças não diagnosticadas, alertando para as consequências da substituição de medicamentos prescritos por estas preparações e ressaltando a importância de consultar os profissionais de saúde.

Ainda, sob orientação dos farmacêuticos residentes, os estudantes esclarecem dúvidas dos pacientes acerca de questões associadas a doenças de maior prevalência e suas farmacoterapias. Os jornadeiros orientam, em todas as residências visitadas, sobre o correto acondicionamento, manuseio, identificação, validade, administração e descarte, visando, assim, a promoção da segurança do uso do medicamento.

## Levantamento da prevalência de diabetes, hipercolesterolemia e hipertensão arterial

No Brasil, os altos índices de óbitos causados por doenças crônicas decorrem do estágio atual da transição demográfico/epidemiológica pela qual passa a população brasileira, resultando no envelhecimento populacional [14]. O diabetes mellitus e a hipertensão arterial estão entre as doenças crônicas não transmissíveis mais prevalentes, cujo manejo frequentemente exige a realização de mudanças no estilo de vida (como com a prática de atividade física e adoção de dietas saudáveis), além da farmacoterapia adequada. Estas intervenções podem afetar significativamente a qualidade de vida do paciente, ressaltando a importância de que o paciente esteja ciente das possíveis complicações destas doenças, bem como das consequências da não adesão ao tratamento de forma adequada [15, 16].

Diante desse cenário, julgou-se ser de grande importância à implementação de uma campanha para detecção de indicadores destas doenças crônicas não transmissíveis, como glicemia, colesterol e pressão arterial de cada indivíduo. O intuito da aquisição desses dados é orientar e incentivar o monitoramento desses parâmetros pelos indivíduos, de forma a contribuir para o diagnóstico precoce e promoção da saúde (Figura 5).

Figura 5. Campanhas de Anemia e de Diabetes, Hipercolesterolemia e Hipertensão Arterial. Coleta de amostra de sangue (esquerda) e orientação à população (direita). Fotografias por Thiago André.



A campanha de prevenção e diagnóstico de diabetes, hipercolesterolemia e hipertensão arterial são realizadas nos finais de semana. Como mencionado anteriormente, os acadêmicos da JCAFB são capacitados previamente para a campanha e são devidamente paramentados com equipamentos de proteção individual – avental e luvas descartáveis. Após aceitação do termo de consentimento, aplica-se um questionário para avaliar o histórico familiar e os hábitos do indivíduo com relação à diabetes, hipertensão, hipercolesterolemia, tabagismo, alcoolismo, entre outros. Em seguida, os participantes são encaminhados para testes rápidos de glicemia e colesterol total, bem como aferição da pressão arterial. Por fim, recebem orientações individuais sobre as doenças, bem como o papel de hábitos saudáveis na prevenção, com base em sua rotina e o resultado dos testes realizados no dia. Por ano, realizam-se cerca de 600 exames durante as campanhas de diabetes, hipercolesterolemia e hipertensão, que envolvem a orientação de mais de 200 pessoas a cada edição do projeto.

### **Capacitação dos agentes comunitários de saúde**

O ACS atua na Estratégia de Saúde da Família cujo objetivo principal é interligar a equipe de serviços de saúde com a comunidade, por meio de ações diretas, envolvendo os mais diversos profissionais da saúde. A JCAFB almeja enriquecer o trabalho da equipe de ACSs do município atendido, através de atividades complementares sobre educação em saúde, como educação sanitária e medidas preventivas contra doenças metabólicas e enteroparasitárias que acometem a região.

A capacitação consiste na aplicação de um questionário para identificação das demandas locais e coleta de informações sobre os trabalhos realizados, após apresentação e assinatura do Termo de Consentimento Livre e Esclarecido. Além disso, são oferecidas visitas ao laboratório local da JCAFB, além de palestras e oficinas sobre temas atuais, bem como os principais problemas de saúde encontrados no município e dinâmicas para valorização do trabalho. Ainda, são disponibilizados materiais didáticos de suporte sobre educação em saúde, constando medidas profiláticas básicas e reconhecimento de sintomas destes problemas, a fim de serem utilizados como ferramentas de ação. O objetivo da capacitação é aprimorar os profissionais e complementar, de forma efetiva, a atuação na abordagem, conscientização e orientação da população.

### **Determinação da qualidade da água para consumo**

A análise microbiológica da água é realizada para a detecção de coliformes fecais e totais como indicadores de prováveis contaminações por patógenos. Adicionalmente, a análise de parâmetros físico-químicos, como a concentração de cloro residual e o pH, é essencial para a avaliação da efetividade do sistema de tratamento de água. As amostras de água são coletadas em diversos pontos da cidade, incluindo residências de famílias atendidas pelo projeto, unidade básica de saúde, reservatórios e postos de abastecimento de água, escolas locais e estabelecimentos comerciais da cidade. Para fins de comparação, amostras de água esterilizadas são utilizadas como controle negativo. Os dados são avaliados segundo padrões microbiológicos e físico-químicos,

descritos na Portaria nº 2914/2011 do Ministério da Saúde [5]. Os resultados são analisados em conjunto com os dados socioeconômicos e os exames coproparasitológicos da população. Ao todo, são realizadas cerca de 80 análises de água durante a estada do projeto em cada cidade.

### Transdisciplinaridade

#### » Intercâmbio de ideias

A participação de alunos de outras unidades e institutos da Universidade de São Paulo, tanto de graduação como de pós-graduação, tem auxiliado no crescimento do projeto e no desenvolvimento de novas atividades e perspectivas de atuação. Desde 2012, a JCAFB conta com o apoio e participação de graduandos de outros cursos da área da saúde da USP (medicina, nutrição, enfermagem, gestão em saúde pública, dentre outros), fruto de um convênio com a Jornada Universitária da Saúde (JUS). Esta parceria prevê a participação de dois coordenadores da JUS, sob responsabilidade da Faculdade de Saúde Pública da USP, nas atividades da JCAFB. Em contrapartida, coordenadores da JCAFB participam das atividades da JUS. Este intercâmbio visa melhorias da esfera organizacional, estrutural e de seleção dos participantes de ambos os projetos, permitindo uma troca de experiências de forma mais profunda, além de uma atuação mais enriquecida, uma vez que incentiva o contato entre áreas de formação distintas.

#### » Interface com a saúde animal

Atualmente, a concepção de família é baseada em vínculos afetivos em detrimento do parentesco familiar de fato, e os animais são membros importantes desta família multiespécie [17]. Médicos veterinários têm sido inseridos em equipes multiprofissionais de assistência à saúde da família, e em 2011, incluído no Núcleo de Apoio à Saúde da Família.

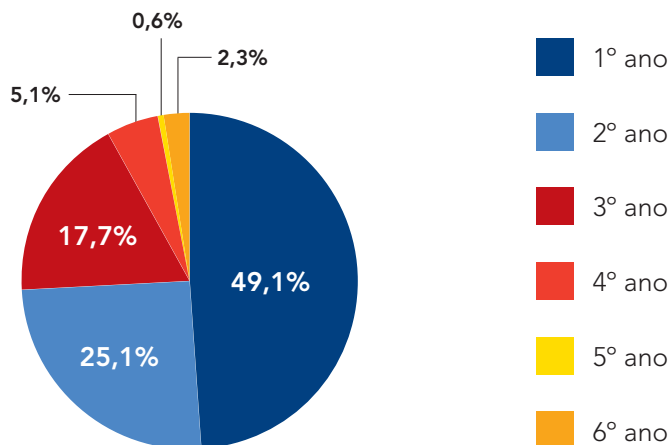
Neste contexto, em 2015, foi estabelecida parceria com o Programa de Residência em Área Profissional da Saúde em Medicina Veterinária e o Programa de Aperfeiçoamento Profissional em Medicina Veterinária, ambos associados ao Hospital Veterinário da Faculdade de Medicina Veterinária e Zootecnia da USP (Hovet/FMVZ/USP). Este trabalho inclui ações de educação em saúde e atenção primária aos animais, com visitas domiciliares com avaliação clínica, levantamento epidemiológico por meio de questionários, campanhas de vermifugação e de vacinação, e principalmente orientações básicas referentes à nutrição, uso de antiparasitários, imunizações, métodos contraceptivos, bem-estar animal e zoonoses. Já no primeiro ciclo, foram atendidos cerca de 200 cães e gatos. A consolidação desta parceria visa a expansão das atividades dos médicos veterinários residentes, com enfoque em zoonoses, doenças sexualmente transmissíveis e métodos de contracepção, especialmente em cães e gatos.

#### » Formação do graduando

A JCAFB tem como missão o aprendizado científico, humanitário e social dos estudantes que atuam no projeto. A grande maioria dos jornadeiros (74,2%) encontram-se

nos dois primeiros anos da graduação (Figura 6). Sendo assim, a participação em um projeto de extensão universitária de grande complexidade, como a JCAFB, cria a oportunidade de vivência, logo no início da formação acadêmica, de uma experiência de aproximação da plenitude da profissão farmacêutica, catalisando o contato dos alunos com a atuação do farmacêutico como um profissional de saúde. Ainda, o modelo transdisciplinar junto às diferentes profissões da área da saúde cria um ambiente rico para a discussão de ideias e para a quebra de paradigmas. Fomenta-se, então, a visão de que, para a eficaz promoção da saúde, é crucial uma ação conjunta da equipe multiprofissional. Dessa forma, o projeto viabiliza a construção de um perfil profissional pautada no conhecimento teórico, prático e, concomitantemente, crítico acerca das funções e limitações dos serviços de saúde.

**Figura 6** – Distribuição, por ano no curso de Farmácia e Bioquímica, dos graduandos participantes da JCAFB.



## CONCLUSÃO

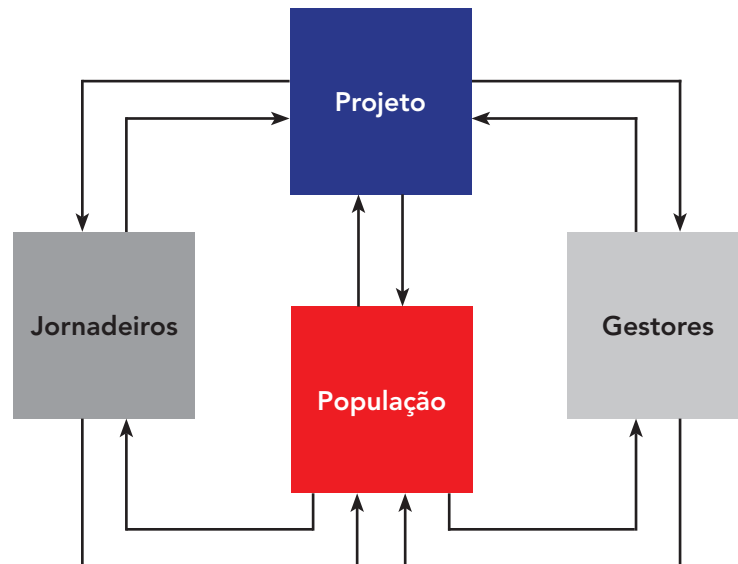
Durante um aparente curto período de 20 dias, repetidos em um ciclo de cerca de 4 anos, a JCAFB promove um impacto positivo significativo sobre a saúde e a educação da população, por meio de abordagem e linguagem diferenciadas, que despertam o interesse local pelos temas. São levantadas informações epidemiológicas que revelam importantes aspectos acerca da saúde em cidades do estado de São Paulo, estimulando a pesquisa e a elaboração de instrumentos de intervenção, uma vez que um relatório circunstanciado é anualmente enviado à Secretaria de Saúde e à Prefeitura do município atendido.

A crescente procura dos acadêmicos pela JCAFB evidencia o interesse pela integração entre profissão, sociedade e cidadania. Tanto para a equipe coordenadora quanto para a equipe de alunos participantes, a experiência da aproximação entre

farmacêutico e população resgata o caráter humanitário da profissão. A participação dos graduandos nas atividades práticas de inserção social desperta o interesse do futuro farmacêutico para o desenvolvimento e valorização de ações primárias à saúde, bem como o olhar crítico à promoção de saúde, por meio de uma formação profissional e cidadã.

O projeto tem, como objetivo principal, despertar o interesse da população pela promoção da saúde, bem como discutir conhecimentos teóricos e práticos junto às comunidades, como meio de melhorar a qualidade de vida local. Assim, a JCAFB possibilita a interação prática entre pesquisa, ensino e extensão, fomentando a construção do conhecimento e a criação de ferramentas que promovam ação continuada das ideias propostas. Sendo assim, preservando o princípio da indissociabilidade do tripé universitário, a JCAFB proporciona aos estudantes a vivência do papel do farmacêutico enquanto profissional da saúde. Após o término de cada ciclo, as autoridades e lideranças locais obtém, como fruto de um trabalho conjunto com a população e a JCAFB, informações necessárias para intervirem em demandas iminentes, incentivando a perpetuação do projeto. Portanto, a atuação da JCAFB é constituída de ações interdependentes, no qual a contribuição mútua entre os jornadeiros, a população e os gestores é crucial (Figura 7). Enfim, a Jornada Científica atua com o ideal de construir uma sociedade mais justa e fundamentada no bem-estar coletivo.

**Figura 7** – Esquema representativo do ciclo de ação da JCAFB – interação múltipla entre o projeto, os jornadeiros, a população e os gestores.



## REFERÊNCIAS

- [1] ARTIGAS, P.T.; PEREZ, M.D.; OTSUKO, J.M.; NISHIMORI, G. Levantamentos parasitológicos, em particular a esquistossomose mansônica, nas cidades de Itanhaém e Mongaguá (Litoral Sul do Estado de São Paulo). **Rev. Saúde Pública**, v. 4, n. 1, p. 35-43, 1970.
- [2] PEREZ, M. D.; ARTIGAS, P. T. Contribuição ao levantamento da carta planorbídica do estado de São Paulo. Pesquisa de focos com formas evolutivas do *Schistosoma mansoni*. II. Município de Peruíbe (litoral sul do estado de São Paulo, Brasil). **Rev. Saúde Pública**, v. 3, n. 2, p. 149-152, 1969.
- [3] PIZA, J.T.; RAMOS, A.S.; MORAES, L.V.C.; CORRÊA, R.R.; PINTO, A.C.M. **Carta planorbídica do Estado de São Paulo**. São Paulo (SP): Secretaria de Estado da Saúde de São Paulo, 1972.
- [4] BELO, V.S.; OLIVEIRA, R.B.; FERNANDES, P.C.; NASCIMENTO, B.W.L.; FERNANDES, F.V.; CASTRO, C.L.F.; SANTOS, W.B.; SILVA, E.S. Fatores associados à ocorrência de parasitoses intestinais em uma população de crianças e adolescentes. **Rev. Paul. Pediatr.**, v. 30, n. 2, p. 195-201, 2012.
- [5] BRASIL. Portaria nº 2914, de 12 de dezembro de 2011. Procedimentos de controle e de vigilância da qualidade da água para consumo humano e seu padrão de potabilidade. **Diário Oficial da União, Brasília**, DF, 14 dez. 2011, Seção 1, p. 39-46.
- [6] VISSER, S.; GIATTI, L.L.; CARVALHO, R.A.C.; GUERREIRO, J.C.H. Estudo da associação entre fatores socioambientais e prevalência de parasitose intestinal em área periférica da cidade de Manaus (AM, Brasil). **Ciênc. Saúde Coletiva**, v.16, n.8, p.3481-3492, 2011.
- [7] CARDOSO, G.S, SANTANA, A.D.C., AGUIAR, C.P. Prevalência e aspectos epidemiológicos da giardíase em creches no município de Aracaju, Sergipe, Brasil. **Rev. Soc. Bras. Med. Trop.**, n.28, p.25-31, 1995.
- [8] GOMES DOS SANTOS, Marilena et al. Educação em saúde em escolas pública de 1º grau da periferia de Belo Horizonte, MG, Brasil: II - conhecimentos, opiniões e prevalência de helmintíase entre alunos e professores. **Rev. Inst. Med. Trop. SP**, v.35, n.6, p.573-579, 1993.
- [9] REY, L. **Parasitologia**. 3. ed. [s.l.] Editora Guanabara Koogan, 2001.
- [10] FERREIRA, H. DA S. **Desnutrição: magnitude, significado social e possibilidade de prevenção**. [s.l.] Edefal, 2000.
- [11] D'ORSI, E.; XAVIER, A. J.; RAMOS, L. R. Trabalho, suporte social e lazer protegem idosos da perda funcional: estudo epidioso. **Rev. Saúde Pública**, v. 45, n. 4, p. 685-692, 2011.
- [12] BRASIL. Lei nº 8.842, de 04 de janeiro de 1994. Lei da Política Nacional do Idoso. **Diário Oficial da União**, Brasília, DF, 05 jan. 1994, Seção 1, p.77.
- [13] BRASIL. Portaria nº 2528, de 19 de outubro de 2006. Política Nacional de Saúde da Pessoa Idosa. **Diário Oficial da União**, Brasília, DF, 20 out. 2006, Seção 1, p. 142
- [14] CORRÊA FILHO, H. R. Vigilância das doenças crônicas e ocupacionais: como passar das propostas às ações? **Saúde e Sociedade**, v. 4, n. 1-2, p. 99-105, 1995.
- [15] JARDIM, A.D.I.; LEAL, A.M.O. Qualidade da informação sobre diabéticos e

- hipertensos registrada no Sistema HIPERDIA em São Carlos-SP, 2002-2005. **Physis: Rev. Saúde Coletiva**, v. 19, n. 2, p. 405-417, 2009.
- [16] MARCOPITO, L.F.; RODRIGUES, S.S.F.; PACHECO, M.A.; SHIRASSU, M.M.; GOLDFEDER, A.J.; MORAES, M.A. Prevalência de alguns fatores de risco para doenças crônicas na cidade de São Paulo. **Rev. Saúde Pública**, v. 39, n. 5, p. 738-745, 2005.

## AGRADECIMENTOS

Agradecemos à Pró-Reitoria de Cultura e Extensão Universitária da USP e à FIPFARMA, pelo apoio financeiro; à Diretoria, Corpo Docente e Comissão de Cultura e Extensão Universitária da FCF/USP, ao HU/USP, à FMVZ/USP e à JUS/USP, pelo apoio institucional; às empresas AFIP, Roche, Merck S.A., Horiba ABX, P&G e CLVsol, pelo apoio técnico, material e científico; e, por fim, a todos os jornadaeiros e coordenadores que tornaram, e ainda tornam, a Jornada possível.

**ALICE HERMÍNIA SERPENTINO** *Farmacêutica, Hospital Universitário, Universidade de São Paulo (HU/USP).*

**JOÃO VICTOR CABRAL-COSTA** *Doutorando, Depto. de Bioquímica, Instituto de Química, Universidade de São Paulo (IQ/USP)*

**RODOLFO RIBEIRO DE SOUZA** *Graduando, FCF/USP*

**TAMARA RAMOS JORGE** *Graduanda, FCF/USP*

**SABRINA EIPHANIO PROFESSORA** *Doutora, Depto. de Análises Clínicas e Toxicológicas, FCF/USP*

**JEANINE GIAROLLA PROFESSORA** *Doutora, Depto. de Farmácia, FCF/USP*

**PRIMAVERA BORELLI** *Professora Titular, Depto. de Análises Clínicas e Toxicológicas, Faculdade de Ciências Farmacêuticas, Universidade de São Paulo (FCF/USP) - E-mail: borelli@usp.br*